BULLETIN OF RUSSIAN STATE MEDICAL UNIVERSITY

BIOMEDICAL JOURNAL OF PIROGOV RUSSIAN NATIONAL RESEARCH MEDICAL UNIVERSITY

SUBMISSION http://vestnikrgmu.ru/login?lang=en
CORRESPONDENCE editor@vestnikrgmu.ru
COLLABORATION manager@vestnikrgmu.ru
ADDRESS ul. Ostrovityanova, d. 1, Moscow, Russia, 117997

Indexed in Scopus. CiteScore 2023: 0,8

Indexed in WoS. JCR 2021: 0.5

Five-year h-index is 10

SCImago Journal & Country Rank 2020: 0.14

Listed in HAC 31.01.2020 (№ 507)

Open access to archive

Issue DOI: 10.24075/brsmu.2025-02
The mass media registration certificate № 012769 issued on July 29, 1994
Founder and publisher is Pirogov Russian National Research Medical University (Moscow, Russia)

Approved for print 30.04.2025
Circulation: 100 copies. Printed by Print.Formula
www.print-formula.ru

ВЕСТНИК РОССИЙСКОГО ГОСУДАРСТВЕННОГО МЕДИЦИНСКОГО УНИВЕРСИТЕТА

НАУЧНЫЙ МЕДИЦИНСКИЙ ЖУРНАЛ РНИМУ ИМ. Н. И. ПИРОГОВА

ПОДАЧА РУКОПИСЕЙ http://vestnikrgmu.ru/login
ПЕРЕПИСКА С РЕДАКЦИЕЙ editor@vestnikrgmu.ru
СОТРУДНИЧЕСТВО manager@vestnikrgmu.ru
АДРЕС РЕДАКЦИИ ул. Островитянова, д. 1, г. Москва, 117997

Журнал включен в Scopus. CiteScore 2023: 0,8 — Журнал включен в WoS. JCR 2021: 0,5 — Индекс Хирша (h^5) журнала по оценке Google Scholar: 10

SCImago Journal & Country Rank 2020: 0,14 — Журнал включен в Перечень 31.01.2020 (№ 507) — Здесь находится открытый архив журнала

DOI выпуска: 10.24075/vrgmu.2025-02
Свидетельство о регистрации средства массовой информации № 012769 от 29 июля 1994 г.
Учредитель и издатель — Российский национальный исследовательский медицинский университет имени Н. И. Пирогова (Москва, Россия)

Подписано в печать 30.04.2025
Тираж 100 экз. Отпечатано в типографии Print.Formula
www.print-formula.ru

BULLETIN OF RSMU **2, 2025**
ВЕСТНИК РГМУ

Contents
Содержание

ASSESSING PROLIFERATIVE ACTIVITY AND GLUCOSE METABOLISM IN CELLS OF SALIVARY GLAND MUCOEPIDERMOID CARCINOMA USING DIFFERENT GRADING SYSTEMS

Familia Frias DR[1]✉, Visaitova ZYu[2], Tigay YuO[1], Ivina AA[1], Babichenko II[1,2]

[1] Patrice Lumumba Peoples' Friendship University of Russia, Moscow, Russia

[2] National Medical Research Center of Dentistry and Maxillofacial Surgery, Moscow, Russia

Mucoepidermoid carcinoma (MEC) is the most common malignant tumor of the salivary gland consisting of three main histological components: mucocytes, intermediate and epidermoid cells. Various grading systems (AFIP, Brandwein, modified Healy, MSKCC) are difficult to use. The Ki-67 and GLUT1 markers associated with tumor aggressiveness can improve MEC diagnosis and classification. The study aimed to assess the correlation of the cell proliferative activity and glucose metabolism with the MEC grading systems. Tumors of a total of 40 patients with MEC were analyzed and determined in accordance with the following grading systems: AFIP, Brandwein, modified Healy, and MSKCC. Immunohistochemistry (IHC) was used to estimate Ki-67 proliferation indices and GLUT1 expression intensity. IHC showed high Ki-67 indices and GLUT1 values in epidermoid and intermediate cells, while mucocytes showed low or no expression. There were significant differences in Ki-67 and GLUT1 expression between epidermoid ($p < 0.005$) and intermediate cells ($p < 0.01$). Comparison revealed the increase between grades 1 and 2, 1 and 3, but no differences between grades 2 and 3. Spearman's rank correlation test revealed moderate positive correlations with tumor grades for GLUT1 and Ki-67, and the AFIP system showed the highest correlation (Ki-67: $rs = 0.55$; GLUT1: $rs = 0.50$). Thus, GLUT1 and Ki-67 are most intensely expressed in epidermoid and intermediate cells showing a strong correlation with the tumor grade and aggressiveness, especially in low-grade and intermediate-grade MEC. These markers can improve the diagnosis of MEC malignancy degree. The AFIP system most closely matches these markers in epidermoid and intermediate cells.

Keywords: GLUT-1, Ki-67, MEC grading, AFIP, Brandwein, Modified Healy, MSKCC

Author contribution: Babichenko II — study concept and design; Familia Frias DR, Tigay YuO, Visaitova ZYu — data acquisition and processing; Familia Frias DR — manuscript writing; Babichenko II, Ivina AA — editing.

Compliance with ethical standards: the study was approved by the Ehics Committee of RUDN (protocol No. 3 dated 11 March 2025).

✉ **Correspondence should be addressed:** Diana Rosina Familia Frias
Mikluho-Maklaya, 21, str. 2, Moscow, 117198, Russia; drff26@gmail.com

Received: 13.03.2025 **Accepted:** 27.03.2025 **Published online:** 11.04.2025

DOI: 10.24075/brsmu.2025.017

ОЦЕНКА ПРОЛИФЕРАТИВНОЙ АКТИВНОСТИ И МЕТАБОЛИЗМА ГЛЮКОЗЫ В КЛЕТКАХ МУКОЭПИДЕРМОИДНОЙ КАРЦИНОМЫ СЛЮННЫХ ЖЕЛЕЗ ПРИ РАЗЛИЧНЫХ СИСТЕМАХ ГРАДАЦИИ

Д. Р. Фамилья Фриас[1]✉, З. Ю. Висаитова[2], Ю. О. Тигай[1], А. А. Ивина[1], И. И. Бабиченко[1,2]

[1] Российский университет дружбы народов имени Патриса Лумумбы, Москва, Россия

[2] Национальный медицинский исследовательский центр стоматологии и челюстно-лицевой хирургии, Москва, Россия

Мукоэпидермоидная карцинома (МЭК) является наиболее распространенной злокачественной опухолью слюнных желез и состоит из трех основных гистологических компонентов: мукоцитов, промежуточных и эпидермоидных клеток. Различные системы градации (AFIP, Brandwein, Modified Healy, MSKCC) сложны в применении. Маркеры Ki-67 и GLUT1, связанные с агрессивностью опухоли, могут улучшить диагностику и классификацию МЭК. Целью исследования было провести оценку корреляции пролиферативной активности и метаболизма глюкозы клеток с системами градации МЭК. Были проанализированы опухоли 40 пациентов с МЭК и определены по системам градации: AFIP, Brandwein, Modified Healy и MSKCC. Для оценки индексов пролиферации Ki-67 и интенсивности экспрессии GLUT1 использовали иммуногистохимическое исследование (ИГХ). ИГХ показало высокие индексы Ki-67 и GLUT1 у эпидермоидных и промежуточных клеток, при этом в мукоцитах выявлена низкая или отсутствующая экспрессия. Статистически значимые различия в экспрессии Ki-67 и GLUT1 обнаружены между эпидермоидными ($p < 0,005$) и промежуточными клетками ($p < 0,01$). Сравнения показали увеличение между степенями 1 и 2, 1 и 3, но без различий между степенями 2 и 3. Корреляция Спирмена выявила умеренные положительные связи для GLUT1 и Ki-67 с градацией опухоли, причем система AFIP показала наибольшую корреляцию (Ki-67: $rs = 0,55$; GLUT1: $rs = 0,50$). Таким образом, GLUT1 и Ki-67 наиболее интенсивно экспрессируются в эпидермоидных и промежуточных клетках, сильно коррелируя со степенью и агрессивностью опухоли, особенно при низкой и средней степени МЭК. Эти маркеры могут улучшить точность диагностики степени злокачественности МЭК. Система AFIP наиболее точно соответствует этим маркерам в эпидермоидных и промежуточных клетках.

Ключевые слова: GLUT-1, Ki-67, градация МЭК, AFIP, Brandwein, Modified Healy, MSKCC

Вклад авторов: И. И. Бабиченко — концепция и дизайн исследования; Д. Р. Фамилия Фриас, Ю. О. Тигай, З. Ю. Висаитова — сбор и обработка материала; Д. Р. Фамилия Фриас — написание текста; И. И. Бабиченко, А. А. Ивина — редактирование.

Соблюдение этических стандартов: исследование одобрено этическим комитетом РУДН (протокол № 3 от 11 марта 2025 г.).

✉ **Для корреспонденции:** Диана Р. Фамилья Фриас
ул. Миклухо-Маклая, 21, к. 2, г. Москва, 117198, Россия; drff26@gmail.com

Статья получена: 13.03.2025 **Статья принята к печати:** 27.03.2025 **Опубликована онлайн:** 11.04.2025

DOI: 10.24075/vrgmu.2025.017

Mucoepidermoid carcinoma (MEC) is the most common malignant tumor of the salivary gland and occurs in 30% of cases of malignant tumors salivary glands [1]. MEC most often affects large salivary glands, specifically the parotid gland (60% of cases), but can also affect minor salivary glands [2, 3].

As for MEC histopathological structure, mucocytes, intermediate and epidermoid cells are distinguished as the main components, but there can also be cylindrical, clear cells, and oncocytes, which leads to diagnostic difficulties for pathologists [4–6]. These components form various histological structures, such as cystic (the most common and well differentiated), solid (rare, with necrosis and considerable cellular and nuclear atypia) or solid cystic structures more typical for tumors that are more prone to invasive growth and metastasis [7, 8].

MEC can be diagnosed based on its histological features only, without any additional testing, such as immunohistochemistry (IHC) or genetic testing, however it is often difficult to establish the final diagnosis [1]. To date, many grading systems have been created for MEC classification. However, there is no universally acknowledged unified system [9]. MEC is classified as low-grade (G1), intermediate-grade (G2) or high-grade (G3) tumor based on four different grading systems, such as Goode, Auclair, and Ellis AFIP (Armed Forces Institute of Pathology), as well as the Brandwein system used in routine histopathology practice [1, 4, 6], along with the modified Healy and MSKCC grading systems of qualitative nature (Table 1). The AFIP and Brandwein methods are not always consistent when used to classify the same tumor, especially when it comes down to determination of certain differences between G2 and G3 tumors. Comparative studies of grading systems have revealed differences when describing major and minor salivary glands [7, 10].

Carcinogenesis is a multi-step process, in which glucose metabolism disturbances can play an important role due to rapid cell proliferation typical for malignant growth [11]. Modern studies have revealed high energy metabolism of malignant tumors and glucose involvement in their growth. Glucose is the main energy source for mammalian cells, and glucose transporters (GLUT) on the cytoplasmic membrane promote glucose cell entry. Thus, GLUT represents the important enzymes mediating glucose metabolism during carcinogenesis [12]. High GLUT1 expression in malignant tumors is associated with invasion and metastasis, including head and neck cancer [13]. The Ki-67 proliferation marker represents a gold standard of assessing the salivary gland malignancies. The role of Ki-67 in the diagnosis and classification of salivary gland tumors is huge: it is directly correlated to the cell proliferation rate being a key indicator of tumor aggressiveness [14].

The study aimed to estimate various MEC grading systems based on proliferative activity and glucose metabolism of the MEC cells in order to determine the grade.

METHODS

Retrospective analysis of the paraffin blocks of tumors of 40 patients (female and male) diagnosed with mucoepidermoid carcinoma from the archive of the Pathology Laboratory of the Central Research Institute of Dental and Maxillofacial Surgery of the Ministry of Health of the Russian Federation for the period 2014–2023 was conducted.

Table 1. Mucoepidermoid carcinoma grading systems

Criteria	AFIP	Brandwein	Modified Healey	MSKCC
Cystic component	(< 20%) 2	(< 25%) 2	L: macro + microcysts I: microcysts + solid H: solid ± microcysts	L: prediminantly cystic (> 80%) I: prediminantly solid H: any (usually solid)
Perineural invasion (PI)	2	3	H: present	n/a*
Necrosis (N)	3	3	n/a	L: absent I: absent H: present
Mitoses	3 (≥ 4/10 HPF)	3 (≥ 4/10 HPF)	L: rare I: rare H: many	L: 0–1/10 HPF I: 2–3/10 HPF H: 4+ /10 HPF
Nuclear anaplasia / pleomorphism	4	2	L: absent/minimal I: minimal/moderate H: prominent (including nucleoli)	L: negligible I: negligible H: any
Border / invasion front	n/a	2	L: broad/ circumscribed I: uncircumscribed H: soft tissue / perineural / vascular invasion	L: well-defined I: well-defined or infiltrative H: any (usually infiltrative)
Lymphovascular invasion	n/a	3	H: present	n/a
Bone invasion	n/a	3	n/a	n/a
Intermediate cells	n/a	n/a	L: rare I: more frequent H: predominant	n/a
Stroma	n/a	n/a	L: extravasated mucin + fibrosis + CI I: fibrosis separating nests + CI H: desmoplasia, minimal CI	n/a
Architecture	n/a	n/a	L: daughter cysts from larger ones I: larger canals are less prominent H: variable architectural pattern/cell morphology	n/a
Grading	L — 0–4 I — 5–6 H — 7–14	L — 0 I — 2, 3 H — ≥ 4	L — low grade I — intermediate grade H — high grade	

Note: n/a — not applicable.

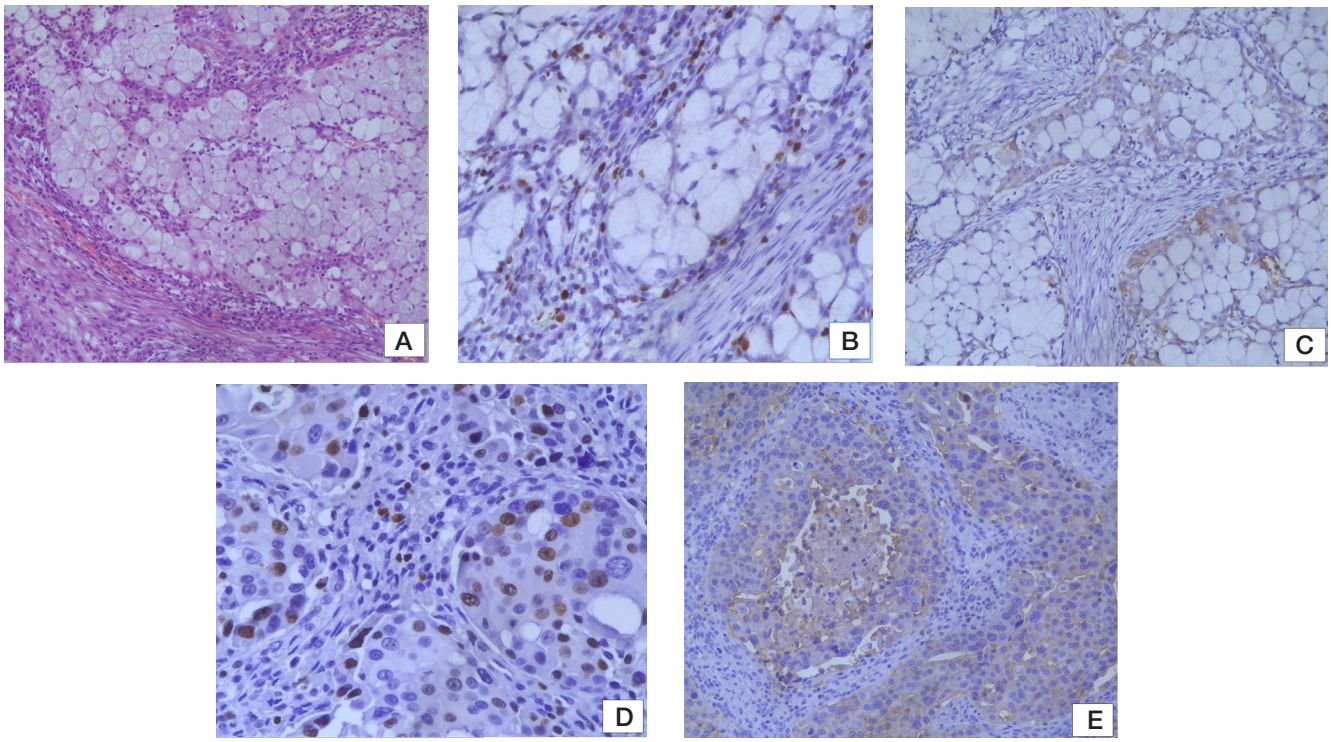

Fig. 1. MEC, hematoxylin and eosin stain ×100 **(A)**. Immunohistochemical reaction with antibody against Ki-67 ×200 **(B)**. GLUT1 cytoplasm staining in epidermoid and intermediate cells, weak response in mucin-producing cells ×100 **(C)**. High proliferative activity based on Ki-67 in epidermoid cells ×400 **(D)**. Intense GLUT1 cytoplasmic membrane staining in epidermoid cells ×200 **(E)**. IHC reaction with the background Mayer's hematoxylin DAB stain

Morphology assessment was performed in accordance with the standard hematoxylin and eosin stain protocols. Histological specimens were assessed using the following four grading systems: modified Healy grading, MSKCC grading, AFIP grading, and Brandwein grading. These systems were compared with the final estimates for each case and correlated to IHC assessment.

Histological and IHC assessment was conducted in accordance with the standard protocol. All biopsy specimens were stained with the Thermo Scientific anti-Ki-67 rabbit monoclonal antibody (USA, clone SP6), Thermo Scientific anti-GLUT1 rabbit polyclonal antibody (USA). The material collected was assessed using the Axioplan 2 Imaging microscope (Karl Zeiss, Germany), and the AxioCam ERc5s camera was used to take images of specimens (Karl Zeiss, Germany). IHC imaging was accomplished using the UltraVision Quanto Detection System HRP DAB (USA) system. The Ki-67 proliferation protein expression was estimated based on proliferation activity index (percentage of cells with the intensely stained nuclei per 300 nuclei of each MEC cell type). GLUT1 expression was assessed based on the cytoplasm and/or cytoplasmic membrane stain and scored based on conditional criteria: no expression — 0, weak expression — 1, moderate expression — 2, strong expression — 3.

MEC was graded using four grading systems, and correlations between the marker, cellular components, and grades were analyzed using the Kruskal–Wallis test, Dunn–Bonferroni test for pairwise comparison, and Spearman's rank correlation. Statistical analysis was conducted using the SPSS Statistics 23 software package for Windows 10 (IBM Corporation, USA).

RESULTS

Histological grading

The AFIP grading system showed a more conservative approach, allowing one to classify the largest number of tumors considered to be low-grade (G1) (40%) compared to other systems. Tumors classified as intermediate-grade accounted for 35%, while high-grade tumors (G3) accounted for only 25%. Such distribution suggests that tumors are assigned lower grades based on the AFIP system, which results in potential underestimation of tumor aggressiveness relative to other systems.

The Brandwein grading system is characterized by the more aggressive approach: the smallest number of tumors are assigned low grade (G1) (20%), while the largest number are classified as high-grade tumors (G3) (45%). Tumors assessed as intermediate-grade ones (G2) account for 35%, which is similar to the results of using AFIP. This suggests that in the Brandwein system preference is given to classification of higher grades, more tumors are assessed as potentially aggressive, but in some cases there is a risk to overestimate the disease severity.

The Modified Healy grading system presents a more balanced grade distribution: 25% of tumors were classified as low-grade ones (G1), 50% as intermediate-grade (G2) (the largest share among all systems), and 25% as high-grade ones (G3). This grading system focuses on the intermediate category, which makes it potentially more useful for identification of borderline or moderately aggressive tumors.

The MSKCC grading system showed the conservative approach similar to that of AFIP: 35% of tumors were classified as low-grade ones (G1) and 45% as intermediate-grade ones (G2). However, the lowest number of tumors were assigned high grade (G3) (20%), which reflects the trend towards the decrease in the number of cases of higher grade MEC. In some cases, this can result in underestimation of tumor aggressiveness.

Immunohistochemistry assessment

Assessment of the hematoxylin and eosin stained MEC slides revealed mucocytes, intermediate and epidermoid cells (Fig. 1A).

Table 2. Pairwise comparison (Dunn–Bonferroni test)

Cellular component	Comparison	Significance ($p < 0,05$)
Epidermoid	G1–G2	0.003
	G1–G3	0.0003
	G2–G3	0.067
Intermediate	G1–G2	0.036
	G1–G3	0.003
	G2–G3	0.23
Mucocytes	G1–G2	0.12
	G1–G3	0.12
	G2–G3	0.12

IHC assessment effectively complements the diagnosis of the hematoxylin and eosin stained slides. In this study, detection of the Ki-67 nuclear antigens associated with the cell cycle made it possible to estimate cell proliferation intensity, and GLUT1 was used as an indicator of glucose metabolism in MEC.

In all the MEC cellular components, Ki-67 protein was found in the cell nuclei (Fig. 1C, D) and GLUT1 was found in the cytoplasm and on the cytoplasmic membrane (Fig. 1C, E). There were considerable differences in distribution of the Ki-67 proliferation indices between three MEC components (epidermoid, intermediate, mucoid). In-depth statistical analysis showed high proliferation rate of epidermoid cells based on Ki-67, for which the median was 13.3% (9.3; 20.0). Intermediate cells demonstrated lower proliferation rates compared to epidermoid cells, and the median was 6.7% (3.5; 10.7), while mucocytes showed minimal Ki-67 expression, and the median was 1.3% (0.0; 2.7).

The Kruskal–Wallis test and pairwise comparison were applied to assess the correlation between Ki-67 indices and the tumor grade. Significant differences in Ki-67 indices between tumor grades were reported for epidermoid ($H = 16.25$, $p = 0.0003$) and intermediate cells ($H = 10.85$, $p = 0.0045$), but not for mucocytes ($H = 4.12$, $p = 0.12$).

Pairwise comparison performed using the Dunn–Bonferroni test revealed significant differences for epidermoid and intermediate cells (Table 2). Mucocytes showed no considerable differences based on grades.

The use of the statistical Spearman's rank correlation test revealed a significant correlation between the Ki-67-based proliferation indices and the MEC grade for three studied components. The strongest correlation was reported for epidermoid cells (0.53, $p = 0.0005$). This indicator suggests that the Ki-67 proliferation index in epidermoid cells increases incrementally with increasing tumor grade, which makes it valuable for assessment of the neoplastic process aggressiveness and makes it possible to use it as a marker of tumor aggressiveness. A moderate positive correlation has been also reported for intermediate cells ($rs = 0.47$, $p = 0.0025$), which confirms their contribution to tumor progression, although lesser than that of epidermoid cells. In contrast, mucocytes have shown a weak non-significant correlation ($rs = 0.25$, $p = 0.12$), which reflects their minimal proliferative activity and limited importance for tumor grading (Fig. 1D).

MEC grading based on calculating proliferative activity of epidermoid and intermediate cells suggests low grade (G1) with the activity below 10%, intermediate grade (G2) with the activity between 10% and 15%, and high grade (G3) with the activity exceeding 15–20%. These grades based on the Ki-67 labeling provide important information about the MEC biological behavior allowing one to determine tumor grade using quantitative indicators of proliferation of various cell populations within the tumor.

The analysis of GLUT1 staining intensity in all specimens revealed considerable differences between three components. Intermediate and epidermoid cells showed the highest staining intensity with the median score of 2 points (1; 3), which suggested moderate variability, while mucocytes showed the lowest intensity with the median score of 0 points (0; 0), suggesting consistently low or no GLUT1 expression in this component (Fig. 1E).

The Kruskal–Wallis test allowed us to reveal considerable differences in GLUT1 staining intensity by tumor grades for epidermoid ($p = 0.005$) and intermediate cells ($p = 0.01$), but not for mucocytes ($p = 0.15$). Pairwise comparison involving the use of the Dunn–Bonferroni test showed that in epidermoid and intermediate cells the staining intensity increased considerably between grade 1 and grade 2, as well as between grade 1 and grade 3. However, no significant differences between grades 2 and 3 were reported for both components, which suggested the GLUT1 expression plateau in higher grade tumors. Mucoid cells showed low staining intensity and uniformity, regardless of the salivary gland neoplasm malignancy degree; no significant differences were also revealed.

In addition to statistical analysis, we applied Spearman's rank correlation test to determine the correlation between the GLUT1 staining intensity and the tumor grade. The following results were obtained: epidermoid cells — $rs = 0.48$ ($p = 0.003$), intermediate cells — $rs = 0.42$ ($p = 0.008$). These data indicate a moderate positive correlation with the tumor grade and suggest a progressive GLUT1 expression increase with increasing tumor aggressiveness. In contrast, mucocytes showed a weak non-significant correlation ($rs = 0.15$, $p = 0.36$), which reflected their minor contribution to tumor grading.

In MEC, GLUT1 staining intensity in various cellular components allows one to achieve critical understanding of metabolic activity associated with various tumor grades. Epidermoid and intermediate cells demonstrate a progressive increase in GLUT1 expression. Such progression demonstrates a considerable increase in metabolic activity with increasing tumor grade: from low grade with minimal GLUT1 expression indicating the decreased metabolic demands to high grade, in which the staining intensity is close to maximum suggesting high metabolic activity that is necessary for rapid tumor growth and tumor aggressiveness.

Correlation between GLUT1 and Ki-67 in various MEC components

Spearman's rank correlation test allowed us to reveal a strong positive correlation between the GLUT1 and Ki-67 staining

Table 3. Correlation between GLUT1 and Ki-67 and tumor grades

Correlation between GLUT1 and tumor grades		
Grading system	Correlation coefficient (*rs*)	*p*-value
AFIP	0.5	0.001
Brandwein	0.45	0.003
Modified Healy	0.48	0.002
MSKCC	0.4	0.01
Correlation between Ki-67 and tumor grades		
Grading system	Correlation coefficient (*rs*)	*p*-value
AFIP	0.55	0.0005
Brandwein	0.48	0.002
Modified Healy	0.52	0.001
MSKCC	0.45	0.003

intensity in epidermoid cells ($rs = 0.68$, $p < 0.001$). This suggests that higher GLUT1 expression is stably associated with the increased proliferative activity for this component. A moderate positive correlation was reported for intermediate cells ($rs = 0.52$, $p = 0.004$), which suggested a significant, but less strong, association between two markers. In contrast, mucocytes showed a weak non-significant correlation ($rs = 0.20$, $p = 0.18$), which reflected a minimal interplay between the GLUT1 expression and Ki-67 proliferation in this component.

Both markers, GLUT1 and Ki-67, showed high correlation and strong relationship in epidermoid and intermediate cells. In epidermoid cells, the following values were obtained for GLUT1 and Ki-67: $rs = 0.48$ ($p = 0.003$) and $rs = 0.53$ ($p = 0.0005$). Similar values were reported for intermediate cells: GLUT1 — $rs = 0.42$ ($p = 0.008$) and Ki-67 — $rs = 0.47$ ($p = 0.0025$). This indicates moderate correlation with the malignancy degree, which makes the markers selected important for tumor progression assessment. When assessing the correlation with the malignancy degree, in contrast to epidermoid and intermediate cells, mucocytes showed weak correlations for both GLUT1, where $rs = 0.15$ at $p = 0.36$, and Ki-67, where $rs = 0.25$ at $p = 0.12$, which once more emphasized their limited contribution to tumor grading.

GLUT1 correlation with tumor grading systems

GLUT1 staining intensity showed a moderate positive correlation with tumor grades for all grading systems. The strongest correlation was reported for the AFIP system ($rs = 0.50$, $p = 0.001$), which suggests that GLUT1 agrees well with the tumor aggressiveness determined by the AFIP criteria. The modified Healy system ($rs = 0.48$, $p = 0.002$) also showed a comparable correlation. The Brandwein ($rs = 0.45$, $p = 0.003$) and MSKCC ($rs = 0.40$, $p = 0.01$) systems showed weaker correlation, which suggests less full GLUT1 compliance with the grading ctiteria.

Ki-67 correlation with tumor grading systems

Ki-67 proliferation indices showed stronger correlation with tumor grades, than GLUT1, for all grading systems. The highest correlation was reported for the AFIP system ($rs = 0.55$, $p = 0.0005$) that was followed by the modified Healy system ($rs = 0.52$, $p = 0.001$). These findings emphasize the effectiveness of Ki-67 as a reliable tumor progression marker, especially within the limits of these grading systems. The Brandwein ($rs = 0.48$, $p = 0.002$) and MSKCC ($rs = 0.45$, $p = 0.003$) also showed moderate correlations, but weaker, than the AFIP and modified Healy systems.

Comparison of grading systems

Among four grading systems assessed, AFIP consistently showed the strongest correlation with both GLUT1 and Ki-67 expression, which suggests being most close to tumor biology reflected by these markers. The modified Healy system showed almost the same results, especially for Ki-67, which makes it one more reliable basis for tumor aggressiveness assessment. The Brandwein and MSKCC systems showed a slightly weaker correlation, especially for GLUT1, which indicates lower coordination with metabolic and proliferative activity (Table 3).

DISCUSSION

In this study we assessed proliferative activity (Ki-67) and activity of the glucose transporter protein (GLUT1) in various MEC components, which were found in all cellular components. High expression of the selected proteins was revealed in the MEC epidermoid and intermediate cells, which indicates growth and neoplastic process aggressiveness. The findings are similar to the earlier reported data [15, 16], according to which GLUT1 expression was higher in the epidermoid component and high-grade tumors, respectively.

The Ki-67 index serves as the most important biomarker to determine the MEC grade that complements conventional histological assessment. Thus, in 46 patients, low Ki-67 index was correlated to favorable outcomes, while higher index values indicated the increased risk of aggressive disease course [17]. In contrast to more subjective histological assessment involving indirect measurement of proliferative activity based on the share of solid areas, the Ki-67 index allows one to directly determine proliferation through enumeration of the actively dividing cells. Such a direct approach makes it a more objective and reliable marker allowing one to clearly distinguish indolent and aggressive MEC forms [14, 17]. Thus, using the Ki-67 index along with histological assessment can considerably improve accuracy of predicting the clinical course of such tumors, ensuring invaluable guidance for targeted therapeutic strategies.

Mostly, such grading systems, as AFIP and MSKCC, are prone to conservative grading, which highlights low and intermediate classification, while the Brandwein system is characterized by the more aggressive approach and higher effectiveness when dealing with high-grade tumors. The modified Healy system is more effective when dealing with intermediate-grade tumors. Such variation emphasizes the impact of grading criteria on tumor classification and the importance of matching the grading system to clinical goals, such as risk stratification or treatment planning.

CONCLUSIONS

The study emphasizes the key role of GLUT1 and Ki-67 in assessing metabolic and proliferative activity of salivary gland MEC. High expression of these markers revealed in epidermoid and intermediate cells corresponded to the following values: low grade — Ki-67 below 10%, GLUT1 intensity 1–2; intermediate grade — Ki-67 between 10 and 15%, GLUT1 intensity 2; high grade — Ki-67 >15%, GLUT1 intensity 3. The data obtained were correlated to tumor grade, while mucocytes demonstrated the lowest activity. GLUT1 and Ki-67 help effectively distinguish low-grade tumors (G1) from intermediate-grade (G2) and high-grade (G3) ones, and the plateau effect is observed between grades 2 and 3. Among four grading systems assessed, AFIP has shown the strongest correlation with these biomarkers, which suggests that it agrees with the MEC biological behavior. The modified Healy system has also shown good results, it is suitable for medium-grade tumors, while the Brandwein system is better suited for dealing with highly aggressive poorly differentiated tumors; the MSKCC seems to be more conservative. These findings highlight potential value of integrating IHC markers, such as GLUT1 and Ki-67, into MEC grading protocols in order to improve accuracy of the diagnosis and prognostic evaluation. However, mismatch between grading systems emphasizes the need for standardized approaches. Further large-scale studies are necessary to confirm these results and assess the effectiveness of additional markers for improvement of the MEC diagnosis, grading, and treatment planning.

References

1. Peraza A, Gómez R, Beltran J, Amarista FJ. Mucoepidermoid carcinoma. An update and review of the literature. J Stomatol Oral Maxillofac Surg. 2020; 121: 713–20.
2. Ullah A, Khan J, Waheed A, et al. Mucoepidermoid Carcinoma of the Salivary Gland: Demographics and Comparative Analysis in U.S. Children and Adults with Future Perspective of Management. Cancers (Basel). 2022; 15 (1): 250. Published 2022. DOI: 10.3390/cancers15010250.
3. Robinson L, van Heerden MB, Ker-Fox JG, Hunter KD, van Heerden WFP. Expression of Mucins in Salivary Gland Mucoepidermoid Carcinoma. Head Neck Pathol. 2021; 15 (2): 491–502. DOI: 10.1007/s12105-020-01226-z.
4. El-Naggar AK, Chan JKC, Rubin-Grandis J, Takata T, Slootweg PJ, International Agency for Research on Cancer. World Health Organization classification of tumours. 4th ed. Lyon: International Agency for Research on Cancer, 2017.
5. Donempudi P, Bhayya H, Venkateswarlu M, Avinash Tejasvi M L, Paramkusam G. Mucoepidermoid carcinoma of the minor salivary gland: Presenting as ranula. J Can Res Ther. 2018; 14: 1418–21.
6. Fehr A, Werenicz S, Trocchi P et al. Mucoepidermoid carcinoma of the salivary glands revisited with special reference to histologic grading and CRTC1/3-MAML2 genotyping. Virchows Arch (2021). Available from: https://doi.org/10.1007/s00428-021-03146-x.
7. Lin HH, Limesand KH, Ann DK. Current State of Knowledge on Salivary Gland Cancers. Crit Rev Oncog. 2018; 23 (3–4): 139–51. DOI: 10.1615/CritRevOncog.2018027598.
8. Gotoh S, Nakasone T, Matayoshi A, et al. Mucoepidermoid carcinoma of the anterior lingual salivary gland: A rare case report. Mol Clin Oncol. 2022; 16 (1): 7. DOI: 10.3892/mco.2021.2444.
9. Cipriani NA, Lusardi JJ, McElherne J, Pearson AT, Olivas AD, Fitzpatrick C, et al. Mucoepidermoid carcinoma: A comparison of histologic grading systems and relationship to MAML2 rearrangement and prognosis. Am J Surg Pathol. 2019; 43: 885–97.
10. Qannam A, Bello IO. Comparison of histological grading methods in mucoepidermoid carcinoma of minor salivary glands. Indian J Pathol Microbiol. 2016; 59: 457–62. DOI: 10.4103/0377-4929.191765.
11. Sampedro-Núñez M, Bouthelier A, Serrano-Somavilla A, et al. LAT-1 and GLUT1 Carrier Expression and Its Prognostic Value in Gastroenteropancreatic Neuroendocrine Tumors. Cancers (Basel). 2020; 12 (10): 2968. Available from: https://doi.10.3390/cancers12102968.
12. Yang H, Zhong JT, Zhou SH, Han HM. Roles of GLUT1 and HK-II expression in the biological behavior of head and neck cancer. Oncotarget. 2019; 10 (32): 3066–83. DOI: 10.18632/oncotarget.24684.
13. Kang F, Ma W, Ma X, et al. Propranolol inhibits glucose metabolism and 18F-FDG uptake of breast cancer through posttranscriptional downregulation of hexokinase-2. J Nucl Med. 2014; 55 (3): 439–45. DOI: 10.2967/jnumed.113.121327.
14. Kaza S, Rao TJM, Mikkilineni A, Ratnam GV, Rao DR. Ki-67 Index in Salivary Gland Neoplasms. Int J Phonosurg Laryngol. 2016; 6 (1): 1–7.
15. de Souza LB, de Oliveira LC, Nonaka CFW, et al. Immunoexpression of GLUT1 and angiogenic index in pleomorphic adenomas, adenoid cystic carcinomas, and mucoepidermoid carcinomas of the salivary glands. Eur Arch Otorhinolaryngol. 2017; 274: 2549–56. Available from: https://doi.org/10.1007/s00405-017-4530-y.
16. Demasi APD, Costa AF, Altemani A, Furuse C, Araújo NS and Araújo VC. Glucose transporter protein 1 expression in mucoepidermoid carcinoma of salivary gland: correlation with grade of malignancy. International Journal of Experimental Pathology. 2010; 91: 107–13. Available from: https://doi.org/10.1111/j.1365-2613.2009.00702.x.
17. Skalova A, Lehtonen H, von Boguslawsky K, Leivo I. Prognostic significance of cell proliferation in mucoepidermoid carcinomas of the salivary gland: clinicopathological study using MIB 1 antibody in paraffin sections. Hum Pathol. 1994; 25 (9): 929–35. DOI: 10.1016/0046-8177(94)90014-0.

Литература

1. Peraza A, Gómez R, Beltran J, Amarista FJ. Mucoepidermoid carcinoma. An update and review of the literature. J Stomatol Oral Maxillofac Surg. 2020; 121: 713–20.
2. Ullah A, Khan J, Waheed A, et al. Mucoepidermoid Carcinoma of the Salivary Gland: Demographics and Comparative Analysis in U.S. Children and Adults with Future Perspective of Management. Cancers (Basel). 2022; 15 (1): 250. Published 2022. DOI: 10.3390/cancers15010250.
3. Robinson L, van Heerden MB, Ker-Fox JG, Hunter KD, van Heerden WFP. Expression of Mucins in Salivary Gland Mucoepidermoid Carcinoma. Head Neck Pathol. 2021; 15 (2): 491–502. DOI: 10.1007/s12105-020-01226-z.
4. El-Naggar AK, Chan JKC, Rubin-Grandis J, Takata T, Slootweg PJ, International Agency for Research on Cancer. World Health Organization classification of tumours. 4th ed. Lyon: International Agency for Research on Cancer, 2017.
5. Donempudi P, Bhayya H, Venkateswarlu M, Avinash Tejasvi M L, Paramkusam G. Mucoepidermoid carcinoma of the minor salivary gland: Presenting as ranula. J Can Res Ther. 2018; 14: 1418–21.
6. Fehr A, Werenicz S, Trocchi P et al. Mucoepidermoid carcinoma of the salivary glands revisited with special reference to histologic grading and CRTC1/3-MAML2 genotyping. Virchows Arch (2021). Available from: https://doi.org/10.1007/s00428-021-03146-x.
7. Lin HH, Limesand KH, Ann DK. Current State of Knowledge on Salivary Gland Cancers. Crit Rev Oncog. 2018; 23 (3–4): 139–51. DOI: 10.1615/CritRevOncog.2018027598.
8. Gotoh S, Nakasone T, Matayoshi A, et al. Mucoepidermoid carcinoma of the anterior lingual salivary gland: A rare case report.

Mol Clin Oncol. 2022; 16 (1): 7. DOI: 10.3892/mco.2021.2444.
9. Cipriani NA, Lusardi JJ, McElherne J, Pearson AT, Olivas AD, Fitzpatrick C, et al. Mucoepidermoid carcinoma: A comparison of histologic grading systems and relationship to MAML2 rearrangement and prognosis. Am J Surg Pathol. 2019; 43: 885–97.
10. Qannam A, Bello IO. Comparison of histological grading methods in mucoepidermoid carcinoma of minor salivary glands. Indian J Pathol Microbiol. 2016; 59: 457–62. DOI: 10.4103/0377-4929.191765.
11. Sampedro-Núñez M, Bouthelier A, Serrano-Somavilla A, et al. LAT-1 and GLUT1 Carrier Expression and Its Prognostic Value in Gastroenteropancreatic Neuroendocrine Tumors. Cancers (Basel). 2020; 12 (10): 2968. Available from: https://doi.10.3390/cancers12102968.
12. Yang H, Zhong JT, Zhou SH, Han HM. Roles of GLUT1 and HK-II expression in the biological behavior of head and neck cancer. Oncotarget. 2019; 10 (32): 3066–83. DOI: 10.18632/oncotarget.24684.
13. Kang F, Ma W, Ma X, et al. Propranolol inhibits glucose metabolism and 18F-FDG uptake of breast cancer through posttranscriptional downregulation of hexokinase-2. J Nucl Med. 2014; 55 (3): 439–45. DOI: 10.2967/jnumed.113.121327.
14. Kaza S, Rao TJM, Mikkilineni A, Ratnam GV, Rao DR. Ki-67 Index in Salivary Gland Neoplasms. Int J Phonosurg Laryngol. 2016; 6 (1): 1–7.
15. de Souza LB, de Oliveira LC, Nonaka CFW, et al. Immunoexpression of GLUT1 and angiogenic index in pleomorphic adenomas, adenoid cystic carcinomas, and mucoepidermoid carcinomas of the salivary glands. Eur Arch Otorhinolaryngol. 2017; 274: 2549–56. Available from: https://doi.org/10.1007/s00405-017-4530-y.
16. Demasi APD, Costa AF, Altemani A, Furuse C, Araújo NS and Araújo VC. Glucose transporter protein 1 expression in mucoepidermoid carcinoma of salivary gland: correlation with grade of malignancy. International Journal of Experimental Pathology. 2010; 91: 107–13. Available from: https://doi.org/10.1111/j.1365-2613.2009.00702.x.
17. Skalova A, Lehtonen H, von Boguslawsky K, Leivo I. Prognostic significance of cell proliferation in mucoepidermoid carcinomas of the salivary gland: clinicopathological study using MIB 1 antibody in paraffin sections. Hum Pathol. 1994; 25 (9): 929–35. DOI: 10.1016/0046-8177(94)90014-0.

PD1 EXPRESSION IN IMMUNE CELLS WITHIN THE TUMOR MICROENVIRONMENT OF PATIENTS WITH NON-SMALL CELL AND SMALL CELL LUNG CANCER

Kalinchuk AYu, Tsarenkova EA, Loos DM, Mokh AA, Rodionov EO, Miller SV, Grigoryeva ES ✉, Tashireva LA

The Laboratory of Molecular Therapy of Cancer, Cancer Research Institute, Tomsk National Research Medical Center, Russian Academy of Sciences, Tomsk, Russia

The clinical significance of programmed cell death protein 1 (PD-1) expression in the tumor microenvironment (TME) of lung cancer, particularly in the context of immunotherapy, remains poorly understood. This study aimed to evaluate PD-1 expression in tumor-infiltrating immune cells and its association with clinical outcomes in lung cancer patients. In a study of 20 patients (17 men and three women, average age 56 ± 6.9 years) with lung cancer, four key immune cell populations involved in the immunotherapy response were analyzed using multiplexed *in situ* immunofluorescence. The focus was on PD-1 expression patterns and their correlation with progression-free survival (PFS). Our findings revealed that PD-1 expression was predominantly observed on $CD8^+$ lymphocytes, albeit at low levels (~5%), suggesting a state of T-cell exhaustion. Notably, PD-1-expressing immune cells were rare in both non-small-cell and small-cell lung cancer microenvironments, indicating that most immune cells remain functionally active. This deficit of $PD\text{-}1^+$ cells may explain the limited therapeutic efficacy of anti-PD-1 antibodies. Furthermore, we identified $CD20^+$ B-cell infiltration as an independent predictor of poorer PFS (HR = 0.17, 95% CI: 0.02–0.65, p = 0.0454), highlighting a previously underappreciated role of B cells in lung cancer progression. Additionally, the presence of distant metastases (stage M1), a high proportion of $PD\text{-}1^+CD163^+$ macrophages, and a low proportion of $PD\text{-}1^+FoxP3^+$ lymphocytes were associated with shorter PFS, underscoring the complex interplay between immunosuppressive and immunostimulatory cell populations in the TME. These findings suggest that PD-1-expressing immune subsets, particularly cytotoxic lymphocytes and regulatory T cells, may serve as prognostic markers and potential therapeutic targets.

Keywords: PD1 expression, tumor microenvironment, immune checkpoint, lung cancer

Funding: the study was supported by the Russian Science Foundation (grant № 20-75-10033-П).

Author contribution: Kalinchuk AYu — literature search, obtaining and statistically processing the results, writing the article; Tsarenkova EA — obtaining and analyzing data; Loos DM — obtaining and analyzing data; Mokh AA — patients' curation; Rodionov EO — patients' curation; Miller SV — data collection; ES Grigoryeva — editing the article; Tashireva LA — study planning and supervision, analysis, and interpretation of results, writing the article.

Compliance with ethical standards: The study was approved by the Ethics Committee of the Tomsk National Research Medical Center Oncology Research Institute (protocol № 7, 25 August 2020; protocol № 18, 25 August 2023), conducted in accordance with federal laws of the Russian Federation and the 1964 Helsinki Declaration with all subsequent additions and amendments regulating scientific research on biomaterial obtained from humans. All participants signed informed voluntary consent to participate in the study.

✉ **Correspondence should be addressed:** Evgenia S. Grigoryeva
pereulok Kooperativny, 5, Tomsk, Russia; 634009; grigoryeva.es@gmail.com

Received: 04.03.2025 **Accepted:** 17.03.2025 **Published online:** 24.03.2025

DOI: 10.24075/brsmu.2025.014

ЭКСПРЕССИЯ PD-1 В ИММУННЫХ КЛЕТКАХ МИКРООКРУЖЕНИЯ ОПУХОЛИ У ПАЦИЕНТОВ С НЕМЕЛКОКЛЕТОЧНЫМ И МЕЛКОКЛЕТОЧНЫМ РАКОМ ЛЕГКОГО

А. Ю. Калинчук, Е. А. Царенкова, Д. М. Лоос, А. А. Мох, Е. О. Родионов, С. В. Миллер, Е. С. Григорьева ✉, Л. А.Таширева

Научно-исследовательский институт онкологии, Томский национальный исследовательский медицинский центр Российской академии наук, Томск, Россия

Клиническое значение экспрессии белка PD-1 в микроокружении опухоли рака легких, особенно в контексте иммунотерапии, остается плохо изученным. Целью исследования было оценить экспрессию PD-1 в инфильтрирующих опухоль иммунных клетках и ее связь с клиническими исходами у пациентов с раком легких. У 20 пациентов (17 мужчин и три женщины, средний возраст составил 56 ± 6,9 лет) с раком легкого с помощью мультиплексной иммунофлуоресценции *in situ* был проведен анализ четырех ключевых популяций иммунных клеток, вовлеченных в ответ на иммунотерапию, с фокусом внимания на паттернах экспрессии PD-1 и их корреляции с выживаемостью без прогрессирования (progression-free survival, PFS). Экспрессию PD-1 преимущественно наблюдали на $CD8^+$-лимфоцитах, хотя и на низком уровне (~5%), что предполагает состояние истощения Т-клеток. Иммунные клетки, экспрессирующие PD-1, встречались редко в микроокружении как немелкоклеточного, так и мелкоклеточного рака легких, возможно в связи с тем, что большинство иммунных клеток остаются функционально активными. Дефицитом клеток $PD\text{-}1^+$ можно объяснить ограниченную терапевтическую эффективность антител против PD-1. Выявлено, что инфильтрация $CD20^+$ В-клетками является независимым предиктором низкой PFS (HR = 0,17; 95% CI: 0,02–0,65; p = 0,0454), и это подчеркивает ранее недооцененную роль В-клеток в прогрессировании рака легких. Показано также, что наличие отдаленных метастазов (стадия М1), высокая доля макрофагов $PD\text{-}1^+CD163^+$ и низкая доля лимфоцитов $PD\text{-}1^+FoxP3^+$ связаны с более короткой PFS, что подчеркивает сложное взаимодействие между популяциями клеток в опухолевом микроокружении. Эти результаты свидетельствуют о том, что иммунные субпопуляции, экспрессирующие PD-1, в частности цитотоксические лимфоциты и регуляторные Т-клетки, могут служить прогностическими маркерами и потенциальными терапевтическими мишенями.

Ключевые слова: экспрессия PD-1, микроокружение опухоли, иммунные контрольные точки, рак легкого

Финансирование: исследование поддержано Российским научным фондом (грант № 20-75-10033-П).

Вклад авторов: А. Ю. Калинчук — поиск литературы, получение и статистическая обработка результатов, написание статьи; Е. А. Царенкова, Д. М. Лоос — получение и анализ данных; А. А. Мох, Е. О. Родионов — курация пациентов; С. В. Миллер — сбор данных; Е. С. Григорьева — редактирование статьи; Л. А. Таширева — планирование и руководство исследованием, анализ и интерпретация результатов, написание статьи.

Соблюдение этических стандартов: исследование одобрено этическим комитетом Томского национального исследовательского медицинского центра НИИ онкологии (протокол № 7 от 25 августа 2020 г. и протокол № 18 от 25 августа 2023 г.), проведено в соответствии с федеральными законами Российской Федерации и Хельсинкской декларацией 1964 г. со всеми последующими дополнениями и изменениями, регламентирующими проведение научных исследований биоматериала, полученного от человека. Все участники подписали добровольное информированное согласие на участие в исследовании.

✉ **Для корреспонденции:** Евгения Сергеевна Григорьева,
пер. Кооперативный, д. 5, г. Томск, 634009, Россия; grigoryeva.es@gmail.com

Статья получена: 04.03.2025 **Статья принята к печати:** 17.03.2025 **Опубликована онлайн:** 24.03.2025

DOI: 10.24075/vrgmu.2025.014

The immune microenvironment within tumors actively participates in the processes of cancer development and progression. This role is underscored by the rapid expansion of therapeutic approaches that aim to modulate the immune microenvironment, including those for lung cancer. A series of fundamental studies in model systems have revealed pathogenetic mechanisms of progression and microenvironment factors associated with resistance to immunotherapy in lung cancer [1]. For example, a high percentage of PD-1-expressing cells among $CD8^+$ lymphocytes have been correlated with a limited response to PD-1 blockade during polyclonal T-cell stimulation [2]. During the study of the relationship between immunological parameters and the clinical course of the disease in patients, patterns were identified that indicate the significance of the immune microenvironment [3]. Thus, the classification of the tumor immune microenvironment (TIMT) based on PD-1/PD-L1 and $CD8^+$ tumor-infiltrating lymphocytes (TIL) effectively stratifies lung adenocarcinoma patients into groups with varying survival rates. Notably, the group with low $CD8^+$ lymphocyte counts and high PD-1/PD-L1 expression demonstrates the poorest outcomes [4]. The microenvironment demonstrates equally importance in studies examining its association with responses to immunotherapy. For instance, the IKCscore (Immune-Keratin-Immune Checkpoint score), which is derived from the expression ratios of various genes encoding immune markers and cytokeratins, is a promising indicator for predicting the efficacy of immunotherapy and immunotherapy-based combination therapies in non-small cell lung cancer (NSCLC). Furthermore, the infiltration levels of $CD8^+$ lymphocytes, resting memory $CD4^+$ T cells, and resting dendritic cells are significantly higher in the high IKCscore group than in the low IKCscore group [5]. Expression of programmed death ligand 1 (PD-L1) on tumor cells and tumor mutational burden (TMB) have been identified as predictors of response to immunotherapy. However, the actual clinical scenario shows that these biomarkers alone are insufficient for effectively selecting patients for such type of therapy. Interestingly, despite extensive research into the characteristics of the tumor microenvironment in lung cancer, certain aspects relevant to immunotherapy remain unexplored.

One class of immunotherapeutic agents includes anti-PD1 antibodies, which target the receptor rather than the ligand. Nonetheless, the expression of PD1 within the lung cancer microenvironment is poorly understood. Given the wide availability of therapeutic options that incorporate immune checkpoint inhibitors, understanding the specificities of the tumor microenvironment becomes crucial. This could enhance the identification of associations with the efficacy of immunotherapy. The aim of this study was to evaluate PD-1 expression in tumor-infiltrating immune cells and its association with clinical outcomes in patients with lung cancer.

METHODS

Patients

The study involved 20 patients (3 women and 17 men) with a morphologically verified diagnosis of lung cancer. Among them, 12 patients had non-small cell lung cancer and 8 had small cell lung cancer. All patients were at disease stage III–IV (10 patients were stage III, 10 — stage IV), with a mean age of 56 ± 6.9 years. Exclusion criteria were stage I–II lung cancer, concomitant autoimmune and inflammatory diseases. The patients completed the full course of treatment in accordance with clinical guidelines recommendations (combination therapy, including first-line and subsequent-line chemotherapy according to the following regimens: Carboplatin/Paclitaxel, Pemetrexed/Carboplatin, Carboplatin/Etoposide, monochemotherapy with taxanes, Denosumab, chemoimmunotherapy; if indicated, patients underwent external beam radiation therapy). The median follow-up period was 12 months.

Tumor microenvironment immunophenotyping

Tumor tissue samples were collected from all patients prior to any treatment, fixed in formalin, and embedded in paraffin using standard techniques. Subsequently, multicolor staining of the lung cancer tissue was carried out employing TSA (tyramide signal amplification) modification in immunohistochemical analysis. The following primary antibodies were used: human anti-CD8 (Ventana, Switzerland, clone SP57, dilution 1 : 10), anti-PD-1 (ABclonal, China, clone AMC0439, dilution 1:500), anti-CD20 (Leica Biosystems, Germany, clone L26, dilution 1 : 600), anti-CD163 (Diagnostic Biosystems, USA, clone 10D6, dilution 1 : 150) and anti-FoxP3 monoclonal antibody (Invitrogen, USA, clone 236A/E7, dilution 1 : 800). The EnVision FLEX/HRP system (Dako, Denmark) and Opal 7-color Fluorophore Kit (Akoya Biosciences, USA), which includes tyramide conjugated with fluorophores, were utilized for detection. The staining procedure was executed on a BOND RXm automated immunohistostainer (Leica, Germany). The protocol included antigen retrieval using Epitope Retrieval Solution 2 buffer (Leica Biosystems, Germany) at 98.5 °C for 20 minutes, followed by five sequential staining cycles. Each cycle consisted of the following steps: a 10-minute incubation of EnVision FLEX Peroxidase-blocking reagent (Dako, Denmark), a 10-minute incubation with Novocastra Protein Block (Leica Biosystems, Germany), a 30-minute incubation with the primary antibody, a 30-minute incubation with EnVision FLEX/HRP, and a 20-minute incubation with Opal dye. After each cycle, depletion complex of primary and secondary antibodies was performed using Epitope Retrieval Solution 2 buffer. Cell nuclei were counterstained manually using Fluoroshield™ with DAPI (Sigma-Aldrich, USA). Visualization and image acquisition (Fig. 1) were carried out using the Vectra® 3.0 system (Akoya Biosciences, USA), and quantitative cell analysis was performed using inForm® software (Akoya Biosciences, USA) based on data collected from seven representative tissue regions.

The densities of $CD8^+$ cytotoxic lymphocytes, $CD20^+$ B-lymphocytes, $CD163^+$ tumor-associated macrophages, and $FoxP3^+$ regulatory T lymphocytes were quantified in tumor tissues obtained from patients with lung cancer (Fig. 1). The results were represented as the percentage of each cell type relative to the total cell count in the tumor stroma. Statistical analyses of the results were performed using Prism 10 software (GraphPad, USA). The Friedman test was used to detect differences in the number of immune cells within the tumor microenvironment, while the nonparametric Mann–Whitney test was employed for comparing independent groups. Both univariate and multivariate Cox regression analyses were conducted to determine the associations between key clinical and pathological parameters, as well as tumor microenvironment parameters, with progression-free survival. All criteria were two-sided, and differences were deemed significant at $p < 0.05$.

RESULTS

In the tumor microenvironment of NSCLC, the median proportion of PD-1-positive cells was 1.04 (0.17–1.70)%, in small cell lung cancer (SCLC) — 0.27 (0.03–2.93)%. The frequency of PD-1-positive $CD8^+$ cytotoxic lymphocytes was 83.3%

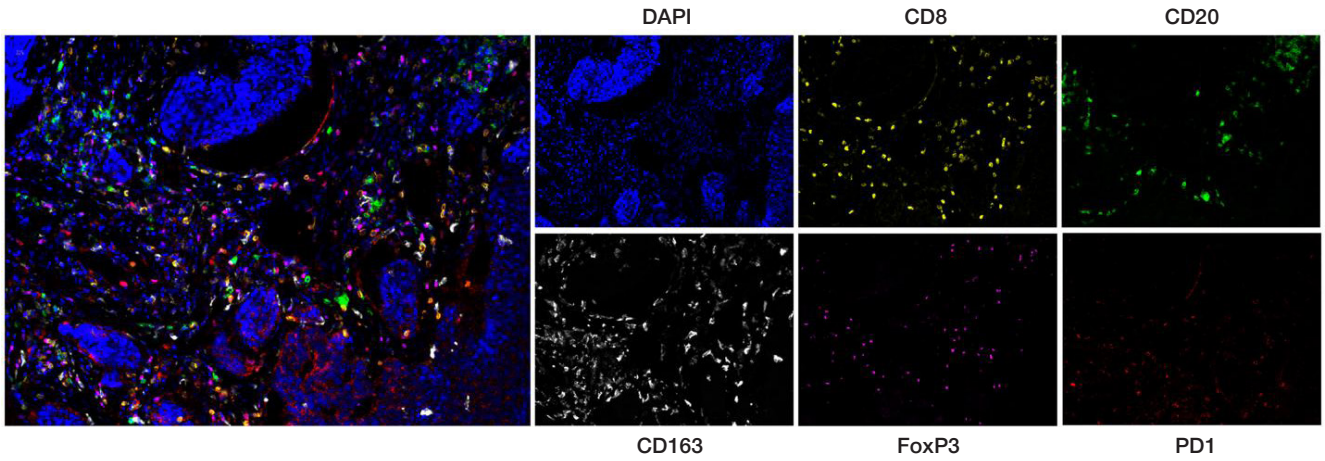

Fig. 1. Tumor microenvironment of lung cancer. Multiplex image, 400x magnification

(10/12) in patients with NSCLC and 37.5% (3/8) in patients with SCLC. While the frequency of PD-1-positive CD20⁺ B-lymphocytes were 8.3% (1/12) and 12.5% (1/8), PD-1-positive FoxP3⁺ T-regulatory lymphocytes were 25% (3/12) and 12.5% (1/8), and PD-1-positive CD163⁺ macrophages were 25% (3/12) and 20% (2/8), respectively. We studied the proportion of PD-1-positive CD8⁺ cytotoxic lymphocytes, CD20⁺ B-lymphocytes, FoxP3⁺ T-regulatory lymphocytes and CD163⁺ macrophages, as well as the proportion of other PD-1-positive cells (without immunophenotype determination) in the tumor microenvironment of patients with non-small-cell and small-cell lung cancer (Fig. 2).

When assessing the cell fraction among all cells in the immune infiltrate of NSCLC, PD-1-positive CD8⁺ cytotoxic lymphocytes and other PD-1-positive immune cells were predominant among lymphocytes, accounting for 0.24% (range: 0.08–0.46%) and 0.39% (range: 0.00–1.05%), respectively. No significant differences in the quantity of PD-1-expressing immune cells were observed in the SCLC microenvironment. The proportions of PD-1-expressing cells among all studied immunophenotypes were also determined for both NSCLC and SCLC (Table 1).

When comparing the proportions of PD-1-expressing cells between patients with NSCLC and SCLC, no significant differences were observed (Fig. 3).

The analysis of immune microenvironment parameters in conjunction with clinical and pathological factors in lung cancer patients revealed no significant correlations between the studied cell populations and patient age, smoking status, or the presence of distant metastases (stage M1). However, a statistically significant association was observed between disease stage and the proportion of CD8⁺ lymphocytes in patients with SCLC. Specifically, patients with stage III–IV disease demonstrated a significantly lower proportion of CD8⁺ lymphocytes in the tumor microenvironment compared to those with stage II (3.49% [range: 3.07–1.19%] vs. 4.82% [range: 3.76–9.88%], $p = 0.0286$). Furthermore, the relationship between tumor microenvironment characteristics and long-term treatment outcomes was evaluated using Cox regression analysis (Table 2).

An increased proportion of CD20⁺ lymphocytes in the tumor microenvironment has been identified as a significant independent factor associated with poor progression-free survival in lung cancer patients (HR = 0.17 [0.02–0.65], $p = 0.0454$), compared to factors such as stage, histological type, smoking status, presence of regional lymph node metastases, and distant metastases (stage M1). Furthermore, an analysis of the prognostic value of PD-1-expressing immune cell populations in relation to clinicopathological parameters revealed that independent predictors of shorter progression-free survival in lung cancer include the presence of distant metastases (stage M1), a high proportion of PD-1-expressing CD163⁺ macrophages, and a low proportion of PD-1-expressing FoxP3⁺ lymphocytes (Table 3).

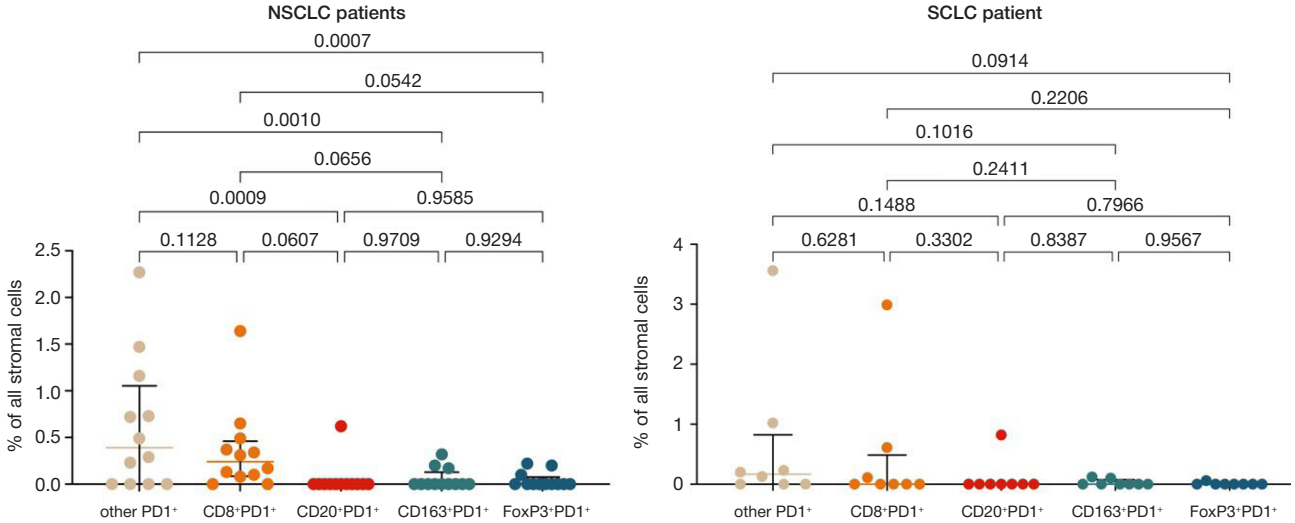

Fig. 2. The proportion of PD-1-positive CD8⁺ cytotoxic lymphocytes, CD20⁺ B-lymphocytes, FoxP3⁺ T-regulatory lymphocytes and CD163⁺ macrophages, and other PD-1-positive cells (without immunophenotype determination) in the tumor microenvironment of NSCLC and SCLC patients

Table 1. Proportion of PD-1-Expressing Cells Among All Cells of the Studied Immunophenotype in Patients with Lung Cancer, Median (Q_1–Q_3)

Parameter	NSCLC		SCLC	
1. CD8⁺PD1⁺	5.20 (1.15-35.33)	p_{1-2} = 0.0005 p_{1-3} = 0.0006 p_{1-4} = 0.0010	0.00 (0.00–12.02)	p_{1-2} = 0.0527 p_{1-3} = 0.0547 p_{1-4} = 0.0381
2. CD20⁺PD1⁺	0.00 (0.00-0.00)	p_{2-3} = 0.9465 p_{2-4} = 0.8265	0.00 (0.00–0.00)	p_{2-3} = 0.9864 p_{2-4} = 0.8784
3. CD163⁺PD1⁺	0.00 (0.00-1.05)	p_{3-4} = 0.8791	0.00 (0.00–0.87)	p_{3-4} = 0.8650
4. FoxP3⁺PD1⁺	0.00 (0.00-1.07)		0.00 (0.00–0.00)	

DISCUSSION

The clinical significance of PD-1 expression, particularly in the context of immunotherapy, remains poorly understood. Limited and controversial data on the prognostic value of determining PD-1 expression are available in the literature. The study by Dan A. et al. demonstrated that patients with early-stage non-small cell lung cancer (NSCLC) who exhibited PD-1 expression of ≥10% on tumor-infiltrating lymphocytes experienced unfavorable 10-year overall survival rates. [6]. Conversely, the study by Sun C. et al. revealed that positive PD-1 expression, coupled with high lymphocyte counts (CD3, CD4, CD8, and FOXP3), was associated with significantly improved survival rates compared to negative PD-1 expression in conjunction with lower lymphocyte counts. [7]. In our study, for the first time, we assessed PD-1 expression while considering the immunophenotype of cells. We focused on the four most relevant populations for which there is evidence suggesting an association with a response to immunotherapy, since the patients included in our study are potential candidates for anti-PD-1 antibody therapy in future treatment lines.

When discussing the prognostic significance of PD-1 expression in the context of immunotherapy, it is important to mention the findings of the study by Mazzaschi G. et al., which demonstrated that, a low incidence of PD-1 expression among CD8⁺ lymphocytes was a distinguishing feature of patients treated with nivolumab, and this was also associated with clinical benefits and extended PFS (HR = 4,51; 95% CI, 1,45–13,94) [8]. In our study, PD-1 expression was found predominantly on CD8⁺ lymphocytes, although the proportion of PD-1⁺ cells in the CD8⁺ lymphocyte population was about 5% and was not associated with PFS. It is known that effector functions are gradually lost during the progressive depletion of T cells; in a recent study, an inverse correlation between T cell function and the level of PD-1 expression was noted [9]. Thus, PD-1 expression on cytotoxic lymphocytes indicates a state of depletion. It is important to note that our study reveals that PD-1-expressing immune cells are extremely sparse within both the non-small-cell and small-cell lung cancer microenvironments. This indicates that the majority of immune cells in the lung cancer environment are predominantly in an active functional state. Our findings suggest that the cells targeted by therapeutic anti-PD-1 antibodies are few within the lung cancer microenvironment, and mainly consist of PD-1-expressing cytotoxic lymphocytes. Blocking the checkpoint in these few cells could potentially restore their depleted function. At the same time, the low number of these cells may explain the limited therapeutic effects observed with the use of anti-PD-1 antibodies.

Currently, we are unable to evaluate the correlation between specific characteristics of the tumor microenvironment's cellular composition and treatment outcomes in these patients, as their therapy is still ongoing. Nevertheless, this study enabled us to assess the relationship between various tumor microenvironment parameters and PFS. Our results underscore the crucial importance of immune cell composition within the tumor microenvironment in determining PFS in lung cancer patients. Notably, an increased presence of CD20⁺ lymphocytes has been identified as a significant independent predictor of poorer PFS, exhibiting a hazard ratio (HR) of 0.17 (95% CI: 0.02-0.65, p = 0.0454). This association appears more substantial than conventional prognostic factors, including tumor stage, histological subtype, smoking status, and the presence of regional or distant metastases (stage M1). The results suggest that B-cell infiltration may play a previously underestimated role in lung cancer progression, possibly due to its implications in immune suppression or modulation within the TME. Further studies are required to explore the functional impact of CD20⁺ lymphocytes in lung cancer, aiming to elucidate their role in tumor biology and resistance to treatment effectively.

Moreover, our analysis concerning PD-1-expressing immune cell populations has unveiled new insights about the

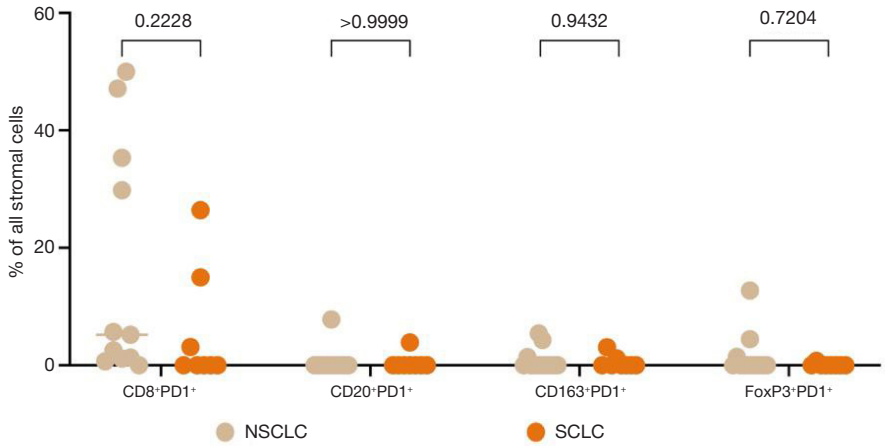

Fig. 3. Comparison of the proportion of PD-1-expressing cells between NSCLC and SCLC patients

Table 2. Univariate and multivariate regression analysis of the significance of clinicopathological parameters and immune cell populations in the duration of progression-free survival in patients with lung cancer

Parameter	Single-factor analysis			Multifactor analysis		
	HR	95% CI	*P* value	HR	95% CI	*P* value
Smoking status	1.23	0.37–4.75	0.7366	0.4716	0.07–3.12	0.4167
Histological type	0.83	0.24–2.93	0.7659	1.236	0.15–9.33	0.8365
Stage	1.4	0.69–3.16	0.367	0.6977	0.11–4.17	0.6798
Lymph node metastasis	1.29	0.71–2.44	0.4074	1.54	0.69–4.14	0.3158
Distant metastasis (stage M1)	0.79	0.23–3.11	0.7177	0.07	0.001–1.13	0.1158
CD8	1.01	0.86–1.17	0.8213	1.58	0.91–4.00	0.237
CD20	0.42	0.09–0.88	0.1532	0.17	0.02–0.65	0.0454
CD163	1	0.84–1.16	0.9954	1	0.78–1.29	0.9392
FoxP3	0.89	0.69–1.11	0.3567	0.6	0.20–1.25	0.2925

Table 3. Univariate and multivariate regression analysis of the Influence of Clinicopathological Parameters and PD1-Expressing Immune Cell Populations on the Duration of Progression-Free Survival in Patients with Lung Cancer

Parameter	Single-factor analysis			Multifactor analysis		
	HR	95% CI	*P* value	HR	95% CI	*P* value
Smoking status	1.23	0.37–4.75	0.7366	3.85	0.33–125.70	0.3402
Histological type	0.83	0.24–2.93	0.7659	4	0.06–186.10	0.481
Stage	1.4	0.69–3.16	0.367	2.32	0.30–71.80	0.549
Lymph node metastasis	1.29	0.71–2.44	0.4074	0.8	0.17–2.81	0.7545
Distant metastasis (stage M1)	0.79	0.23–3.11	0.7177	0.004	0.0003–0.26	0.0349
%$CD8^+PD1^+$	1.011	0.97–1.04	0.5361	1.019	0.93–1.11	0.6532
%$CD20^+PD1^+$	0.001	–	>0.9999	0.001	–	>0.9999
%$CD163^+PD1^+$	1.39	0.95–1.97	0.0619	4.78	1.35–33.64	0.041
%$FoxP3^+PD1^+$	1.06	0.85–1.22	0.4517	0.44	0.16–0.89	0.0484

links between immune checkpoint expression and clinical outcomes. The presence of distant metastases (stage M1), a high proportion of PD-1-positive $CD163^+$ macrophages, and a low proportion of PD-1-positive $FoxP3^+$ lymphocytes have been identified as predictors of shorter PFS. These observations underscore the complexity of immune regulation within the TME, where a delicate balance between immunosuppressive and immunostimulatory cell populations critically influences disease progression. The association of $PD\text{-}1^+CD163^+$ macrophages with poor outcomes has predominantly been observed in animal models [10]. Conversely, the anti-tumor effect observed in $PD\text{-}1^+FoxP3^+$ lymphocytes suggest a potential regulatory function, although Tregs are generally associated with poor outcomes in the existing literature [11].

These findings carry substantial implications for the development of predictive biomarkers and the formulation of immunotherapeutic strategies in lung cancer. The identification of PD-1-expressing immune subsets as prognostic markers underlines the necessity for an enhanced understanding of the TME. Targeting these populations, either through direct modulation or in combination with existing immune checkpoint inhibitors, could pave the way for improved therapeutic outcomes. Nevertheless, the functional heterogeneity within these cell populations calls for more detailed mechanistic studies to clarify their roles in tumor immunity and identify optimal therapeutic targets.

CONCLUSIONS

Our study provides compelling evidence that the immune landscape of the TME, particularly the composition of PD-1-expressing immune cells, is significantly associated with lung cancer outcomes. These findings highlight the critical importance of the immune contexture in determining cancer prognosis and informing therapeutic strategies. Future research should concentrate on validating these findings in larger, independent cohorts and further exploring their predictive potential concerning immunotherapy in lung cancer patients.

References

1. Hynds RE, Frese KK, Pearce DR, Grönroos E, Dive C, Swanton C. Progress towards non-small-cell lung cancer models that represent clinical evolutionary trajectories. Open Biol. 2021; 11 (1): 200247. DOI: 10.1098/rsob.200247.
2. Thommen DS, Schreiner J, Müller P, Herzig P, Roller A, Belousov A, et al. Progression of Lung Cancer Is Associated with Increased Dysfunction of T Cells Defined by Coexpression of Multiple Inhibitory Receptors. Cancer immunology research. 2015; 3: 1344–55. DOI: 10.1158/2326-6066.CIR-15-0097.
3. Enfield KSS, Colliver E, Lee C, Magness A, Moore DA, Sivakumar M, et al. Spatial Architecture of Myeloid and T Cells Orchestrates Immune Evasion and Clinical Outcome in Lung Cancer. Cancer Discov. 2024; 14 (6): 1018–47. DOI: 10.1158/2159-8290.CD-23-1380.
4. Lin Z, Gu J, Cui X, Huang L, Li S, Feng J et al. Deciphering

Microenvironment of NSCLC based on CD8+ TIL Density and PD-1/PD-L1 Expression. J Cancer. 2019; 10 (1): 211–22. DOI:10.7150/jca.26444.
5. Wu J, Wang Y, Huang Z, Wu J, Sun H, Zhou R, et al. Tumor microenvironment assessment-based signatures for predicting response to immunotherapy in non-small cell lung cancer. iScience. 2024; 27 (12): 111340. DOI: 10.1016/j.isci.2024.111340.
6. Dan A, Aricak O, Rounis K, Montero-Fernandez MA, Guijarro R, Ekman S. et al. PD-1 expression in tumor infiltrating lymphocytes as a prognostic marker in early-stage non-small cell lung cancer. Front Oncol. 2024; 14: 1414900. DOI: 10.3389/fonc.2024.1414900.
7. Sun C, Zhang L, Zhang W, Liu Y, Chen B, Zhao S, et al. Expression of PD-1 and PD-L1 on Tumor-Infiltrating Lymphocytes Predicts Prognosis in Patients with Small-Cell Lung Cancer. OncoTargets and Therapy. 2020; 13: 6475–83. Available from: https://doi.org/10.2147/OTT.S252031.
8. Mazzaschi G, Madeddu D, Falco A, Bocchialini G, Goldoni M, Sogni F et al. Low PD-1 Expression in Cytotoxic CD8+ Tumor-Infiltrating Lymphocytes Confers an Immune-Privileged Tissue Microenvironment in NSCLC with a Prognostic and Predictive Value. Clin Cancer Res. 2018; 24 (2): 407–19. DOI: 10.1158/1078-0432.CCR-17-2156.
9. Kansy BA, Concha-Benavente F, Srivastava RM, Jie HB, Shayan G, Lei Y, et al. PD-1 Status in CD8(+) T Cells Associates with Survival and Anti-PD-1 Therapeutic Outcomes in Head and Neck Cancer. Cancer Res. 2017; 77: 6353–64. DOI: 10.1158/0008-5472.CAN-16-3167.
10. Chen L, Cao MF, Xiao JF, Ma QH, Zhang H, Cai RL, et al. Stromal PD-1+ tumor-associated macrophages predict poor prognosis in lung adenocarcinoma. Hum Pathol. 2020; 97: 68–79. DOI: 10.1016/j.humpath.2019.12.007.
11. Tao H, Mimura Y, Aoe K, Kobayashi S, Yamamoto H, Matsuda E, et al. Prognostic potential of FOXP3 expression in non-small cell lung cancer cells combined with tumor-infiltrating regulatory T cells. Lung Cancer. 2012; 75 (1): 95–101. DOI: 10.1016/j.lungcan.2011.06.002.

Литература

1. Hynds RE, Frese KK, Pearce DR, Grönroos E, Dive C, Swanton C. Progress towards non-small-cell lung cancer models that represent clinical evolutionary trajectories. Open Biol. 2021; 11 (1): 200247. DOI: 10.1098/rsob.200247.
2. Thommen DS, Schreiner J, Müller P, Herzig P, Roller A, Belousov A, et al. Progression of Lung Cancer Is Associated with Increased Dysfunction of T Cells Defined by Coexpression of Multiple Inhibitory Receptors. Cancer immunology research. 2015; 3: 1344–55. DOI: 10.1158/2326-6066.CIR-15-0097.
3. Enfield KSS, Colliver E, Lee C, Magness A, Moore DA, Sivakumar M, et al. Spatial Architecture of Myeloid and T Cells Orchestrates Immune Evasion and Clinical Outcome in Lung Cancer. Cancer Discov. 2024; 14 (6): 1018–47. DOI: 10.1158/2159-8290.CD-23-1380.
4. Lin Z, Gu J, Cui X, Huang L, Li S, Feng J et al. Deciphering Microenvironment of NSCLC based on CD8+ TIL Density and PD-1/PD-L1 Expression. J Cancer. 2019; 10 (1): 211–22. DOI:10.7150/jca.26444.
5. Wu J, Wang Y, Huang Z, Wu J, Sun H, Zhou R, et al. Tumor microenvironment assessment-based signatures for predicting response to immunotherapy in non-small cell lung cancer. iScience. 2024; 27 (12): 111340. DOI: 10.1016/j.isci.2024.111340.
6. Dan A, Aricak O, Rounis K, Montero-Fernandez MA, Guijarro R, Ekman S. et al. PD-1 expression in tumor infiltrating lymphocytes as a prognostic marker in early-stage non-small cell lung cancer. Front Oncol. 2024; 14: 1414900. DOI: 10.3389/fonc.2024.1414900.
7. Sun C, Zhang L, Zhang W, Liu Y, Chen B, Zhao S, et al. Expression of PD-1 and PD-L1 on Tumor-Infiltrating Lymphocytes Predicts Prognosis in Patients with Small-Cell Lung Cancer. OncoTargets and Therapy. 2020; 13: 6475–83. Available from: https://doi.org/10.2147/OTT.S252031.
8. Mazzaschi G, Madeddu D, Falco A, Bocchialini G, Goldoni M, Sogni F et al. Low PD-1 Expression in Cytotoxic CD8+ Tumor-Infiltrating Lymphocytes Confers an Immune-Privileged Tissue Microenvironment in NSCLC with a Prognostic and Predictive Value. Clin Cancer Res. 2018; 24 (2): 407–19. DOI: 10.1158/1078-0432.CCR-17-2156.
9. Kansy BA, Concha-Benavente F, Srivastava RM, Jie HB, Shayan G, Lei Y, et al. PD-1 Status in CD8(+) T Cells Associates with Survival and Anti-PD-1 Therapeutic Outcomes in Head and Neck Cancer. Cancer Res. 2017; 77: 6353–64. DOI: 10.1158/0008-5472.CAN-16-3167.
10. Chen L, Cao MF, Xiao JF, Ma QH, Zhang H, Cai RL, et al. Stromal PD-1+ tumor-associated macrophages predict poor prognosis in lung adenocarcinoma. Hum Pathol. 2020; 97: 68–79. DOI: 10.1016/j.humpath.2019.12.007.
11. Tao H, Mimura Y, Aoe K, Kobayashi S, Yamamoto H, Matsuda E, et al. Prognostic potential of FOXP3 expression in non-small cell lung cancer cells combined with tumor-infiltrating regulatory T cells. Lung Cancer. 2012; 75 (1): 95–101. DOI: 10.1016/j.lungcan.2011.06.002.

CHARACTERISTICS OF THE METASTASIS-ASSOCIATED CIRCULATING CELLS: FEATURES OF SIDE SCATTER PARAMETERS

Buzenkova AV[1] ✉, Grigoryeva ES[1], Alifanov VV[1], Tashireva LA[1], Savelieva OE[3], Pudova ES[1], Zavyalova MV[2], Cherdyntseva NV[1], Perelmuter VM[1]

[1] Cancer Research Institute, Tomsk National Research Medical Center of the Russian Academy of Sciences, Tomsk, Russia
[2] Siberian State Medical University, Tomsk, Russia
[3] Saint Petersburg State Pediatric Medical University, Saint Petersburg, Russia

It is difficult to detect the circulating tumor cells (CTCs) being through the epithelial–mesenchymal transition (EMT) terminal phase, since these do not express epithelial markers or show weak expression of those. This hampers assessment of the CTC prognostic potential. It has been shown that the circulating cells (CCs) with the $CD45^{-}EpCAM^{-}CK7/8^{-}CD24^{+}N\text{-}cadherin^{-}$ phenotype are associated with the risk of metastasis in breast cancer (BC). The study aimed to test CCs based on the side scatter parameters considering the expression of epithelial cell markers and CD11b. CC phenotypes were assessed by flow cytometry within the regions with low (SSC^{low}) and high (SSC^{high}) side scatter in 11 donors and 20 female patients with BC. All the $CD45^{-}EpCAM^{-}CK7/8^{-}CD24^{+}N\text{-}cadherin^{-}$ CCs were represented by the $CD11b^{-}$ and $CD11b^{+}$ phenotypes found in both SSC^{low} and SSC^{high} regions. Among eight $CD45^{-}mEpCAM^{-}CK7/8^{-}CD24^{+}N\text{-}cadherin^{-}$ CC phenotypes with different variants of co-expression of epithelial markers (E-cadherin, panCK, and icEpCAM) and CD11b found in patients, six showed signs of epithelial nature based on one of the markers, while another two showed no epithelial traits and predominated over other phenotypes (only these two phenotypes were found in donors). The differences in light scattering parameters of the CCs with the same phenotype is one more characteristic, the prognostic value of which remains to be uncovered. The E-cadherin and panCK expression in the absence of mEpCAM and presence of icEpCAM suggest that some CCs are tumor cells in the state of pronounced EMT. CCs showing co-expression of CD11b and epithelial markers can emerge due to hybridization with myeloid cells.

Keywords: breast cancer, circulating cells, flow cytometry, side scatter

Funding: the study was supported by the RSF grant No. № 23-15-00135.

Author contribution: Buzenkova AV — literature review, data analysis, acquisition and statistical processing of the results, manuscript writing; Grigoryeva ES — flow cytometry, data analysis, interpretation of the results, manuscript writing; Alifanov VV — flow cytometry, manuscript editing; Tashireva LA, Savelieva OE — discussion, manuscript editing; Pudova ES — flow cytometry; Zavyalova MV — manuscript editing; Cherdyntseva NV — study planning and design, discussion; Perelmuter VM — study planning and management, interpretation of the results, manuscript writing.

Compliance with ethical standards: the study was approved by the Ethics Committee of the Cancer Research Institute, Tomsk National Research Medical Center of the Russian Academy of Sciences (protocol No. 8 dated 17 June 2016) and conducted in accordance with Federal Laws of the Russian Federation (No. 152, 323, etc.), the Declaration of Helsinki (1964) and all later amendments and additions that regulate scientific research involving human biomaterial. All subjects submitted the informed consent to participation in the study.

✉ **Correspondence should be addressed:** Angelina V. Buzenkova
Kooperativny per., 5, Tomsk, 634009, Russia; buzenkova_av@mail.ru

Received: 11.03.2025 **Accepted:** 26.03.2025 **Published online:** 18.04.2025

DOI: 10.24075/brsmu.2025.019

ХАРАКТЕРИСТИКА МЕТАСТАЗ-АССОЦИИРОВАННЫХ ЦИРКУЛИРУЮЩИХ КЛЕТОК ПРИ РАКЕ МОЛОЧНОЙ ЖЕЛЕЗЫ: ОСОБЕННОСТИ ПАРАМЕТРОВ БОКОВОГО СВЕТОРАССЕЯНИЯ

А. В. Бузенкова[1] ✉, Е. С. Григорьева[1], В. В. Алифанов[1], Л. А. Таширева[1], О. Е. Савельева[3], Е. С. Пудова[1], М. В. Завьялова[2], Н. В. Чердынцева[1], В. М. Перельмутер[1]

[1] Научно-исследовательский институт онкологии, Томский национальный исследовательский медицинский центр Российской академии наук, Томск, Россия
[2] Сибирский государственный медицинский университет, Томск, Россия
[3] Санкт-Петербургский государственный педиатрический медицинский университет, Санкт-Петербург, Россия

Детекция циркулирующих опухолевых клеток (ЦОК), находящихся в терминальной стадии эпителиально-мезенхимального перехода (ЭМП), затруднена, поскольку они не экспрессируют или имеют слабую экспрессию эпителиальных маркеров. Это осложняет изучение их прогностического потенциала. Показано, что циркулирующие клетки (ЦК) с фенотипом $CD45^{-}EpCAM^{-}CK7/8^{-}CD24^{+}N\text{-}cadherin^{-}$ ассоциированы с риском метастазирования при раке молочной железы (РМЖ). Целью исследования было изучить ЦК в зависимости от параметров бокового светорассеяния, с учетом экспрессии маркеров эпителиальности и CD11b. У 11 доноров и 20 пациенток с РМЖ методом проточной цитометрии проводили оценку фенотипов ЦК в областях с низким (SSC^{low}) и высоким (SSC^{high}) боковым светорассеянием. Все $CD45^{-}EpCAM^{-}CK7/8^{-}CD24^{+}N\text{-}cadherin^{-}$ ЦК были представлены фенотипами $CD11b^{-}$ и $CD11b^{+}$, которые встречались как в SSC^{low}, так и в SSC^{high} областях. Из восьми обнаруженных у пациенток фенотипов $CD45^{-}mEpCAM^{-}CK7/8^{-}CD24^{+}N\text{-}cadherin^{-}$ ЦК с разными вариантами коэкспрессии эпителиальных маркеров (E-cadherin, panCK, и icEpCAM) и CD11b, шесть имели признаки эпителиальности по одному из маркеров, еще два не имели признаков эпителиальности и преобладали над прочими (у доноров встречались только такие два фенотипа). Различие параметров светорассеяния ЦК с одинаковыми фенотипами является дополнительной характеристикой, прогностическое значение которой предстоит выяснить. Экспрессия E-cadherin и panCK при отсутствии mEpCAM и наличие icEpCAM позволяют полагать, что часть ЦК являются опухолевыми в состоянии выраженного ЭМП. ЦК, коэкспрессирующие CD11b и эпителиальные маркеры, могут возникать вследствие гибридизации с миелоидными клетками.

Ключевые слова: рак молочной железы, циркулирующие клетки, проточная цитометрия, боковое светорассеяние

Финансирование: работа выполнена при финансовой поддержке гранта РНФ № 23-15-00135.

Вклад авторов: А. В. Бузенкова — анализ литературы, анализ данных, получение и статистическая обработка результатов, написание статьи; Е. С. Григорьева — проточная цитометрия, анализ данных, интерпретация результатов, написание статьи; В. В. Алифанов — проточная цитометрия, редактирование статьи; Л. А. Таширева, О. Е. Савельева — обсуждение результатов, редактирование статьи; Е. С. Пудова — проточная цитометрия; М. В. Завьялова — редактирование статьи; Н. В. Чердынцева — планирование, дизайн исследования, обсуждение результатов; В. М. Перельмутер — планирование и руководство исследованием, интерпретация результатов, написание статьи.

Соблюдение этических стандартов: исследование одобрено этическим комитетом НИИ онкологии Томского НИМЦ (протокол № 8 от 17 июня 2016 г.), проведено в соответствии с федеральными законами Российской Федерации (№ 152, 323 и др.) и Хельсинкской декларацией 1964 г. и всеми последующими дополнениями и изменениями, регламентирующими научные исследования на биоматериале, полученном у людей. Все участники подписали добровольное информированное согласие об участии в исследовании.

✉ **Для корреспонденции:** Ангелина Владиславовна Бузенкова
пер. Кооперативный, д. 5, г. Томск, 634009, Россия; buzenkova_av@mail.ru

Статья получена: 11.03.2025 **Статья принята к печати:** 26.03.2025 **Опубликована онлайн:** 18.04.2025

DOI: 10.24075/vrgmu.2025.019

Distant metastasis is the main cause of malignant neoplasm adverse outcomes. Cells of primary tumors capable of intravasation and generating the circulating tumor cells (CTCs) are the source of hematogenous metastasis. CELLSEARCH, the conventional method to determine CTCs, is based on isolation of CD45-negative, EpCAM-positive, and cytokeratin 8-, 18- and/or 19-positive CTCs from peripheral blood [1]. To date, various CTC detection and isolation techniques have been developed: separation by density gradient centrifugation; dielectrophoresis (method to isolate CTCs based on the cells' dielectric properties); microfluidic chip-based cell separation method; CTC enrichment involving the use of the magnetic-activated cell sorting (MACS) system (involves CTC labeling with the MACS superparamagnetic microspheres covered with the antibodies specific for the CTC surface antigens); use of magnetic beads covered with a thin layer of the hydrogel containing antibodies against EpCAM; reverse transcription polymerase chain reaction (RT-PCR); flow-cytometry-based detection methods [2]. In patients with late-stage breast cancer (BC), CTCs are found in 60% of cases, while in patients with early-stage disease these are found in 20–30% of cases [3]. The use of flow cytometry allows one to identify a broad range of functional markers in each CTC. With this technology, heterogeneity of stemness sign manifestations and the epithelial–mesenchymal transition manifestations in BC has been shown [4, 5]. In BC, progression-free survival is associated with CTCs. With the CTC counts ≥ 6, relapses and metastasis are more frequent, and survival rate is lower [6]. We have previously reported the cells in peripheral blood with the $CD45^{-}mEpCAM^{-}CK7/8^{-}CD24^{+}N\text{-}cadherin^{-}$ phenotype, which are associated with high risk of metastasis, along with the classic CTCs that express membrane EpCAM (mEpCAM) [7]. In contrast to CTCs, these cells have been classified as circulating cells (CCs). The nature and origin of CCs are poorly understood.

The important characteristics of any cell present in the bloodstream, including tumor cells, involve biophysical parameters that can partially reflect their morphofunctional state. Measurement of the cells' biophysical properties (such as electrical impedance, radio-frequency conductivity, light scattering from cells at various angles) has provided the basis for the automated hematology analysis methods. Flow cytometry techniques enable gathering information about the cells' size and structure through the detection of forward and side scatter parameters. As cells passes through the light stream emitted by a laser, both cell fluorescence and light scattering in various directions are recorded. Forward scatter (FSC) considers intensity of the light scattered at small angles of up to 10° (with detectors located along the laser beam) and provides data about cell size. Side scatter (SSC) considers intensity of the light scattered at the angles of up to 90° (with detectors positioned perpendicularly to the laser beam direction), depends on cell density, and characterizes the complexity of intracellular structures [8] and the extent of cytoplasmic granularity [9]. Furthermore, studies suggest that various cell structures have a subtle impact on side scatter parameters. For instance, light scattering at an angle of 5–30° is primarily caused by the cell nucleus, while scattering at angles of 50–130° is attributed by small organelles, such as mitochondria, peroxisomes, lysosomes, and granules [10].

In 2023, advancements in this method led to the development of an approach where cell granularity, as estimated based on SSC, can be used to differentiate functional lymphocyte subpopulations. Specifically, naïve undifferentiated lymphocytes were within the SSClow region, whereas cytotoxic lymphocytes characterized by high granule contents were detected in the SSC^{high} region [9].

The study aimed to clarify phenotypic characteristics of the $CD45^{-}mEpCAM^{-}CK7/8^{-}CD24^{+}N\text{-}cadherin^{-}$ cells in blood of female patients with breast cancer. The investigation focused on the analysis of these cells based on side scatter (SSC) properties and evaluation of epithelial cell markers such as E-cadherin, cytokeratins AE1/AE3 (pan Cytokeratin), as well as intracellular expression of the EpCAM adhesion molecules (icEpCAM). We assessed the indicated parameters in both female patients with invasive ductal carcinoma of no special type (IDC NST) and healthy donors.

METHODS

A prospective study involved 11 donors and 20 patients with IDC NST, who underwent treatment at the Cancer Research Institute, Tomsk National Research Medical Center RAS. Inclusion criteria for the study group: morphologically verified diagnosis of invasive ductal carcinoma of no special type; primary tumor extent T_1-$4N_0$-$3M_0$; luminal B $Her2^{-}$ (9 patients), luminal B $Her2^{+}$ (4 patients), triple negative (5 patients) and $HER2^{+}$ (2 patients) molecular biological subtypes. Exclusion criteria for the study group: other breast cancer histologic types; multiple primary malignant tumors; exacerbation of chronic inflammatory disorder. The group of donors was matched to patients based on age, and the primary inclusion criterion was the absence of any exacerbation of chronic inflammatory disorders. Venous blood samples were collected into EDTA-treated vacuum test tubes before surgery and neoadjuvant chemotherapy. Further sample preparation was performed in accordance with the previously reported protocol [11]. Monoclonal antibodies were used to stain surface markers: BV570-anti-CD45 (clone HI30, mouse IgG1; Sony Biotechnology, USA), PE-Cy7-anti-N-cadherin (clone 8C11, mouse IgG1; Sony Biotechnology, USA), BB700-anti-CD24 (clone ML5, mouse IgG2a; BD Horizont, USA), R718-anti-EpCAM (CD326) (clone EBA-1, mouse IgG1; BD Biosciences, USA), BV-421-anti-CD11b (clone ICRF44, mouse IgG1; BioLegend, UK), PE-Dazzle594-anti-E- cadherin (CD324) (clone 67A4, rat IgG1; Sony Biotechnology, USA). Intracellular staining was performed using the following: PE-anti-CK7/8 (clone CAM 5.2, mouse IgG2a; BD Biosciences, USA), eFlour660-anti-panCK (clone AE1/3, mouse IgG1; Invitrogen, USA), BV605-anti-EpCAM (CD326) (clone 9C4, IgG2b; Sony Biotechnology, USA). The MCF-7 breast cancer cells were used as positive controls when estimating fluorescence of antibodies against epithelial markers, whereas U937 promonocytic cells served as negative controls. The events detected within the high signal intensity region (7^{th} decade and above) were considered to be positive based on epithelial markers.

Immunofluorescence was conducted using the Novocyte 3000 flow cytofluorometer (ACEA Biosciences, USA) with the acompanying the NovoExpress 1.3.0 software package (ACEA Biosciences, USA). The granularity of the cells was evaluated based on the side scatter (SSC) parameter individually for each case. In the FSC/SSC two-dimensional plot, the SSC^{low}-circulating cells were localized within the region corresponding to populations of agranulocytes, which include lymphocytes and monocytes. SSC^{high}-cells were positioned within the region corresponding to the granulocyte population on the FSC/SSC two-dimensional plot. The median levels of the boundary between the SSC^{low} and SSC^{high} regions for this cytometer was 0.40 (0.36–0.45) (Fig. 1).

Statistical data processing was performed using the GraphPadPrism 9 software package (GraphPad Software, San

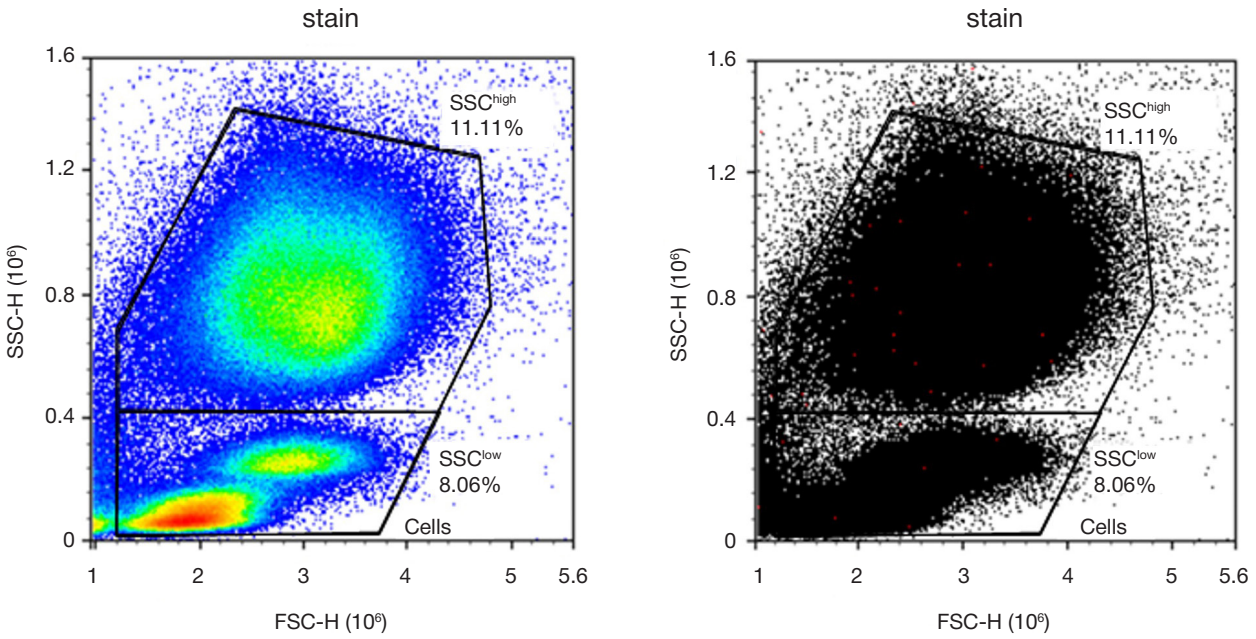

Fig. 1. Distribution of CCs ($CD45^-mEpCAM^-CK7/8^-CD24^+Ncadh^-$) within the SSC^{low} and SSC^{high} regions (cells of interest are *highlighted in red*)

Diego, CA, USA). Fischer's exact test was used to compare the abundance of various cell phenotypes. The cell phenotype counts were compared with each other using the nonparametric Wilcoxon test, and the nonparametric Mann–Whitney test was used to compare cell phenotype counts between donors and patients; the data were presented as Me (Q_1; Q_3). The results were considered significant at $p < 0.05$.

RESULTS

CC abundance and counts within the SSC^{low} and SSC^{high} regions in donors and patients with IDC NST

To clarify the CC nature we evaluated expression of the CD11b marker of myeloid origin, as well as of epithelial cell markers: E-cadherin, pan-Cytokeratin, and intracellular EpCAM (icEpCAM). Among 16 possible CC phenotypes, eight were found in the peripheral blood of patients with IDC NST. Furthermore, each cell expressed only one of the above epithelial markers. We compared the abundance (Table 1) and counts (Table 2) of these cell populations based on the side scatter degree: SSC^{low} or SSC^{high}.

Table 1 represents only those cell phenotypes that were detected in blood of patients with IDC NST. There were no differences in the abundance of cells with the studied CC phenotypes between the SSC^{low} and SSC^{high} regions. Regardless of the SSC parameter and CD11b expression, in the majority of cases (85–100%) CCs with phenotypes 1 and 5 showing no expression of epithelial markers were found. In 20–35% of cases, there were E-cadherin$^+$ cells among CCs. In six CC phenotypes, expression of only one studied epithelial marker was observed.

The total number of cells showing expression of epithelial markers (regardless of the CD11b expression and SSC parameter) was 1.9 cells per 1 mL of whole blood. CCs with phenotypes 1 and 5 were not only more often found in blood, but were the most numerous. The median of other six phenotypes was close to zero.

The number of CCs with phenotype 5 within the SSC^{high} region was 24 times higher, than that within the SSC^{low} region ($p < 0.0001$) (Table 2). In contrast to breast cancer patients, only two phenotypes of the studied cells were found in donors. It should be noted that these were the same most abundant phenotypes 1 and 5. There were no differences in abundance of the specified cell phenotypes depending on their location within the SSC^{low} and SSC^{high} regions, and the counts were not the same. The number of cells with phenotype 5 $CD11b^+Ecadherin^-panCK^-icEpCAM^-$ was 12.5 times higher within the SSC^{high} region compared to the SSC^{low} region ($p = 0.0020$), while the number of cells with phenotype 1 $CD11b^-E\text{-}cadherin^-panCK^-icEpCAM^-$, on the contrary, was 7.5 times higher within the SSClow region

Table 1. Comparison of CC abundance within the SSC^{low} and SSC^{high} regions in patients with IDC NST

CC phenotype ($CD45^-mEpCAM^-CK7/8^-CD24^+Ncadh^-$)	Abundance, % (abs.)	
	$n = 20$	
	SSC^{low}	SSC^{high}
(№1) $CD11b^-E^-cadh^-panCK^-icEpCAM^-$	85 (17/20)	100 (20/20)
(№2) $CD11b^-E^-cadh^-panCK^-icEpCAM^+$	0 (0/20)	10 (2/20)
(№3) $CD11b^-E^-cadh^-panCK^+icEpCAM^-$	5 (1/20)	10 (2/20)
(№4) $CD11b^-E^-cadh^+panCK^-icEpCAM^-$	35 (7/20)	20 (4/20)
(№5) $CD11b^+E^-cadh^-panCK^-icEpCAM^-$	95 (19/20)	100 (20/20)
(№6) $CD11b^+E^-cadh^-panCK^-icEpCAM^+$	10 (2/20)	10 (2/20)
(№7) $CD11b^+E^-cadh^-panCK^+icEpCAM^-$	10 (2/20)	25 (5/20)
(№8) $CD11b^+E^-cadh^+panCK^-icEpCAM^-$	15 (3/20)	25 (5/20)

Table 2. Comparison of CC counts within the SSC^{low} and SSC^{high} regions in patients with IDC NST

CC phenotype (CD45$^-$mEpCAM$^-$CK7/8$^-$CD24$^+$Ncadh$^-$)	Number of cells Me (Q_1–Q_3) / mL		p
	n = 20		
	SSC^{low}	SSC^{high}	
	a	b	
(№1) CD11b$^-$E$^-$cadh$^-$panCK$^-$icEpCAM$^-$	47.25 (10.38–97.25)	19.50 (3.13–48.50)	
(№5) CD11b$^+$E$^-$cadh$^-$panCK$^-$icEpCAM$^-$	11.75 (5.00–36.50)	287.00 (73.00–1132.00)	$p_{a-b} < 0.0001$

Table 3. Comparison of CC abundance and counts within the SSC^{low} and SSC^{high} regions in donors

CC phenotype (CD45$^-$mEpCAM$^-$CK7/8$^-$CD24$^+$Ncadh$^-$)			SSC^{low}	SSC^{high}	p
			a	b	
(№1) CD11b$^-$Ecadh$^-$panCK$^-$icEpCAM$^-$	abundance, % (abs.)	1	91 (10/11)	82 (9/11)	
	number of cells Me (Q_1–Q_3)	2	7.50 (1.50–12.50)	1.00 (0.50–7.50)	$p_{a-b} = 0.0156$
(№5) CD11b$^+$Ecadh$^-$panCK$^-$icEpCAM$^-$	abundance, % (abs.)	3	100 (11/11)	100 (11/11)	
	number of cells Me (Q_1–Q_3)	4	2.00 (1.00–7.50)	25.00 (3.50–61.00)	$p_{a-b} = 0.0020$; $p_{2-4} = 0.0020$

compared to the SSC^{high} region (p = 0.0156). Furthermore, in the SSC^{high} region, the number of cells with phenotype 5 CD11b$^+$Ecadherin$^-$panCK$^-$icEpCAM$^-$ was 25 times higher, than the number of cells with phenotype 1 CD11b$^-$Ecadherin$^-$panCK$^-$icEpCAM$^-$ (p = 0.0020) (Table 3). It is noteworthy that donors had no CCs showing expression of any epithelial cell marker used.

Comparison of the abundance and counts of various CC phenotypes in donors and patients with IDC NST

Comparison of the abundance and counts of various CC phenotypes in blood of donors and patients with IDC NST is of special interest due to the possibility that there is an association between CC identification in blood and the presence of cancer. We compared the abundance of CCs with the CD45$^-$mEpCAM$^-$CK7/8$^-$CD24$^+$Ncadherin$^-$ phenotypes and different variants of CD11b, E-cadherin, pan-Cytokeratin, and icEpCAM co-expression within the SSClow and SSChigh regions (Fig. 2). Two CC phenotypes were most often found within the SSC^{low} and SSC^{high} regions in both donors and patients with IDC NST: phenotype 1 CD11b$^-$Ecadherin$^-$panCK$^-$icEpCAM$^-$ and phenotype 5 CD11b$^+$Ecadherin$^-$panCK$^-$icEpCAM$^-$, i.e. cells the do not express the E-cadherin, pan-Cytokeratin, and icEpCAM epithelial cell markers (Fig. 2A, B). The same CC phenotypes (1 and 5) turned out to be both most abundant and most numerous in both regions (Fig. 2C, D). Cells with phenotype 4 CD45$^-$mEpCAM$^-$CK7/8$^-$CD24$^+$Ncadherin–CD11b$^-$Ecadherin$^+$panCK$^-$icEpCAM$^-$ were significantly more often found within the SSC^{low} region (p = 0.0331) (Fig. 2A), and the counts were higher at the division level (p = 0.0522) (Fig. 2C) in patients with IDC NST compared to donors. It is worthwhile to emphasize once again that no cells showing expression of epithelial cell markers were found in donors. In patients with IDC NST, CCs showing expression of epithelial cell markers were found, but the abundance was low.

The abundance of the cells showing expression of any epithelial marker within the SSC^{low} region was higher in patients with IDC NST, than in donors (no such cells were found in donors), regardless of the CD11b expression (p = 0.0331 and p = 0.0331, respectively), while within the SSC^{high} region this was reported for the CD11b$^+$ cells only (p = 0.0116) (Fig. 3A). The counts of such cells were higher in patients with IDC NST compared to donors only for the CD11b$^+$ cells within the SSChigh region (p = 0.0129) (Fig. 3B).

DISCUSSION

The assessment of the side scatter parameter (SSC) divided the studied cells into two distinct populations, which are located within the SSC^{low} and SSC^{high} regions. This division indicates differing level of cellular organization complexity, as suggested by the physical nature of the SSC parameter. Specifically, these differences encompass variations in the number of organoids and the extent of cytoplasmic granularity [8].

This criterion is likely to actually show cytoplasmic granularity, since the number of cells within the SSC^{low} and SSC^{high} regions depended on the CD11b myeloid marker expression in the cells. The number of the CCs with phenotype 5, which expressed CD11b, in both donors and cancer patients was higher within the SSC^{high} region, than within the SSC^{low} region. At the same time, there were no differences in the number of the CCs having the same phenotype, but showing no CD11b expression (phenotype 1) between the SSC^{low} and SSC^{high} regions. Assesment of the abundance has shown that each of the eight CC phenotypes was equally likely to be found within the the SSC^{low} and SSC^{high} regions. This suggests that the cells showing expression of the same cytokeratins and/or CD11b show different intracellular organization complexity. Based on the results of the study of lymphocytes with different functional activity [9], it can be noted that the cells showing high activity are located within the SSC^{high} region. This observation can likely to be applied for the studied CCs. Thus, CCs with identical phenotypes but differing in biophysical properties — and consequently in functional characteristics — may vary in their association with metastasis mechanisms. This nuanced understanding underscores the complexity of cellular behavior in cancer metastasis and underscores the potential significance of SSC parameters in evaluating cellular function and malignancy potential.

When discussing the CC epithelial traits, some methodological features of the study should be clarified. The study involved the utilization of the anti-EpCAM monoclonal antibodies labeled with two different fluorescent markers. This dual-labeling technique permitted the distinct detection and differentiation of EpCAM expression at the membrane and within the cell.

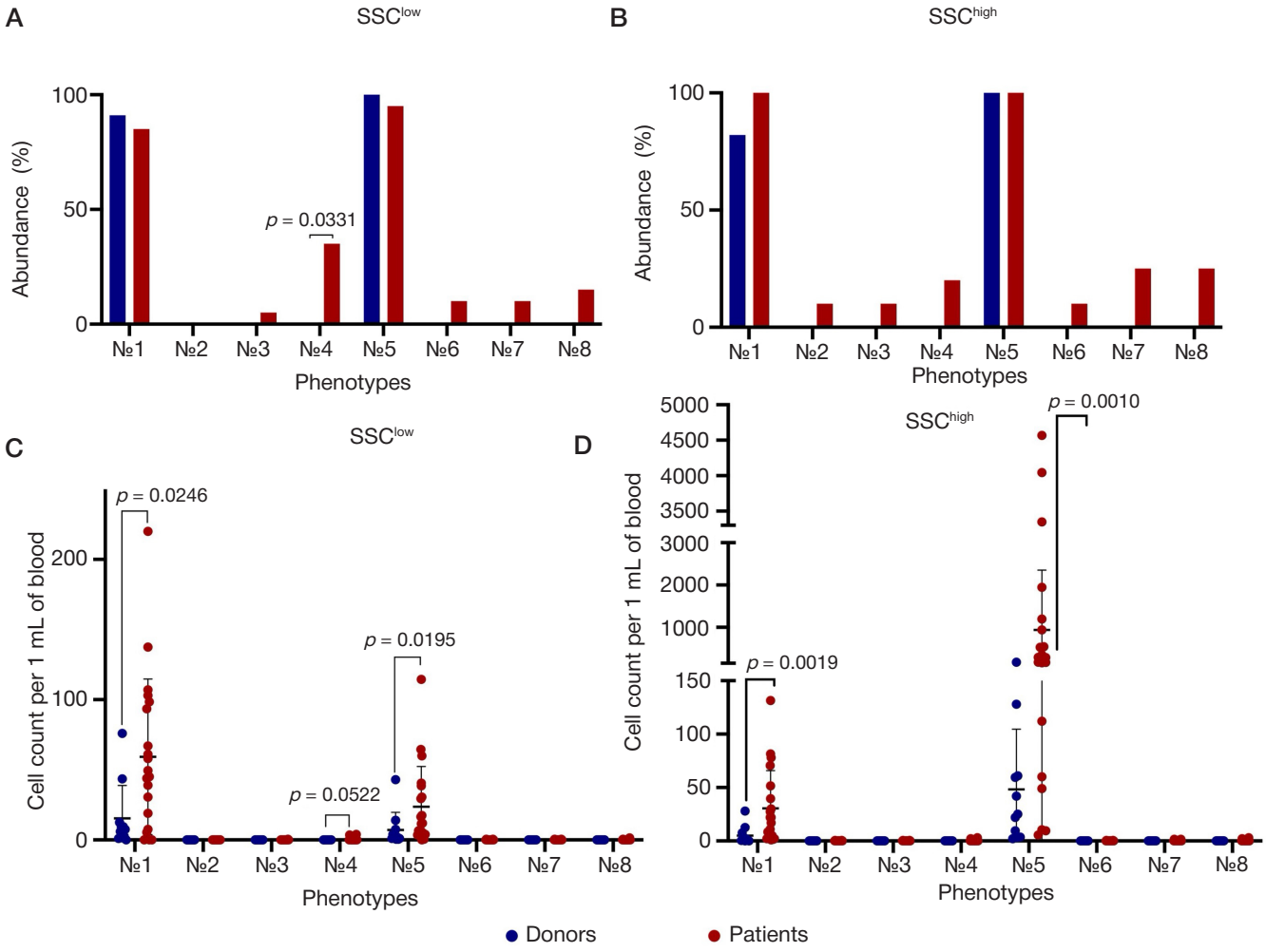

Fig. 2. Comparison of the abundance and counts in blood of donors and patients with IDC NST (main phenotype: CD45⁻mEpCAM⁻CK7/8⁻CD24⁺Ncadh⁻ — with co-expression of CD11b, E-cadherin, pan-Cytokeratin и icEpCAM) within the SSC^{low} and SSC^{high} regions. **A.** Comparison of CC abundance in donors and patients within the SSC^{low} region. **B.** Comparison of CC abundance in donors and patients within the SSChigh region. **C.** Comparison of CC counts in donors and patients within the SSC^{low} region. **D.** Comparison of CC counts in donors and patients within the SSC^{high} region

Specifically, antibodies with the first label were used for surface staining, while those with the second label were added post-permeabilization. The anti-EpCAM antibodies used in our study were produced by the EBA-1 and 9C4 cell clones. These antibodies are designed to detect the EpCAM marker both on the membrane and inside the cell, contingent upon whether the permeabilization phase is included in the procedure. [12]. It is noteworthy that staining following permeabilization may not exclusively reveal intracellular EpCAM expression due to the potential presence of accessible antigenic epitopes on the surface, even after the use of excess antibodies in the initial surface staining phase. However, in our study, not a single case exhibited cells with simultaneous EpCAM expression on both the membrane and intracellularly (within the cytoplasm or nucleus). This observation strongly suggests a genuine intracellular localization of EpCAM expression in the cells we analyzed.

The loss of membrane EpCAM expression during the EMT may occur due to molecule translocation [13, 14] or result from regulated intramembrane proteolysis (RIP) and endocytosis of mEpCAM, leading to its eventual degradation in proteosomes [15, 16]. In cases where there is an absence of mEpCAM and presence of icEpCAM alongside the expression of the other epithelial markers (E-cadherin and pan-Cytokeratin), it is plausable that some of the studied CCs are tumor cells undergoing pronounced EMT. These cells could, therefore, be considered CTCs. However, contemporary research suggests that these CCs may also be of non-tumor origins; for example, bone marrow-derived epithelial progenitor cells have been identified [17, 18]. There are data that the cells originating from the bone marrow can express proteins of epithelial cells and become epithelial cells in many organs. These cells do not express CD45 leukocyte marker, however, they do exhibit cytokeratins expression and are detected only following prior epithelial damage. This is considered to be an argument in favor of the fact that the bone marrow-derived epithelial progenitor cells are intended for regeneration [19–21]. Given these findings, it's possible that the studied CCs expressing epithelial markers—yet showing no CD45 expression—might be normal cells originating from the bone marrow. The absence of such cells in healthy donors does not contradict this hypothesis, as their prevalence might only rise to detectable levels under specific conditions, such as in loci undergoing regeneration or

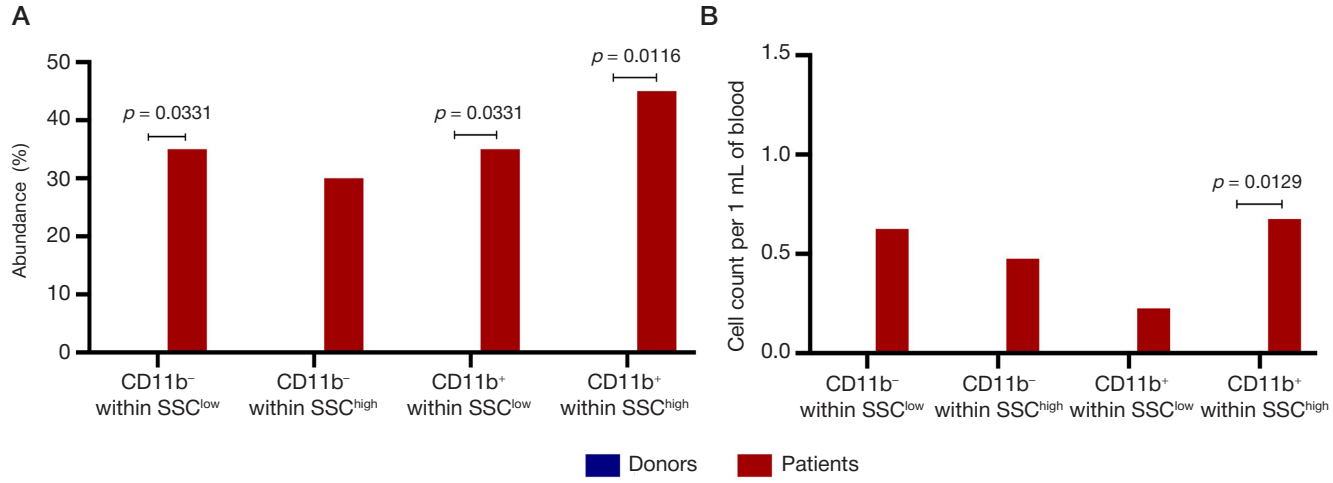

Fig. 3. Total abundance and counts of the CD11b⁻ and CD11b⁺ cell that express any epithelial cell marker (main phenotype: CD45⁻mEpCAM⁻CK7/8⁻CD24⁺Ncadh⁻, epithelial cell markers: E-cadh, panCK, icEpCAM) within the SSC^{low} and SSC^{high} regions. **A.** Comparison of the total abundance of the CC epithelial markers in donors and patients with IDC NST within the SSC^{low} and SSC^{high} regions. **B.** Comparison of total counts of the CC epithelial markers in donors and patients with IDC NST within the SSC^{low} and SSC^{high} regions

within the carcinoma microenvironment, which is commonly described as a "non-healing wound" [22, 23].

Two CC phenotypes, 1 and 5, are deprived of epithelial cell markers. CCs with phenotype 1 expressed CD24 only, while that with phenotype 5 expressed both CD24 and CD11b⁺. CCs with phenotypes 1 and 5 were not only more often found compared to other phenotypes detected in blood, but were also most numerous. As for origin of such cells, it can be assumed that these are epithelial cells, in which epithelial traits have been lost after achieving the EMT terminal phase, or these CCs are of non-epithelial origin and belong to another unknown population.

The CC phenotypes 1–4 were similar to phenotypes 5–8 based on eight studied markers out of nine. The only difference between these groups of phenotypes was CD11b⁺ expression in CCs with phenotypes 5–8. As is well known, integrin CD11b is expressed mainly on monocytes/macrophages and neutrophils, as well as some subpopulations of dendritic cells. CD11b represents an integrin alpha-M subunit (αM CD11bCD18), which is part of the αMβ2 heterodimer. This integrin serves as a receptor of fibrinogen and the ICAM-1 endothelial adhesion molecule [24]. CD11b mediates cell adhesion, chemotaxis, migration, phagocytic activity and inhibits inflammatory responses initiated via Toll-like receptors [25]. Immunosuppression is one of the most important functions of the myeloid cells that express CD11b [26]. What could be the origin of the CD11b⁺ CCs that we found? The CD11b expression is observed at the rather late promonocytic differentiation stage, while CD45 has to be expressed much earlier: at the monoblast stage [27]. In this regard, it is doubtful that the CD45⁻D11b⁺ CCs considered can belong to myeloid elements (especially cells that express epithelial markers). It is appropriate to consider the CCs showing co-expression of CD11b⁺ and epithelial markers as the hybrid cells emerging due to hybridization with myeloid cells. In this case, expression of leukocyte markers is expected. Not excluded the rarely studied and discussed EMT mechanism, in which not fibroblastic, but leukocyte traits manifest itself. Such EMT variant is substantiated in one of the reports [28]. Finally, if we accept the hypothesis of bone marrow origin of the CCs with epithelial traits, the presence of a myeloid marker can result from the nonlinear bone marrow stem cell differentiation process with the presence of cells with atypical phenotypes in the differentiation continuum.

It is important to note several limitations of the study:

The prospective character of the study has made it impossible to find out whether phenotypic features of the combination of SSC parameters with the CD11b⁺ expression and the presence of epithelial cell traits are associated with hematogenous metastasis and metastasis-free survival. A longer monitoring period will be required to adequately address these questions.

A small sample of donors (n = 11) could limit detection of rare CC phenotypes in the control group. The control group expansion will make it possible to clarify the presence of CCs showing expression of epithelial markers in donors.

Heterogeneity of the studied group of patients with IDC NST also represents a limitation of the study. Perhaps, assessment of the studied parameters in the groups of patients more homogenous based on molecular biological subtype will make it possible to reveal the associations of the CCs having epithelial traits with the less favorable BC subtypes.

CONCLUSIONS

The studied CCs represent a heterogenous population. All cell phenotypes were found within both SSC^{low} and SSC^{high} regions. There was a larger number of the CCs showing CD11b expression within the SSC^{high} region (p = 0.0020 for donors; p < 0.0001 for patients with IDC NST). In BC patients, among eight detected CC CD45⁻mEpCAM⁻CK7/8⁻CD24⁺N-cadherin⁻ phenotypes with different variants of co-expression of the epithelial markers (E-cadherin, pan-Cytokeratin, and icEpCAM) and CD11b, six phenotypes had epithelial cell traits based on one marker only. All the CC phenotypes were represented by two variants depending on the CD11b expression. Cells with two phenotypes, CD45⁻mEpCAM⁻CK7/8⁻CD24⁺N-Ecadherin⁻panCK⁻icEpCAM⁻CD11b⁻ and CD45⁻mEpCAM⁻CK7/8⁻CD24⁺N-Ecadherin⁻panCK⁻icEpCAM⁻CD11b⁺, were most frequently detected and numerous. Only these two CC phenotypes without epithelial traits were found in donors. The side scatter values of the CCs with the same phenotype represent an additional characteristic. Future studies will need to clarify the role of this trait in the association of the studied CCs with distant metastasis.

References

1. Riethdorf S, Fritsche H, Müller V, Rau T, Schindlbeck C, Rack B, et al. Detection of circulating tumor cells in peripheral blood of patients with metastatic BC: A validation study of the CellSearch system. Clin Cancer Res. 2007; 13 (3): 920–8. DOI: 10.1158/1078-0432.CCR-06-1695. PMID: 17289886.
2. Vidlarova M, Rehulkova A, Stejskal P, Prokopova A, Slavik H, Hajduch M, et al. Recent Advances in Methods for Circulating Tumor Cell Detection. Int J Mol Sci. 2023; 24 (4): 3902. DOI: 10.3390/ijms24043902. PMID: 36835311.
3. Fabisiewicz A, Szostakowska-Rodzos M, Zaczek AJ, Grzybowska EA. Circulating Tumor Cells in Early and Advanced Breast Cancer; Biology and Prognostic Value. Int J Mol Sci. 2020; 21 (5): 1671. DOI: 10.3390/ijms21051671. PMID: 32121386.
4. Tashireva LA, Savelieva OE, Grigoryeva ES, Nikitin YV, Denisov EV, et al. Heterogeneous Manifestations of Epithelial-Mesenchymal Plasticity of Circulating Tumor Cells in Breast Cancer Patients. Int J Mol Sci. 2021; 22 (5): 2504. DOI: 10.3390/ijms22052504. PMID: 33801519.
5. Savelieva OE, Tashireva LA, Kaigorodova EV, Buzenkova AV, Mukhamedzhanov RKh, Grigoryeva ES, et al. Heterogeneity of Stemlike Circulating Tumor Cells in Invasive Breast Cancer. Int J Mol Sci. 2020; 21 (8): 2780. DOI: 10.3390/ijms21082780. PMID: 32316333.
6. Xu W, Yuan F. Detection of Circulating Tumor Cells in the Prognostic Significance of Patients with Breast Cancer: A Retrospective Study. J Clin Lab Anal. 2025; 39 (1): e25126. DOI: 10.1002/jcla.25126. PMID: 39692703.
7. Perelmuter VM, Grigoryeva ES, Savelieva OE, Alifanov VV, Andruhova ES, Zavyalova MV, et al. EpCAM–CD24+ circulating cells associated with poor prognosis in breast cancer patients. Sci Rep. 2024; 14 (1): 12245. DOI: 10.1038/s41598-024-61516-2. EDN: XZHVTO.
8. Chabot-Richards DS, George TI. White blood cell counts. Clin Lab Med. 2015; 35 (1): 11–24. DOI: 10.1016/j.cll.2014.10.007. PMID: 25676369.
9. Wu T, Tan JHL, Sin WX, Luah YH, Tan SY, Goh M, et al. Cell granularity reflects immune cell function and enables selection of lymphocytes with superior attributes for immunotherapy. Adv Sci. 2023; 10 (28): e2302175. DOI: 10.1002/advs.202302175. PMID: 37544893.
10. Watson D, Hagen N, Diver J, Marchand P, Chachisvilis M. Elastic light scattering from single cells: orientational dynamics in optical trap. Biophys J. 2004; 87 (2): 1298–306. DOI: 10.1529/biophysj.104.042135. PMID: 15298932.
11. Grigoryeva ES, Tashireva LA, Alifanov VV, Savelieva OE, Vtorushin SV, Zavyalova MV, et al. Molecular subtype conversion in CTCs as indicator of treatment adequacy associated with metastasis-free survival in breast cancer. Sci Rep. 2022; 12 (1): 20949. DOI: 10.1038/s41598-022-25609-0. PMID: 36470982.
12. Sterzynska K, Kempisty B, Zawierucha P, Zabel M. Analysis of the specificity and selectivity of anti-EpCAM antibodies in breast cancer cell lines. Folia Histochem Cytobiol. 2012; 50 (4): 534–41. DOI: 10.5603/17845. PMID: 23264216.
13. Gorges TM, Tinhofer I, Drosch M, Röse L, Zollner TM, Krahn T, et al. Circulating tumor cells escape from EpCAM-based detection due to epithelial-to-mesenchymal transition. BMC cancer. 2012; 50 (4): 534–41. DOI: 10.1186/1471-2407-12-178. PMID: 22591372.
14. Königsberg R, Obermayr E, Bises G, Pfeiler G, Gneist M, Wrba F, et al. Detection of EpCAM positive and negative circulating tumor cells in metastatic breast cancer patients. Acta Oncol. 2011; 50 (5): 700–10. DOI: 10.3109/0284186X.2010.549151. PMID: 21261508.
15. Driemel C, Kremling H, Schumacher S, Will D, Wolters J, Lindenlauf N, et al. Context-dependent adaption of EpCAM expression in early systemic esophageal cancer. Oncogene. 2014; 33 (41): 4904–15. DOI: 10.1038/onc.2013.441. PMID: 24141784.
16. Perelmuter VM, Manskikh VN. Prenisha as the missing link of the metastatic niche concept explaining selective metastasis of malignant tumors and the pattern of metastatic disease. Biochemistry (Mosc). 2012; 77 (1): 111-8. DOI: 10.1134/S0006297912010142. PMID: 22339641.
17. Fox JM, Chamberlain G, Ashton BA. Recent advances into the understanding of mesenchymal stem cell trafficking. Br J Haematol. 2007; 137 (6): 491–502. DOI: 10.1111/j.1365-2141.2007.06610. x. PMID: 17539772.
18. Huang Y, Chanou A, Kranz G, Pan M, Kohlbauer V, Ettinger A, et al. Membrane-associated epithelial cell adhesion molecule is slowly cleaved by γ-secretase prior to efficient proteasomal degradation of its intracellular domain. JBC. 2019; 294 (9): 3051–64. DOI: 10.1074/jbc.RA118.005874. PMID: 30598504.
19. Schreier S & Triampo W. The blood circulating rare cell population. What is it and what is it good for? Cells. 2020; 9 (4): 790. DOI: 10.3390/cells9040790. PMID: 32218149.
20. Holtorf S, Boyle J, Morris R. Evidence for EpCAM and cytokeratin expressing epithelial cells in normal human and murine blood and bone marrow. JoVE. 2023; (194): 10.3791/65118. DOI: 10.3791/65118. PMCID: PMC10653199.
21. Kassmer SH & Krause DS. Detection of bone marrow–derived lung epithelial cells. Exp Hematol. 2010; 38 (7): 564–73. DOI: 10.1016/j.exphem.2010.04.011. PMID: 20447442.
22. Van Arnam JS, Herzog E, Grove J, Bruscia E, Ziegler E, Swenson S. Engraftment of bone marrow-derived epithelial cells. Stem Cell Rev. 2005; 1 (1): 21–7. DOI: 10.1385/SCR:1:1:021. PMID: 17132871.
23. Borue X, Lee S, Grove J, Herzog EL, Harris R, Diflo T, et al. Bone marrow-derived cells contribute to epithelial engraftment during wound healing. Am J Pathol. 2004; 165 (5): 1767–72. DOI: 10.1016/S0002-9440(10)63431-1. PMID: 15509544.
24. Solovjov DA, Pluskota E, Plow EF. Distinct roles for the alpha and beta subunits in the functions of integrin alphaMbeta2. JBC. 2005; 280 (2): 1336–45. DOI: 10.1074/jbc.M406968200. PMID: 15485828.
25. Han C, Jin J, Xu S, Liu H, Li N, Cao X. Integrin CD11b negatively regulates TLR-triggered inflammatory responses by activating Syk and promoting degradation of MyD88 and TRIF via Cbl-b. Nat Immunol. 2010; 11 (8): 734–42. DOI: 10.1038/ni.1908. PMID: 20639876.
26. Schmid MC, Khan SQ, Kaneda MM, Pathria P, Shepard R, Louis TL, et al. Integrin CD11b activation drives anti-tumor innate immunity. Nat Commun. 2018; 9 (1): 5379. DOI: 10.1038/s41467-018-07387-4. PMID: 30568188.
27. Lambert C, Preijers FW, Yanikkaya Demirel G, Sack U. Monocytes and macrophages in flow: an ESCCA initiative on advanced analyses of monocyte lineage using flow cytometry. Cytometry B Clin Cytom. 2017; 92 (3): 180–8. DOI: 10.1002/cyto.b.21280. PMID: 26332381.
28. Johansson J, Tabor V, Wikell A, Jalkanen S, Fuxe J. TGF-β1-Induced Epithelial-Mesenchymal Transition Promotes Monocyte/Macrophage Properties in Breast Cancer Cells. Front Oncol. 2015; 5: 3. DOI: 10.3389/fonc.2015.00003. PMID: 25674539.

Литература

1. Riethdorf S, Fritsche H, Müller V, Rau T, Schindlbeck C, Rack B, et al. Detection of circulating tumor cells in peripheral blood of patients with metastatic BC: A validation study of the CellSearch system. Clin Cancer Res. 2007; 13 (3): 920–8. DOI: 10.1158/1078-0432.CCR-06-1695. PMID: 17289886.
2. Vidlarova M, Rehulkova A, Stejskal P, Prokopova A, Slavik H, Hajduch M, et al. Recent Advances in Methods for Circulating Tumor Cell Detection. Int J Mol Sci. 2023; 24 (4): 3902. DOI: 10.3390/ijms24043902. PMID: 36835311.
3. Fabisiewicz A, Szostakowska-Rodzos M, Zaczek AJ, Grzybowska EA. Circulating Tumor Cells in Early and Advanced Breast Cancer; Biology and Prognostic Value. Int J Mol Sci. 2020; 21 (5): 1671. DOI: 10.3390/ijms21051671. PMID: 32121386.
4. Tashireva LA, Savelieva OE, Grigoryeva ES, Nikitin YV, Denisov EV, et al. Heterogeneous Manifestations of Epithelial-Mesenchymal Plasticity of Circulating Tumor Cells in Breast Cancer Patients. Int J Mol Sci. 2021; 22 (5): 2504. DOI: 10.3390/ijms22052504. PMID: 33801519.
5. Savelieva OE, Tashireva LA, Kaigorodova EV, Buzenkova AV, Mukhamedzhanov RKh, Grigoryeva ES, et al. Heterogeneity of Stemlike Circulating Tumor Cells in Invasive Breast Cancer. Int J

Mol Sci. 2020; 21 (8): 2780. DOI: 10.3390/ijms21082780. PMID: 32316333.
6. Xu W, Yuan F. Detection of Circulating Tumor Cells in the Prognostic Significance of Patients with Breast Cancer: A Retrospective Study. J Clin Lab Anal. 2025; 39 (1): e25126. DOI: 10.1002/jcla.25126. PMID: 39692703.
7. Perelmuter VM, Grigoryeva ES, Savelieva OE, Alifanov VV, Andruhova ES, Zavyalova MV, et al. EpCAM–CD24+ circulating cells associated with poor prognosis in breast cancer patients. Sci Rep. 2024; 14 (1): 12245. DOI: 10.1038/s41598-024-61516-2. EDN: XZHVTO.
8. Chabot-Richards DS, George TI. White blood cell counts. Clin Lab Med. 2015; 35 (1): 11–24. DOI: 10.1016/j.cll.2014.10.007. PMID: 25676369.
9. Wu T, Tan JHL, Sin WX, Luah YH, Tan SY, Goh M, et al. Cell granularity reflects immune cell function and enables selection of lymphocytes with superior attributes for immunotherapy. Adv Sci. 2023; 10 (28): e2302175. DOI: 10.1002/advs.202302175. PMID: 37544893.
10. Watson D, Hagen N, Diver J, Marchand P, Chachisvilis M. Elastic light scattering from single cells: orientational dynamics in optical trap. Biophys J. 2004; 87 (2): 1298–306. DOI: 10.1529/biophysj.104.042135. PMID: 15298932.
11. Grigoryeva ES, Tashireva LA, Alifanov VV, Savelieva OE, Vtorushin SV, Zavyalova MV, et al. Molecular subtype conversion in CTCs as indicator of treatment adequacy associated with metastasis-free survival in breast cancer. Sci Rep. 2022; 12 (1): 20949. DOI: 10.1038/s41598-022-25609-0. PMID: 36470982.
12. Sterzynska K, Kempisty B, Zawierucha P, Zabel M. Analysis of the specificity and selectivity of anti-EpCAM antibodies in breast cancer cell lines. Folia Histochem Cytobiol. 2012; 50 (4): 534–41. DOI: 10.5603/17845. PMID: 23264216.
13. Gorges TM, Tinhofer I, Drosch M, Röse L, Zollner TM, Krahn T, et al. Circulating tumor cells escape from EpCAM-based detection due to epithelial-to-mesenchymal transition. BMC cancer. 2012; 50 (4): 534–41. DOI: 10.1186/1471-2407-12-178. PMID: 22591372.
14. Königsberg R, Obermayr E, Bises G, Pfeiler G, Gneist M, Wrba F, et al. Detection of EpCAM positive and negative circulating tumor cells in metastatic breast cancer patients. Acta Oncol. 2011; 50 (5): 700–10. DOI: 10.3109/0284186X.2010.549151. PMID: 21261508.
15. Driemel C, Kremling H, Schumacher S, Will D, Wolters J, Lindenlauf N, et al. Context-dependent adaption of EpCAM expression in early systemic esophageal cancer. Oncogene. 2014; 33 (41): 4904–15. DOI: 10.1038/onc.2013.441. PMID: 24141784.
16. Перельмутер В. М., Манских В. Н. Прениша как отсутствующее звено концепции метастатических ниш, объясняющее избирательное метастазирование злокачественных опухолей и форму метастатической болезни. Биохимия. 2012; 77 (1): 130–9.
17. Fox JM, Chamberlain G, Ashton BA. Recent advances into the understanding of mesenchymal stem cell trafficking. Br J Haematol. 2007; 137 (6): 491–502. DOI: 10.1111/j.1365-2141.2007.06610. x. PMID: 17539772.
18. Huang Y, Chanou A, Kranz G, Pan M, Kohlbauer V, Ettinger A, et al. Membrane-associated epithelial cell adhesion molecule is slowly cleaved by γ-secretase prior to efficient proteasomal degradation of its intracellular domain. JBC. 2019; 294 (9): 3051–64. DOI: 10.1074/jbc.RA118.005874. PMID: 30598504.
19. Schreier S & Triampo W. The blood circulating rare cell population. What is it and what is it good for? Cells. 2020; 9 (4): 790. DOI: 10.3390/cells9040790. PMID: 32218149.
20. Holtorf S, Boyle J, Morris R. Evidence for EpCAM and cytokeratin expressing epithelial cells in normal human and murine blood and bone marrow. JoVE. 2023; (194): 10.3791/65118. DOI: 10.3791/65118. PMCID: PMC10653199.
21. Kassmer SH & Krause DS. Detection of bone marrow–derived lung epithelial cells. Exp Hematol. 2010; 38 (7): 564–73. DOI: 10.1016/j.exphem.2010.04.011. PMID: 20447442.
22. Van Arnam JS, Herzog E, Grove J, Bruscia E, Ziegler E, Swenson S. Engraftment of bone marrow-derived epithelial cells. Stem Cell Rev. 2005; 1 (1): 21–7. DOI: 10.1385/SCR:1:1:021. PMID: 17132871.
23. Borue X, Lee S, Grove J, Herzog EL, Harris R, Diflo T, et al. Bone marrow-derived cells contribute to epithelial engraftment during wound healing. Am J Pathol. 2004; 165 (5): 1767–72. DOI: 10.1016/S0002-9440(10)63431-1. PMID: 15509544.
24. Solovjov DA, Pluskota E, Plow EF. Distinct roles for the alpha and beta subunits in the functions of integrin alphaMbeta2. JBC. 2005; 280 (2): 1336–45. DOI: 10.1074/jbc.M406968200. PMID: 15485828.
25. Han C, Jin J, Xu S, Liu H, Li N, Cao X. Integrin CD11b negatively regulates TLR-triggered inflammatory responses by activating Syk and promoting degradation of MyD88 and TRIF via Cbl-b. Nat Immunol. 2010; 11 (8): 734–42. DOI: 10.1038/ni.1908. PMID: 20639876.
26. Schmid MC, Khan SQ, Kaneda MM, Pathria P, Shepard R, Louis TL, et al. Integrin CD11b activation drives anti-tumor innate immunity. Nat Commun. 2018; 9 (1): 5379. DOI: 10.1038/s41467-018-07387-4. PMID: 30568188.
27. Lambert C, Preijers FW, Yanikkaya Demirel G, Sack U. Monocytes and macrophages in flow: an ESCCA initiative on advanced analyses of monocyte lineage using flow cytometry. Cytometry B Clin Cytom. 2017; 92 (3): 180–8. DOI: 10.1002/cyto.b.21280. PMID: 26332381.
28. Johansson J, Tabor V, Wikell A, Jalkanen S, Fuxe J. TGF-β1-Induced Epithelial-Mesenchymal Transition Promotes Monocyte/Macrophage Properties in Breast Cancer Cells. Front Oncol. 2015; 5: 3. DOI: 10.3389/fonc.2015.00003. PMID: 25674539.

MODERN TUMOR IMAGING MODELS FOR RODENTS: POTENTIAL AND PROSPECTS IN TRANSLATIONAL MEDICINE

Fadeeva AA[1], Osipova ZM[1,2], Chepurnykh TV[1], Myshkina NM[1]✉

[1] Shemyakin–Ovchinnikov Institute of Bioorganic Chemistry of the Russian Academy of Sciences, Moscow, Russia
[2] Pirogov Russian National Research Medical University, Moscow, Russia

Rodent neoplastic process models are extensively used in pre-clinical practice to assess the dynamics of tumor development and test anti-cancer drugs, which ensures flexibility of choosing both basic and advanced personalized tumor development models for researchers. Various modern model tumor imaging methods are considered, including fluorescence and bioluminescence imaging, which enable comprehensive assessment, from qualitative evaluation to *in vivo* monitoring. We believe that the development of autonomous bioluminescent systems in mammalian cells will provide new possibilities for noninvasive imaging of animal physiological processes, including long-term monitoring of tumor progression.

Keywords: bioluminescence, bioimaging, biomedical research, autonomous bioluminescence, tumor models

Funding: the study was supported by the Russian Science Foundation grant, project No. 24-74-10105 (https://rscf.ru/project/24-74-10105/).

Author contribution: Fadeeva AA — literature review, manuscript writing; Myshkina NM — paper concept, literature review, manuscript writing, project management; Chepurnykh TV — manuscript writing and editing; Osipova ZM — data processing, manuscript editing.

✉ **Correspondence should be addressed:** Nadezhda M. Myshkina
Miklukho-Maklaya, 16/10, Moscow, 117997, Russia; markina.nadya@gmail.com

Received: 04.03.2025 **Accepted:** 18.03.2025 **Published online:** 27.03.2025

DOI: 10.24075/brsmu.2025.015

СОВРЕМЕННЫЕ МОДЕЛИ ВИЗУАЛИЗАЦИИ ОПУХОЛЕЙ У ГРЫЗУНОВ: ВОЗМОЖНОСТИ И ПЕРСПЕКТИВЫ В ТРАНСЛЯЦИОННОЙ МЕДИЦИНЕ

А. А. Фадеева[1], З. М. Осипова[1,2], Т. В. Чепурных[1], Н. М. Мышкина[1]✉

[1] Институт биоорганической химии имени М. М. Шемякина и Ю. А. Овчинникова Российской академии наук, Москва, Россия
[2] Российский национальный исследовательский медицинский университет имени Н. И. Пирогова, Москва, Россия

Моделирование опухолевых процессов в грызунах активно применяют в доклинической практике для изучения динамики развития опухолей и тестирования противораковых препаратов, что дает исследователям гибкость в выборе как базовых, так и сложных персонализированных моделей опухолеобразования. Рассмотрены разнообразные современные методы визуализации модельных опухолей, включая флуоресцентный и биолюминесцентный имиджинг, которые позволяют проводить всесторонние исследования, начиная с качественной оценки и заканчивая *in vivo*-мониторингом. По мнению авторов, разработка автономных биолюминесцентных систем в клетках млекопитающих создаст новые возможности для неинвазивной визуализации физиологических процессов у животных, включая продолжительный мониторинг прогрессии опухолей.

Ключевые слова: биолюминесценция, биоимиджинг, биомедицинские исследования, автономная биолюминесценция, опухолевые модели

Финансирование: исследование выполнено за счет гранта Российского научного фонда № 24-74-10105 (https://rscf.ru/project/24-74-10105/).

Вклад авторов: А. А. Фадеева — анализ литературы, написание статьи; Н. М. Мышкина — идея публикации, анализ литературы, написание статьи, руководство проектом; Т. В. Чепурных — написание и редактирование статьи; З. М. Осипова — обработка данных, редактирование статьи.

✉ **Для корреспонденции:** Надежда Михайловна Мышкина
ул. Миклухо-Маклая, д. 16/10, г. Москва, 117997, Россия; markina.nadya@gmail.com

Статья получена: 04.03.2025 **Статья принята к печати:** 18.03.2025 **Опубликована онлайн:** 27.03.2025

DOI: 10.24075/vrgmu.2025.015

Cancer represents one of the most diverse categories in terms of both tumor development and treatment. Despite this fact, it is possible to distinguish common traits and even model the disease course in other animal species (for example, in rodents) for many types of neoplasms. Given obvious differences in anatomy and genome structure between humans and rodents, such models are still optimal for pre-clinical trials [1]. The neoplastic process modeling is constantly evolving and has changed considerably over more than half a century since the first models were reported. As in other fields of biomedical science, the researchers prefer methods allowing them to obtain more precise information using a lower number of experimental objects and with fewer costs. Thus, the focus is shifting towards life-time noninvasive methods to assess model tumors using simple equipment. In particular, fluorescence and bioluminescence imaging methods enable long-term high-sensitivity monitoring of tumor development and treatment in rodents. An example of the tumor suitable for such monitoring is the highly invasive fluorescent/bioluminescent patient-derived orthotopic model of glioblastoma in mice created under the direction of Vladimir Baklaushev [2]. For the first time the researchers managed to noninvasively record tumor development in less than a week after inoculation and then trace its development by two orthogonal imaging methods (bioluminescence and fluorescence) at once.

Current review is aimed at considering modern rodent tumor models and imaging methods for those, as well as assuming which methods will develop most actively in the near future, providing researchers with the broadest opportunities.

A wide selection of model animals and typical tumor models makes it possible to choose an optimal approach for each particular trial. The main model rodent species include mice

(*Mus musculus*) [3], rats (*Rattus norvegicus*) [4], guinea pigs (*Cavia porcellus*), and Syrian golden hamsters (*Mesocricetus auratus*) [5] (Fig. 1A). However, the list is not limited to these species: marmots, voles, squirrels, degus, and other rodents are also used [6]. The methods to create model tumors include syngeneic models, xenotransplantation models, in situ tumor models, genetic engineering mouse models, patient-derived xenograft models (PDX), and the carcinogen-induced cancer model [4] (Fig. 1B).

Syngeneic models and xenograft models have been known since the 1960s. These are tumors developing from *in vitro* cultured transformed cells introduced into the model organism; depending on the model type, the organism species are either the same (syngeneic models), or different (xenotransplantation models) — in the latter case immunodeficient model animals are used. Despite the fact that such models fail to reliably reproduce tumor microenvironment, these are suitable for primary testing of anti-tumor drugs. Furthermore, syngeneic models of mouse tumors can be used to assess the efficacy of CAR-T therapy of solid tumors [7].

The patient-derived xenograft model is largely similar to the above models. However, a model immunodeficient animal is injected with tumor biopsy fragments obtained directly from the patient for experimental selection of personalized therapy. Such an approach allows one to identify response biomarkers and treatment targets for the tumor subgroups that can be distinguished based on the molecular profile [8].

In situ modeling that makes it possible to achieve tumor development in a certain organ through local gene editing largely overlaps with the carcinogen-induced cancer models that can also be local. Both approaches are used to develop the animal's own tumor, which ensures better reproduction of, inter alia, blood supply. However, the use of the approaches for simulation of human carcinogenesis is limited. An example of the carcinogen-induced mouse model is a novel colitis-associated colorectal cancer mouse model obtained through intraperitoneal administration of azoxymethane to the CD4-dnTGFβRII mice [9].

Finally, all the variants of mice with the sustainably modified genotype are used in the genetic engineering mouse models: in some cases, these are more prone to spontaneous carcinogenesis in certain organs due to knockout of regulatory genes, in other cases these mimic human immune system (humanized mice) and are optimal for introduction of human tumor cells. Long production cycles and high cost can be considered the shortcomings of genetic engineering mouse models. An example of the genetic engineering mouse model is the mouse lineage overexpressing the luteinizing hormone receptor, which is prone to spontaneous endometrial cancer development [10].

Imaging of neoplastic processes in animal models has evolved from standard assessment of tumor location and size to advanced multimodal assessment of molecular, physiological, genetic, immunological, and biochemical events at microscopic and macroscopic levels performed noninvasively and sometimes in the real-time mode [11]. In contrast to necropsy, noninvasive imaging methods allow one to assess a tumor lesion in the body without having to sacrifice the experimental animal. Owing to noninvasive nature, the long-term monitoring becomes available yielding more accurate results and reducing the number of the animals needed [12]. Recently, such imaging techniques as magnetic resonance imaging (MRI), micro computed tomography (micro-CT), bioluminescence and fluorescence imaging, positron emission tomography (PET), etc. have become available for tumor imaging in small animals. Multimodal imaging allows one to trace structural and

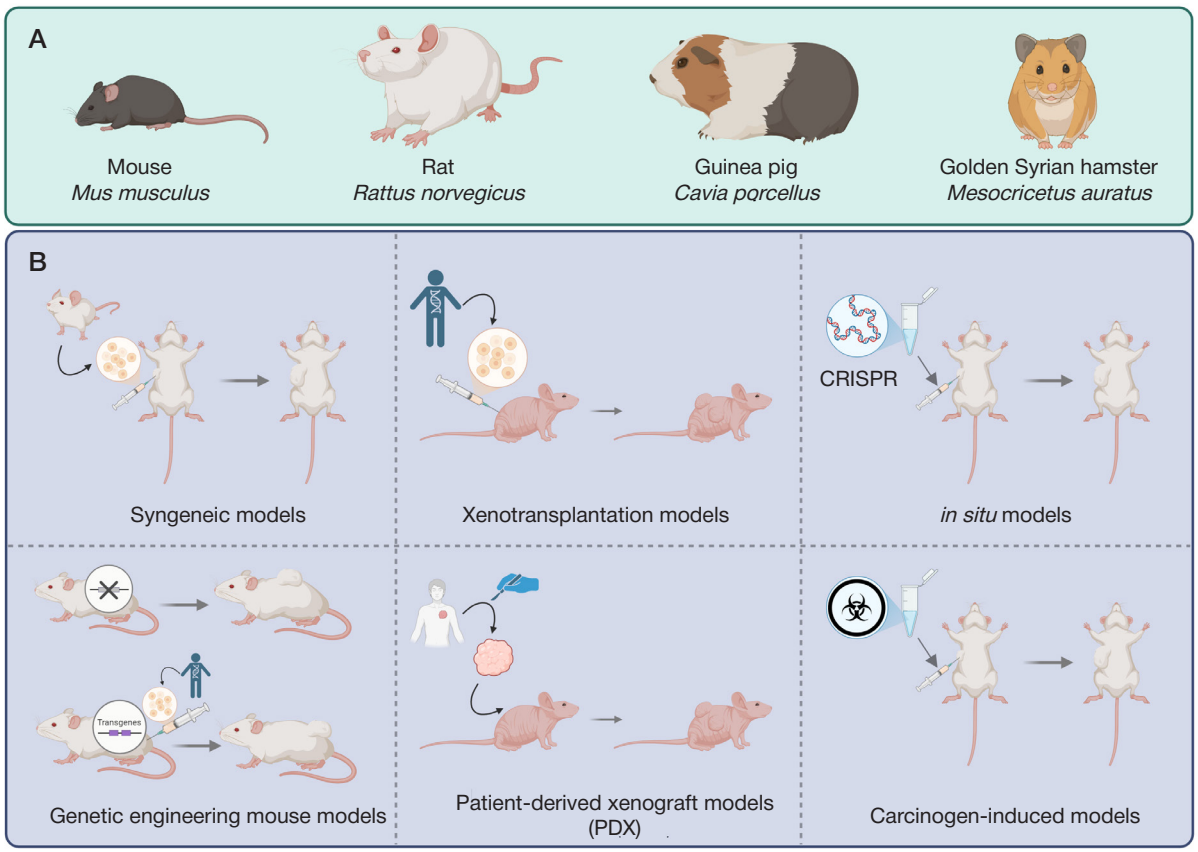

Fig. 1. The main models used to test anti-cancer drugs. **A**. Animal species used in the majority of experimental models. **B**. The most common methods to model animal tumors (exemplified by mice)

physiological alterations, metabolic processes, transplanted cells and target molecules, as well as to accomplish tumor imaging in distinct organs and the entire animal's body. The use of nanoparticles is a powerful supplementary tool for the above methods due to high resolution, selectivity, and versatile nature [13, 14].

Among all imaging methods, MRI is one of the most informative due to high resolution and excellent contrast, which can be enhanced by adding exogenous paramagnetic contrast agents. This method enables detection of extra-small tumors (up to 0.2 mm in diameter) in well-structured tissues and represents a "gold standard" for orthotopic brain tumors; it is also widely used for detection of metastases in other soft tissues, including the liver and lungs [15]. It has been shown that the weight of colorectal carcinoma calculated based on MRI data *in vivo* is rather accurately correlated to the carcinoma weight measured *ex vivo*, while the correlation with the bioluminescence signal intensity is rather weak, and the difference between the correlations is considerable. However, high cost and limitation of monitoring the neoplastic process at early stages after implantation are definitely the MRI shortcomings [16].

Compared to MRI, CT is considerably inferior in soft tissue and organ recognition quality. However, the main advantages of micro-CT are its high resolving power (<50 μm) and rapid visualization of the lung and bone tissue allowing one to detect cancerous neoplasms. Since bones represent a common metastatic focus for the major types of malignant neoplasms (including breast and prostate carcinomas), some studies report the use of high-resolution (10 μm) micro-CT for detection of metastases of breast carcinomas of different etiology to the bone tissue [17]. Moreover, micro-CT is particularly well suited for acquisition of high-quality anatomic information about the lungs [18]. Thus, the use of 3D analysis allows one to obtain accurate data on the tumor number, size, and progression. It is superior to conventional histology or lung resection. Extra administration of contrast agents is needed to record soft tissue tumors, which complicates the procedure [19].

Widely used methods also include nuclear diagnostic procedures, during which images are acquired by introducing the short-lived radioisotopes and recording their decay using SPECT or PET scanner, which eventually shows spatial and temporal distribution of radioactive substances and drugs specific for certain targets. PET with ^{18}F-fluorodeoxyglucose (^{18}FDG) is the most common imaging method used in both pre-clinical and clinical trials [20]. This method is characterized by high specificity and sensitivity, as well as by positive prognostic value when used to detect tumors. At the same time, it is necessary to somehow prepare model animals for the ^{18}FDG-PET scan; in particular, strict dietary restrictions are necessary to ensure that basal glucose metabolism levels do not mask the test results [21].

Fluorescence imaging is used for visualization of biological processes throughout the body involving the use of the genetically encoded fluorescent proteins or fluorescent dyes [22]. Bioluminescence imaging also represents a noninvasive imaging method based on biochemical reaction of the substrate (luciferin) oxidation by atmospheric oxygen under exposure to specific enzyme (luciferase) with light emission. In contrast to fluorescence, bioluminescence does not require any external light source and, therefore, does not have the related side effects, such as autofluorescence and photobleaching [23]. Obvious advantages of bioluminescence imaging include relative simplicity of use, image acquisition speed, lower cost compared to MRI, and high sensitivity, which makes the method popular in pre-clinical trials. Potential shortcomings of the method include the need for genetic modification of the cells and the need for exogenous substrate supplementation. It should be noted that both bioluminescence and fluorescence imaging methods show high efficacy when used to detect small nonpalpable tumors, but both methods suffer from the signal decrease due to tissue absorption and scattering, which limits the depth at which tumor visualization is possible and hampers acquisition of quantitative data from deeper tissues [24].

It is possible to overcome fundamental flaws in bioluminescence imaging of model tumors *in vivo* through a shift towards autonomous bioluminescent systems. Such systems do not require exogenous substrate supplementation, which both reduces the cost of their use and simplifies measurement. The fundamental possibility of creating a fully autonomous bioluminescent mouse has been confirmed [25], and tumors of such mice are suitable for production of at least syngeneic models. There is also a possibility of gene modification of the tumor cells only for autonomous bioluminescence. In this case, viruses specifically targeting cancer cells may be used to deliver genes of autonomous bioluminescent systems: depending on cancer type these may include adenoviruses, poxviruses, herpes simplex virus 1 (HSV-1), coxsackieviruses, poliovirus, measles virus, Newcastle disease virus (NDV), reoviruses, etc. [26]. Delivery of appropriate mRNA using lipid nanoparticles may become an alternative [14]. It is possible to improve the method sensitivity via treatment of rodent skin with specific dyes showing high absorption in violet and blue spectral regions, which reversibly make the skin transparent in visible light while alive [27, 28].

Today, the key shortcoming is low brightness of autonomous bioluminescent systems, however, research teams in different countries are working to improve these, specifically due to the use of natural orthologs of essential enzymes or their modifications obtained by site-directed mutagenesis [29]. We believe that in the future autonomous bioluminescent models of rodent tumors will be introduced widely into pre-clinical practice along with conventional models.

CONCLUSION

Modern methods to create rodent tumor models reported in this review combined with innovative imaging approaches have expanded the possibilities of pre-clinical trials. In the near future, autonomous bioluminescent models that use the genetically encoded luciferases and luciferin biosynthesis enzymes for noninvasive tumor monitoring have a significant development potential. Such systems enable long-term monitoring with high spatiotemporal resolution without the need for exogenous substrate supplementation, which is especially important for investigation of metastases and monitoring of tumor alterations when treating with therapeutic agents. The approaches based on autonomous bioluminescence can become a valuable translational oncology tool, contributing to a shift towards more personalized pre-clinical trials.

References

1. Hollingshead MG. Antitumor efficacy testing in rodents. J Natl Cancer Inst. 2008; 100: 1500–10. DOI: 10.1093/jnci/djn351.
2. Yuzhakova D, Kiseleva E, Shirmanova M, Shcheslavskiy V, Sachkova D, Snopova L, et al. Highly invasive fluorescent/bioluminescent patient-derived orthotopic model of glioblastoma in mice. Front Oncol. 2022; 12: 897839. DOI: 10.3389/fonc.2022.897839.
3. Utz B, Turpin R, Lampe J, Pouwels J, Klefström J. Assessment of the WAP-Myc mouse mammary tumor model for spontaneous metastasis. Sci Rep. 2020; 10: 18733. DOI: 10.1038/s41598-020-75411-z.
4. Guo H, Xu X, Zhang J, Du Y, Yang X, He Z, et al. The pivotal role of preclinical animal models in anti-cancer drug discovery and personalized cancer therapy strategies. Pharmaceuticals (Basel). 2024; 17: 1048. DOI: 10.3390/ph17081048.
5. Wang Z, Cormier RT. Golden Syrian hamster models for cancer research. Cells. 2022; 11: 2395. DOI: 10.3390/cells11152395.
6. Jackson RK. Unusual laboratory rodent species: Research uses, care, and associated biohazards. ILAR J. 1997; 38: 13–21. DOI: 10.1093/ilar.38.1.13.
7. Ahmed EN, Cutmore LC, Marshall JF. Syngeneic mouse models for pre-clinical evaluation of CAR T cells. Cancers (Basel). 2024; 16: 3186. DOI: 10.3390/cancers16183186.
8. Zanella ER, Grassi E, Trusolino L. Towards precision oncology with patient-derived xenografts. Nat Rev Clin Oncol. 2022; 19: 719–32. DOI: 10.1038/s41571-022-00682-6.
9. Uragami T, Ando Y, Aoi M, Fukui T, Matsumoto Y, Horitani S, et al. Establishment of a novel colitis-associated cancer mouse model showing flat invasive neoplasia. Dig Dis Sci. 2023; 68: 1885–93. DOI: 10.1007/s10620-022-07774-4.
10. Lottini T, Iorio J, Lastraioli E, Carraresi L, Duranti C, Sala C, et al. Transgenic mice overexpressing the LH receptor in the female reproductive system spontaneously develop endometrial tumour masses. Sci Rep. 2021; 11: 8847. DOI: 10.1038/s41598-021-87492-5.
11. Serkova NJ, Glunde K, Haney CR, Farhoud M, De Lille A, Redente EF, et al. Preclinical applications of multi-platform imaging in animal models of cancer. Cancer Res. 2021; 81: 1189–200. DOI: 10.1158/0008-5472.CAN-20-0373.
12. Bausart M, Bozzato E, Joudiou N, Koutsoumpou X, Manshian B, Préat V, et al. Mismatch between bioluminescence imaging (BLI) and MRI when evaluating glioblastoma growth: Lessons from a study where BLI suggested “regression” while MRI showed “progression”. Cancers (Basel). 2023; 15: 1919. DOI: 10.3390/cancers15061919.
13. Yin C, Hu P, Qin L, Wang Z, Zhao H. The current status and future directions on nanoparticles for tumor molecular imaging. Int J Nanomedicine. 2024; 19: 9549–9574. DOI: 10.2147/IJN.S484206.
14. Liu B, Zhou H, Tan L, Siu KTH, Guan X-Y. Exploring treatment options in cancer: Tumor treatment strategies. Signal Transduct Target Ther. 2024; 9: 175. DOI: 10.1038/s41392-024-01856-7.
15. Green AL, DeSisto J, Flannery P, Lemma R, Knox A, Lemieux M, et al. BPTF regulates growth of adult and pediatric high-grade glioma through the MYC pathway. Oncogene. 2020; 39: 2305–27. DOI: 10.1038/s41388-019-1125-7.
16. Ravoori MK, Margalit O, Singh S, Kim S-H, Wei W, Menter DG, et al. Magnetic resonance imaging and bioluminescence imaging for evaluating tumor burden in orthotopic colon cancer. Sci Rep. 2019; 9: 6100. DOI: 10.1038/s41598-019-42230-w.
17. Previdi S, Abbadessa G, Dalò F, France DS, Broggini M. Breast cancer-derived bone metastasis can be effectively reduced through specific c-MET inhibitor tivantinib (ARQ 197) and shRNA c-MET knockdown. Mol Cancer Ther. 2012; 11: 214–23. DOI: 10.1158/1535-7163.MCT-11-0277.
18. Pennati F, Leo L, Ferrini E, Sverzellati N, Bernardi D, Stellari FF, et al. Micro-CT-derived ventilation biomarkers for the longitudinal assessment of pathology and response to therapy in a mouse model of lung fibrosis. Sci Rep. 2023; 13: 4462. DOI: 10.1038/s41598-023-30402-8.
19. Tan MJ, Fernandes N, Williams KC, Ford NL. In vivo micro-computed tomography imaging in liver tumor study of mice using Fenestra VC and Fenestra HDVC. Sci Rep. 2022; 12: 22399. DOI: 10.1038/s41598-022-26886-5.
20. Hesketh RL, Wang J, Wright AJ, Lewis DY, Denton AE, Grenfell R, et al. Magnetic resonance imaging is more sensitive than PET for detecting treatment-induced cell death-dependent changes in glycolysis. Cancer Res. 2019; 79: 3557–69. DOI: 10.1158/0008-5472.CAN-19-0182.
21. Toner YC, Prévot G, van Leent MMT, Munitz J, Oosterwijk R, Verschuur AVD, et al. Macrophage PET imaging in mouse models of cardiovascular disease and cancer with an apolipoprotein-inspired radiotracer. Npj Imaging. 2024; 2: 12. DOI: 10.1038/s44303-024-00009-3.
22. Ito R, Kamiya M, Urano Y. Molecular probes for fluorescence image-guided cancer surgery. Curr Opin Chem Biol. 2022; 67: 102112. DOI: 10.1016/j.cbpa.2021.102112.
23. Townsend KM, Prescher JA. Recent advances in bioluminescent probes for neurobiology. Neurophotonics. 2024; 11: 024204. DOI: 10.1117/1.NPh.11.2.024204.
24. Gleneadie HJ, Dimond A, Fisher AG. Harnessing bioluminescence for drug discovery and epigenetic research. Front Drug Discov (Lausanne). 2023; 3: 1249507. DOI: 10.3389/fddsv.2023.1249507.
25. Kiszka KA, Dullin C, Steffens H, Koenen T, Rothermel E, Alves F, et al. Autonomous bioluminescence emission from transgenic mice. bioRxiv. 2024. DOI: 10.1101/2024.06.13.598801.
26. Kaufman HL, Kohlhapp FJ, Zloza A. Oncolytic viruses: a new class of immunotherapy drugs. Nat Rev Drug Discov. 2016; 15: 660. DOI: 10.1038/nrd.2016.178.
27. Ou Z, Duh Y-S, Rommelfanger NJ, Keck CHC, Jiang S, Brinson K Jr, et al. Achieving optical transparency in live animals with absorbing molecules. Science. 2024; 385: eadm6869. DOI: 10.1126/science.adm6869.
28. Keck CHC, Schmidt EL, Roth RH, Floyd BM, Tsai AP, Garcia HB, et al. Color-neutral and reversible tissue transparency enables longitudinal deep-tissue imaging in live mice. bioRxivorg. 2025. p. 2025.02.20.639185. DOI: 10.1101/2025.02.20.639185.
29. Shakhova ES, Karataeva TA, Markina NM, Mitiouchkina T, Palkina KA, Perfilov MM, et al. An improved pathway for autonomous bioluminescence imaging in eukaryotes. Nat Methods. 2024; 21: 406–10. DOI: 10.1038/s41592-023-02152-y.

Литература

1. Hollingshead MG. Antitumor efficacy testing in rodents. J Natl Cancer Inst. 2008; 100: 1500–10. DOI: 10.1093/jnci/djn351.
2. Yuzhakova D, Kiseleva E, Shirmanova M, Shcheslavskiy V, Sachkova D, Snopova L, et al. Highly invasive fluorescent/bioluminescent patient-derived orthotopic model of glioblastoma in mice. Front Oncol. 2022; 12: 897839. DOI: 10.3389/fonc.2022.897839.
3. Utz B, Turpin R, Lampe J, Pouwels J, Klefström J. Assessment of the WAP-Myc mouse mammary tumor model for spontaneous metastasis. Sci Rep. 2020; 10: 18733. DOI: 10.1038/s41598-020-75411-z.
4. Guo H, Xu X, Zhang J, Du Y, Yang X, He Z, et al. The pivotal role of preclinical animal models in anti-cancer drug discovery and personalized cancer therapy strategies. Pharmaceuticals (Basel). 2024; 17: 1048. DOI: 10.3390/ph17081048.
5. Wang Z, Cormier RT. Golden Syrian hamster models for cancer research. Cells. 2022; 11: 2395. DOI: 10.3390/cells11152395.
6. Jackson RK. Unusual laboratory rodent species: Research uses, care, and associated biohazards. ILAR J. 1997; 38: 13–21. DOI: 10.1093/ilar.38.1.13.
7. Ahmed EN, Cutmore LC, Marshall JF. Syngeneic mouse models for pre-clinical evaluation of CAR T cells. Cancers (Basel). 2024; 16: 3186. DOI: 10.3390/cancers16183186.
8. Zanella ER, Grassi E, Trusolino L. Towards precision oncology with patient-derived xenografts. Nat Rev Clin Oncol. 2022; 19: 719–32. DOI: 10.1038/s41571-022-00682-6.
9. Uragami T, Ando Y, Aoi M, Fukui T, Matsumoto Y, Horitani S, et al. Establishment of a novel colitis-associated cancer mouse model showing flat invasive neoplasia. Dig Dis Sci. 2023; 68: 1885–93. DOI: 10.1007/s10620-022-07774-4.

10. Lottini T, Iorio J, Lastraioli E, Carraresi L, Duranti C, Sala C, et al. Transgenic mice overexpressing the LH receptor in the female reproductive system spontaneously develop endometrial tumour masses. Sci Rep. 2021; 11: 8847. DOI: 10.1038/s41598-021-87492-5.
11. Serkova NJ, Glunde K, Haney CR, Farhoud M, De Lille A, Redente EF, et al. Preclinical applications of multi-platform imaging in animal models of cancer. Cancer Res. 2021; 81: 1189–200. DOI: 10.1158/0008-5472.CAN-20-0373.
12. Bausart M, Bozzato E, Joudiou N, Koutsoumpou X, Manshian B, Préat V, et al. Mismatch between bioluminescence imaging (BLI) and MRI when evaluating glioblastoma growth: Lessons from a study where BLI suggested "regression" while MRI showed "progression". Cancers (Basel). 2023; 15: 1919. DOI: 10.3390/cancers15061919.
13. Yin C, Hu P, Qin L, Wang Z, Zhao H. The current status and future directions on nanoparticles for tumor molecular imaging. Int J Nanomedicine. 2024; 19: 9549–9574. DOI: 10.2147/IJN.S484206.
14. Liu B, Zhou H, Tan L, Siu KTH, Guan X-Y. Exploring treatment options in cancer: Tumor treatment strategies. Signal Transduct Target Ther. 2024; 9: 175. DOI: 10.1038/s41392-024-01856-7.
15. Green AL, DeSisto J, Flannery P, Lemma R, Knox A, Lemieux M, et al. BPTF regulates growth of adult and pediatric high-grade glioma through the MYC pathway. Oncogene. 2020; 39: 2305–27. DOI: 10.1038/s41388-019-1125-7.
16. Ravoori MK, Margalit O, Singh S, Kim S-H, Wei W, Menter DG, et al. Magnetic resonance imaging and bioluminescence imaging for evaluating tumor burden in orthotopic colon cancer. Sci Rep. 2019; 9: 6100. DOI: 10.1038/s41598-019-42230-w.
17. Previdi S, Abbadessa G, Dalò F, France DS, Broggini M. Breast cancer-derived bone metastasis can be effectively reduced through specific c-MET inhibitor tivantinib (ARQ 197) and shRNA c-MET knockdown. Mol Cancer Ther. 2012; 11: 214–23. DOI: 10.1158/1535-7163.MCT-11-0277.
18. Pennati F, Leo L, Ferrini E, Sverzellati N, Bernardi D, Stellari FF, et al. Micro-CT-derived ventilation biomarkers for the longitudinal assessment of pathology and response to therapy in a mouse model of lung fibrosis. Sci Rep. 2023; 13: 4462. DOI: 10.1038/s41598-023-30402-8.
19. Tan MJ, Fernandes N, Williams KC, Ford NL. In vivo micro-computed tomography imaging in liver tumor study of mice using Fenestra VC and Fenestra HDVC. Sci Rep. 2022; 12: 22399. DOI: 10.1038/s41598-022-26886-5.
20. Hesketh RL, Wang J, Wright AJ, Lewis DY, Denton AE, Grenfell R, et al. Magnetic resonance imaging is more sensitive than PET for detecting treatment-induced cell death-dependent changes in glycolysis. Cancer Res. 2019; 79: 3557–69. DOI: 10.1158/0008-5472.CAN-19-0182.
21. Toner YC, Prévot G, van Leent MMT, Munitz J, Oosterwijk R, Verschuur AVD, et al. Macrophage PET imaging in mouse models of cardiovascular disease and cancer with an apolipoprotein-inspired radiotracer. Npj Imaging. 2024; 2: 12. DOI: 10.1038/s44303-024-00009-3.
22. Ito R, Kamiya M, Urano Y. Molecular probes for fluorescence image-guided cancer surgery. Curr Opin Chem Biol. 2022; 67: 102112. DOI: 10.1016/j.cbpa.2021.102112.
23. Townsend KM, Prescher JA. Recent advances in bioluminescent probes for neurobiology. Neurophotonics. 2024; 11: 024204. DOI: 10.1117/1.NPh.11.2.024204.
24. Gleneadie HJ, Dimond A, Fisher AG. Harnessing bioluminescence for drug discovery and epigenetic research. Front Drug Discov (Lausanne). 2023; 3: 1249507. DOI: 10.3389/fddsv.2023.1249507.
25. Kiszka KA, Dullin C, Steffens H, Koenen T, Rothermel E, Alves F, et al. Autonomous bioluminescence emission from transgenic mice. bioRxiv. 2024. DOI: 10.1101/2024.06.13.598801.
26. Kaufman HL, Kohlhapp FJ, Zloza A. Oncolytic viruses: a new class of immunotherapy drugs. Nat Rev Drug Discov. 2016; 15: 660. DOI: 10.1038/nrd.2016.178.
27. Ou Z, Duh Y-S, Rommelfanger NJ, Keck CHC, Jiang S, Brinson K Jr, et al. Achieving optical transparency in live animals with absorbing molecules. Science. 2024; 385: eadm6869. DOI: 10.1126/science.adm6869.
28. Keck CHC, Schmidt EL, Roth RH, Floyd BM, Tsai AP, Garcia HB, et al. Color-neutral and reversible tissue transparency enables longitudinal deep-tissue imaging in live mice. bioRxivorg. 2025. p. 2025.02.20.639185. DOI: 10.1101/2025.02.20.639185.
29. Shakhova ES, Karataeva TA, Markina NM, Mitiouchkina T, Palkina KA, Perfilov MM, et al. An improved pathway for autonomous bioluminescence imaging in eukaryotes. Nat Methods. 2024; 21: 406–10. DOI: 10.1038/s41592-023-02152-y.

DETERMINATION OF THE RATE OF AUTOANTIBODY CARRIER STATE IN PATIENTS WITH CELIAC DISEASE BY MONO- AND MULTIPLEX IMMUNOASSAY

Nuralieva NF[1]✉, Yukina MYu[1], Bykova SV[2], Savvateeva EN[3], Nikankina LV[1], Kulagina EV[3], Shaskolskiy BL[3], Gryadunov DA[3], Troshina EA[1]

[1] Endocrinology Research Centre, Moscow, Russia
[2] Loginov Moscow Clinical Scientific Centre, Moscow, Russia
[3] Engelhardt Institute of Molecular Biology of the Russian Academy of Sciences, Moscow, Russia

The search for concomitant autoimmune disorders (ADs) in patients with celiac disease is a pressing issue. The study aimed to determine the rate of the carrier state for antibodies (Abs) being the markers of AD development in patients with celiac disease using various immunological approaches. Enzyme-linked immunoassay and hydrogel microarray-based multiplex immunoassay (MI) were used to determine Abs against thyroid peroxidase (TPO), thyroglobulin (TG), glutamate decarboxylase (GAD), pancreatic islet cells (ICA), tyrosine phosphatase (IA2), 21-hydroxylase (P450c21), Castle's intrinsic factor, tissue transglutaminase (TGM2) in blood serum of patients with celiac disease (group 1, $n = 27$) and healthy individuals (group 2, $n = 16$). The microarray also enables testing of Abs against interferons (IFN) alpha and omega, interleukin 22. In group 1, Abs against IA2 (30%), TPO (22%), TG (19%), GAD (19%) were detected by the enzyme-linked immunoassay, and in group 2 Abs against IA2 (38%), TPO (19%), GAD (19%) were detected. In group 1, Abs against TPO (11%), TG (11%), P450c21 (4%), IFN-alpha (4%), ICA (4%) were detected using the microarray, and in group 2 Abs against TPO (13%), ICA (13%), TG (6%), IFN-alpha (6%) were identified. No significant differences in the rate of elevated Abs in the groups were revealed ($p > 0.05$). Patients, in whom the Ab carrier state was established using microarrays, with negative results enzyme-linked immunoassay can develop the delayed ADs, which suggests prognostic value of MI. The lack of significant differences in the rate of elevated Abs in patients with celiac disease and healthy individuals can result from small size of the studied groups and can suggest high prevalence of potential AD forms in these cohorts.

Keywords: celiac disease, autoimmune diseases, screening, multiplex immunoassay, hydrogel microarray

Funding: the study was supported by the Foundation for Scientific and Technological Development of Yugra (No. 2023-571-05/2023).

Author contribution: Nuralieva NF — literature review, study concept and design, patient assessment, material collection, laboratory testing, analysis and interpretation of the results, manuscript writing; Yukina MYu — literature review, study concept and design, patient assessment, material collection, laboratory testing, analysis and interpretation of the results, manuscript writing and editing; Bykova SV — patient assessment, material collection, manuscript editing; Savvateeva EN — literature review, study concept and design; laboratory microarray testing; analysis and interpretation of the results; Kulagina EV, Nikankina LV — laboratory testing (ELISA); Shaskolskiy BL — analysis of the autoantibody multiplex testing results; Gryadunov DA — study concept and design; manuscript editing; Troshina EA — manuscript editing.

Compliance with ethical standards: the study was approved by the Ethics Committee of the Endocrinology Research Centre (protocol No. 14 dated 29 July 2022). All the patients and conditionally healthy individuals submitted the informed consent to participation in the study.

✉ **Correspondence should be addressed:** Nurana F. Nuralieva
Dmitriya Ulyanova, 11, Moscow, 117292, Russia; nnurana@yandex.ru

Received: 02.04.2025 **Accepted:** 16.04.2025 **Published online:** 23.04.2025

DOI: 10.24075/brsmu.2025.020

ОПРЕДЕЛЕНИЕ ЧАСТОТЫ НОСИТЕЛЬСТВА АУТОАНТИТЕЛ У ПАЦИЕНТОВ С ЦЕЛИАКИЕЙ МЕТОДАМИ МОНО- И МУЛЬТИПЛЕКСНОГО ИММУНОАНАЛИЗА

Н. Ф. Нуралиева[1]✉, М. Ю. Юкина[1], С. В. Быкова[2], Е. Н. Савватеева[3], Л. В. Никанкина[1], Е. В. Кулагина[3], Б. Л. Шаскольский[3], Д. А. Грядунов[3], Е. А. Трошина[1]

[1] Национальный медицинский исследовательский центр эндокринологии Министерства здравоохранения Российской Федерации, Москва, Россия
[2] Московский клинический научно-практический центр имени А. С. Логинова Департамента здравоохранения города Москвы, Москва, Россия
[3] Институт молекулярной биологии имени В. А. Энгельгардта Российской академии наук, Москва, Россия

Поиск сопутствующих аутоиммунных заболеваний (АИЗ) у пациентов с целиакией является актуальной задачей. Целью исследования было определить частоту носительства антител (АТ) — маркеров развития АИЗ у пациентов с целиакией с помощью различных иммунологических подходов. У пациентов с целиакией (группа 1, $n = 27$) и здоровых лиц (группа 2, $n = 16$) в сыворотке крови с использованием ИФА и метода мультиплексного иммуноанализа (МИ) на гидрогелевом биочипе определены АТ к тиреоидной пероксидазе (ТПО), тиреоглобулину (ТГ), глутаматдекарбоксилазе (GAD), островковым клеткам поджелудочной железы (ICA), тирозинфосфатазе (IA2), 21-гидроксилазе (P450c21), внутреннему фактору Кастла, тканевой трансглутаминазе (TGM2). Биочип также позволяет проводить исследование АТ к интерферонам (ИФН) альфа и омега, интерлейкину 22. Методом ИФА в группе 1 выявлены АТ к IA2 (30%), ТПО (22%), ТГ (19%), GAD (19%), в группе 2 — к IA2 (38%), ТПО (19%), GAD (19%). В группе 1 с использованием биочипа обнаружены АТ к ТПО (11%), ТГ (11%), P450c21 (4%), ИФН-альфа (4%), ICA (4%), в группе 2 — к ТПО (13%), ICA (13%), ТГ (6%), ИФН-альфа (6%). Значимых различий в частоте повышения АТ в группах не выявлено ($p > 0,05$). У пациентов с носительством АТ, выявленных на биочипах, при отрицательном результате ИФА не исключается развитие АИЗ в отсроченном периоде, что позволяет предположить прогностическую значимость МИ. Отсутствие значимых различий в частоте повышения АТ среди пациентов с целиакией и здоровых лиц может быть обусловлено ограниченной численностью групп наблюдения и свидетельствовать о высокой распространенности потенциальных форм АИЗ в данных когортах.

Ключевые слова: целиакия, аутоиммунные заболевания, скрининг, мультиплексный иммуноанализ, гидрогелевый биочип

Финансирование: исследование выполнено за счет гранта Фонда научно-технологического развития Югры № 2023-571-05/2023.

Вклад авторов: Н. Ф. Нуралиева — анализ литературы, концепция и дизайн исследования, обследование пациентов, сбор материала, лабораторные исследования, анализ и интерпретация результатов, написание статьи; М. Ю. Юкина — анализ литературы, концепция и дизайн исследования, обследование пациентов, сбор материала, лабораторные исследования, анализ и интерпретация результатов, написание и редактирование статьи; С. В. Быкова — обследование пациентов, сбор материала, редактирование статьи; Е. Н. Савватеева — анализ литературы, концепция и дизайн исследования, лабораторные исследования на биочипах, анализ и интерпретация результатов; Е. В. Кулагина, Л. В. Никанкина — лабораторные исследования (ИФА); Б. Л. Шаскольский — анализ результатов мультиплексного исследования аутоантител; Д. А. Грядунов — концепция и дизайн исследования; редактирование статьи; Е. А. Трошина — редактирование статьи.

Соблюдение этических стандартов: исследование одобрено этическим комитетом ФГБУ «Национальный медицинский исследовательский центр эндокринологии» Минздрава России (протокол № 14 от 29 июля 2022 г.). Все пациенты и условно здоровые лица подписывали добровольное информированное согласие на участие в исследовании.

✉ **Для корреспонденции:** Нурана Фейзуллаевна Нуралиева
ул. Дмитрия Ульянова, д. 11, г. Москва, 117292, Россия; nnurana@yandex.ru

Статья получена: 02.04.2025 **Статья принята к печати:** 16.04.2025 **Опубликована онлайн:** 23.04.2025

DOI: 10.24075/vrgmu.2025.020

Celiac disease is an autoimmune disorder (AD) resulting from gluten intolerance in genetically predisposed individuals and characterized by damage to the small intestinal mucosa. The celiac disease clinical manifestations include diarrhea, weight loss, as well as delayed growth and development in children. It should be noted that classic gastrointestinal symptoms (abdominal pain, nausea, flatulence) associated with celiac disease are currently less prevalent due to the disease morphogenesis alteration in the last 30 years. Celiac disease often has atypical course and manifests with skin lesions, reproductive disorders, and neurological symptoms [1]. It is well known that celiac disease is often associated with other ADs, such as type 1 diabetes mellitus (T1D), Hashimoto's thyroiditis (HT), autoimmune hepatitis, dermatitis herpetiformis [2–4], as well as Sjogren's syndrome, selective IgA deficiency, juvenile chronic arthritis, autoimmune myocarditis [5]. The data have been published on the celiac disease comorbidity with primary biliary cirrhosis, primary sclerosing cholangitis, Addison's disease, vitiligo, alopecia areata, dermatomyositis, peripheral neuropathy, rheumatoid arthritis, and other ADs [6]. Moreover, some of the above ADs are considered to be clinical "masks" of celiac disease, for example alopecia areata [1]. Thus, patients with ADs represent the group at risk of developing celiac disease. To ensure timely diagnosis, patients with ADs require screening for celiac disease. At the same time, individuals with the established diagnosis of celiac disease should be recommended assessment aimed to rule out possible concomitant ADs. In particular, in the published studies, the analysis of antibodies (Abs) being the markers of T1D, autoimmune thyroiditis, Sjogren's syndrome, anti-nuclear, anti-mitochondrial Abs, Abs against DNA, to the Smith antigen, neutrophils, smooth muscles, microsomes, stomach parietal cells to the Smith antigen, is conducted [7]. The authors have not revealed higher rate of the carrier state for Abs specific for ADs in patients with celiac disease compared to healthy subjects. The researchers believe that such results are due to small number of patients and their adherence to gluten-free diet. However, the paper reports higher rate of concomitant ADs in patients with celiac disease relative to healthy individuals. Thus, the authors draw a conclusion about the need for both clinical and laboratory testing of patients with celiac disease in case of suspected concomitant AD and recommend to go beyond blood testing for antibodies.

Considering the large number of potential ADs the patient can develop, it can be very difficult to conduct regular screening by ELISA due to high cost and duration of testing, as well as the need to collect a large amount of biomaterial. In this regard, it is feasible to consider the possibility of using the multiplex immunoassay allowing one to obtain information about the presence/absence of a large number of Abs specific for various ADs in a small volume blood sample (5 μL) in a short time in order to optimize the assessment algorithm for patients with celiac disease. The hydrogel microarray-based multiplex immunoassay is used for the diagnosis and screening of celiac disease. Currently, the diagnostic kits are produced allowing one to simultaneously detect Abs against gliadin and tissue transglutaminase (TGM2) in a patient [8, 9], along with Abs against the endomysium [10]. The results obtained using the multiplex immunoassay match the data yielded by monoplex methods [10] and are characterized by high sensitivity and specificity [9]. It is assumed that due to preanalytical, analytical and cost advantages, as multiplex immunoassays are implemented, the need for biopsy to confirm the diagnosis will be significantly reduced [8].

Considering high risk of developing several ADs by one patient, the multiplex immunoassay-based diagnostic kits have been designed allowing one to assess Abs specific not only for celiac disease, but also for other ADs. The multiplex electrochemiluminescence analysis method has been proposed for detection of Abs against insulin, glutamate decarboxylase (GAD), tyrosine phosphatase (IA2), tissue transglutaminase, thyroid peroxidase (TPO), thyroglobulin (TG), IFN-alpha [11]. At the same time, there are no published studies focused on assessing the rate of the Abs carrier state, including Abs specific for endocrine ADs, in patients with celiac disease by multiplex immunoassay.

The study aimed to determine the rate of the carrier state for antibodies being the markers of autoimmune disorders in patients with celiac disease by ELISA and multiplex immunoassay.

METHODS

Study site and period

The study was conducted at the Loginov Moscow Clinical Scientific Centre of Moscow Healthcare Department, Endocrinology Research Centre of the Ministry of Health of the Russian Federation, and Engelhardt Institute of Molecular Biology of the Russian Academy of Sciences.

Material was collected in March–June 2023, laboratory testing was performed in March–December 2023; analysis of the results was conducted in January–June 2024.

Studied cohorts

Cohort of patients with celiac disease (group 1)

Inclusion criteria: male or female sex; age 18 years and over; the diagnosis of celiac disease verified based on the clinical, immunological, and instrumental testing data (in accordance with the data of medical records provided). Exclusion criteria: pregnancy, lactation; acute infection; exacerbation of chronic disorder; severe life-threatening conditions (decompensated chronic heart failure, chronic kidney disease (stage 3b and above), pulmonary failure and liver failure; immune system disorder (including congenital and acquired immunodeficiency; hypersensitivity reactions occurring within the period of participation in the study); use of drugs affecting the immune system function (interleukins, interferons, immunoglobulins, immunosuppressants, cytostatics) within a month before inclusion in the study; vaccination/revaccination within a month before inclusion in the study (in accordance with the data of medical records provided).

Cohort of conditionally healthy participants (group 2)

Inclusion criteria: male or female sex; age 18 years and over, no subclinical/overt autoimmune disorder (in accordance with the data of medical records provided). Exclusion criteria: symptoms of celiac disease (diarrhea, anemia, weight loss), pregnancy, lactation; acute infection; exacerbation of chronic disorder; severe life-threatening conditions (decompensated chronic heart failure, chronic kidney disease (stage 3b and above), pulmonary failure and liver failure; immune system disorder (including congenital and acquired immunodeficiency; hypersensitivity reactions occurring within the period of participation in the study); use of drugs affecting the immune system function (interleukins, interferons, immunoglobulins,

immunosuppressants, cytostatics) within a month before inclusion in the study; vaccination/revaccination within a month before inclusion in the study.

A total of 27 patients aged 29–51 years (median age 36 years) were included in group 1, among them 17 (63%) were females. Group 2 included 16 participants aged 30–52 years (median age 41 years), among them 12 (75%) were females. In patients of group 1, the disease duration at the time of inclusion in the study was 7 [3; 21], (1, 36) years. In group 1, concomitant ADs were diagnosed in three patients (11%), including Hashimoto's thyroiditis (HT) in two patients (7%) and hypoparathyroidism in one patient (4%).

Sampling method for several studied cohorts

A continuous sampling method was used.

Study design

Multicenter, interventional, cross-sectional, two-sample comparative study.

Methods

Criteria to establish the diagnosis of celiac disease

The diagnosis of celiac disease was established based on comprehensive assessment of the patient considering clinical features of the disease, elevated serological markers (levels of antibodies against tissue transglutaminase (IgA and IgG) above the reference values), as well as morphological features of the small intestinal mucosa (signs of hyperregenerative type small intestinal mucosal atrophy based on the Marsh–Oberhuber classification) in accordance with the guidelines of the all-Russian consensus on the diagnosis and treatment of celiac disease in adults and children [4].

All the individuals enrolled underwent determination of Abs markers of ADs by ELISA methods, chemiluminescence analysis, and hydrogel microarray-based multiplex immunoassay.

Enzyme-linked immunoassay

All the patients enrolled underwent assessment of the levels of Abs being the markers of autoimmune thyroiditis (against TPO, TG), type 1 diabetes mellitus (against GAD, pancreatic islet cells (ICA), IA2), autoimmune adrenal insufficiency (against 21-hydroxylase (P450c21)), autoimmune gastritis (Castle's intrinsic factor), celiac disease (levels of IgA against tissue TGM2) within the framework of screening for concomitant ADs.

Blood was collected from the cubital vein into vacuum test tubes with inert gel in the morning (08:00–10:00) in the fasting state (fasting for at least 8 h and no more than 14 h before blood collection). The resulting samples were centrifuged within 15 min after blood collection using the Eppendorf 5810R centrifuge (Eppendorf, USA) at a temperature of 4 °C and 3000 rpm for 15 min, and then processed. The levels of Abs against TPO, TG were determined on the day of blood collection. Serum samples for further determination of the levels of Abs against P450c21, GAD, IA2, ICA, Castle's intrinsic factor, and tissue TGM2 were temporarily frozen in micro test tubes at a temperature of –80 °C. Abs against TG were determined using the Cobas 6000 electrochemiluminescence analyzer (Roche, Germany); Abs against TPO were determined by chemiluminescence immunoassay using the Architect i2000 automated analyzer (Abbott, USA). Abs against P450c21, IA-2, GAD, ICA, Castle's intrinsic factor, tissue TGM2 were determined by ELISA using the commercially available kits (BioVendor, Czech Republic (Abs against P450c21); Medipan, Germany (Abs against IA-2); Biomerica, USA (Abs against GAD, ICA); Orgentec Diagnostika, Germany (Abs against Castle's intrinsic factor); Xema, Russia (Abs against tissue TGM2, total IgA)). The reference ranges of blood immunological indicators were as follows: Abs against P450c21 — < 0.4 U/mL, TPO — 0–5.6 IU/mL, TG — 0–115 IU/mL, GAD — < 1 U/mL (1–1.05 — "gray zone", > 1.05 — positive test), IA2 — < 8 U/mL (8–10 — "gray zone", ≥ 10 — positive test), ICA — < 0.95 U/mL (0.95–1.05 — "gray zone", > 1.05 — positive test), Castle's intrinsic factor — < 6 U/mL, IgA Ab against tissue TGM2 — ≤ 20 U/mL, total IgA — 0.9–5.0 g/L. The values within the"gray zone" were considered as elevated levels.

Hydrogel microarray-based multiplex immunoassay

Hydrogel microarrays were produced by the copolymerization immobilization method based on the hydrogel microarray technique developed at the Engelhardt Institute of Molecular Biology RAS. The earlier designed and tested microarray [12] allowing of the one to identify both organ-specific Abs (against P450c21, GAD, IA-2, ICA, TG, and TPO) and Abs against cytokines (against IFN-omega, IFN-alpha, and interleukin 22) was modified for identification of the IgA Abs against tissue TGM2. For that the microarray was supplemented with the hydrogel elements containing tissue TGM2 (R&D Systems, USA). To ensure simultaneous detection of the G and A class antibodies, the mixture of antibodies against human IgG labeled with the Cy5.5 fluorescence dye and antibodies against human IgA labeled with the Cy3 fluorescence dye was used. Conjugates of the F(ab')2-fragments of the goat antibody against human immunoglobulin G (Invitrogen, USA) and F(ab')2- fragments of the goat antibody against human immunoglobulin A (Invitrogen, USA) were produced in accordance by the method developed by the manufacturer of fluorescence dyes Cy5.5 and Cy3, respectively (Lumiprobe RUS, Russia). Fluorescent microarray images recording and fluorescent signal calculation were accomplished using the analyzer and software (Engelhardt Institute of Molecular Biology RAS, Russia). Interpretation of the microarray-based assay of the results and determination of the Abs presence/absence in blood serum was performed as previously reported [12].

Statistical analysis

Statistical processing of the results was performed by standard methods using the STATISTICA 13 (StatSoft, USA, 2017) and MedCalc (MedCalc Software Ltd, Belgium, 2020) software packages. The median and the interquartile range were specified for quantitative traits. Nonparametric tests were used, since the trait distribution was non-normal. To compare quantitative data of two independent samples, the Mann–Whitney *U*-test was used; qualitative traits were compared using the Chi-squared test and Yates's Chi-squared test. When testing statistical hypotheses, the critical significance level was considered to be equal to 0.05. Bonferroni correction was applied to counteract the multiple comparison problem. After applying correction, p-values within the range between the calculated value and 0.05 were interpreted as a statistical trend.

Multiparametric analysis of the signals reported based on the results of the microarray-based blood serum sample testing, which corresponded to autoantibody levels, considering the

Table 1. Levels of antibodies assessed by enzyme-linked immunoassay and the rate of elevated Abs in groups 1 and 2

Antibody level***				Rate of elevated antibodies, *n* (%)			
Antibodies	Group 1 *n* = 27	Group 2 *n* = 16	*p**	Antibodies	Group 1 *n* = 27	Group 2 *n* = 16	*p***
against TPO, IU/mL	0.8 [0.5; 4.1]	0.5 [0.3; 2.0]	0.315	against TPO	6 (22)	3 (19)	0.907
against TG, IU/mL	16.4 [13.6; 83.1]	14.0 [12.2; 18.2]	0.149	against TG	5 (19)	2 (13)	0.929
against GAD, U/mL	0.5 [0.5; 0.8]	0.5 [0.4; 0.8]	0.734	against GAD	5 (19)	3 (19)	0.699
against IA2, U/mL	3.6 [1.0; 8.4]	1.0 [1.0; 9.5]	0.792	against IA2	8 (30)	6 (38)	0.595
ICA, U/mL	0.4 [0.3; 0.5]	0.3 [0.3; 0.5]	0.49	ICA	2 (7)	0	0.715
against P450c21, U/mL	0.1 [0.1; 0.1]	0.1 [0; 0.1]	0.866	against P450c21	0	0	–
against Castle's intrinsic factor, U/mL	3.2 [0; 4.6]	1.7 [1.1; 2.6]	0.253	against Castle's intrinsic factor	4 (15)	–	–
against TGM2, U/mL	1.2 [0.7; 3.5]	0.9 [0.6; 1.5]	0.125	against TGM2	0	0	–
				At least one Ab	20 (74)	10 (63)	0.424

Note: * — Mann–Whitney *U*-test. Threshold p_0 = 0.004 (after applying Bonferroni correction: 14 comparisons). ** — Chi-squared test and Yates's Chi-squared test. Threshold p_0 = 0.004 (after applying Bonferroni correction: 14 comparisons). *** — Median value, [Q_1; Q_3] Note: TPO — thyroid peroxidase; TG — thyroglobulin; GAD — glutamate decarboxylase; ICA — pancreatic islet cell antibodies; IA2 — tyrosine phosphatase; P450c21 — 21-hydroxylase, TGM2 — tissue transglutaminase.

presence or absence of the diagnosis of celiac disease was conducted by the decision tree method for construction of a single tree in accordance with the classification and regression algorithm (CART). The resulting division into classes based on the signal value ranges was assessed using the Fischer's exact test to test the homogeneity hypothesis. Then the Fischer's exact test for pairwise comparison and Bonferroni correction were used to conduct post-hoc analysis. Calculations and construction of figures were accomplish in R using the rpart v. 4.1.24, rpart.plot v. 3.1.2, ggplot2 v. 3.5.1, rstatix v. 0.7.2 software packages.

RESULTS

No significant intergroup age (p = 0.372) and sex (p = 0.633) differences were revealed. The levels of Abs assessed by ELISA and the rate of detecting elevated levels are provided in Table 1. Elevated IgA against tissue TGM2 was detected in none of the study participants. In group 1, no elevated Abs were detected in seven patients (26%), one elevated Ab was reported in 13 patients (48%), two elevated Abs — in five (19%), three elevated Abs — in one (4%), four elevated Abs — in one patient (4%). In group 2, no elevated Abs were detected in six assessed individuals (38%), one elevated Ab was reported in eight individuals (50%), two elevated Abs — in one (6%), four elevated Abs — in one individual (6%). The median total IgA level determined by ELISA in patients with celiac disease was 1.1 g/L [95% CI: 0.9; 1.5], while in the group of healthy individuals it was 1.1 g/L [95% CI: 1.0; 1.4]. In one patient of group 1, the total IgA level was below the detection limit (< 0.06 g/L).

Values of signals of the microarray elements corresponding to the test Abs levels, that were obtained by multiplex immunoassay, and the rate of detecting elevated levels are provided in Table 2. Antibodies against TGM2 (TGM2-IgA) were also found in none of the patients. In group 1, no Abs were detected in 18 patients (66%), one Ab was reported in eight patients (30%), two Abs — in one patient (4%). In group 2, no Abs were detected in 12 assessed individuals (75%), one Ab was found in three (19%), three Abs — in one individual (6%).

In the whole studied cohort (n = 43) there were eight Abs carriers (18.6%), in whom more than one Ab against the target

Table 2. Values of the microarray element signals corresponding to the levels of studied Abs obtained by multiplex immunoassay and the rate of elevated Abs in groups 1 and 2

Values of microarray element signals, relative units***				Rate of elevated Abs, *n* (%)			
Antibodies	Group 1 *n* = 27	Group 2 *n* = 16	*p**	Antibodies	Group 1 *n* = 27	Group 2 *n* = 16	*p***
against TPO	1.1 [0.9; 1.4]	1.4 [1.0; 1.8]	0.247	against TPO	3 (11)	2 (13)	0.383
against TG	0.8 [0.7; 1.0]	0.95 [0.7; 1.2]	0.496	against TG	3 (11)	1 (6)	0.446
against GAD	1.0 [0.9; 1.1]	0.9 [0.8; 1.0]	0.126	against GAD	0	0	–
against IA2	1.0 [0.9; 1.0]	0.9 [0.8; 1.1]	0.724	against IA2	0	0	–
ICA	1.0 [0.9; 1.3]	1.4 [0.8; 2.1]	0.358	ICA	1 (4)	2 (13)	0.37
against P450c21	0.9 [0.8; 1.0]	1.1 [0.8; 1.9]	0.097	against P450c21	1 (4)	0	0.297
against IFN-omega	1.0 [0.7; 1.1]	0.85 [0.5; 1.0]	0.529	against IFN-omega	0	0	–
against IFN-alpha	0.9 [0.8; 1.2]	1.2 [0.9; 1.7]	0.346	against IFN-alpha	1 (4)	1 (6)	0.31
against IL-22	1.0 [1.0; 1.3]	0.9 [0.8; 1.1]	0.449	against IL-22	0	0	–
against TGM-2 (IgA)	1.1 [0.9; 1.1]	0.8 [0.3; 1.2]	0.065	against TGM-2 (IgA)	0	0	–
				At least one Ab	8 (30)	3 (19)	0.668

Note: * — Mann–Whitney *U*-test. Threshold p_0 = 0.003 (after applying Bonferroni correction: 16 comparisons). ** — Chi-squared test and Yates's Chi-squared test. Threshold p_0 = 0.003 (after applying Bonferroni correction: 16 comparisons). *** — Median value, [Q_1; Q_3] Note: TPO — thyroid peroxidase; TG — thyroglobulin; GAD — glutamate decarboxylase; ICA — pancreatic islet cell antibodies; IA2 — tyrosine phosphatase; P450c21 — 21-hydroxylase; IFN — interferon; IL-22 — interleukin 22, TGM2 — tissue transglutaminase

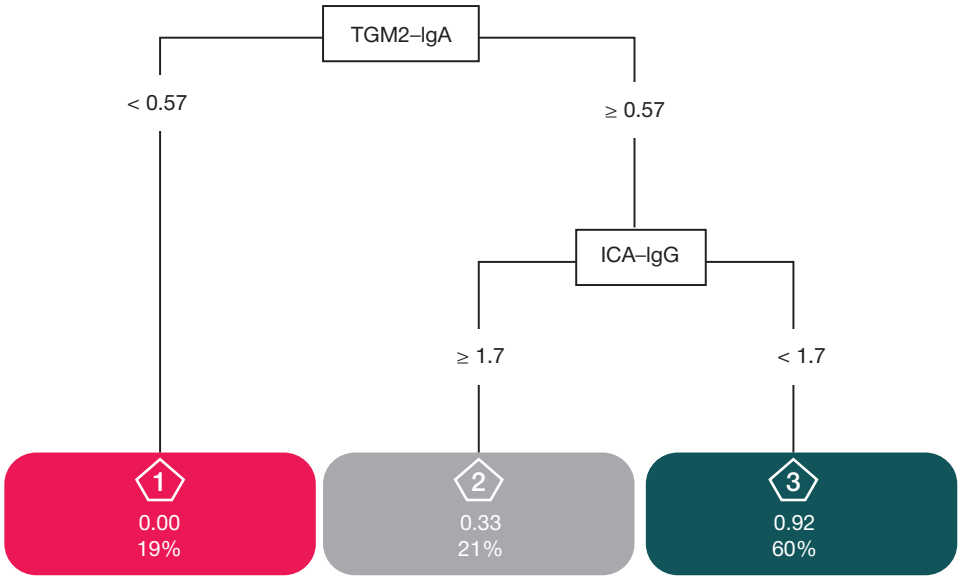

Fig. 1. Classification and regression tree (CART). Each terminal node of the tree (leaf) contains the name of the identified class (here: 1, 2, 3), likelihood of being diagnosed with celiac disease (here: 0.00, 0.33, 0.92), share of patients in the class relative to the entire sample (here: 19%, 21%, 60%)

group of proteins were found and/or the Abs identified were confirmed by two methods: two carriers of Abs against protein marker of diabetes mellitus — a patient with celiac disease and a healthy individual; six carriers of anti-thyroid Abs — five patients with celiac disease and no established diagnosis of autoimmune thyroiditis and one conditionally healthy patient with no established diagnosis of autoimmune thyroiditis. It was determined using multiplex assay that two patients were carriers of the Abs against interferon alpha (a conditionally healthy patient with MEN-1 and a patient with celiac disease). In four patients with celiac disease, the Abs against Castle's intrinsic factor associated with autoimmune gastritis were detected by enzyme-linked immunoassay.

Due to the fact that none of the methods detected elevated levels of the IgA Abs against tissue TGM2 in patients with celiac disease, we conducted multiparametric analysis of the signals of microarray elements based on the results of testing blood serum samples of the studied groups. A classification and regression tree (CART) was constructed based on the input array of signals obtained using microarrays corresponding to various levels of ten studied Abs (Fig. 1).

The resulting tree demonstrates the probability of being diagnosed with celiac disease in a patient with the accuracy of 0.92, if two criteria are met: TGM2-IgA 0.57, ICA–IgG < 1.7. Distribution of patients across the classes of the tree constructed based on the diagnosis of celiac disease (Fig. 2, Table 3) was assessed using the Fisher's exact test. The *p*–value obtained was < 0.0001.

The results of post-hoc analysis involving the use of the Fisher's exact test and Bonferroni correction (Table 4) suggest the differences at the significance level of $p < 0.005$ in classes 2 and 3, classes 1 and 3. The difference between classes 1 and 2 is negligible.

DISCUSSION

The sample of patients with celiac disease can be considered representative based on sex (predominance of females is reported) and age of the disease onset.

This study has revealed elevated Abs against tissue TGM2 in none of the samples. Among possible causes of false-negative

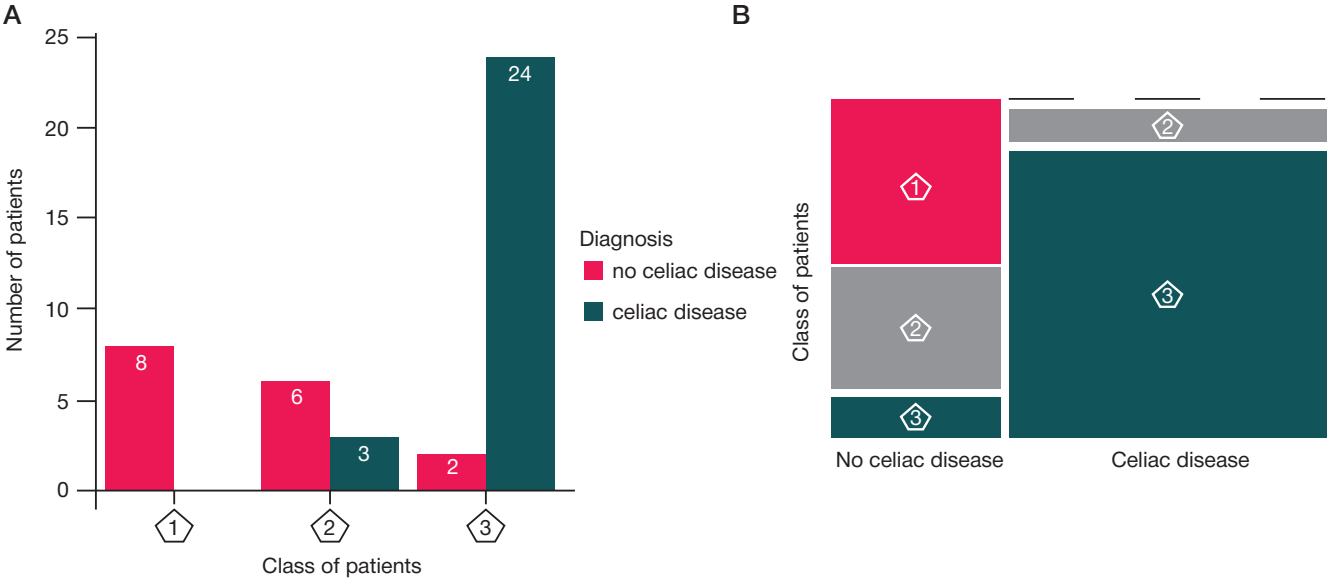

Fig. 2. Distribution of patients across the classes based on the fact of being diagnosed with celiac disease in the form of the column a) and mosaic b) charts. The corresponding classes are designated by numbers in pentagons

Table 3. Distribution of patients across the classes depending on the signals acquired using microarrays and the fact of being diagnosed with celiac disease

Diagnosis of celiac disease	Class 1	Class 2	Class 3
Yes	0	3	24
No	8	6	2

serological testing results in celiac disease, selective IgA deficiency, gluten intake reduction or gluten-free diet, use of corticosteroids or immunosuppressants are distinguished [13].

To rule out IgA deficiency in patients and healthy donors by ELISA, serum total IgA levels were determined. IgA deficiency was found by ELISA in one patient of group 1 (male, 33 years): the total IgA level was below the detection limit. Other patients of group 1 had total IgA levels within normal range, the same was reported for group 2. Celiac disease is an autoimmune disorder associated with IgA deficiency. However, the data on the prevalence of IgA deficiency among patients with celiac disease in different populations vary within wide limits: between 0.55 and 16.67% [16]. The results of the patient sample assessed are consistent with the earlier published data (IgA deficiency was found in one patient out of 27; 3.7%). Thus, since 26 patients out of 27 have no immunoglobulin A deficiency, negative results of testing for IgA against tissue TGM2 result from the long celiac disease duration and adherence to gluten-free diet in the majority of patients.

In patients with celiac disease, HT at the time of enrollment was found only in 7% of cases (n = 2). In one of these patients, ELISA revealed both elevated Abs against TG and elevated Abs against TPO, while multiplex immunoassay revealed none of these Abs. In the second patient, only elevated Abs against TG was detected by both methods. According to the results reported by other authors, the prevalence of HT among patients with celiac disease is 5.7%–18.9% [15, 16]. Considering the fact that the patients are young and the rate of elevated Abs against TPO and TG is high (the rate of elevated Abs against TPO and TG determined by ELISA is 22% and 19%, respectively), it is highly likely that the rate of HT in this group will increase with time.

Hypoparathyroidism was diagnosed in one patient. Sporadic cases of the combination of celiac disease and hypoparathyroidism are reported in the literature. It is assumed that hypoparathyroidism is not a primary disorder, but results from cross reactivity between Abs against endomysium and parathyroid antigens [17]. It is important to note that this patient was also diagnosed with diabetes mellitus against the background of decreased C-peptide levels and normal levels of Abs against insulin, GAD, IA2, zinc transporter 8 (ZnT8), ICA (testing of the expanded panel of T1D Abs markers was conducted before inclusion in the study). Thus, the autoimmune genesis of the disease has not been confirmed. Previous genetic testing revealed a pathogenic mutation in the gene *GCK*, thereby confirming maturity-onset diabetes of the young (MODY). No increase in Abs against Castle's intrinsic factor, 21-hydroxylase, IFN-alpha, and IFN-omega was found in this patient. As for Abs against thyroid tissue, ambiguous results were obtained: the levels of Abs against TG measured by two methods were within normal range, the same as the levels of Abs against TPO determined by ELISA, while multiplex immunoassay determined that the levels of Abs against TPO were within the “gray zone”. The patient’s history is notable for the development of subacute thyroiditis requiring prescription of prednisolone. However, treatment had been terminated before blood collection (euthyroidism was confirmed).

It should be noted that the rate of concomitant ADs determined in our study (11%) is lower compared to the previously reported data [13]: 33.7% of patients had at least one AD, among them 8.1% had multiple autoimmune disorders; the most prevalent was HT (18.9%), T1D (13.5%) and other disorders were less frequent. This is probably due to small number of study participants.

We have found no significant differences in the rate of elevated Ab markers of endocrine and non-endocrine ADs using both ELISA and multiplex assay when comparing the groups. Similar results were reported in the literature, when the rate of carrier state was assessed for Abs against TPO, TG, GAD, ICA in patients with celiac disease and healthy subjects [7]. At the same time, there are reports of the higher rate of Abs against GAD among patients with celiac disease [18]. It should be noted that the rate of elevated Abs against TPO in patients with celiac disease varies considerably; according to the data provided by different authors, it is 3.9–30.5% [7, 13, 19, 20–22], which is likely to result from the differences in the subjects’ age and the diagnostic kit sensitivity. According to the literature data, the rate of elevated Abs against TG in celiac disease is 11.2–11.7% [20, 23], against GAD — 0–13.5% [7, 13, 18, 19, 24], against IA2 — 1–1.25% [18, 19], against stomach parietal cells — 10.9% [19], against P450c21 — 2.2% [19].

In the assessed cohort of patients with celiac disease, the rate of elevated Abs was significantly higher compared to the data obtained in other studies: 13 assessed patients out of 74 (17.6%) were carriers of one Ab, 9 (12.2%) were carriers of two or more Abs [15]. However, it should be noted that the authors analyzed Abs against GAD, TPO and the anti-nuclear Abs only. In the study conducted by other authors, the carrier state for at least one Ab was reported in 31.5% of 92 surveyed patients (the study was focused on determining Abs against insulin, GAD, IA2, ZnT8, TPO, stomach parietal cells, P450c21) [19]. In contrast to our study, in this paper the carrier state for at least one Abs was significantly more frequent in individuals with celiac disease, than in the cohort of healthy individuals (a total of 237 individuals were assessed). The authors note that the rate of the Ab carrier state increases with age: thus, in the group aged 34–50 years elevated Abs levels are found in 34.8% of cases, while in patients aged 18–34 years these are found

Table 4. Results of pairwise comparison of classes

Classes	p	p-adjusted*
1 and 2	0.206	0.618
1 and 3	0.00000248	0.00000744
2 and 3	0.0012	0.0036

Note: * — Bonferroni adjusted p-value.

in 28.3% of cases. In our cohort, the multiplex immunoassay revealed Abs against P450c21 (2.8 relative units) in one patient of group 1, which can be also associated with the patient's age (76 years).

We used multiplex immunoassay to assess Abs against type 1 interferons (IFN-alpha and IFN-omega) and interleukin 22, along with organ-specific Abs. Abs against interleukin 22 associated with mucocutaneous candidiasis and Abs against IFN-omega were found in none of the patients of groups 1 and 2. High titers of Abs against type 1 interferons showing high specificity for type 1 autoimmune polyglandular syndrome can be also detected in patients with some other disorders, including systemic lupus erythematosus, myasthenia gravis, thymic tumor [25]. A rather low titer of Abs against IFN-alpha (2.5 relative units) was found in one patient with celiac disease, in whom other antibodies were within reference ranges and for whom no data on concomitant ADs were obtained. Abs against IFN-alpha (5.6 relative units) were also found in one patient of group 2 having type 1 multiple endocrine neoplasia (MEN-1), including hyperparathyroidism and insulinoma. It is noteworthy that our previously published paper [12] also reported the patient, who was a carrier of Abs against IFN-alpha having the MEN-1 syndrome, the components of which also included insulinoma and hyperparathyroidism. These data need the accumulations followed by a thorough analysis. Also noteworthy is one feature typical for the IFN-alpha Ab carrier state: as shown by the previously reported study, this is associated with the risk of severe COVID-19 course [26].

The lack of significant differences in the rate of elevated Abs in groups 1 and 2 can result from small size of the studied groups and suggest high prevalence of potential AD forms in the surveyed cohorts; is also confirms conditional nature of the term "healthy".

In group 1, markers of T1D and HT were most often detected by both ELISA and multiplex immunoassay, which is consistent with the literature data on the high risk of these disorders in individuals with celiac disease [6]. It is important to note that the Abs carrier state was more often determined using ELISA that is currently considered to be a "gold standard" in clinical practice, than using multiplex immunoassay in both group 1 and group 2. However, in three cases multiplex immunoassay allowed us to reveal the Ab carrier state (Ab against P450c21 in one patient of group 1 and ICA Abs in two subjects of group 2), while ELISA yielded a negative result. No signs of hypocorticism and T1D were found when assessing hormonal profiles of patients with elevated Abs, but we continued follow-up of these subjects (since delayed development of ADs was quite possible) in order to correctly estimate prognostic value of the results obtained.

Thus, since the results of determining this or that indicator by different immunological methods can differ, detection of one Ab in a patient having no clinical signs of the disease during screening requires clarification testing.

Due to the complexity of multidimensional data analysis and the non-obviousness of the conclusions drawn, it is necessary to use mathematical methods to interpret such data arrays. The decision tree methods, specifically the classification and regression tree (CART), are used for analysis of medical data due to the capability of discovering complex interactions between variables and providing visual representation of the results interpreted [27]. In the study conducted we analyzed ten-dimensional data arrays in the form of microarray signal values for 43 patients. It has been shown that when conducting the microarray-based multiplex assay, it is possible to classify patients into one of three classes, in which the third is significantly ($p < 0.005$) different from the first and second in the rate of detecting subjects with celiac disease. Furthermore, class 1 included only healthy subjects, class 2 included both healthy individuals and patients with celiac disease, whose test results were within the conditional "gray zone", and class 3 was constituted by 89% of patients with celiac disease and two (12.5%) subjects of group 2. It should be noted that one conditionally healthy patient classified into class 3 was diagnosed with idiopathic hypoparathyroidism and Fahr's syndrome. The second conditionally healthy individual is a carrier of Abs against gliadin. However, elevation of these Abs is nonspecific and does not constitute grounds for the diagnosis of celiac disease.

Introduction of new approaches to ruling out celiac disease in individuals adherent to gluten-free diet is currently a pressing issue, to resolve which special methods are being developed [28]. The decrease in the levels of various autoantibodies in patients with celiac disease adherent to gluten-free diet has been reported earlier [29, 30]. In particular, in patients with celiac disease, the gluten-free diet is associated with reduction or extinction of the islet-specific autoantibodies, including ICA-IgG [30]. The decrease in the values of ICA-IgG and P450c21-IgG (data not shown) in patients with celiac disease relative to the group of healthy individuals was reported for our sample. Inclusion of the ICA-IgG values together with the TGM2-IgA values in the CART algorithm ensured the best division of patients into classes based on the fact of being diagnosed with celiac disease with the accuracy of 0.92.

CONCLUSIONS

The lack of marker Abs against tissue TGM2 in patients with celiac disease can result from the disease duration and adherence to gluten-free diet. The rate of elevated Ab markers of endocrine ADs in patients with celiac disease is not significantly different from that in healthy individuals. The lack of significant differences in the rate of elevated Abs in the groups of patients with celiac disease and healthy individuals can be due to small size of the studied groups and can suggest high prevalence of potential ADs forms in these cohorts; it also confirms the conditional nature of the term "healthy". Patients, who are Abs carriers based on the multiplex immunoassay data, and have negative ELISA results can develop delayed ADs, which suggests prognostic value of the multiplex immunoassay method. Multiparametric analysis of autoimmune disease markers determined using microarrays has demonstrated the possibility of diagnosing celiac disease in patients on a gluten-free diet when the levels of antibodies against tissue TGM2 are within normal range. Thus, it has been shown that the multiplex immunoassay method can be used in the phase of the celiac disease diagnosis verification and for screening of organ-specific Abs in blood of patients with ADs.

References

1. Ahmedova JeF, Belinskaja VA. Gnezdnaja alopecija kak osnovnoe projavlenie celiakii. Jeksperimental'naja i klinicheskaja gastrojenterologija. 2022; 205 (9): 303–07. DOI: 10.31146/1682-8658-ecg-205-9-303-307. Russian.
2. Bykova SV, Sabel'nikova EA, Zadiran EI, Parfenov AI. Osvedomlennost' vrachej o celiakii: rezul'taty oprosa. Jeffektivnaja farmakoterapija. 2021; 17 (16): 92–100. DOI: 10.33978/2307-3586-2021-17-16-92-100. Russian.
3. Parfenov AI. Celiakija (bolezn' Gi–Gertera–Gejbnera). M.: Medicinskoe informacionnoe agentstvo, 2023; 488 c. Russian.
4. Parfenov AI, Bykova SV, Sabel'nikova EA, Maev IV, Baranov AA, Bakulin IG, i dr. Vserossijskij konsensus po diagnostike i lecheniju celiakii u detej i vzroslyh. Terapevticheskij arhiv. 2017; 89 (3): 94–107. DOI: 10.17116/terarkh201789394-107. Russian.
5. Kocsis D, Csaplár M, Jócsák E, Pák P, Tóth Z, Miheller P, et al. Celiac disease association with other autoimmune disorders: Three case reports. Case Reports in Internal Medicine. 2015; 2 (1): 23–29. DOI: 0.5430/crim.v2n1p23.
6. Lauret E, Rodrigo L. Celiac disease and autoimmune-associated conditions. Biomed Research International. 2013; 2013: 127589. DOI: 10.1155/2013/127589.
7. Caglar E, Ugurlu S, Ozenoglu A, Can G, Kadioglu P, Dobrucali A. Autoantibody frequency in celiac disease. Clinics. 2009; 64 (12): 1195–200. DOI: 10.1590/S1807-59322009001200009.
8. Lochman I, Martis P, Burlingame RW, Lochmanová A. Multiplex assays to diagnose celiac disease. Annals of the New York Academy of Sciences. 2007; 1109: 330–7. DOI: 10.1196/annals.1398.039.
9. Holding S, Wilson F, Spradbery D. Clinical evaluation of the BioPlex 2200 Celiac IgA and IgG Kits — a novel multiplex screen incorporating an integral check for IgA deficiency. Journal of Immunological Methods. 2014; 405: 29–34. DOI: 10.1016/j.jim.2014.01.002.
10. Abdukhakimova D, Dossybayeva K, Grechka A, Almukhamedova Z, Boltanova A, Kozina L, et al. Reliability of the multiplex CytoBead CeliAK immunoassay to assess Anti-tTG IgA for celiac disease screening. Frontiers in Medicine. 2021; 8: 731067. DOI: 10.3389/fmed.2021.731067.
11. Gu Y, Zhao Z, Waugh K, Miao D, Jia X, Cheng J, et al. High-throughput multiplexed autoantibody detection to screen type 1 diabetes and multiple autoimmune diseases simultaneously. EBioMedicine. 2019; 47: 365–72. DOI: 10.1016/j.ebiom.2019.08.036.
12. Savvateeva EN, Yukina MY, Nuralieva NF, Filippova MA, Gryadunov DA, Troshina EA. Multiplex autoantibody detection in patients with autoimmune polyglandular syndromes. International Journal of Molecular Sciences. 2021; 22 (11): 5502. DOI: 10.3390/ijms22115502.
13. Rashid M, Lee J. Serologic testing in celiac disease: Practical guide for clinicians. Canadian Family Physician. 2016; 62 (1): 38–43.
14. Odineal DD, Gershwin ME. The epidemiology and clinical manifestations of autoimmunity in selective IgA deficiency. Clinical Reviews in Allergy & Immunology. 2020; 58 (1): 107–33. DOI:10.1007/s12016-019-08756-7.
15. Gupta V, Singh A, Makharia GK. Prevalence of auto-antibodies and autoimmune disorders in patients with celiac disease. Scandinavian Journal of Gastroenterology. 2020; 55 (7): 785. DOI: 10.1080/00365521.2020.1785544.
16. Volta U, De Franceschi L, Molinaro N, Tetta C, Bianchi FB. Organ-specific autoantibodies in coeliac disease: do they represent an epiphenomenon or the expression of associated autoimmune disorders? Italian Journal of Gastroenterology and Hepatology. 1997; 29: 18–21.
17. Patel SR, Shashaty RJ, Denoux P. Nutritional Nightmare: Hypoparathyroidism Secondary to Celiac Disease. The American Journal of Medicine. 2017; 130 (12): e525–e526. DOI: 10.1016/j.amjmed.2017.07.032.
18. Ghozzi M, Souguir D, Melayah S, Abidi S, Faleh M, Ghedira I. Frequency of auto-antibodies of type 1 diabetes in adult patients with celiac disease. Journal of Clinical Laboratory Analysis. 2021; 35 (9): e23941. DOI: 10.1002/jcla.23941.
19. Tiberti C, Panimolle F, Borghini R, Montuori M, Trovato CM, Filardi T, et al. Type 1 diabetes, thyroid, gastric and adrenal humoral autoantibodies are present altogether in almost one third of adult celiac patients at diagnosis, with a higher frequency than children and adolescent celiac patients. Scandinavian Journal of Gastroenterology. 2020; 55 (5): 549–54. DOI: 10.1080/00365521.2020.1754898.
20. Ventura A, Neri E, Ughi C, Leopaldi A, Citta A, Not T. Gluten-dependent diabetes-related and thyroid-related autoantibodies in patients with celiac disease. The Journal of Pediatrics. 2000; 137: 263–65. DOI: 10.1067/mpd.2000.107160.
21. Velluzzi F, Caradonna A, Boy MF, Pinna MA, Cabula R, Lai MA, et al. Thyroid and celiac disease: clinical, serological, and echographic study. American Journal of Gastroenterology. 1998; 93: 976–979. DOI: 10.1111/j.1572-0241.1998.291_u.x.
22. Carta MG, Hardoy MC, Boi MF, Mariotti S, Carpiniello B, Usai P. Association between panic disorder, major depressive disorder and celiac disease: a possible role of thyroid autoimmunity. Journal of Psychosomatic Research. 2002; 53: 789–93. DOI: 10.1016/s0022-3999(02)00328-8.
23. Gaibi S, Mohammad Amini H, Feizollah Zadeh S. Investigating the prevalence of autoimmune thyroid diseases in children with celiac disease in Urmia city, Iran. Studies in Medical Sciences. 2023; 34(6): 330–37.
24. Hadjivassiliou M, Aeschlimann D, Grünewald RA, Sanders DS, Sharrack B, Woodroofe N. GAD antibody-associated neurological illness and its relationship to gluten sensitivity. Acta Neurologica Scandinavica. 2011; 123 (3): 175–80. DOI: 10.1111/j.1600-0404.2010.01356.x.
25. Gupta S, Tatouli IP, Rosen LB, Hasni S, Alevizos I, Manna ZG, et al. Distinct functions of autoantibodies against interferon in systemic lupus erythematosus: a comprehensive analysis of anticytokine autoantibodies in common rheumatic diseases. Arthritis & Rheumatology. 2016; 68 (7): 1677–87. DOI: 10.1002/art.39607.
26. Savvateeva E, Filippova M, Valuev-Elliston V, Nuralieva N, Yukina M, Troshina E, et al. Microarray-based detection of antibodies against SARS-CoV-2 proteins, common respiratory viruses and type I interferons. Viruses. 2021; 13: 2553. DOI: 10.3390/v13122553.
27. Zimmerman RK, Balasubramani GK, Nowalk MP, Eng H, Urbanski L, Jackson M L, et al. Classification and Regression Tree (CART) analysis to predict influenza in primary care patients. BMC Infectious Diseases. 2016; 16 (1): 503. DOI: 10.1186/s12879-016-1839-x.
28. Sarna VK, Lundin KEA, Mørkrid L, Qiao SW, Sollid LM, Christophersen A. HLA-DQ-gluten tetramer blood test accurately identifies patients with and without celiac disease in absence of gluten consumption. Gastroenterology. 2018; 154 (4): 886–896. e6. DOI: 10.1053/j.gastro.2017.11.006.
29. Elia ZN, Berwary NJA. Effectiveness of a gluten-free diet on the autoantibody frequency of endocrine and neuron disorders in patients with celiac disease. Journal of Advanced Biotechnology and Experimental Therapeutics. 2024; 7 (1): 34–43. DOI: 10.5455/jabet.2024.d03.
30. Tiberti C, Montuori M, Trovato CM, Panimolle F, Filardi T, Valitutti F, et al. Gluten-free diet impact on dynamics of pancreatic islet-specific autoimmunity detected at celiac disease diagnosis. Pediatric Diabetes. 2020; 21 (5): 774–80. DOI: 10.1111/pedi.13054.

Литература

1. Ахмедова Э. Ф., Белинская В. А. Гнездная алопеция как основное проявление целиакии. Экспериментальная и клиническая гастроэнтерология. 2022; 205 (9): 303–07. DOI: 10.31146/1682-8658-ecg-205-9-303-307.
2. Быкова С. В., Сабельникова Е. А., Задиран Е. И., Парфенов А. И. Осведомленность врачей о целиакии: результаты опроса. Эффективная фармакотерапия. 2021; 17 (16): 92–100. DOI: 10.33978/2307-3586-2021-17-16-92-100.
3. Парфенов А. И. Целиакия (болезнь Ги–Гертера–Гейбнера). М.: Медицинское информационное агентство, 2023; 488 с.
4. Парфенов А. И., Быкова С. В., Сабельникова Е. А., Маев И. В., Баранов А. А., Бакулин И. Г. и др. Всероссийский консенсус по диагностике и лечению целиакии у детей и взрослых. Терапевтический архив. 2017; 89 (3): 94–107. DOI:

10.17116/terarkh201789394-107.
5. Kocsis D, Csaplár M, Jócsák E, Pák P, Tóth Z, Miheller P, et al. Celiac disease association with other autoimmune disorders: Three case reports. Case Reports in Internal Medicine. 2015; 2 (1): 23–29. DOI: 0.5430/crim.v2n1p23.
6. Lauret E, Rodrigo L. Celiac disease and autoimmune-associated conditions. Biomed Research International. 2013; 2013: 127589. DOI: 10.1155/2013/127589.
7. Caglar E, Ugurlu S, Ozenoglu A, Can G, Kadioglu P, Dobrucali A. Autoantibody frequency in celiac disease. Clinics. 2009; 64 (12): 1195–200. DOI: 10.1590/S1807-59322009001200009.
8. Lochman I, Martis P, Burlingame RW, Lochmanová A. Multiplex assays to diagnose celiac disease. Annals of the New York Academy of Sciences. 2007; 1109: 330–7. DOI: 10.1196/annals.1398.039.
9. Holding S, Wilson F, Spradbery D. Clinical evaluation of the BioPlex 2200 Celiac IgA and IgG Kits — a novel multiplex screen incorporating an integral check for IgA deficiency. Journal of Immunological Methods. 2014; 405: 29–34. DOI: 10.1016/j.jim.2014.01.002.
10. Abdukhakimova D, Dossybayeva K, Grechka A, Almukhamedova Z, Boltanova A, Kozina L, et al. Reliability of the multiplex CytoBead CeliAK immunoassay to assess Anti-tTG IgA for celiac disease screening. Frontiers in Medicine. 2021; 8: 731067. DOI: 10.3389/fmed.2021.731067.
11. Gu Y, Zhao Z, Waugh K, Miao D, Jia X, Cheng J, et al. High-throughput multiplexed autoantibody detection to screen type 1 diabetes and multiple autoimmune diseases simultaneously. EBioMedicine. 2019; 47: 365–72. DOI: 10.1016/j.ebiom.2019.08.036.
12. Savvateeva EN, Yukina MY, Nuralieva NF, Filippova MA, Gryadunov DA, Troshina EA. Multiplex autoantibody detection in patients with autoimmune polyglandular syndromes. International Journal of Molecular Sciences. 2021; 22 (11): 5502. DOI: 10.3390/ijms22115502.
13. Rashid M, Lee J. Serologic testing in celiac disease: Practical guide for clinicians. Canadian Family Physician. 2016; 62 (1): 38–43.
14. Odineal DD, Gershwin ME. The epidemiology and clinical manifestations of autoimmunity in selective IgA deficiency. Clinical Reviews in Allergy & Immunology. 2020; 58 (1): 107–33. DOI:10.1007/s12016-019-08756-7.
15. Gupta V, Singh A, Makharia GK. Prevalence of auto-antibodies and autoimmune disorders in patients with celiac disease. Scandinavian Journal of Gastroenterology. 2020; 55 (7): 785. DOI: 10.1080/00365521.2020.1785544.
16. Volta U, De Franceschi L, Molinaro N, Tetta C, Bianchi FB. Organ-specific autoantibodies in coeliac disease: do they represent an epiphenomenon or the expression of associated autoimmune disorders? Italian Journal of Gastroenterology and Hepatology. 1997; 29: 18–21.
17. Patel SR, Shashaty RJ, Denoux P. Nutritional Nightmare: Hypoparathyroidism Secondary to Celiac Disease. The American Journal of Medicine. 2017; 130 (12): e525–e526. DOI: 10.1016/j.amjmed.2017.07.032.
18. Ghozzi M, Souguir D, Melayah S, Abidi S, Faleh M, Ghedira I. Frequency of auto-antibodies of type 1 diabetes in adult patients with celiac disease. Journal of Clinical Laboratory Analysis. 2021; 35 (9): e23941. DOI: 10.1002/jcla.23941.
19. Tiberti C, Panimolle F, Borghini R, Montuori M, Trovato CM, Filardi T, et al. Type 1 diabetes, thyroid, gastric and adrenal humoral autoantibodies are present altogether in almost one third of adult celiac patients at diagnosis, with a higher frequency than children and adolescent celiac patients. Scandinavian Journal of Gastroenterology. 2020; 55 (5): 549–54. DOI: 10.1080/00365521.2020.1754898.
20. Ventura A, Neri E, Ughi C, Leopaldi A, Citta A, Not T. Gluten-dependent diabetes-related and thyroid-related autoantibodies in patients with celiac disease. The Journal of Pediatrics. 2000; 137: 263–65. DOI: 10.1067/mpd.2000.107160.
21. Velluzzi F, Caradonna A, Boy MF, Pinna MA, Cabula R, Lai MA, et al. Thyroid and celiac disease: clinical, serological, and echographic study. American Journal of Gastroenterology. 1998; 93: 976–979. DOI: 10.1111/j.1572-0241.1998.291_u.x.
22. Carta MG, Hardoy MC, Boi MF, Mariotti S, Carpiniello B, Usai P. Association between panic disorder, major depressive disorder and celiac disease: a possible role of thyroid autoimmunity. Journal of Psychosomatic Research. 2002; 53: 789–93. DOI: 10.1016/s0022-3999(02)00328-8.
23. Gaibi S, Mohammad Amini H, Feizollah Zadeh S. Investigating the prevalence of autoimmune thyroid diseases in children with celiac disease in Urmia city, Iran. Studies in Medical Sciences. 2023; 34(6): 330–37.
24. Hadjivassiliou M, Aeschlimann D, Grünewald RA, Sanders DS, Sharrack B, Woodroofe N. GAD antibody-associated neurological illness and its relationship to gluten sensitivity. Acta Neurologica Scandinavica. 2011; 123 (3): 175–80. DOI: 10.1111/j.1600-0404.2010.01356.x.
25. Gupta S, Tatouli IP, Rosen LB, Hasni S, Alevizos I, Manna ZG, et al. Distinct functions of autoantibodies against interferon in systemic lupus erythematosus: a comprehensive analysis of anticytokine autoantibodies in common rheumatic diseases. Arthritis & Rheumatology. 2016; 68 (7): 1677–87. DOI: 10.1002/art.39607.
26. Savvateeva E, Filippova M, Valuev-Elliston V, Nuralieva N, Yukina M, Troshina E, et al. Microarray-based detection of antibodies against SARS-CoV-2 proteins, common respiratory viruses and type I interferons. Viruses. 2021; 13: 2553. DOI: 10.3390/v13122553.
27. Zimmerman RK, Balasubramani GK, Nowalk MP, Eng H, Urbanski L, Jackson M L, et al. Classification and Regression Tree (CART) analysis to predict influenza in primary care patients. BMC Infectious Diseases. 2016; 16 (1): 503. DOI: 10.1186/s12879-016-1839-x.
28. Sarna VK, Lundin KEA, Mørkrid L, Qiao SW, Sollid LM, Christophersen A. HLA-DQ-gluten tetramer blood test accurately identifies patients with and without celiac disease in absence of gluten consumption. Gastroenterology. 2018; 154 (4): 886–896. e6. DOI: 10.1053/j.gastro.2017.11.006.
29. Elia ZN, Berwary NJA. Effectiveness of a gluten-free diet on the autoantibody frequency of endocrine and neuron disorders in patients with celiac disease. Journal of Advanced Biotechnology and Experimental Therapeutics. 2024; 7 (1): 34–43. DOI: 10.5455/jabet.2024.d03.
30. Tiberti C, Montuori M, Trovato CM, Panimolle F, Filardi T, Valitutti F, et al. Gluten-free diet impact on dynamics of pancreatic islet-specific autoimmunity detected at celiac disease diagnosis. Pediatric Diabetes. 2020; 21 (5): 774–80. DOI: 10.1111/pedi.13054.

COMPARISON OF EXTRACORPOREAL PHOTOPHERESIS AND GLATIRAMER ACETATE EFFICACY IN THE TREATMENT OF MULTIPLE SCLEROSIS

Kildyushevsky AV, Kotov SV, Sidorova OP ✉, Borodin AV, Bunak MS

Vladimirsky Moscow Regional Research and Clinical Institute, Moscow, Russia

Multiple sclerosis is an autoimmune disorder, the development of which involves humoral and cellular immunity. The disease-modifying drugs (DMDs) for multiple sclerosis slow down the disease progression, but the therapy prescribed is not always well tolerated by patients; allergy and other side effects are possible. In this regard, the development of new methods, including non-pharmacological ones, is relevant. These methods include extracorporeal photopheresis involving UV exposure of peripheral blood lymphocytes and its modification — transimmunization (involving incubation of lymphocytes after UV exposure). The study aimed to compare and within a year assess the transimmunization and glatiramer acetate efficacy in patients with relapsing-remitting multiple sclerosis. A total of 19 adult patients with relapsing-remitting multiple sclerosis, who had been prescribed transimmunization, were assessed. Patients over the age of 18, who did not receive treatment by other methods (DMDs for multiple sclerosis, etc.), were included in the study. The comparison group consisted of 48 adult patients with relapsing-remitting multiple sclerosis, who were prescribed subcutaneous glatiramer acetate 20 mg daily. Clinical assessment was performed using EDSS. Brain and spinal cord MRI was performed in the 3.0 and 1.5 T scanners. When performing transimmunization, the decrease in the median overall EDSS score from 2 to 1.5 points was reported. In the comparison group of patients receiving glatiramer acetate, the median EDSS score changed from 1.75 to 2 points. Therefore, transimmunization is comparable with first-line DMDs for multiple sclerosis and can be used to stabilize the disease course.

Keywords: multiple sclerosis, extracorporeal photopheresis, transimmunization, autoimmune disease, glatiramer acetate

Author contribution: Kildyushevsky AV — study planning, literature review, extracorporeal photopheresis (transimmunization), data interpretation, manuscript writing; Kotov SV — study planning, literature review, data interpretation, manuscript writing; Sidorova OP — literature review, data acquisition and interpretation, patient assessment using EDSS, manuscript writing; Borodin AV — literature review, data acquisition and interpretation, patient assessment using EDSS, manuscript writing; Bunak MS — literature review, data acquisition and interpretation, MRI, manuscript writing.

Compliance with ethical standards: the study was approved by the Ethics Committee (protocol No. 16 dated 26 November 2020); the informed consent to participation in the study was submitted by all subjects.

✉ **Correspondence should be addressed:** Olga P. Sidorova
Shhepkina 61/2, Moscow, 129110, Russia; sidorovaop2019@mail

Received: 02.04.2025 **Accepted:** 19.04.2025 **Published online:** 29.04.2025

DOI: 10.24075/brsmu.2025.023

СРАВНЕНИЕ ЭФФЕКТИВНОСТИ ЭКСТРАКОРПОРАЛЬНОГО ФОТОФЕРЕЗА И ГЛАТИРАМЕРА АЦЕТАТА В ЛЕЧЕНИИ РАССЕЯННОГО СКЛЕРОЗА

А. В. Кильдюшевский, С. В. Котов, О. П. Сидорова ✉, А. В. Бородин, М. С. Бунак

Московский областной научно-исследовательский клинический институт имени М. Ф. Владимирского, Москва, Россия

Рассеянный склероз — аутоиммунное заболевание, в развитии которого играет роль гуморальный и клеточный иммунитет. Препараты, изменяющие течение рассеянного склероза (ПИТРС), замедляют прогрессирование болезни, но не все пациенты хорошо переносят назначаемое лечение, возможны аллергические реакции и другие побочные эффекты. В связи с этим актуальна разработка новых методов лечения, включая немедикаментозные. К таким методам относят экстракорпоральный фотоферез, при котором проводится воздействие ультрафиолетовыми лучами на лимфоциты периферической крови, и его модификация — трансиммунизация (с инкубацией лимфоцитов после ультрафиолетового воздействия). Целью работы было сравнить и оценить через год эффективность трансиммунизации и препарата глатирамира ацетата у пациентов с ремиттирующим течением рассеянного склероза. Обследовали 19 взрослых пациентов с ремитирующим рассеянным склерозом, которым назначали трансиммунизацию. В исследование были включены пациенты старше 18 лет, которым не проводили другие методы лечения (ПИТРС и др.). Группу сравнения составили 48 взрослых пациентов с ремитирующим течением рассеянного склероза, которым был назначен глатирамера ацетат в дозе 20 мг подкожно ежедневно. Клиническую оценку проводили по шкале EDSS. МРТ головного и спинного мозга осуществляли на аппаратах с напряженностью магнитного поля 3,0 и 1,5 Тл. При проведении трансиммунизации отмечено снижение медианы общего показателя EDSS с 2 до 1,5 баллов. В группе сравнения пациентов, получающих глатирамера ацетат, медиана EDSS изменялась от 1,75 балла до 2 баллов. Следовательно, трансиммунизация сопоставима с ПИТРС первой линии и может быть применена для стабилизации течения заболевания.

Ключевые слова: рассеянный склероз, экстракорпоральный фотоферез, трансиммунизация, аутоиммунное заболевание, глатирамира ацетат

Вклад авторов: А. В. Кильдюшевский — планирование исследования, анализ литературы, проведение экстракорпорального фотофереза (трансиммунизации), интерпретация данных, написание статьи; С. В. Котов — планирование исследования, анализ литературы, интерпретация данных, написание статьи; О. П. Сидорова — анализ литературы, сбор и интерпретация данных, обследование пациентов по шкале EDSS, написание статьи; А. В. Бородин — анализ литературы, сбор и интерпретация данных, обследование пациентов по шкале EDSS, написание статьи; М. С. Бунак — анализ литературы, сбор и интерпретация данных, проведение МРТ, написание статьи.

Соблюдение этических стандартов: исследование одобрено этическим комитетом (протокол № 16 от 26 ноября 2020 г.); все участники подписали добровольное согласие на участие в исследовании.

✉ **Для корреспонденции:** Ольга Петровна Сидорова
ул. Щепкина, 61/2, г. Москва, 129110, Россия; sidorovaop2019@mail

Статья получена: 02.04.2025 **Статья принята к печати:** 19.04.2025 **Опубликована онлайн:** 29.04.2025

DOI: 10.24075/vrgmu.2025.023

Multiple sclerosis is an autoimmune disorder, the development of which involves humoral and cellular immunity. The use of disease-modifying drugs (DMDs) for multiple sclerosis has contributed greatly to slowing down the disease progression, improvement of patients' longevity and quality of life, prevention of exacerbations. However, the therapy prescribed is not always well tolerated by patients; allergy and other side effects are possible. In this regard, the development of new methods, including non-pharmacological ones, is relevant. Such methods include extracorporeal photopheresis (ECP) involving UV exposure of peripheral blood lymphocytes (involving incubation of lymphocytes after UV exposure). Extracorporeal photopheresis was proposed by Richard Edelson (Yale University, USA) in 1987 as a method for cutaneous T-cell lymphoma treatment [1]. The method was originally used for effective treatment of cutaneous T-cell lymphoma. Later indications for its use were expanded: it was used to prevent transplant rejection, for autoimmune disorders [2–13]. Phototherapy with UV radiation has various effects, such as anti-inflammatory, immunosuppressive, and cytotoxic ones. The mechanisms of its action are poorly understood, but include altered antigen presentation, decreased natural killer (NK cell) activity, and apoptosis of T cells and keratinocytes. Photopheresis results in the fact that dendritic cells acquire an antigen from apoptotic lymphocytes, which causes a specific immune response without systemic immunosuppression [14]. Globally, more than 70,000 patients have undergone a total of 3 million procedures.

Positive effect of extracorporeal photopheresis on the course of experimental autoimmune encephalomyelitis (EAE) in animals has been shown [15]. The decrease in severity of clinical disease manifestations has been reported in experimental animals. Histological assessment showed that during treatment by ECP mononuclear cell infiltrates were less prominent, that in the control group. The anti-myelin basic protein antibody (anti-MBP) levels in the Lewis rats with encephalomyelitis, which received ECP, were lower, than in untreated rats (p = 0.03). After receiving ECP animals with experimental autoimmune encephalomyelitis showed a significant decrease in the levels of pro-inflammatory cytokine — tumor necrosis factor alpha (TNFα). Thus, the study results demonstrated ECP efficacy in changing EAE severity and clinical course.

Later the ECP method was used in patients with multiple sclerosis. It was shown that ECP could be effective when used for treatment of the relapsing-remitting disease form, but it did not significantly change the course of the primary progressive form [16–20]. The authors reported safety of the method and some preliminary data on the efficacy obtained when using ECP for treatment of five patients with relapsing-remitting multiple sclerosis: in the majority of cases ECP led to the decrease in relapse rate and EDSS, MRI stabilization. The authors confirmed ECP safety and tolerability; they believe that this therapy can be useful as a therapeutic alternative in the subgroup of patients with relapsing-remitting multiple sclerosis.

The search is being conducted for adequate combinations of extracorporeal photopheresis with other extracorporeal hemocorrection and drug therapy methods that can result in the improved efficacy of autoimmune disorder treatment [21, 22].

The study aimed to compare the efficacy of transimmunization and glatiramer acetate in patients with relapsing-remitting multiple sclerosis within a year.

METHODS

A total of 19 adult patients with relapsing-remitting multiple sclerosis underwent treatment by transimmunization (modified ECP method) at the Vladimirsky Moscow Regional Research and Clinical Institute. Patients over the age of 18, who did not receive treatment by other methods (DMDs for multiple sclerosis, etc.), were included in the study.

Inclusion criteria: the diagnosis of multiple sclerosis verified in accordance with the 2005 revision of the MacDonald international criteria; patients' age at the time of enrollment 18–60 years; no therapy with DMDs for multiple sclerosis before ECP prescription; EDSS disability score below 6.0 at the time of enrollment; the ability to submit the informed consent.

Exclusion criteria: unreliable diagnosis of multiple sclerosis; secondary progressive or primary progressive course; use of DMDs for multiple sclerosis before the beginning of the study; EDSS disability score over 6.0; severe cognitive impairment.

The comparison group consisted of 48 adult patients with relapsing-remitting multiple sclerosis, who were prescribed subcutaneous glatiramer acetate 20 mg daily.

Clinical assessment of the treatment efficacy was based on the data on the patients' neurological status. The Expanded Disability Status Scale (EDSS) was used. EDSS is used to determine the degree of disability depending on the patient's ability to move, as well on the impairment degree based on the FS score. EDSS scores are in the range between 0 points (normal neurological status) and 10 points (fatal outcome of multiple sclerosis). The Kurtzke scales allow one to determine the condition severity, degree of multiple sclerosis progression, and efficacy of treatment measures.

The patients' neurological status was assessed before therapy, then before each ECP course and in case of the disease exacerbation — before prescription of glucocorticoid therapy and after it.

The following 3.0 and 1.5 T MRI scanners were used for brain and spinal cord MRI:

1) Achieva 3.0 T MRI scanner with the superconducting magnet: magnetic field strength 3.0 T, sampling interval 3–5 mm; product license No. 2004/708; certificate of conformity No. ROSS NL CH01B 84154 (Philips Medical Systems Nederland B.V., Netherlands).

2) Optima MR 450 w Gem 1.5 T MRI scanner with the superconducting magnet: magnetic field strength 1.5 T, sampling interval 3–5 mm; product license No. 95/112; hygiene certificate No. 7.99.04.944.D.000967.02.01; certificate of conformity No. ROSS FR IM 02.B08001 (General Electric, USA).

MRI was performed to verify the diagnosis before ECP, every 6 months during follow-up, and in cases of suspected exacerbation of the disease.

ECP method (transimmunization)

Equipment

1. MSC+ blood component collection system (Heamonetics Corporation, USA).

Product license of the Ministry of Health of the Russian Federation 2005/119/28.09.05.

Mononuclear cells are isolated in accordance with the RBCP protocol (stem cell isolation).

Specifications:
– width: 37 cm, length: 57 cm;
– height 44 cm (when closed), 67 cm (when operated);
– weight: 28 kg;
– power supply: 220 V, 60 Hz;
– pump speed: 20–250 mL/min;
– centrifuge speed: 3000–7000 rpm;
– anticoagulant/blood ratio: from 1 : 8 to 1 : 16.

Table 1. Patient distribution by age

Age	18–27 years	28–37 years	38–47 years	48–57 years	58–67 years	≥ 68 years
Number of individuals (*n*)	8	5	3	2	1	–

Table 2. Synoptic table of medical history data

Parameters	Median (LQ, UQ, minimum, maximum)
Males / females	2/17
Age at initiation of therapy (years)	30 [LQ = 26; UQ = 47] 20–60
Age of onset (years)	23 [LQ = 21; UQ = 30] 11–51
Disease duration (years)	6 [LQ = 2,5; UQ = 10] 1–37

Anticoagulant used: sodium citrate 2.2%, citric acid monohydrate 0.8%, glucose monohydrate 2.45%, water for injection to 1000 mL.

2. Julia extracorporeal blood irradiation system OKUFKE-320/400-600/650-01 (Metom, Russia).

Product license of the Ministry of Health of the Russian Federation 29/01040502/4362-02/25.09.2002.

Specifications:

– wavelength range: LUFT-6 quartz lamp — 320–400 nm; LK-6 lamp — 600–650 nm;

– value of incident irradiance of the cell surface within the light spot equal to the dimensions of the cell flow part, at least 3 mW\cm^2 for one lamp;

– AC power supply (220 V);

– power input: no more than 50 VA;

– operation mode cycle: 20 min (operation), 10 min (break);

– weight: no more than 2 kg.

Dimensions 270 × 160 × 80 mm.

3. Disposable container for blood and its components TU 64-2-361-85. Product license number 86/1027-12-1.

4. Photosensitizing drug Ammifurin (8-methoxypsoralen) (VILAR, Russia).

Product license number LS-002598 of 26.10.2011, 20 mg pills

Extracorporeal photochemotherapy (transimmunization) procedure

The patients took oral Ammifurin (8-methoxypsoralen) 2 h before the procedure. The Haemonetics MCS+ cell separator (USA) was used to isolate mononuclear cells in accordance with the PBSC protocol. Then mononuclear cells were exposed to UV radiation for 90 min and incubated for 20 h at a temperature of 37 °C. On the next day the cells were reinfused to the patient. The procedure was conducted twice a week every month throughout 6 months.

In the beginning of treatment ECP was performed once a month throughout 6 months. Then the interval was increased by a month every time. Later treatment was performed once every 6 months. The follow-up gadolinium-enhanced brain MRI was performed once every 6 months. Methylprednisolone pulse therapy was used in cases of clinical exacerbation based on the MRI data.

Statistical analysis

Statistical processing was performed in RStudio 2023.09.0 using R v. 4.3.1. As descriptive statistics for quantitative variables, mean values and standard deviations (M ± SD), median and quartiles (Me [LQ; UQ]), minimum and maximum were calculated. The Mann-Whitney *U* test or Wilcoxon test (for related samples) was used to compare quantitative variables in two groups. Absolute (*n*) and relative (%) rates were calculated for qualitative variables. Comparison of qualitative variables in two groups was performed using Fischer's exact test. The significance level (α) was considered to be 0.05 (null hypotheses were rejected when $p < \alpha$).

RESULTS

A total of 19 patients with relapsing-remitting multiple sclerosis, who had been receiving ECP — transimmunization, had been followed-up within a year. Most of patients were aged 18–27 years (42.1%) (Table 1).

The patients' median age was 30 years (LQ = 26; UQ = 47), between 20 and 60 years (Table 2).

The majority of patients were females (89.5% females and 10.5% males). The male to female ratio was 2/17. The median age of onset was 23 years (LQ = 21; UQ = 30), between 11 and 51 years. The median disease duration was 6 years (LQ = 2.5; UQ = 10), between 1 year and 37 years.

In the majority of cases (42.11%), visual impairment was the first clinical symptom of the disease (Table 3). Sensory disorders ranked second (31.58%). The emergence of pyramidal disorder at the disease onset was reported in 10.52% of cases. Polysymptomatic onset was observed in 15.79% of cases. It included visual impairment, sensory and cerebellar disorders, brain stem and pyramidal disorders, pyramidal disorders and disorders of the pelvis.

Table 4 presents the multiple sclerosis patients' degree of disability based on the EDSS score before treatment. The highest proportion was mild disability (EDSS score ≤ 2.5). It was reported in 15 patients (78.5% of cases). Moderate disability (EDSS score 3.0–5.5) was reported in four patients (21.5%). These patients were able to move without any assistance.

The median EDSS score in the overall group of patients with relapsing-remitting multiple sclerosis, who underwent

Table 3. Clinical manifestations at the disease onset

Clinical manifestations	Abs. (%)
Visual impairment	8 (42.11%)
Sensory disorders	6 (31.58%)
Pyramidal disorders	2 (10.52%)
Polysymptomatic onset	3 (15.79%)

Table 4. Disability severity based on the EDSS score before treatment

EDSS	Group I
0–2.5 (mild disability)	78.95% (15)
3.0–5.5 (moderate disability)	21.05% (4)
Over 6.0 (severe disability)	–
Median EDSS score	1.5 [LQ = 1.5; UQ = 2.5] 1–5.5

extracorporeal photopheresis, was 2 (LQ = 1.5; UQ = 2.5), between 1 and 5.5. This score did not change after a year of treatment: 1.5 (LQ = 1; UQ = 2), between 0 and 3.5. The decrease in EDSS scores was reported in seven patients (36.84%) (see Figure).

Thus, the increase in EDSS scores in the overall group of patients relative to the previous values was reported in 5.26% of cases. In five patients, foci accumulating the contrast agent in the white matter were revealed on MRI within a year after the beginning of treatment.

In the comparison group of patients with relapsing-remitting multiple sclerosis, who underwent treatment with glatiramer acetate, the median EDSS score was 1.75 (LQ = 1.5; UQ = 2.5), between 1 and 5. The difference between this group of patients and the group of patients, who received transimmunization, was non-significant (p = 0.748). In a year the median EDSS score was 2 (LQ = 1.5; UQ = 3), between 1 and 5. The increase in EDSS score within a year after the beginning of treatment was reported in 29.27% of cases. The median EDSS scores reported after a year of treatment with extracorporeal photopheresis — transimmunization showed no negative results relative to the use of first-line DMD for multiple sclerosis, glatiramer acetate (Fig. 1).

Clinical case

The female patient aged 40 years complained of gait disorder, intermittent urinary incontinence. She got ill at the age of 29 years: weakness in the left limbs and a speech disorder emerged. Multiple demyelination foci were found on brain MRI. The ophthalmologist diagnosed partial atrophy of the optic nerve. As for neurological status, the EDSS score of 5.5 was reported. After a single ECP procedure the EDSS score decreased to 5, after four procedures — to 4.5, and after five procedures it was 2.5. Later there was a disease exacerbation, and the EDSS score increased to 3.5, but it did not get worse before the beginning of treatment. Thus, a beneficial outcome was achieved given high EDSS score and long disease duration (11 years).

DISCUSSION

The data on the use of extracorporeal photochemotherapy method and its modification (with blood lymphocyte incubation) in patients with relapsing-remitting multiple sclerosis are reported. The method has proven itself over a long time in various disorders associated of autoimmune manifestations (graft-versus-host disease, autoimmune manifestations in coronavirus infection, Crohn's disease, etc.) [23]. A number of authors used the ECP method without lymphocyte incubation in combination with plasmapheresis in 40 patients with multiple sclerosis [24–26]. When the anti-myelin basic protein antibody levels exceeded 500 μg/L, plasma was removed, and lymphocytes were exposed to UV radiation. When the anti-myelin basic protein antibody concentration was below 500 μg/L, the extracted plasma with the lymphocyte suspension was irradiated and then reinfused. In 36 patients (90%), good and satisfactory therapeutic effect was achieved assessed based on the neurological deficit regression according to the EDSS scores (good effect — 2 points, satisfactory effect — 1 point). In four patients, the effect was considered to be negligible. Patient's condition deterioration or side effect was reported in none of the cases. A one-year follow-up revealed no disease progression. Improvement in the form of EDSS score decrease by 1–2 points was observed. The anti-myelin basic protein antibody titer decreased 2-fold relative to baseline. The decrease in the CD16 natural killer cell and CD4 T helper counts, as well as in mitogen-induced γ-IFN production was

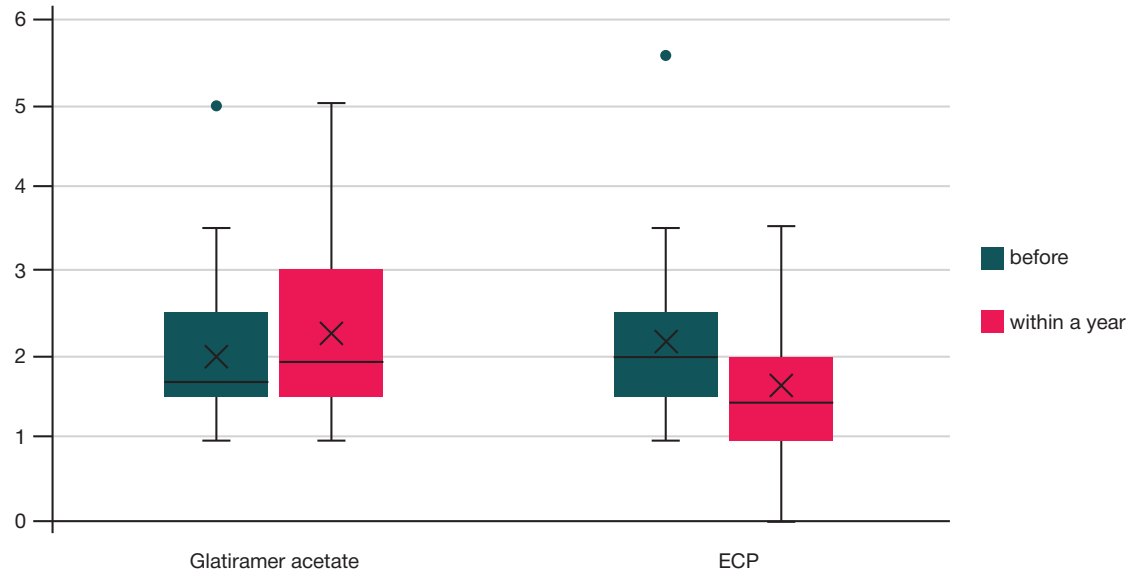

Fig. Changes in EDSS scores of patients with multiple sclerosis treated using extracorporeal photopheresis (ECP) and glatiramer acetate

reported. Examination of patients within 6 months of follow-up revealed no disease exacerbation.

In this study we compared the modified ECP (transimmunization) and glatiramer acetate efficacy in patients with relapsing-remitting multiple sclerosis during the one-year follow-up. The findings show that transimmunization can be comparable with conventional treatment methods, such as glatiramer acetate, which shows that new approaches to therapy of this disease are possible.

Multiple sclerosis is a complex autoimmune disorder, and treatment of the disorder requires a personalized approach. The use of ECP based on the lymphocyte UV exposure has shown its efficacy in terms of decreasing the median EDSS score in patients receiving transimmunization from 2 to 1.5 points. Such a decrease indicates neurological status improvement and stability of the condition in a large number of patients, which represents an important aspect of multiple sclerosis treatment.

Comparison with the group of patients taking glatiramer acetate has shown that the median EDSS score of this group has remained fairly constant: it increased from 1.75 to 2 points. This suggests that transimmunization may not only be effective, but also more preferable for patients, who do not tolerate conventional treatment methods or have side effects.

It is important to note that ECP and its modifications, such as transimmunization, cause no allergy or generation of autoantibodies, which makes these a safe alternative for patients having contraindications for drugs. This is particularly true in the light of the growing need for the development of new treatment methods considering the patients' individual characteristics. However, it should be considered that in our study the increase in EDSS score was observed in some patients, which emphasizes the importance of continuous monitoring of patients' condition and possible use of pulse therapy for rapid exacerbation management. When performing further research, it is necessary to focus on the longer patient follow-up and assessment of the long-term transimmunization effects, as well as on studying its combinations with other treatment methods.

Our findings confirm the possibility of using transimmunization as an effective method for treatment of relapsing-remitting multiple sclerosis.

CONCLUSIONS

The data of the one-year follow-up of patients with relapsing-remitting multiple sclerosis undergoing non-pharmacological treatment by transimmunization, the modified ECP method, are reported. The procedure was prescribed every month throughout up to six months, then the interval was increased by a month every time, and then transimmunization was performed once every six months. The patients had mild-to-moderate disability based on the EDSS scores before the beginning of treatment. During the one-year follow-up we noted a decrease in the median total EDSS score from 2 to 1.5 points. In one case, the increase in EDSS score following the improvement of the patient's clinical condition within six months of transimmunization, but it did not reach the value reported before the beginning of treatment. In the comparison group of patients taking glatiramer acetate, there were also cases of the EDSS score increase relative to baseline requiring methylprednisolone pulse therapy. We have revealed no negative effect of transimmunization on the course of multiple sclerosis within a year of patient follow-up. Thus, the use of blood transimmunization is comparable with the use of first-line DMDs for multiple sclerosis, it causes no allergy or addiction (generation of antibodies against the protein drug), and can be recommended as both initial therapy and therapy after unsuccessful use of first-line DMDs for multiple sclerosis due to side effects. Since it is impossible to completely modify the patients' immune status, the disease exacerbations and the use of pulse therapy for rapid suppression of the active autoimmune process accompanied by inflammation in the central nervous system are possible when performing ECP, as when using other multiple sclerosis treatment methods. To assess the ECP effect on the course of multiple sclerosis, it is possible to follow up these patients undergoing treatment over a longer time. This method can be used in clinical practice for patients with multiple sclerosis as one of the first-line methods to prevent the disease progression. Further studies can be aimed to assess the transimmunization mechanism of action at the cellular level and assess its efficacy when combined with other non-pharmacological treatment methods.

References

1. Edelson R, Berger C, Gasparro F, Jegasothy B, Heald P, Wintroub B, et al. New therapies for cutaneous T-cell lymphoma. N Engl J Med. 1987; 316 (6): 297–303. DOI: 10.1056/NEJM198702053160603.
2. Michallet M, Sobh M, Deloire A, Revesz D, Chelgoum Y, El-Hamri M. Second line extracorporeal photopheresis for cortico-resistant acute and chronic GVHD after allogeneic hematopoietic cell transplantation for hematological malignancies: Long-term results from a real-life study. Transfus Apher Sci. 2024; 63 (3): 103899. DOI: 10.1016/j.transci.2024.103899.
3. Rastogi S, Kim EJ, Gelfand JM, Loren AW, Baumrin E. Chronic Graft-versus-Host Disease-Associated Muscle Cramps: Severity and Response to Immunomodulatory Therapies. Transplant Cell Ther. 2024; 30 (3): 338.e1–338.e6. DOI: 10.1016/j.jtct.2023.12.674.
4. Kim D, Taparia M, Robinson E, Mcgee M, Merali T. Navigating the Complexity of Chronic Graft-vs-Host Disease: Canadian Insights into Real-World Treatment Sequencing.Transplant Proc. 2024; 56 (2): 409–15. DOI: 10.1016/j.transproceed.2023.12.021.
5. Ruf T, Rahimi F, Anz D, Tufman A, Salzer S, Zierold S, et al. Extracorporeal Photopheresis as a Treatment Option for Immune-Related Adverse Events: Two Case Reports and a Prospective Study. J Immunother. 2024. DOI: 10.1097/CJI.0000000000000510.
6. Lin Y, Cheng Z, Zhong Y, Zhao Y, Xiang G, Li L, et al. Extracorporeal photopheresis reduces inflammation and joint damage in a rheumatoid arthritis murine model. J Transl Med. 2024; 22 (1): 305. DOI: 10.1186/s12967-024-05105-x.
7. Fisher AJ, White M, Goudie N, Kershaw A, Phillipson J, Bardgett M, et al. Extracorporeal photopheresis (ECP) in the treatment of chronic lung allograft dysfunction (CLAD): a prospective, multicentre, open-label, randomised controlled trial studying the addition of ECP to standard care in the treatment of bilateral lung transplant patients with CLAD (E-CLAD UK). BMJ Open Respir Res. 2024; 11 (1): e001995. DOI: 10.1136/bmjresp-2023-001995.
8. Lionet A, Van Triempon M, Figeac M, Fages V, Gibier JB, Provot F, et al. Extracorporeal Photopheresis Reduces Fibrotic and Inflammatory Transcriptomic Biological Marker of Chronic Antibody-mediated Kidney Rejection. Transplant Direct. 2024; 10 (3): e1587. DOI: 10.1097/TXD.0000000000001587.
9. Mitsunaga K, Bagot M, Ram-Wolff C, Guenova E, von Gugelberg C, Hodak E, et al. Real-world study on the use of pegylated interferon alpha-2a for treatment of mycosis fungoides/Sézary syndrome using Time to Next Treatment as a measure of clinical benefit: An EORTC CLTG study. Br J Dermatol. 2024: 152. DOI: 10.1093/bjd/ljae152.
10. Castillo-Aleman YM, Krystkowiak PC. Extracorporeal photopheresis in stiff person syndrome. Front Immunol. 2024; 15: 1519032. DOI:

10.3389/fimmu.2024.1519032. eCollection 2024.
11. Szabó BG, Reményi P, Tasnády S, Korózs D, Gopcsa L, Réti M, et al. Extracorporeal Photopheresis as a Possible Therapeutic Approach for Adults with Severe and Critical COVID-19 Non-Responsive to Standard Treatment: A Pilot Investigational Study. J Clin Med. 2023; 12 (15): 5000. DOI: 10.3390/jcm12155000.
12. Kildyushevsky AV, Molochkov AV, Zhuravlev OR, Mitina TA, Belousov KA, Zakharov SG, et al. Jekstrakorporal'nyj fotoferez v lechenii novogo koronavirusnogo zabolevanija COVID-19 (serija klinicheskih nabljudenij). Al'manah klinicheskoj medicinyju. 2020; 48 (Specvypusk 1): 11–19. DOI: 10.18786/2072-0505-2020-48-039. Russian.
13. Neretin V Ya, Kildyushevsky AV, Agafonov BV, Geht BM, Sidorova OP, Ospennikova TP. Fotoferez — novyj metod lechenija miastenii. Zhurnal nevrologii i psihiatrii im. S. S. Korsakova. 2002; 103 (6): 11–14. PMID: 12872619. Russian.
14. Rathod DG, Muneer H, Masood S. Phototherapy In: StatPearls [Internet]. Treasure Island (FL): StatPearls Publishing; 2024. PMID: 33085287.
15. Lolli F, Liuzzi GM, Vergelli M, Massacesi L, Ballerini C, Amaducci L, et al. Antibodies specific for the lipid-bound form of myelin basic protein during experimental autoimmune encephalomyelitis. J Neuroimmunol. 1993; 44: 69–75. DOI: 10.1016/0165-5728(93)90269-5.
16. Cavaletti G, Perseghin P, Dassi M, Oggioni N, Sala F, Lolli F, et al. Extracorporeal photochemopherapy reduces the incidence of relapses in experimental allergic encephalomyelitis in DA rats. J Neurol. 2001; 248 (6): 535–6. DOI: 10.1007/s004150170169.
17. Cavaletti G, Perseghin P, Buscemi F, Dassi M, Oggioni N, Sala F, et al. Immunomodulationg effects of extracorporeal photochemotherapy (ECP) in rats experimental allergic encephalomyelitis (EAE). Int J Tissue React. 2001; 23 (1): 21–31. PMID: 11392060.
18. Cavaletti G, Perseghin P, Dassi M, Oggioni N, Sala F, Braga M, et al. Extracorporeal photochemotherapy reduces the severity of Lewis rat experimental allergic encephalomyelitis through a modulation of the function of peripheral blood mononuclear cells. J Biol Regul Homeost Agents. 2004; 18 (1): 9–17. PMID: 15323355.
19. Cavaletti G, Perdeghin P, Dassi M, Oggioni N, Sala F, Braga M, et al. Extracorporeal photochemotherapy reduces the severity of Lewis rat experimental allergic encephalomyelitis through a modulation of the function of peripheral blood mononuclear cells. J Biological Regulators and Homeostatic Agents. 2004; 18 (1): 9–17. PMID: 15323355.
20. Cavaletti G, Perseghin P, Dassi M, Cavarretta R, Frigo M, Caputo D, et al. Extracorporeal photochemotherapy: a safety and tolerability pilot study with preliminary efficacy results in refractory relapsing-remitting multiple sclerosis. Neurol Sci. 2006; 27 (1): 24–32. PubMed PMID: 16688596.
21. Extracorporeal photopheresis: Medical Coverage Guidelines of the Blue Cross and Blue Shield Association of Arizona. 2012; 5 p.
22. Ninosu N, Melchers S, Kappenstein M, Booken N, Hansen I, Blanchard M, et al. Mogamulizumab Combined with Extracorporeal Photopheresis as a Novel Therapy in Erythrodermic Cutaneous T-cell Lymphoma. Cancers (Basel). 2023; 27–16 (1): 141. DOI: 10.3390/cancers16010141.
23. Neretin VYa, Kildyushevsky AV, Ozerova IV, Kotov SV, Golenkov AK. Method of treatment of patients with autoimmune diseases. The 2000 Russian patent on IPC A61M1/38 A61N5/06 2000-11-27. Publication 1999–01–29. Russian.
24. Neretin VYa, Kotov SV, Kildyushevsky AV, Sidorova OP, Ozerova IV. Jekstrakorporal'naja fotohimioterapija v lechenii bol'nyh rassejannym sklerozom. Uchebnoe posobie. M.: MONIKI, 2003; 11 s. Russian.
25. Ozerova IV, Kotov SV, Neretin VYa, Kildyushevsky AV. Jekstrakorporal'naja fotohimioterapija v lechenii bol'nyh rassejannym sklerozom. V sbornike: Materialy k Respublikanskomu rabochemu soveshhaniju «Voprosy diagnostiki i lechenija demielinizirujushhih zabolevanij nervnoj sistemy»; 23–24 fevralja 1999. Stupino; s. 180–182. Russian.

Литература

1. Edelson R, Berger C, Gasparro F, Jegasothy B, Heald P, Wintroub B, et al. New therapies for cutaneous T-cell lymphoma. N Engl J Med. 1987; 316 (6): 297–303. DOI: 10.1056/NEJM198702053160603.
2. Michallet M, Sobh M, Deloire A, Revesz D, Chelgoum Y, El-Hamri M. Second line extracorporeal photopheresis for cortico-resistant acute and chronic GVHD after allogeneic hematopoietic cell transplantation for hematological malignancies: Long-term results from a real-life study. Transfus Apher Sci. 2024; 63 (3): 103899. DOI: 10.1016/j.transci.2024.103899.
3. Rastogi S, Kim EJ, Gelfand JM, Loren AW, Baumrin E. Chronic Graft-versus-Host Disease-Associated Muscle Cramps: Severity and Response to Immunomodulatory Therapies. Transplant Cell Ther. 2024; 30 (3): 338.e1–338.e6. DOI: 10.1016/j.jtct.2023.12.674.
4. Kim D, Taparia M, Robinson E, Mcgee M, Merali T. Navigating the Complexity of Chronic Graft-vs-Host Disease: Canadian Insights into Real-World Treatment Sequencing.Transplant Proc. 2024; 56 (2): 409–15. DOI: 10.1016/j.transproceed.2023.12.021.
5. Ruf T, Rahimi F, Anz D, Tufman A, Salzer S, Zierold S, et al. Extracorporeal Photopheresis as a Treatment Option for Immune-Related Adverse Events: Two Case Reports and a Prospective Study. J Immunother. 2024. DOI: 10.1097/CJI.0000000000000510.
6. Lin Y, Cheng Z, Zhong Y, Zhao Y, Xiang G, Li L, et al. Extracorporeal photopheresis reduces inflammation and joint damage in a rheumatoid arthritis murine model. J Transl Med. 2024; 22 (1): 305. DOI: 10.1186/s12967-024-05105-x.
7. Fisher AJ, White M, Goudie N, Kershaw A, Phillipson J, Bardgett M, et al. Extracorporeal photopheresis (ECP) in the treatment of chronic lung allograft dysfunction (CLAD): a prospective, multicentre, open-label, randomised controlled trial studying the addition of ECP to standard care in the treatment of bilateral lung transplant patients with CLAD (E-CLAD UK). BMJ Open Respir Res. 2024; 11 (1): e001995. DOI: 10.1136/bmjresp-2023-001995.
8. Lionet A, Van Triempon M, Figeac M, Fages V, Gibier JB, Provot F, et al. Extracorporeal Photopheresis Reduces Fibrotic and Inflammatory Transcriptomic Biological Marker of Chronic Antibody-mediated Kidney Rejection. Transplant Direct. 2024; 10 (3): e1587. DOI: 10.1097/TXD.0000000000001587.
9. Mitsunaga K, Bagot M, Ram-Wolff C, Guenova E, von Gugelberg C, Hodak E, et al. Real-world study on the use of pegylated interferon alpha-2a for treatment of mycosis fungoides/Sézary syndrome using Time to Next Treatment as a measure of clinical benefit: An EORTC CLTG study. Br J Dermatol. 2024: 152. DOI: 10.1093/bjd/ljae152.
10. Castillo-Aleman YM, Krystkowiak PC. Extracorporeal photopheresis in stiff person syndrome. Front Immunol. 2024; 15: 1519032. DOI: 10.3389/fimmu.2024.1519032. eCollection 2024.
11. Szabó BG, Reményi P, Tasnády S, Korózs D, Gopcsa L, Réti M, et al. Extracorporeal Photopheresis as a Possible Therapeutic Approach for Adults with Severe and Critical COVID-19 Non-Responsive to Standard Treatment: A Pilot Investigational Study. J Clin Med. 2023; 12 (15): 5000. DOI: 10.3390/jcm12155000.
12. Кильдюшевский А. В., Молочков А. В., Журавлев О .Р., Митина Т. А., Белоусов К. А., Захаров С. Г., и др. Экстракорпоральный фотоферез в лечении нового коронавирусного заболевания COVID-19 (серия клинических наблюдений). Альманах клинической медициныю. 2020; 48 (Спецвыпуск 1): 11–19. DOI: 10.18786/2072-0505-2020-48-039.
13. Неретин В. Я., Кильдюшевский А. В., Агафонов Б. В., Гехт Б. М., Сидорова О. П., Оспенникова Т. П. Фотоферез — новый метод лечения миастении. Журнал неврологии и психиатрии им. С. С. Корсакова. 2002; 103 (6): 11–14. PMID: 12872619.
14. Rathod DG, Muneer H, Masood S. Phototherapy In: StatPearls [Internet]. Treasure Island (FL): StatPearls Publishing; 2024. PMID: 33085287.
15. Lolli F, Liuzzi GM, Vergelli M, Massacesi L, Ballerini C, Amaducci L, et al. Antibodies specific for the lipid-bound form of myelin basic protein during experimental autoimmune encephalomyelitis. J Neuroimmunol. 1993; 44: 69–75. DOI: 10.1016/0165-5728(93)90269-5.
16. Cavaletti G, Perseghin P, Dassi M, Oggioni N, Sala F, Lolli F, et al. Extracorporeal photochemopherapy reduces the incidence of

relapses in experimental allergic encephalomyelitis in DA rats. J Neurol. 2001; 248 (6): 535–6. DOI: 10.1007/s004150170169.
17. Cavaletti G, Perseghin P, Buscemi F, Dassi M, Oggioni N, Sala F, et al. Immunomodulationg effects of extracorporeal photochemotherapy (ECP) in rats experimental allergic encephalomyelitis (EAE). Int J Tissue React. 2001; 23 (1): 21–31. PMID: 11392060.
18. Cavaletti G, Perseghin P, Dassi M, Oggioni N, Sala F, Braga M, et al. Extracorporeal photochemotherapy reduces the severity of Lewis rat experimental allergic encephalomyelitis through a modulation of the function of peripheral blood mononuclear cells. J Biol Regul Homeost Agents. 2004; 18 (1): 9–17. PMID: 15323355.
19. Cavaletti G, Perdeghin P, Dassi M, Oggioni N, Sala F, Braga M, et al. Extracorporeal photochemotherapy reduces the severity of Lewis rat experimental allergic encephalomyelitis through a modulation of the function of peripheral blood mononuclear cells. J Biological Regulators and Homeostatic Agents. 2004; 18 (1): 9–17. PMID: 15323355.
20. Cavaletti G, Perseghin P, Dassi M, Cavarretta R, Frigo M, Caputo D, et al. Extracorporeal photochemotherapy: a safety and tolerability pilot study with preliminary efficacy results in refractory relapsing-remitting multiple sclerosis. Neurol Sci. 2006; 27 (1): 24–32. PubMed PMID: 16688596.
21. Extracorporeal photopheresis: Medical Coverage Guidelines of the Blue Cross and Blue Shield Association of Arizona. 2012; 5 p.
22. Ninosu N, Melchers S, Kappenstein M, Booken N, Hansen I, Blanchard M, et al. Mogamulizumab Combined with Extracorporeal Photopheresis as a Novel Therapy in Erythrodermic Cutaneous T-cell Lymphoma. Cancers (Basel). 2023; 27–16 (1): 141. DOI: 10.3390/cancers16010141.
23. Неретин В. Я., Кильдюшевский А. В., Озерова И. В., Котов С. В., Голенков А. К. Способ лечения пациентов аутоиммунными заболеваниями. Российский патент 2000 г. по МПК A61M1/38 A61N5/06 2000-11-27. Публикация 1999-01-29.
24. Неретин В. Я., Котов С. В., Кильдюшевский А. В., Сидорова О. П., Озерова И. В. Экстракорпоральная фотохимиотерапия в лечении больных рассеянным склерозом. Учебное пособие. М.: МОНИКИ, 2003; 11 с.
25. Озерова И. В., Котов С. В., Неретин В. Я., Кильдюшевский А. В. Экстракорпоральная фотохимиотерапия в лечении больных рассеянным склерозом. В сборнике: Материалы к Республиканскому рабочему совещанию «Вопросы диагностики и лечения демиелинизирующих заболеваний нервной системы»; 23–24 февраля 1999. Ступино; с. 180–182.

MORPHOLOGICAL SUBCHONDRAL BONE TISSUE CHARACTERISTICS IN KNEE OSTEOARTHRITIS

Minasov BSh[1], Yakupov RR[1], Akbashev VN[1] ✉, Shchekin VS[1], Vlasova AO[1], Minasov TB[1], Karimov KK[2], Akhmeldinova AA[1]

[1] Bashkir State Medical University, Ufa, Russia

[2] Avicenna Tajik State Medical University, Dushanbe, Tajikistan

Morphological subchondral bone tissue alterations associated with knee osteoarthritis represent a key pathogenesis link and can precede articular cartilage destruction. The study aimed to identify typical morphological and morphometric signs of osteosclerosis and osteoporosis in the subchondral zone of the femur and tibia. Analysis of 40 bone tissue fragments collected when performing knee replacement surgery in 20 patients (12 females and 8 males) aged 58–75 years with stage III–IV osteoarthritis was performed. Histological and morphometric assessment involving the use of light microscopy and microfracture index (MFI) calculation revealed significant differences in trabecular thickness, intertrabecular distance, and the degree of microdamage between the sites of sclerosis and osteoporosis. High MFI values in the zones of osteoporosis can reflect reduced subchondral bone strength. The findings confirm the diagnostic value of the subchondral zone morphometry and the prospects of using MFI as a quantitative risk criterion when planning orthopedic treatment.

Keywords: osteoarthritis, subchondral bone, osteosclerosis, osteoporosis, morphometry, microcracks, microfracture index

Author contribution: Minasov BSh — study concept and design, data analysis and interpretation, manuscript editing; Yakupov RR — material collection, morphological assessment, primary data processing; Akbashev VN — statistical processing, visualization of results, manuscript writing; Shchekin VS — literature review, morphology data interpretation; Vlasova AO — preparing illustrations, morphometry analysis, manuscript proofreading; Minasov TB — preparing illustrations, discussion; Karimov KK — material collection, clinical follow-up of patients; Akhmeldinova AA — drawing up inclusion/exclusion criteria, coordination of ethical approval.

Compliance with ethical standards: the study was approved by the Ethics Committee of the Bashkir State Medical University (protocol No. 3 dated 12 March 2025) and conducted in accordance with the World Medical Association Declaration of Helsinki (2013 revision). All patients submitted the informed consent to participation in the study.

✉ **Correspondence should be addressed:** Vladislav N. Akbashev
Lenina, 3, Ufa, 450008, Russia; vlad-akb@mail.ru

Received: 06.04.2025 **Accepted:** 20.04.2025 **Published online:** 30.04.2025

DOI: 10.24075/brsmu.2025.024

МОРФОЛОГИЧЕСКАЯ ХАРАКТЕРИСТИКА СУБХОНДРАЛЬНОЙ КОСТНОЙ ТКАНИ ПРИ ОСТЕОАРТРОЗЕ КОЛЕННОГО СУСТАВА

Б. Ш. Минасов[1], Р. Р. Якупов[1], В. Н. Акбашев[1] ✉, В. С. Щекин[1], А. О. Власова[1], Т. Б. Минасов[1], К. К. Каримов[2], А. А. Ахмельдинова[1]

[1] Башкирский государственный медицинский университет, Уфа, Россия

[2] Таджикский государственный медицинский университет имени Абуали ибни Сино, Душанбе, Таджикистан

Морфологические изменения субхондральной костной ткани при остеоартрозе коленного сустава являются ключевым звеном патогенеза и могут предшествовать разрушению суставного хряща. Целью исследования было выявить характерные морфологические и морфометрические признаки остеосклероза и остеопороза в субхондральной зоне бедренной и большеберцовой костей. Выполняли анализ 40 участков костной ткани, полученных при эндопротезировании коленного сустава у 20 пациентов (12 женщин и 8 мужчин) в возрасте 58–75 лет с остеоартрозом III–IV стадий. При гистологической и морфометрической оценке с использованием световой микроскопии и расчетом индекса микрофрактуринга (MFI) установлены достоверные различия в толщине трабекул, интертрабекулярном расстоянии и степени микроповреждений между участками склероза и остеопороза. Повышенные значения MFI в зонах остеопороза могут отражать снижение прочности субхондральной кости. Полученные данные подтверждают диагностическую значимость морфометрической оценки субхондральной зоны и перспективность применения MFI как количественного критерия риска при планировании ортопедического лечения.

Ключевые слова: остеоартроз, субхондральная, кость, остеосклероз, остеопороз, морфометрия, микротрещины, индекс микрофрактуринга

Вклад авторов: Б. Ш. Минасов — концепция и дизайн исследования, анализ и интерпретация данных, редактирование текста; Р. Р. Якупов — сбор материала, морфологическое исследование, первичная обработка данных; В. Н. Акбашев — статистическая обработка, визуализация результатов, написание рукописи; В. С. Щекин — анализ литературы, интерпретация морфологических данных; А. О. Власова — подготовка иллюстраций, морфометрический анализ, корректирование текста; Т. Б. Минасов — оформление и подготовка иллюстраций, обсуждение; К. К. Каримов — сбор материала, клиническое наблюдение пациентов; А. А. Ахмельдинова — составление критериев включения/исключения, координация этического одобрения.

Соблюдение этических стандартов: исследование одобрено этическим комитетом ФГБОУ ВО «Башкирский государственный медицинский университет» Минздрава России (протокол № 3 от 12 марта 2025 г.), проведено с соблюдением Хельсинкской декларации Всемирной медицинской ассоциации (в редакции 2013 г.). Все пациенты подписали добровольное информированное согласие на участие в исследовании.

✉ **Для корреспонденции:** Владислав Николаевич Акбашев
ул. Ленина, д. 3, г. Уфа, 450008, Россия; vlad-akb@mail.ru

Статья получена: 06.04.2025 **Статья принята к печати:** 20.04.2025 **Опубликована онлайн:** 30.04.2025

DOI: 10.24075/vrgmu.2025.024

Osteoarthritis (OA) is one of the most common and socially significant musculoskeletal disorders representing a progressive multifactorial connective tissue lesion resulting in disturbed kinematic balance of the skeleton. It is accompanied by acute and chronic pain, limited mobility and high disability likelihood, especially in elderly people. According to the WHO data, more than 240 million people suffer from symptomatic OA, and their number continues to grow steadily with increasing longevity [1, 2]. The current understanding of the OA pathogenesis is beyond the limits of local articular cartilage damage. Today, this disorder is considered as a systemic connective tissue biomechanics and metabolism impairment, due to which all joint components are affected: cartilage, subchondral bone, synovial membrane, tendons, capsule, and periarticular muscles [3, 4]. Imbalance between adaptive and destructive processes occurring under exposure to overload, inflammation, and disturbed tissue homeostasis becomes a central element [5]. In recent years, special attention is paid to the subchondral bone as a key link of the OA pathogenesis. It has been found that alterations of its structure, including osteosclerosis, osteoporosis, subchondral microcracks, and trabecular remodeling, can precede cartilage degeneration and significantly affect the disease progression [6–8]. Such alterations are considered as effects of chronic overload and impaired mechanotransduction in the context of unstable biomechanical equilibrium.

Structural failure of the subchondral bone playing a role of both biomechanical cartilage support and metabolic process regulator is among the key links of OA pathogenesis [9]. Clinically, stepwise disease development is manifested by a complex of sclerotic, osteoporotic, and osteolytic processes. A simultaneous presence of those generates heterogeneous morphological features reflecting a conflict between compensatory and destructive alterations. Such transformations are not limited to anatomy: these are associated with impaired kinematic links, changes of the stress load vector and, as a result, clinical manifestations of pain and dysfunction [10].

The OA biomechanical aspect becomes a key issue due to galloping development of excessive lateral pressure syndrome. The joint functions as a single system maintaining the kinematic balance owing to liquid crystal connective tissue organization [11]. Disruption of this balance leads to overload of distinct components and triggers the cascade of destructive and dystrophic responses. The changing landscape of intra-tissue tension oppresses the role of mechanostat cells. The liquid crystal organization imbalance leads to mechanocyte death.

Visualization and quantification of these processes have become possible due to advanced histological and morphometric methods. Assessment of the subchondral bone thin sections involving the use of digital technologies allows one to identify alterations at the micro level, including trabecular architecture rearrangement, subchondral sclerosis, osteophytosis, and osteolysis. These data make it possible to not only clarify the diagnosis, but also evaluate the disease stage, predict the disease course and adaptation resources of the macroorganism [12].

In this regard, an integrative multifactorial approach combining biomechanics, morphology and clinical assessment is becoming increasingly important. True nature of OA, not as a local disorder of the joint, but as the systemic connective tissue dysfunction under conditions of unstable dynamic equilibrium, can be understood only within the limits of this model.

The study aimed to identify morphological and morphometric features of subchondral bone tissue in patients with stage III–IV knee OA, identify the differences between the areas of osteosclerosis and osteoporosis, and substantiate the microfracture index (MFI) as a quantitative criterion of the subchondral zone structural integrity.

METHODS

The study was conducted at the Laboratory of Morphology of the Institute of Fundamental Medicine, Bashkir State Medical University.

Inclusion criteria: patients aged over 55 year; clinically and radiologically verified stage III–IV primary (idiopathic) osteoarthritis according to the Kellgren–Lawrence classification, disease duration of at least 5 years; total knee replacement surgery; availability of the informed consent.

Exclusion criteria: rheumatic disease; systemic metabolic disorder (including osteoporosis verified by densitometry); malignant neoplasms; previous surgical management of the same joint; decompensated chronic disorder; infection in the area of the operated joint; long-term use of steroid hormones; refusal to participate in the study.

Research material

A total of 20 patients (12 females and 8 males) aged 58–75 years (average age 66.4 ± 5.2 years), who underwent elective total knee replacement due to stage III–IV osteoarthritis (according to the Kellgren–Lawrence classification), were included in the study. During surgery specimens were collected by standard method from similar sites determined by the priority force-stress vector and outside this (internal and external condyles of the femur and tibia). The specimen size was 10 × 15 mm. The subchondral bone tissue fragments showing signs of bone compaction (osteosclerosis) or loss (osteoporosis) were identified in all patients. In a number of cases, alterations of both types were found in the same sample, which enabled intra-object comparison.

A total of 40 bone tissue fragments were assessed: 20 showing signs of osteosclerosis and 20 showing signs of osteoporosis. Despite the possibility of obtaining up to 80 fragments (4 zones per patient), 40 most informative ones were selected for morphometric assessment — two zones per patient: one showing signs of osteosclerosis, another showing signs of osteoporosis. This enabled intra-object comparison of different types of alterations, increasing the comparative analysis accuracy.

Histological processing methods

Specimens were immediately fixed in the 10% buffered neutral formalin (Histosafe; Biovitrum, Russia) for 24–48 h at a temperature of +4 °C. Decalcification was performed using the Trilon B solution (AGAT-MED, Russia) until the mineral component was completely removed. Histological processing was performed using the automated carousel-type processor (AGOT-1, Russia) and increasing concentrations of isopropyl alcohols. Paraffin embedding was accomplished using the reagents manufactured by Biovitrum (Russia). The 4 μm slices were cut using the HM340E rotary microtome (Thermo Fisher Scientific, USA). Histological slides were stained with hematoxylin and eosin (Biovitrum, Russia) using the Gemini AS automated slide stainer (Thermo Fisher Scientific, USA).

Microscopy and digital processing

The stained slides were scanned with the Pannoramic 250 digital scanning microscope (3DHISTECH Ltd., Hungary) with the Plan-APOCHROMAT 20× lens (Zeiss, Germany). Histological slides were assessed using the CaseViewer (3DHISTECH Ltd., Hungary) and QuPath v.0.5.1 (Bankhead P. et al., Sci Rep 7, 16878, 2017) software tools.

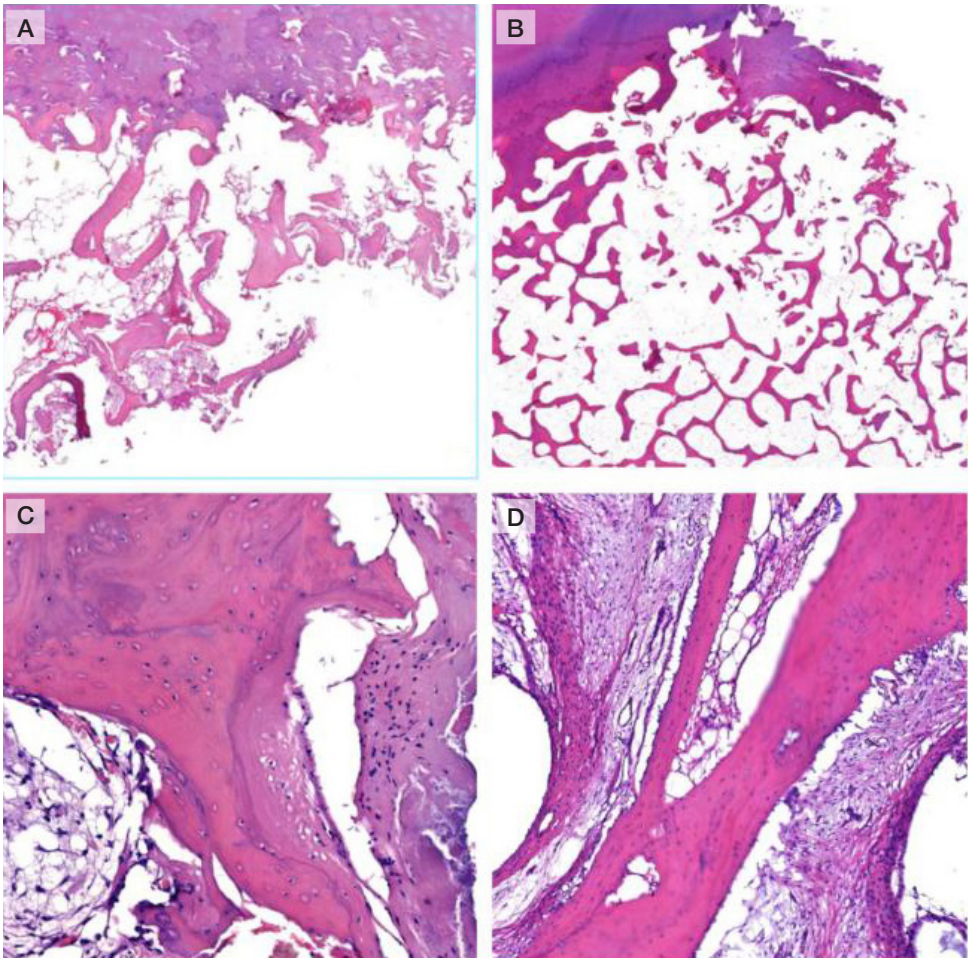

Fig. 1. Morphological alterations in the areas of subchondral bone sclerosis in osteoarthritis. Histological slides stained with hematoxylin and eosin; 20× (**A**, **B**), 200× (**C**, **D**) magnification. **A**. Fragment of the femoral subchondral zone: thickened trabeculae, anastomosing trabecular structure, narrowed intertrabecular spaces. **B**. Fragment of the tibia: huge osteosclerotic trabeculae, chaotic arrangement, reduced number of haversian canals, intratrabecular space partially replaced with fibrous tissue. **C**. Paratrabecular zone showing signs of sclerotic rearrangement: disorganized lamellar structure, foci of replacement with connective tissue. **D**. Bone marrow space: diffuse replacement with fibrous tissue with predominance of collagen fibers, trabeculae with reduced osteocytic lacunae

Morphometry analysis

The following parameters were measured in five independent fields of view with the 100× magnification:

1) trabecular thickness (μm);
2) intertrabecular distance (μm);
3) width of the basophil band (tidemark) at the boundary of the cartilage and subchondral zones (μm).

When performing morphometry, the calcified cartilage zone visualized as the intensely stained basophil layer in the hematoxylin and eosin stained slides was considered the basophil band. Measurements were performed in the most perpendicular areas between the cartilage border and the beginning of the trabecular bone. The stained band width was considered instead of cellular elements.

Morphometry was performed manually using the QuPath features. In addition, the amount of bone tissue microdamage (microcracks) per studied area (mm^2) was calculated.

Statistical analysis

Statistical data processing was performed using the Statistica 13.0 (StatSoft Inc., USA) and GraphPad Prism 9.0 (GraphPad Software, USA) software packages. The distribution of samples was tested for normality using the Shapiro–Wilk test. Since the distribution of most parameters was non-normal, quantitative data were presented as the median and interquartile range (Me (25–75%)). The Mann–Whitney *U* test was used to compare independent groups, and the Kruskal–Wallis H test was used to compare more than two groups, with subsequent pairwise comparison. The differences were considered significant at $p < 0.05$.

RESULTS

Microscopic examination of subchondral bone tissue specimens from the femur and tibia of patients with osteoarthritis revealed typical histological alterations corresponding to two opposing disease processes: osteosclerosis and osteoporosis.

In the areas of bone sclerosis (BS), marked trabecular thickening with enhanced bone matrix production was observed. The trabeculae anastomosed tightly with each other formed coarse fibrous structures (Fig. 1A, B). Intertrabecular spaces were significantly narrowed and partially replaced by fibrous tissue (Fig. 1B). In specific cases, foci of endosteal fibrosis, degenerative changes in osteocytes, and focal osteoblast hyperplasia were reported (Fig. 1C, D).

In the areas of bone tissue loss (BTL), the opposite was observed: severe thinning and fragmentation of bone trabeculae, dilated intertrabecular spaces filled mostly with adipose tissue. Numerous microcracks were reported in atrophic trabeculae, along with sporadic osteoblasts against the background of increased osteoclast counts (Fig. 2).

Morphometric analysis revealed significant differences in trabecular width and intertrabecular distances between BS and

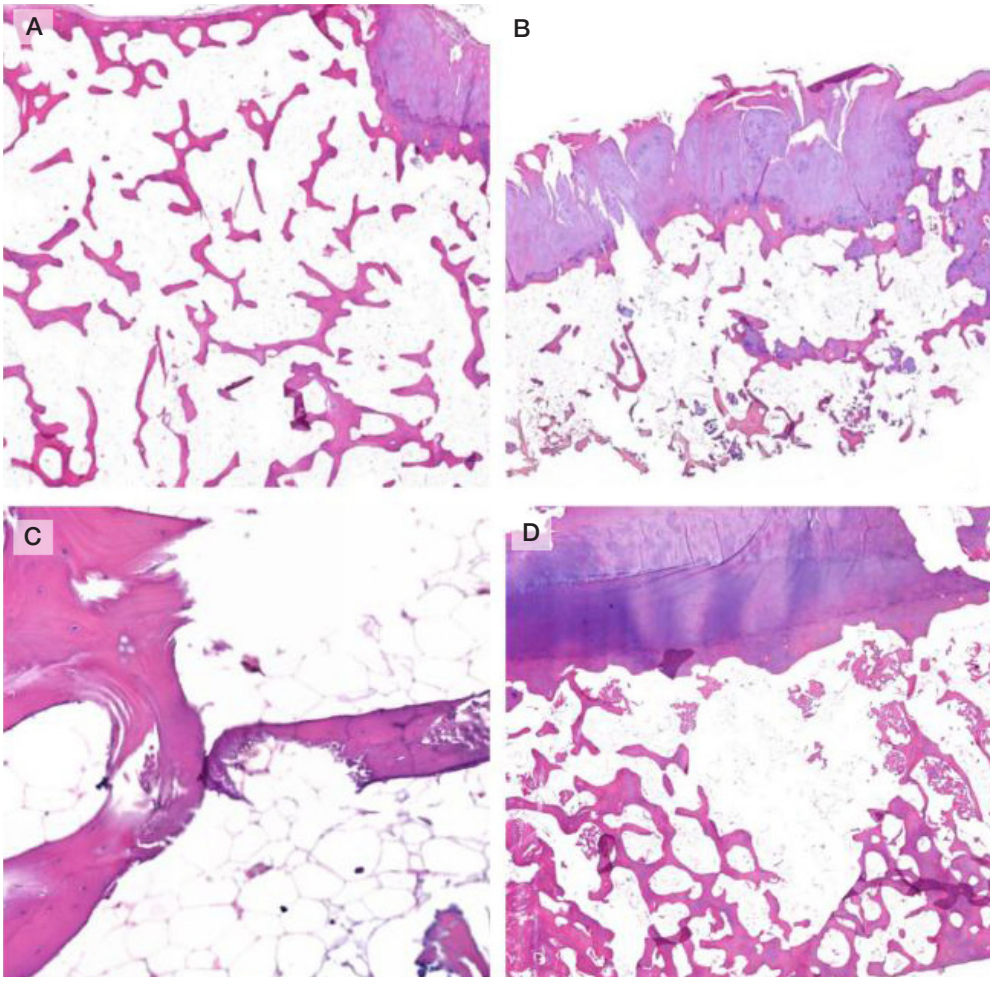

Fig. 2. Morphological characteristics of subchondral bone loss areas in osteoarthritis. Histological slides stained with hematoxylin and eosin; 20× (**A**, **B**), 200× (**C**, **D**) magnification. **A**. Subchondral zone of the femur: thinned trabeculae, dilated intertrabecular spaces, sporadic microcracks. **B**. Fragment of the tibia: disorganized trabecular structure, sparse architecture, disrupted trabeculae. **C**. Paratrabecular zone of the femur: clearly visible intertrabecular spaces filled with bone marrow fat, trabeculae showing signs of thinning. **D**. Bone marrow space of the tibia: areas of fibrous transformation, linear defects within the trabeculae

BTL areas. Trabecular width was significantly larger in the areas of osteosclerosis vs. osteoporosis ($p < 0.001$), while intertrabecular distances were larger in the areas of osteoporosis (Table 1).

Morphometric analysis showed that in the areas of osteosclerosis trabecular width was significantly larger in the tibia, than in the femur ($p = 0.0007$), while intertrabecular distances, in contrast, were larger in the femur ($p = 0.0377$). In the areas of osteoporosis, trabeculae were significantly thinner in the femur relative to similar zones of the tibia ($p = 0.0001$). Such differences reflect the features of the subchondral bone tissue focal remodeling depending on the anatomical region and the type of load. Furthermore, tidemark width was significantly larger in the tibia, than in the femur ($p = 0.0035$), significant differences were revealed when comparing the femur (BS) and the tibia (BTL) ($p = 0.0113$).

Analysis of the number of microcracks (bone fragility index) in the studied specimens was of special interest. It was shown that the median bone fragility index was higher in the areas of bone tissue loss (BTL), 0.25, compared to the areas of compaction (BS), where the index value was 0.20 (Fig. 3). These differences were significant (Mann–Whitney *U* test; $p < 0.05$). Comparison of the data obtained with the control values reported in the literature has shown that both studied conditions are characterized by the increase in the number of microcracks relative to control, but the most pronounced differences from the control group have been found specifically in the areas of osteoporosis [13] (Fig. 4).

Microfracture index as a prognostic criterion

In the specimens assessed, the median MFI for the areas of osteosclerosis was 0.20, while that for the areas of osteoporosis was 0.25. These differences were significant ($p < 0.05$). Preliminary risk scale is proposed based on the distribution of values (Table 2).

Table 1. Subchondral bone morphometric parameters in the studied groups (Me (25–75%))

Parameter	Sclerosis: femur ($n = 10$)	Sclerosis: tibia ($n = 10$)	Osteoporosis: femur ($n = 10$)	Osteoporosis: tibia ($n = 10$)	Kruskal–Wallis H test (p)
Trabecular width, μm	122.4 (89.1–178.6)	139.6 (99.2–193.6)	114.5 (87.8–155.9)	131.4 (95.1–180.8)	H = 41.03 ($p = 0.0001$)
Intertrabecular distance, μm	334.7 (232.6–442.3)	300.7 (219.4–413.9)	289.7 (197.3–402.4)	310.2 (211.4–431.9)	H = 11.01 ($p = 0.0001$)
Tidemark width, μm	62.5 (47.3–78.7)	66.4 (47.7–105.1)	64.3 (44.6–79.5)	81.6 (61.5–113.4)	H = 9.55 ($p = 0.0229$)

Note: the values are presented as the median (25^{th}–75^{th} percentiles). Significance of differences between groups is assessed using the Mann–Whitney *U* test. The differences are considered significant at $p < 0.05$.

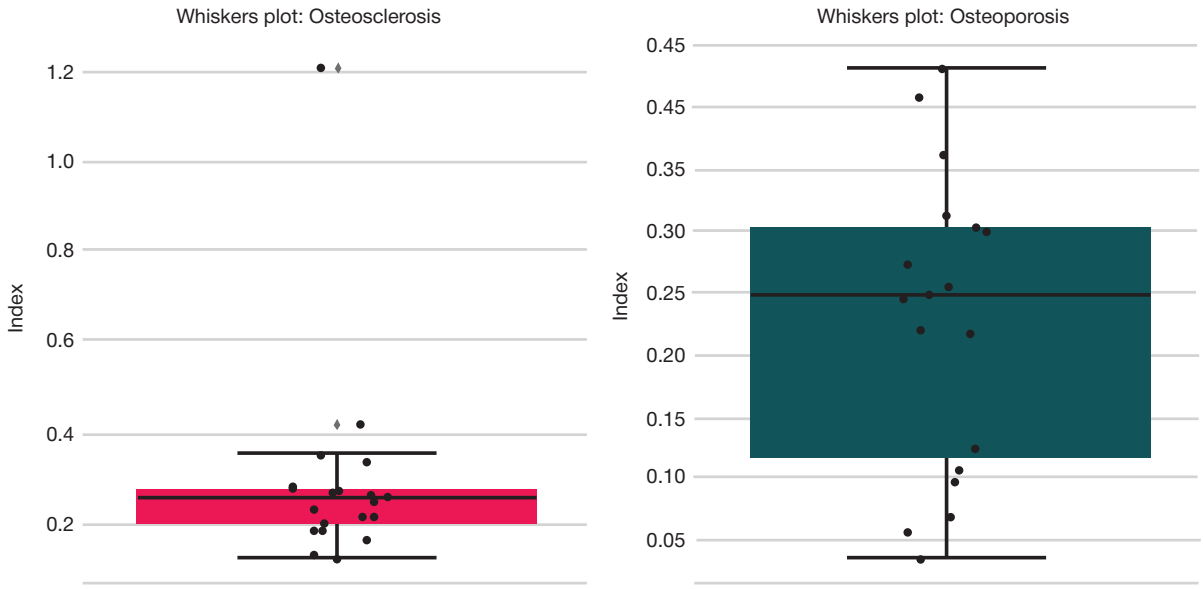

Fig. 3. Distribution of indices in the bone sclerosis and loss areas. The median values and interquartile range are provided. The analysis includes 40 fragments (2 per patient; $n = 20$) collected from the internal and external condyles of the femur and tibia. Areas of osteoporosis are characterized by significantly higher MFI values compared to the areas of sclerosis ($p \leq 0.05$)

DISCUSSION

The findings demonstrate that there are considerable morphological differences between the subchondral bone areas showing signs of osteosclerosis and osteoporosis in knee osteoarthritis. Trabecular width was significantly higher in the areas of sclerosis, while intertrabecular spaces were dilated in the zones of bone tissue loss. Such results confirm that osteoarthritis is accompanied by heterogeneous remodeling processes geared towards both bone sclerosis and structural disorganization in the subchondral zone.

Structural features of the alterations identified are consistent with the literature data emphasizing the key role of subchondral bone in the osteoarthritis pathogenesis. Initial changes of the subchondral bone trabecular architecture can precede chondral degeneration and can be associated with impaired mechanotransduction and microcirculation. The compacted structure with atypical trabecular orientation is formed in the areas of osteosclerosis, which can lead to the depreciation function impairment and increased load on the articular cartilage. In turn, zones of osteoporosis demonstrate the decreased density and microfragmentation, which can contribute to the decreased subchondral zone strength and increased risk of microfractures.

The published data obtained using micro-CT in women aged 32–37 and 78–80 years were used to compare the morphometric characteristics obtained [13]. It should be noted that methodological differences (optical microscopy vs. micro-CT), as well as differences in age and gender make it impossible to use these data as a direct control. However, these were used as a tentative literature model for discussion of age-related bone structure alterations.

The analysis of microfracture index (MFI) has shown its sensitivity to bone morphology alterations. Higher MFI values in the zones of osteoporosis suggest the bone tissue strength decrease and the possibility of using this indicator as a quantitative prognostic criterion of fractures and endoprosthesis instability. In the study conducted, MFI was determined as microcrack density per unit of bone tissue area (mm^2), which allowed one to quantify the degree of microdamage to the subchondral zone.

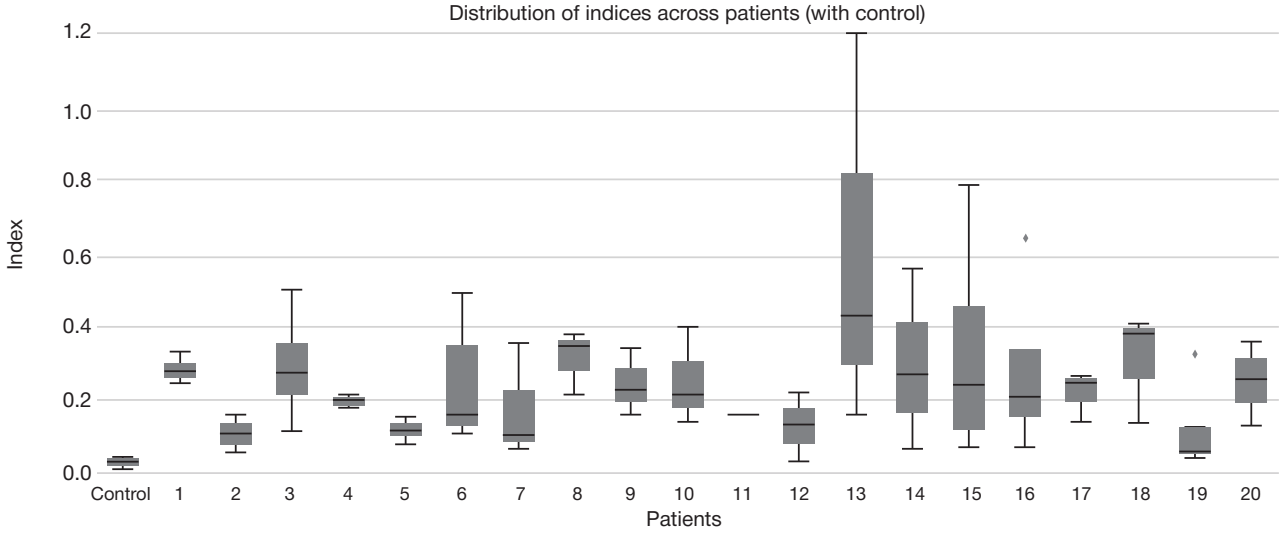

Fig. 4. Bone tissue microfracture index (MFI) in patients with osteoarthritis (based on the data on the areas of osteosclerosis and osteoporosis in the femur and tibia) compared to the literature data [13]. Aggregate MFI values are reported for each patient ($n = 20$), including two areas (of compaction and loss). The literature data are provided for tentative comparison, these have not been used as a control group

Table 2. Microfracture index (MFI)

№	Risk	MFI range	Status description
1	Low	< 0,20	Low number of microcracks, high structural stability
2	Medium	0,20–0,25	Moderate amount of microdamage, potential strength decrease
3	High	≥ 0,25	High density of microcracks, marked bone brittleness

This conclusion is consistent with the results of modern morphometric studies emphasizing the importance of assessing microdamage in the subchondral zone and the interplay between the subchondral zone and the articular cartilage in the context of osteoarthritis [14, 15].

Elevated MFI values can indicate the decreased mechanical bone strength and increased risk of fractures after surgery. In the future this index can be introduced as an additional morphometric criterion for planning of postoperative patient management; this can also be used to substantiate prescription of therapy aimed at remodeling. Further research including clinical follow-up and comparison with the data on actual fractures will make it possible to clarify prognostic value of this indicator and its threshold values with high sensitivity and specificity.

Thus, the structural features identified confirm the need to consider subchondral bone morphology when planning orthopedic treatment, including total knee replacement.

CONCLUSIONS

The study suggests that the subchondral bone tissue demonstrates high morphological heterogeneity in knee osteoarthritis: in distinct zones, signs of osteosclerosis prevail, while signs of osteoporosis prevail in other zones. Morphometric analysis has shown that trabeculae are thickened and intertrabecular spaces are narrowed in the areas of sclerosis, while trabecular thinning and fragmentation, along with dilated intertrabecular spaces are observed in osteoporosis. Microfracture index (MFI) turned out to be significantly higher in the areas of bone tissue loss, which suggests decreased strength and potential instability of the bone. These data indicate the possibility of using morphometric assessment of the subchondral zone, including MFI values, as a prognostic tool when planning orthopedic interventions and total knee replacement.

References

1. Katz JN, Arant KR, Loeser RF. Diagnosis and Treatment of Hip and Knee Osteoarthritis: A Review. JAMA. 2021; 325: 568–78. Available from: https://doi.org/10.1001/jama.2020.22171.
2. GBD 2019 Diseases and Injuries Collaborators. Global burden of 369 diseases and injuries in 204 countries and territories, 1990-2019: a systematic analysis for the Global Burden of Disease Study 2019. Lancet Lond Engl. 2020; 396: 1204–22. Available from: https://doi.org/10.1016/S0140-6736(20)30925-9.
3. Giorgino R, Albano D, Fusco S, Peretti GM, Mangiavini L, Messina C. Knee Osteoarthritis: Epidemiology, Pathogenesis, and Mesenchymal Stem Cells: What Else Is New? An Update. Int J Mol Sci. 2023; 24: 6405. Available from: https://doi.org/10.3390/ijms24076405.
4. Pilipovich AA, Danilov AB. Bol' pri osteoartrite: patogenez i sovremennye vozmozhnosti terapii. Terapija. 2020; 6-3 (37): 117–27. DOI 10.18565/therapy.2020.3.117-127. Russian.
5. Jang S, Lee K, Ju JH. Recent Updates of Diagnosis, Pathophysiology, and Treatment on Osteoarthritis of the Knee. Int J Mol Sci. 2021; 22: 2619. Available from: https://doi.org/10.3390/ijms22052619.
6. Donell S. Subchondral bone remodelling in osteoarthritis. EFORT Open Rev. 2019; 4: 221–9. Available from: https://doi.org/10.1302/2058-5241.4.180102.
7. Suri S, Walsh DA. Osteochondral alterations in osteoarthritis. Bone. 2012; 51: 204–11. Available from: https://doi.org/10.1016/j.bone.2011.10.010.
8. Amir G, Pirie CJ, Rashad S, Revell PA. Remodelling of subchondral bone in osteoarthritis: a histomorphometric study. J Clin Pathol. 1992; 45: 990–2. Available from: https://doi.org/10.1136/jcp.45.11.990.
9. Abramoff B, Caldera FE. Osteoarthritis. Med Clin North Am. 2020; 104: 293–311. Available from: https://doi.org/10.1016/j.mcna.2019.10.007.
10. Diamond LE, Grant T, Uhlrich SD. Osteoarthritis year in review 2023: Biomechanics. Osteoarthritis Cartilage. 2024; 32: 138–47. Available from: https://doi.org/10.1016/j.joca.2023.11.015.
11. Chugaev DV, Kravtsov ED, Kornilov NN, Kulyaba TA. Anatomical and Biomechanical Features of the Lateral Compartment of the Knee and Associated Technical Aspects of Unicompartmental Knee Arthroplasty: Lecture. Traumatol Orthop Russ. 2023; 29: 144–58. Available from: https://doi.org/10.17816/2311-2905-2042.
12. Primorac D, Molnar V, Rod E, Jeleč Ž, Čukelj F, Matišić V, et al. Knee Osteoarthritis: A Review of Pathogenesis and State-Of-The-Art Non-Operative Therapeutic Considerations. Genes. 2020; 11: 854. Available from: https://doi.org/10.3390/genes11080854.
13. Green JO, Nagaraja S, Diab T, Vidakovic B, Guldberg RE. Age-related changes in human trabecular bone: Relationship between microstructural stress and strain and damage morphology. J Biomech. 2011; 44: 2279–85. Available from: https://doi.org/10.1016/j.jbiomech.2011.05.034.
14. Zhang S, Li T, Feng Y, Zhang K, Zou J, Weng X, et al. Exercise improves subchondral bone microenvironment through regulating bone-cartilage crosstalk. Front Endocrinol. 2023; 14: 1159393. Available from: https://doi.org/10.3389/fendo.2023.1159393.
15. Román-Blas JA, Castañeda S, Largo R, Herrero-Beaumont G. Subchondral bone remodelling and osteoarthritis. Arthritis Res Ther. 2012; 14: A6, ar3713. Available from: https://doi.org/10.1186/ar3713.

Литература

1. Katz JN, Arant KR, Loeser RF. Diagnosis and Treatment of Hip and Knee Osteoarthritis: A Review. JAMA. 2021; 325: 568–78. Available from: https://doi.org/10.1001/jama.2020.22171.
2. GBD 2019 Diseases and Injuries Collaborators. Global burden of 369 diseases and injuries in 204 countries and territories, 1990-2019: a systematic analysis for the Global Burden of Disease Study 2019. Lancet Lond Engl. 2020; 396: 1204–22. Available from: https://doi.org/10.1016/S0140-6736(20)30925-9.
3. Giorgino R, Albano D, Fusco S, Peretti GM, Mangiavini L, Messina C. Knee Osteoarthritis: Epidemiology, Pathogenesis, and Mesenchymal Stem Cells: What Else Is New? An Update. Int J Mol Sci. 2023; 24: 6405. Available from: https://doi.org/10.3390/ijms24076405.
4. Пилипович А. А., Данилов А. Б. Боль при остеоартрите: патогенез и современные возможности терапии. Терапия. 2020; 6-3 (37): 117–27. DOI 10.18565/therapy.2020.3.117-127.
5. Jang S, Lee K, Ju JH. Recent Updates of Diagnosis, Pathophysiology, and Treatment on Osteoarthritis of the Knee. Int J Mol Sci. 2021; 22: 2619. Available from: https://doi.org/10.3390/ijms22052619.
6. Donell S. Subchondral bone remodelling in osteoarthritis. EFORT Open Rev. 2019; 4: 221–9. Available from:

https://doi.org/10.1302/2058-5241.4.180102.
7. Suri S, Walsh DA. Osteochondral alterations in osteoarthritis. Bone. 2012; 51: 204–11. Available from: https://doi.org/10.1016/j.bone.2011.10.010.
8. Amir G, Pirie CJ, Rashad S, Revell PA. Remodelling of subchondral bone in osteoarthritis: a histomorphometric study. J Clin Pathol. 1992; 45: 990–2. Available from: https://doi.org/10.1136/jcp.45.11.990.
9. Abramoff B, Caldera FE. Osteoarthritis. Med Clin North Am. 2020; 104: 293–311. Available from: https://doi.org/10.1016/j.mcna.2019.10.007.
10. Diamond LE, Grant T, Uhlrich SD. Osteoarthritis year in review 2023: Biomechanics. Osteoarthritis Cartilage. 2024; 32: 138–47. Available from: https://doi.org/10.1016/j.joca.2023.11.015.
11. Chugaev DV, Kravtsov ED, Kornilov NN, Kulyaba TA. Anatomical and Biomechanical Features of the Lateral Compartment of the Knee and Associated Technical Aspects of Unicompartmental Knee Arthroplasty: Lecture. Traumatol Orthop Russ. 2023; 29: 144–58. Available from: https://doi.org/10.17816/2311-2905-2042.
12. Primorac D, Molnar V, Rod E, Jeleč Ž, Čukelj F, Matišić V, et al. Knee Osteoarthritis: A Review of Pathogenesis and State-Of-The-Art Non-Operative Therapeutic Considerations. Genes. 2020; 11: 854. Available from: https://doi.org/10.3390/genes11080854.
13. Green JO, Nagaraja S, Diab T, Vidakovic B, Guldberg RE. Age-related changes in human trabecular bone: Relationship between microstructural stress and strain and damage morphology. J Biomech. 2011; 44: 2279–85. Available from: https://doi.org/10.1016/j.jbiomech.2011.05.034.
14. Zhang S, Li T, Feng Y, Zhang K, Zou J, Weng X, et al. Exercise improves subchondral bone microenvironment through regulating bone-cartilage crosstalk. Front Endocrinol. 2023; 14: 1159393. Available from: https://doi.org/10.3389/fendo.2023.1159393.
15. Román-Blas JA, Castañeda S, Largo R, Herrero-Beaumont G. Subchondral bone remodelling and osteoarthritis. Arthritis Res Ther. 2012; 14: A6, ar3713. Available from: https://doi.org/10.1186/ar3713.

PROGNOSTIC VALUE OF PROCALCITONIN RAPID TEST IN PURULENT INFLAMMATORY DISEASES OF THE MAXILLOFACIAL REGION

Belchenko VA[1], Chantyr IV[2], Zavgorodnev KD[1,2] ✉, Pakhomova Yul[2]

[1] Maxillofacial Hospital for War Veterans, Pirogov City Clinical Hospital No. 1, Moscow, Russia
[2] Pirogov Russian National Research Medical University, Moscow, Russia

Dental diseases, which exhibit high prevalence within the population, are frequently complicated by odontogenic inflammatory processes in the maxillofacial region (MFR), posing a significant risk of systemic septic complications. Procalcitonin (PCT) is a promising biomarker for the diagnosis of sepsis showing high sensitivity and specificity. However, its prognostic value for purulent inflammatory diseases of the maxillofacial region (PID-MFR) is still understudied. The study aimed to evaluate the diagnostic value of the PCT semi-quantitative rapid test for predicting septic complications in patients with PID-MFR and to evaluate the relationship between PCT levels and clinical/laboratory parameters. The study involved 60 patients (73.3% males, 26.7% females) aged between 21 and 71 years with PID-MFR. Serum PCT levels were determined by a semi-quantitative method. Patients were stratified into two groups: group 1 with PCT > 0.5 ng/mL (23.3%), group 2 with PCT < 0.5 ng/mL (76.7%). Septic complications were observed in 28.57% of patients in group 1, whereas no complications occurred in group 2 (p = 0.001; OR = 0.025). There were no significant differences in clinical and laboratory indicators, number of cellular maxillofacial spaces affected (3.7 ± 1.7), disease duration (5.17 ± 3.39 days), and length of hospital stay (6.50 ± 2.41 bed-days) between groups (p > 0.05). Our findings demonstrate that measuring PCT levels via a semi-quantitative method is an effective and accessible approach to predict septic complications of PID-MFR.

Keywords: procalcitonin, sepsis, purulent inflammatory diseases, maxillofacial region

Author contribution: Belchenko VA, Chantyr IV — study concept and design; Chantyr IV, Zavgorodnev KD — data acquisition and processing; Zavgorodnev KD, Pakhomova Yul — statistical data processing; Chantyr IV, Zavgorodnev KD, Pakhomova Yul — manuscript writing; Pakhomova Yul — illustrating; Belchenko VA — editing.

✉ **Correspondence should be addressed:** Kirill D. Zavgorodnev
Lesteva, 9, Moscow, 115191, Russia; zheme14@mail.ru

Received: 19.03.2025 **Accepted:** 02.04.2025 **Published online:** 15.04.2025

DOI: 10.24075/brsmu.2025.018

ПРОГНОСТИЧЕСКАЯ ЦЕННОСТЬ ЭКСПРЕСС-ТЕСТА НА ПРОКАЛЬЦИТОНИН ПРИ ГНОЙНО-ВОСПАЛИТЕЛЬНЫХ ЗАБОЛЕВАНИЯХ ЧЕЛЮСТНО-ЛИЦЕВОЙ ОБЛАСТИ

В. А. Бельченко[1], И. В. Чантырь[2], К. Д. Завгороднев[1,2] ✉, Ю. И. Пахомова[2]

[1] Городская клиническая больница № 1 имени Н. И. Пирогова филиал Челюстно-лицевой госпиталь для Ветеранов войн, Москва, Россия,
[2] Российский национальный исследовательский медицинский университет имени Н. И. Пирогова, Москва, Россия

Стоматологические заболевания широко распространены среди населения и нередко осложняются развитием одонтогенных воспалительных процессов челюстно-лицевой области (ЧЛО), что создает потенциальный риск развития септических осложнений. Прокальцитонин (ПКТ) — перспективный биомаркер для диагностики сепсиса, обладающий высокой чувствительностью и специфичностью. Однако его прогностическая ценность при гнойно-воспалительных заболеваниях челюстно-лицевой области (ГВЗ ЧЛО) остается недостаточно изученной. Целью исследования было оценить диагностическую ценность полуколичественного экспресс-теста на ПКТ для прогнозирования септических осложнений у пациентов с ГВЗ ЧЛО, а также изучить взаимосвязь между уровнем ПКТ и клинико-лабораторными показателями. В исследование вошли 60 пациентов (73,3% мужчин, 26,7% женщин) в возрасте 21–71 года с ГВЗ ЧЛО. Уровень ПКТ определяли полуколичественным методом. Пациенты были разделены на две группы: в группе 1 ПКТ > 0,5 нг/мл (23,3%), в группе 2 ПКТ < 0,5 нг/мл (76,7%). Септические осложнения отмечены у 28,57% пациентов группы 1; в группе 2 осложнения отсутствовали (p = 0,001; ОШ = 0,025). Статистически значимых различий по клинико-лабораторным показателям, количеству вовлеченных клетчаточных пространств ЧЛО (3,7 ± 1,7), длительности заболевания (5,17 ± 3,39 дня) и госпитализации (6,50 ± 2,41 койко-дней) между группами не установлено (p > 0,05). Результаты исследования демонстрируют, что определение ПКТ полуколичественным методом является эффективным и доступным способом прогнозирования септических осложнений при ГВЗ ЧЛО.

Ключевые слова: прокальцитонин, сепсис, гнойно-воспалительные заболевания, челюстно-лицевая область

Вклад авторов: В. А. Бельченко, И. В. Чантырь — концепция и дизайн исследования; И. В. Чантырь, К. Д. Завгороднев — сбор и обработка материала; К. Д. Завгороднев, Ю. И. Пахомова — статистическая обработка данных; И. В. Чантырь, К. Д. Завгороднев, Ю. И. Пахомова — написание текста; Ю. И. Пахомова — иллюстративное сопровождение; В. А. Бельченко — редактирование.

✉ **Для корреспонденции:** Кирилл Дмитриевич Завгороднев
ул. Лестева, д. 9, г. Москва, 115191, Россия; zheme14@mail.ru

Статья получена: 19.03.2025 **Статья принята к печати:** 02.04.2025 **Опубликована онлайн:** 15.04.2025

DOI: 10.24075/vrgmu.2025.018

According to the WHO Global Oral Health Status Report (2022), dental diseases are among the most common disorders affecting approximately 45% of the world's population (3.5 billion people) [1]. In Russia, annual epidemiological data from the Russian Dental Association indicate over 158 million cases of seeking dental care [2]. Among these conditions are lesions of hard dental tissues, pulpitis, and periapical diseases, the advanced stages of which frequently progress to odontogenic inflammatory disorders of the maxillofacial region (MFR)[3]. Data from the Organizational and Methodological Department

of Dentistry and Maxillofacial Surgery (Moscow Healthcare Department) further reveal that 37% of adults seeking specialized maxillofacial surgical care require intervention for localized or severe forms of purulent inflammatory diseases of the maxillofacial region (PID-MFR) [4].

Much of this category of patients require long-term treatment due to disease severity and high risk of complications, mediastinitis, thrombosis of facial veins and cerebral sinuses, meningitis, meningoencephalitis, etc. Systemic inflammatory response syndrome, sepsis, endotoxic shock, multiple organ failure are conventionally distinguished among life-threatening purulent septic complications [5].

Sepsis remains a critical challenge in surgical disciplines, including MFS. However, the role of odontogenic infection in pathogenesis of systemic inflammatory response, sepsis, and the related complications is still poorly understood.

Despite significant advances in modern medicine, driven by pharmacological innovation and the development of novel diagnostic and therapeutic modalities, the global incidence of infectious inflammatory disorders remains persistently elevated [2, 3, 6]. According to the WHO report on the epidemiology and burden of sepsis (2020), sepsis accounts for approximately 49 million cases and 11 million deaths annually, representing 20% of global mortality [7].

Over the past decades, the scientists searched for an optimal method to diagnose septic complications [8]. Serum procalcitonin (PCT) has become a biomarker of particular interest due to its high sensitivity and specificity in distinguishing bacterial infections from other inflammatory etiologies [9, 10]. The association between elevated PCT levels and bacterial infections was first established in 1993 [11].

Under physiological conditions, PCT is synthesized in parafollicular cells (C-cells) of the thyroid gland, where it undergoes proteolytic cleavage by endoplasmic reticulum endopeptidases into calcitonin and inactive byproducts. This process accounts for its negligible serum concentration in healthy individuals. However, during systemic inflammatory response syndrome (SIRS), PCT production shifts to an extra-thyroidal pathway, wherein diverse organs and tissues synthesize PCT in response to bacterial endotoxins and pro-inflammatory cytokines. The molecular mechanisms governing this alternative synthesis pathway remain incompletely characterized [12].

Elevated serum PCT levels are associated with adverse clinical outcomes, underscoring its utility as a biomarker for guiding therapeutic strategies [9]. While numerous studies have validated PCT's diagnostic value for the diagnosis of inflammatory disorders, its prognostic value in PID-MFR remains poorly understood, which determines the relevance of our study.

The study aimed to evaluate the prognostic value of the PCT semi-quantitative rapid test as a screening tool for stratifying the risk of septic complications in patients with PID-MFR and to assess the relationship between PCT levels and clinical and laboratory parameters.

METHODS

A retrospective cohort study with the elements of prospective analytical observational assessment was conducted at the specialized Maxillofacial Hospital for War Veterans, Pirogov City Clinical Hospital No. 1 specializing in maxillofacial surgical care and dental care provision to adult patients. The study was managed by V. A. Belchenko, D. Sci. (Med), Chief Freelance Specialist of Moscow Healthcare Department.

Between March 12, 2024, and September 23, 2024, 1,784 patients with PID-MFR presented to the emergency department. Of these, 60 patients were enrolled in the study. The cohort comprised 44 males (73.3%) and 16 females (26.7%), with ages ranging from 21 to 71 years (mean age 42.07 ± 13.81 years). Among patients 68.3% (n = 41) were employed, 31.7% (n = 19) were not. Patients were admitted to hospital through the following routes: ambulance — 15.00% of patients (n = 9), 103-outpatient clinic — 85.00% (n = 51).

The minimum sample size was calculated using the formula by N. M. Buderer with the 10% confidence interval. In this study, the minimum sample size was 43 patients.

Inclusion criteria: patients with PID-MFR aged 18–75 years; submitted informed consent for evaluation and treatment; patients who had not taken antibiotics prior to hospitalization; stable and relatively stable patients in accordance with the green and yellow flows of the triage system; serum C-reactive protein (CRP) levels ≥180 mg/L; performing ICA Procalcitonin semi-quantitative rapid test.

Exclusion criteria: patients under 18 and over 75 years; patient's refusal to participate in the study or undergo treatment; taking antibiotics before hospital admission by the patient; patients with life-threatening conditions requiring emergent resuscitation, in accordance with the red flow of the triage system; noncompliance with the laboratory criteria and no indications for the ICA Procalcitonin semi-quantitative test.

The literature review revealed significant variability of CRP levels among patients with PID-MFR. According to the results of the study focused on early diagnosis of sepsis (2021), the range of CRP concentrations was 82.50–95.35 mg/L [13]. In another study (2021) the mean CRP level of 140 mg/L associated with odontogenic infections was reported [14]. According to the data of the study conducted in 2024, the mean CRP admission levels were 185.2 mg/L in males and 189.4 mg/L in females [15]. Based on this evidence, we established a diagnostic CRP threshold of ≥180 mg/L [13–15].

All patients admitted to the emergency department underwent standardized triage assessment. The triage criteria for stratifying patients into green (stable), yellow (semi-stable), and red (critical) categories are summarized in Table 1.

Initial clinical evaluations were conducted by a multidisciplinary team comprising a maxillofacial surgeon and a general practitioner. The following additional tests were performed immediately after evaluation: 1) laboratory analyses — complete blood counts and urinalysis, blood biochemistry panel, coagulation profile; 2) imaging studies — computed tomography (CT) of the chest and maxillofacial region. Based on the evaluation results and inclusion criteria, patients were selected and blood PCT levels were determined by a semi-quantitative method using the ICA Procalcitonin 500 rapid test (Akademinnovacija LLC, Russia) (Fig. 1).

The ICA Procalcitonin 500 assay (Akademinnovatsiya LLC, Russia) is an *in vitro* immunochromatographic rapid test designed for semi-quantitative determination of procalcitonin (PCT) levels in human serum and plasma. The method is based on the immunochromatography analysis principles. When the patient's blood serum or plasma (four drops) is applied to the test strip, interaction with specific monoclonal antibodies against PCT conjugated with the stained marker occurs. The complex produced passes through the test zone with the specific antibodies immobilized on the membrane and forms the stained complex: immobilized antibodies – procalcitonin – antibodies with the marker. The emergence of two parallel stained lines (C and T) in the test window of the cassette indicates a positive result, i.e. that the PCT concentration

Table 1. Triage system criteria for identifying patients into green, yellow and red flows

Indicator	Green flow	Yellow flow	Red flow
HR, bpm	60–90	40–60 90–100	< 40 > 130
RR, per 1 min	8–16	16–25	> 30
BP, mmHg	110/60–140/110	<110/60 >140/110	< 75/30 > 240/140
SpO_2, %	> 95	92–95	< 90
T °C	36.0–37.5	35.0–36.0 37.5–39.0	< 35.0 > 40.0
Morse Fall Scale	0–25	25–50	> 50
Glasgow Coma Scale	15	14	< 13
Pain scale	1–3	4–7	8–10

exceeds 0.5 ng/mL. The presence of only one stained control line (C) indicates a negative result, i.e. that there is no PCT in the sample or that PCT concentration is below 0.5 ng/mL. The lack of stained lines in the test window or the emergence of the test line (T) only indicates that the test result is invalid.

The decision on patient management tactics was made based on the evaluation results: hospitalization and surgical treatment in the specialized hospital or transfer to the multidisciplinary hospital.

Retrospective data acquisition and analysis of the patients' medical records (003/u form) were conducted. The study results obtained were entered in the table and subjected to statistical processing using the StatTech v. 4.0.5 software package (StatTech, Russia).

The statistical analysis conducted included testing the distribution of quantitative indicators for normality using the Kolmogorov–Smirnov test. The normally distributed parameters were presented as the mean (M) with the standard deviation (SD) and 95% confidence interval (CI), while categorical data were presented as absolute values and percentage with the 95% CI calculated by the Clopper–Pearson method. Groups were compared based on quantitative traits using the Student's t-test for samples with equal variances and Welch's *t*-test for samples with unequal variances. Qualitative indicators were analyzed using the Fisher's exact test for contingency tables. The effect size was assessed via odds ratio with the 95% CI; the Haldane–Anscombe correction was applied, when there were zero values in the cells of the table. In all cases, the differences were considered significant at $p < 0.05$.

RESULTS

Patients were stratified into two cohorts based on serum PCT levels measured via the ICA Procalcitonin semi-quantitative immunochromatographic assay. Group 1 (n = 14, 23.3%) comprised individuals with elevated PCT concentrations (>0.5 ng/mL), while Group 2 (n = 46, 76.7%) included patients with subthreshold PCT levels (<0.5 ng/mL). Comparative analyses of the patient groups are provided in Table 2.

The time from symptom onset to seeking care ranged from 1 to 21 days, with a mean of 5.17 ± 3.39 days (95% CI: 4.29–6.04).

The number of the cellular maxillofacial spaces affected by inflammation varied between 1 and 8 with the mean value of 3.7 (95% CI: 3.27–4.13). The mode value for this parameter was 4.00 (Fig. 2).

The analysis of etiological factors showed that in 50.0% of cases (n = 30) the development of PID-MFR was associated with exacerbation of chronic periodontitis in permanent teeth, mostly mandibular molars. Extraction of permanent teeth in outpatient settings caused inflammation in 31.67% of cases (n = 19), and in 18.33% of cases (n = 11) inflammation was attributed to permanent tooth extractions performed in outpatient settings Acute pericoronitis in the mandibular third molars was diagnosed in 6.67% of patients (n = 4). In rare cases,

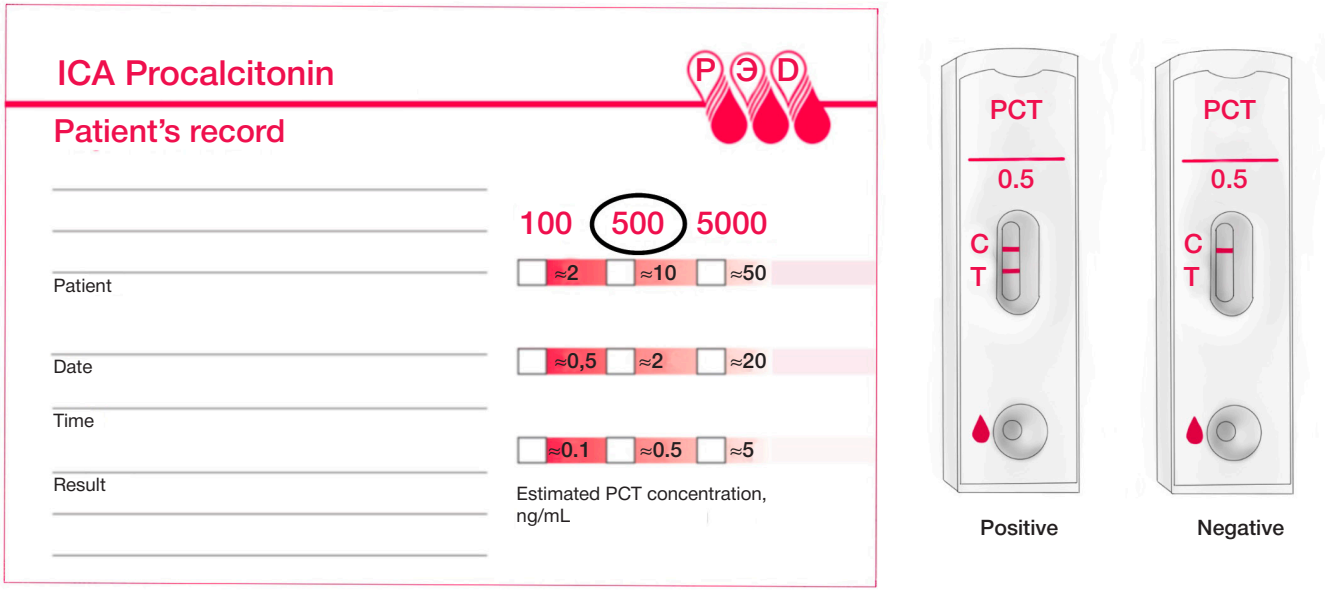

Fig. 1. ICA Procalcitonin 500 test kit (drawing by the author)

Table 2. Comparative characteristics of the studied patient groups

Clinical characteristics	PCT > 0.5 ng/mL	PCT < 0.5 ng/mL
Sex	Males — 85.71% (*n* = 12) Females — 14.29% (*n* = 2)	Males — 69.57% (*n* = 32) Females — 30.43% (*n* = 14)
Age	46.21 ± 17.40 years	40.80 ± 12.48 years
Diagnosis	K12.2 — 14.29% (*n* = 2) L03.2 — 85.71% (*n* = 12)	K12.2 — 19.57% (*n* = 9) L03.2 — 80.43% (*n* = 37)
Concomitant disorders	Cardiovascular disorders — 42,86% (*n* = 6) Diabetes mellitus — 7.14% (*n* = 1) Respiratory disorders — 7.14% (*n* = 1)	Cardiovascular disorders — 30.43% (*n* = 14) Gastrointestinal disorders — 10.87% (*n* = 5) Obesity — 42.86% (*n* = 6) Anemia — 10.87% (*n* = 5) Nervous system disorders — 6.52% (*n* = 3) Impaired glucose tolerance — 6.52% (*n* = 3) Diabetes mellitus — 4.34% (*n* = 2)
Average time since the disease onset	5.79 ± 5.04	4.98 ± 2.75
Average number of bed-days among individuals treated entirely in hospital settings	7.6 ± 1.80	7.02 ± 1.44
Surgical approach	Intra-oral — 14.29% (*n* = 2) External — 64.29% (*n* = 9)	Intra-oral — 19.57% (*n* = 9) External — 80.43% (*n* = 37)

(1.67%, *n* = 1), etiological factors included acute suppurative parotitis, complications after root canal therapy of mandibular second molars, peri-implantitis, post-traumatic osteomyelitis following mandibular fracture, and wound infection.

Among all patients, 95% (n = 57) were admitted to the 24-hour inpatient department of the MFS. After pre-hospitalization evaluation, 3.33% of patients (*n* = 2) required transfer to multidisciplinary hospital due to acute decompensation of preexisting comorbidities exacerbated by SIRS. Another 1.67% of patients (*n* = 1) were transferred to mitigate risks of intraoperative and postoperative complications associated with acute edematous-infiltrative laryngitis.

Depending in inflammation localization, the inflammatory focus debridement was performed via intra-oral route in 18.33% (*n* = 11), via external route in 76.67% (*n* = 46).

Surgical debridement of inflammatory foci was performed through either intraoral or external approaches, depending on the anatomical localization of the infectious process. The intraoral approach was used in 18.33% of cases (*n* = 11), while the external approach was used in the majority of patients (76.67%, *n* = 46).

During surgical procedures biomaterial was collected from all patients for culture-based microbiological analysis. According to microbiological testing results, the most common pathogens causing PID were *Streptococcus viridans* — 31.58% (*n* = 18) and *Neisseria spp*. — 14.04% (*n* = 8). Colonies of *Streptococcus oralis* — 10.52% (n = 6), *Streptococcus constellatus* — 7.01% (*n* = 4), *Streptococcus pyogenes* — 7.01% (*n* = 4), *Streptococcus anginosus* — 5.26% (*n* = 3), *Staphylococcus aureus* — 3.51% (*n* = 2), *Staphylococcus warneri* — 3.51% (*n* = 2), *Eikenella corrodens* — 1.75% (*n* = 1), *Enterobacter cloacae* — 1.75% (*n* = 1), and *Acinetobacter baumannii* — 1.75% (*n* = 1) were less frequent. Polymicrobial communities, predominantly comprising *Streptococcus viridans* and *Neisseria spp*., were identified in 14.04% of cases (*n* = 8). No microbial growth was observed in 17.54% of specimens (*n* = 10).

The length of hospitalization ranged from 4 to 11 bed-days, with a medico-economic standard (MES 73.180) of 8 bed-days. Patients with procalcitonin (PCT) levels >0.5 ng/mL exhibited a mean hospital stay of 7.6 ± 1.80 bed-days, compared to 7.02 ± ± 1.44 bed-days in those with PCT levels <0.5 ng/mL. The overall mean hospitalization duration was 6.50 ± 2.41 bed-days.

No significant correlation was observed between PCT levels and inflammatory biomarkers (C-reactive protein, leukocyte count, fibrinogen) in patients with PID-MFR ($p > 0.05$, Student's *t*-test and Welch's *t*-test).The results are provided in Fig. 3.

PCT levels showed no association with clinical parameters, including hospitalization duration, number of involved maxillofacial

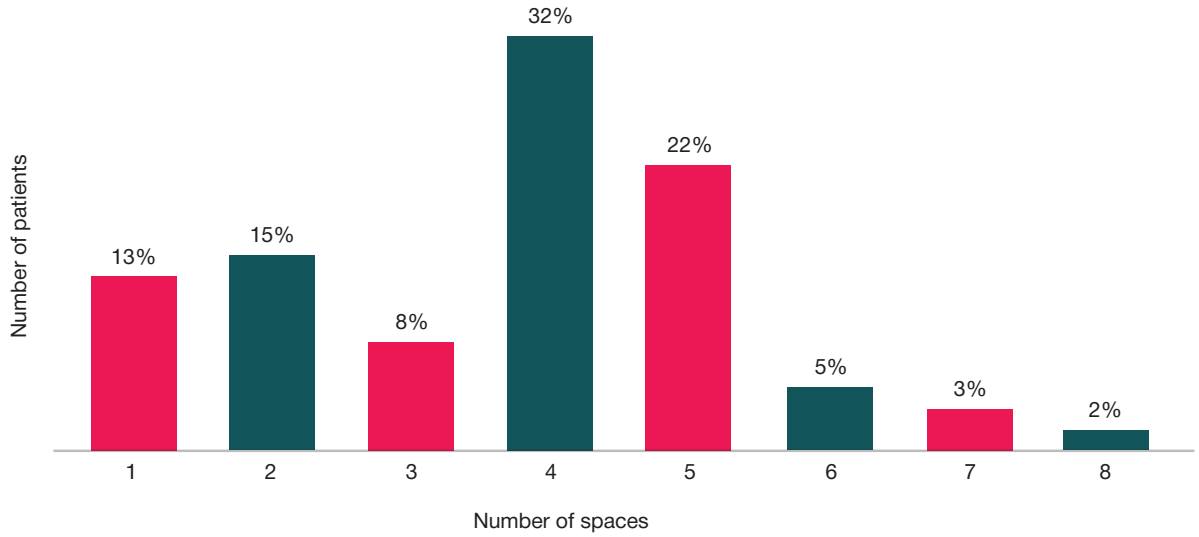

Fig. 2. Mode of the number of cellular maxillofacial spaces affected by inflammation

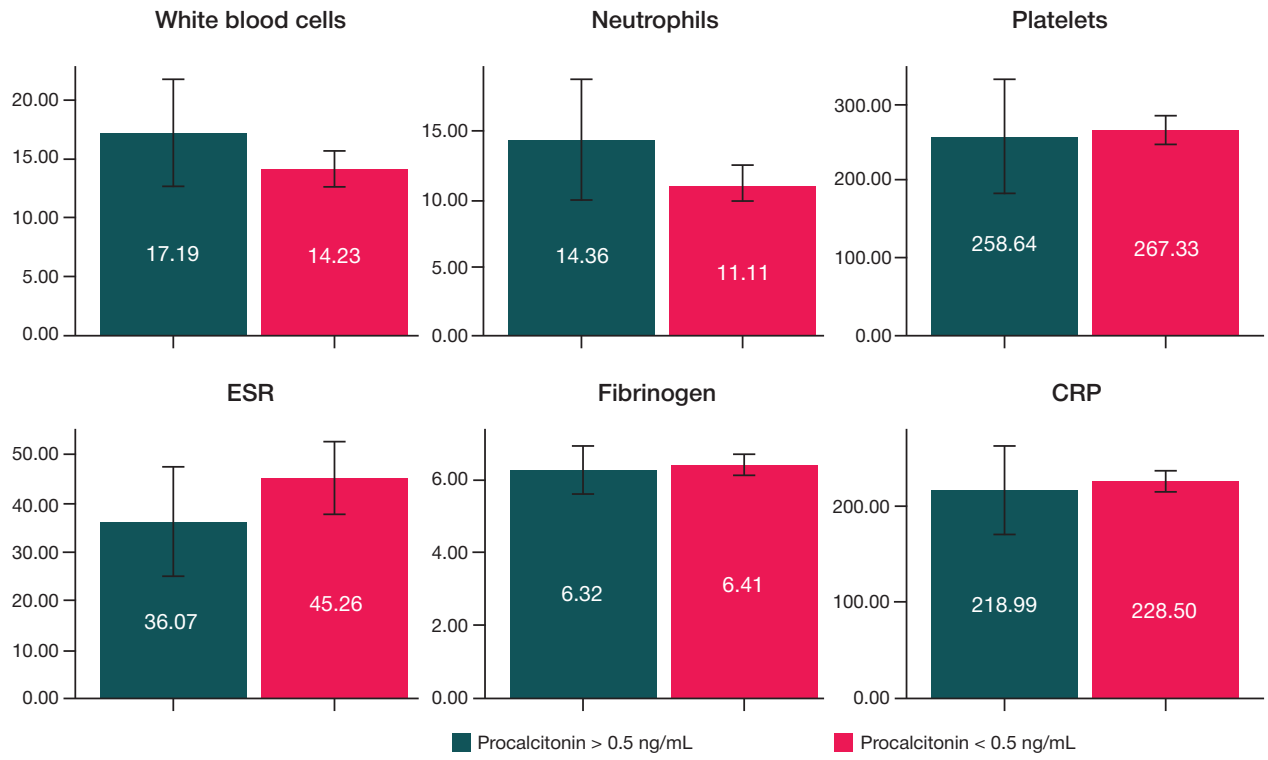

Fig. 3. Dependence of the main inflammation biomarkers on procalcitonin levels

fascial spaces, or disease progression time ($p > 0.05$; Student's *t*-test and Fisher's exact test).

Complications such as SIRS, sepsis, and endotoxic shock were diagnosed in 28.57% of PCT-positive patients ($n = 4$), with a statistically significant odds ratio (OR = 0.025; 95% CI: 0.001–0.503; $p = 0.001$, Fisher's exact test; Fig. 4). The analysis of the results are provided in Fig. 4.

Patients with negative PCT results demonstrated a 39.86-fold lower risk of complications compared to the PCT-positive cohort (OR = 0.025; 95% CI: 0.001–0.503).

Age did not significantly influence complication risk ($p > 0.05$; Student's *t*-test; Fig. 5).

Positive prognostic value of the ICA Procalcitonin 500 semi-quantitative test was 28.57%.

DISCUSSION

The incidence of septic complications in PID-MFR remains relatively low. A retrospective analysis of 483 PID-MFR patients revealed sepsis in only 3.3% of cases [16]. Nevertheless, the potential for life-threatening complications necessitates a multidisciplinary approach to diagnosis and treatment, particularly in severe PID-MFR cases characterized by systemic involvement.

In 2001–2016, sepsis diagnosis relied on the presence of ≥2 SIRS criteria. However, the limited specificity of SIRS prompted a paradigm shift in 2016 with the publication of the Third International Consensus Definitions for Sepsis and Septic Shock (Sepsis-3), which redefined sepsis as life-threatening organ dysfunction arising from a dysregulated host response to infection [17]. Representation of odontogenic sepsis pathogenesis is provided in Fig. 6.

Standard clinical and laboratory inflammatory markers, such as CRP and leukocyte counts, demonstrate limited predictive accuracy for severe septic complications. Early diagnosis facilitated by biomarkers like PCT enables timely therapeutic intervention, which is critical for improving patient outcomes. The results of our study confirm that PCT is a reliable

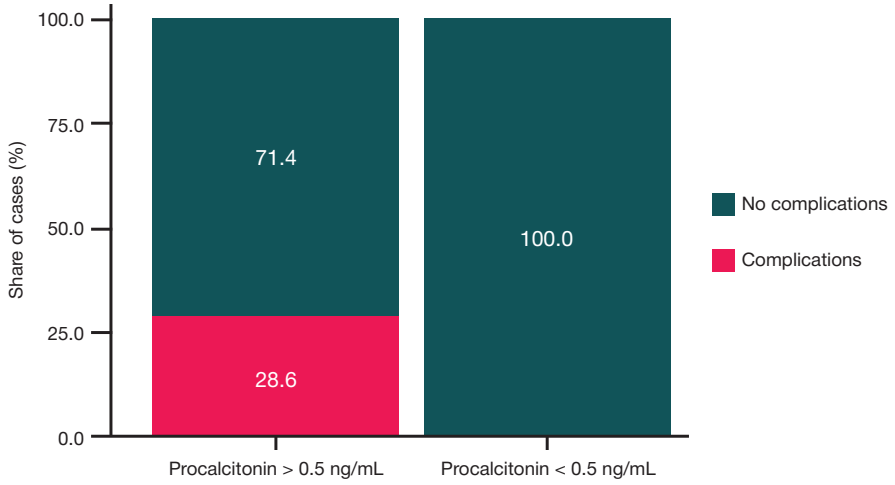

Fig. 4. Analysis of the development of complications depending on procalcitonin levels

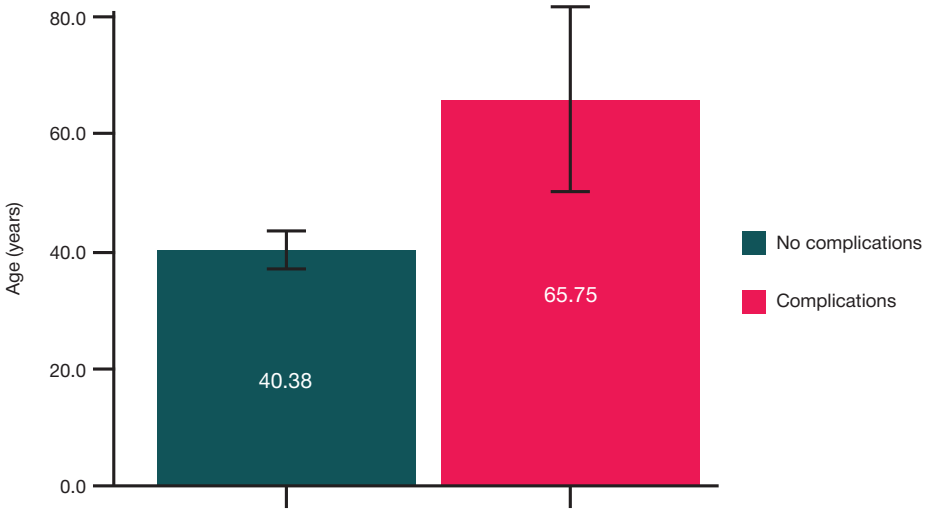

Fig. 5. Analysis of the development of complications depending on the patient's age

prognostic marker of sepsis [8, 10, 18]. A major advantage of PCT is its early appearance in blood serum — within 3–4 hours of synthesis — with peak concentrations reached at 6–12 hours and a half-life of approximately 24 hours. Under effective treatment, PCT levels typically decrease by 50% per day. In contrast, microbiological diagnostic methods require at least 48 hours and may yield false-negative results in 60–70% of cases [8, 18]. Thus, determination of PCT levels using the ICA Procalcitonin 500 rapid test and analogues ensures fast decision-making, thereby significantly improving the patient's outcome.

In this study we analyzed clinical and laboratory data of two groups of patients with PID MFR, 23.33% of patients

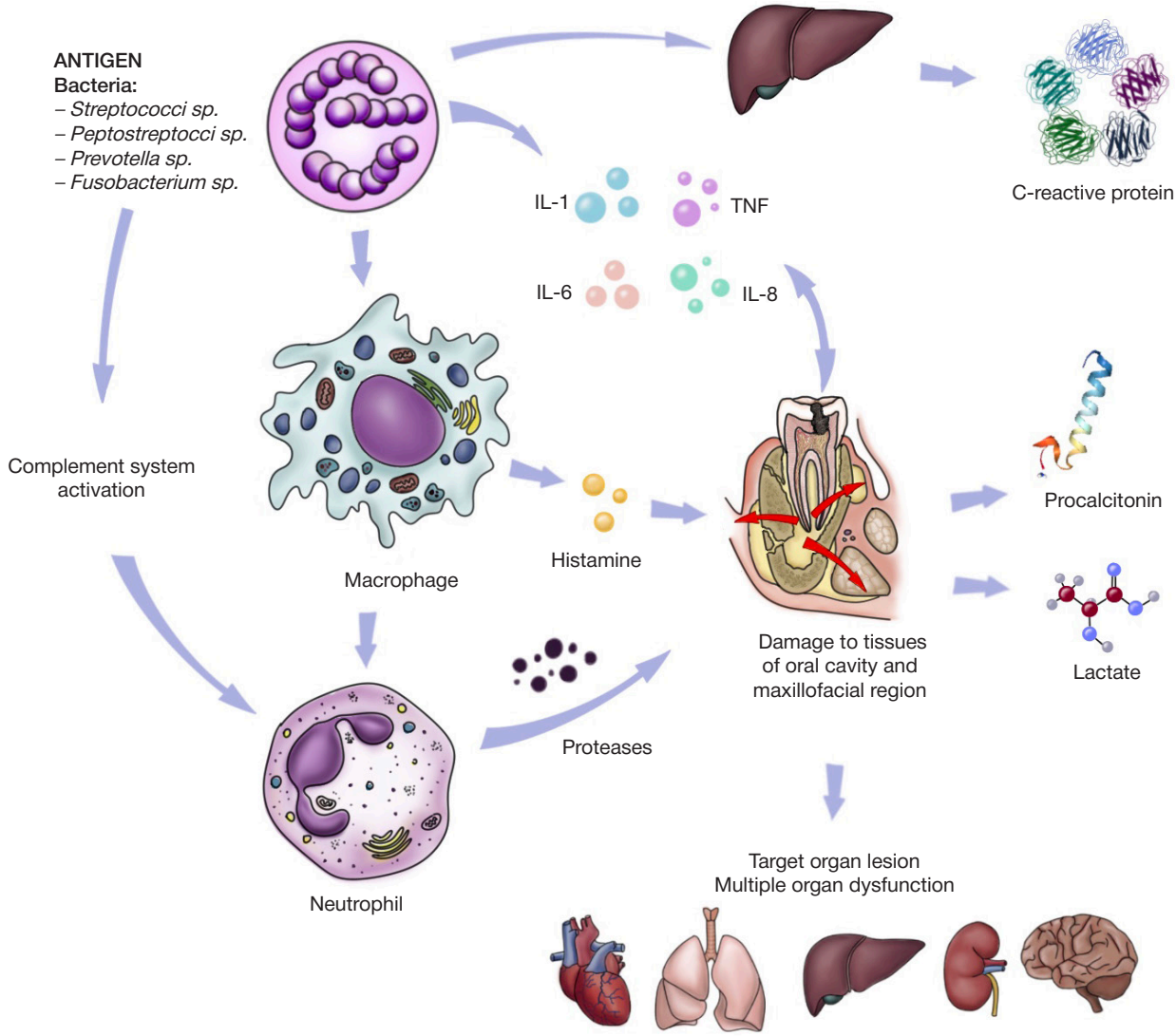

Fig. 6. Sheme of odontogenic sepsis pathogenesis (drawing by the author)

ВЕСТНИК РГМУ | 2, 2025 | VESTNIK.RSMU.PRESS | DOI: 10.24075/VRGMU.2025.018

tested positive for elevated PCT levels, with 28.57% of this subgroup developing complications such as SIRS or sepsis. No significant differences were found between the groups with regard to key clinical and laboratory indicators, including hospital stay duration, number of affected fascial spaces, disease duration, leukocyte, neutrophil and platelet counts, ESR, CRP, and fibrinogen levels. However, a significant correlation was observed between a positive PCT test result, increased patient age, and the risk of developing complications related to PID-MFR. These findings are consistent with the results reported in previous studies, supporting the use of PCT testing as a screening tool in the clinical practice of maxillofacial surgery [14, 18].

One of the limitations of the study is the relatively small sample size.

The predominance of outpatient referrals (85%) underscores the assay's potential for pre-hospital risk stratification. The semi-quantitative PCT test combines diagnostic efficacy, operational simplicity, and rapid turnaround, making it a promising screening method for identifying and predicting complications in both outpatient and inpatient settings.

CONCLUSIONS

The semi-quantitative rapid PCT test demonstrates effectiveness in stratifying the risk of septic complications among patients with PID-MFR. The absence of significant correlations between PCT levels and conventional inflammatory markers — such as CRP, leukocyte count, and fibrinogen — as well as clinical parameters (hospital stay duration, number of affected fascial spaces) underscores its independent prognostic value in evaluating systemic inflammatory response severity. The positive predictive value of 28.57%, coupled with statistically significant intergroup differences, confirm the clinical feasibility of integrating this assay into routine practice. Implementation of the PCT rapid test aligns with contemporary specialized care standards, facilitating early diagnosis and evidence-based therapeutic decision-making.

References

1. Global oral health status report. Towards universal health coverage for oral health by 2030. 2022. Ssylka aktivna na 24.12.2024. Available from: https://www.who.int/publications/i/item/9789240061484.
2. Rabinovich SA, Zavodilenko LA. Materialy 21-go Vserossijskogo stomatologicheskogo foruma. Bezopasnoe obezbolivanie v stomatologii. Rossijskaja stomatologija. 2024; 17 (3): 75–76. Dostupno po ssylke: http://doi.org/10.17116/rosstomat20241703140. Russian.
3. Salahov AK, Ksembaev SS, Bajkeev RF, Silagadze EM. Stomatologicheskaja zabolevaemost' naselenija Rossii. Kazanskij medicinskij zhurnal. 2020; 101 (5): 713–8. Dostupno po ssylke: http://doi.org/10.17816/KMJ2020-713. Russian.
4. Belchenko VA, Chantyr IV. Marshrutizacija pacientov s cheljustno-licevoj patologiej v uslovijah megapolisa: vyzovy i reshenija. Zdorov'e megapolisa. 2022; 3 (3): 46–57. Dostupno po ssylke: https://doi.org/10.47619/2713-2617.zm.2022.v.3i3;46-57. Russian.
5. Rybakova MG. Sepsis: ot sindroma sistemnoj vospalitel'noj reakcii do organnoj disfunkcii. Arhiv patologii. 2021; 83 (1): 67–72. Dostupno po ssylke: https://doi.org/10.17116/patol20218301167. Russian.
6. Bajramova SS, Cygankova OV, Nikolaev KYu, Timoshhenko OV, Nasirova ShT, Starichkov A A. Primenenie polukolichestvennogo jekspress-testa na prokal'citonin v diagnostike vnebol'nichnoj pnevmonii u pacientov s VICh-infekciej. Vestnik terapevta. 2024; 2 (63): 28–36. Dostupno po ssylke: https://doi.org/10.31550/2712-8601-VT-2024-2-4. Russian.
7. Global report on the epidemiology and burden of sepsis: current evidence, identifying gaps and future directions. Geneva: World Health Organization; 2020. Ссылка активна на 24.12.2024. Available from: https://www.who.int/publications/i/item/9789240010789.
8. Yankov YG, Bocheva Y. Comparative Characterization of Procalcitonin (Sensitivity, Specificity, Predictability, and Cut-Off Reference Values) as a Marker of Inflammation in Odontogenic Abscesses of the Head and Neck in the Female Population. Cureus Journal. 2023; 15 (11): e48207. Available from: https://doi.org/10.7759/cureus.48207.
9. Paudel R, Dogra P, Montgomery-Yates AA, Coz Yataco A. Procalcitonin: A promising tool or just another overhyped test? International Journal of Medical Sciences. 2020; 17 (3): 332–7. Available from: https://doi.org/10.7150/ijms.39367.
10. Kabanova AA, Pohodenko-Chudakova IO, Kabanova SA. Sindrom sistemnogo vospalitel'nogo otveta i syvorotochnyj prokal'citonin pri odontogennoj infekcii cheljustno-licevoj oblasti. Rossijskij mediko-biologicheskij vestnik imeni akademika I. P. Pavlova. 2023; 31 (1): 119–25. Available from: https://doi.org/10.17816/PAVLOVJ106281. Russian.
11. Assicot M, Gendrel D, Carsin H, Raymond J, Guilbaud J, Bohuon C. High serum procalcitonin concentrations in patients with sepsis and infection. Lancet Journal. 1993; 341 (8844): 515–28. Available from: https://doi.org/10.1016/0140-6736(93)90277-n.
12. Aloisio E, Dolci A, Panteghini M. Procalcitonin: Between evidence and critical issues. Clinica Chimica Acta Journalю 2019; 496: 7–12. Available from: https://doi.org/10.1016/j.cca.2019.06.010.
13. Hausfater P, Robert Boter N, Morales Indiano C, Cancella de Abreu M, Marin AM, Pernet J, Quesada D, Castro I, Careaga D, Arock M, Tejidor L, Velly L. Monocyte distribution width (MDW) performance as an early sepsis indicator in the emergency department: comparison with CRP and procalcitonin in a multicenter international European prospective study. Crit Care. 2021; 25 (1): 227. Available from: https://doi.org/10.1186/s13054-021-03622-5.
14. Bègue L, Schlund M, Raoul G, Ferri J, Lauwers L, Nicot R. Biological factors predicting the length of hospital stay in odontogenic cellulitis. Journal of Stomatology oral and Maxillofacial Surgery. 2021; 123 (3): 303–8. Available from: https://doi.org/10.1016/j.jormas.2021.07.007.
15. Novikova IS, Gulenko OV, Gerbova TV. Ocenka urovnej ferritina i C-reaktivnogo belka u pacientov s odontogennymi flegmonami cheljustno-licevoj oblasti. Operativnaja hirurgija i klinicheskaja anatomija (Pirogovskij nauchnyj zhurnal). 2024; 8 (4): 49–54. Available from: https://doi.org/10.17116/operhirurg2024804149. Russian.
16. Weise H, Naros A, Weise C. Severe odontogenic infections with septic progress — a constant and increasing challenge: a retrospective analysis. BMC Oral Health Journal. 2019; 19 (1): 173. Available from: https://doi.org/10.1186/s12903-019-0866-6.
17. Dave M, Barry S, Coulthard P. An evaluation of sepsis in dentistry. British Dental Journal. 2021; 230 (6): 351–7. Available from: https://doi.org/10.1038/s41415-021-2724-6.
18. Kim J-K, Lee J-H. Clinical utility of procalcitonin in severe odontogenic maxillofacial infection. Maxillofacial Plastic and Reconstructive Surgery Journal. 2021; 43 (1): 3. Available from: https://doi.org/10.1186/s40902-020-00288-x.

Литература

1. Global oral health status report. Towards universal health coverage for oral health by 2030. 2022. Ssylka aktivna na 24.12.2024. Available from: https://www.who.int/publications/i/item/9789240061484.
2. Рабинович С. А., Заводиленко Л. А. Материалы 21-

го Всероссийского стоматологического форума. Безопасное обезболивание в стоматологии. Российская стоматология. 2024; 17 (3): 75–76. Доступно по ссылке: http://doi.org/10.17116/rosstomat20241703140.
3. Салахов А. К., Ксембаев С. С., Байкеев Р. Ф., Силагадзе Е. М. Стоматологическая заболеваемость населения России. Казанский медицинский журнал. 2020; 101 (5): 713–8. Доступно по ссылке: http://doi.org/10.17816/KMJ2020-713.
4. Бельченко В. А., Чантырь И. В. Маршрутизация пациентов с челюстно-лицевой патологией в условиях мегаполиса: вызовы и решения. Здоровье мегаполиса. 2022; 3 (3): 46–57. Доступно по ссылке: https://doi.org/10.47619/2713-2617.zm.2022.v.3i3;46-57.
5. Рыбакова М. Г. Сепсис: от синдрома системной воспалительной реакции до органной дисфункции. Архив патологии. 2021; 83 (1): 67–72. Доступно по ссылке: https://doi.org/10.17116/patol20218301167.
6. Байрамова С. С., Цыганкова О. В., Николаев К. Ю., Тимощенко О. В., Насирова Ш. Т., Старичков А. А. Применение полуколичественного экспресс-теста на прокальцитонин в диагностике внебольничной пневмонии у пациентов с ВИЧ-инфекцией. Вестник терапевта. 2024; 2 (63): 28–36. Доступно по ссылке: https://doi.org/10.31550/2712-8601-VT-2024-2-4.
7. Global report on the epidemiology and burden of sepsis: current evidence, identifying gaps and future directions. Geneva: World Health Organization; 2020. Ссылка активна на 24.12.2024. Available from: https://www.who.int/publications/i/item/9789240010789.
8. Yankov YG, Bocheva Y. Comparative Characterization of Procalcitonin (Sensitivity, Specificity, Predictability, and Cut-Off Reference Values) as a Marker of Inflammation in Odontogenic Abscesses of the Head and Neck in the Female Population. Cureus Journal. 2023; 15 (11): e48207. Available from: https://doi.org/10.7759/cureus.48207.
9. Paudel R, Dogra P, Montgomery-Yates AA, Coz Yataco A. Procalcitonin: A promising tool or just another overhyped test? International Journal of Medical Sciences. 2020; 17 (3): 332–7. Available from: https://doi.org/10.7150/ijms.39367.
10. Кабанова А. А., Походенько-Чудакова И. О., Кабанова С. А. Синдром системного воспалительного ответа и сывороточный прокальцитонин при одонтогенной инфекции челюстно-лицевой области. Российский медико-биологический вестник имени академика И. П. Павлова. 2023; 31 (1): 119–25. Available from: https://doi.org/10.17816/PAVLOVJ106281.
11. Assicot M, Gendrel D, Carsin H, Raymond J, Guilbaud J, Bohuon C. High serum procalcitonin concentrations in patients with sepsis and infection. Lancet Journal. 1993; 341 (8844): 515–28. Available from: https://doi.org/10.1016/0140-6736(93)90277-n.
12. Aloisio E, Dolci A, Panteghini M. Procalcitonin: Between evidence and critical issues. Clinica Chimica Acta Journalю 2019; 496: 7–12. Available from: https://doi.org/10.1016/j.cca.2019.06.010.
13. Hausfater P, Robert Boter N, Morales Indiano C, Cancella de Abreu M, Marin AM, Pernet J, Quesada D, Castro I, Careaga D, Arock M, Tejidor L, Velly L. Monocyte distribution width (MDW) performance as an early sepsis indicator in the emergency department: comparison with CRP and procalcitonin in a multicenter international European prospective study. Crit Care. 2021; 25 (1): 227. Available from: https://doi.org/10.1186/s13054-021-03622-5.
14. Bègue L, Schlund M, Raoul G, Ferri J, Lauwers L, Nicot R. Biological factors predicting the length of hospital stay in odontogenic cellulitis. Journal of Stomatology oral and Maxillofacial Surgery. 2021; 123 (3): 303–8. Available from: https://doi.org/10.1016/j.jormas.2021.07.007.
15. Новикова И. С., Гуленко О. В., Гербова Т. В. Оценка уровней ферритина и С-реактивного белка у пациентов с одонтогенными флегмонами челюстно-лицевой области. Оперативная хирургия и клиническая анатомия (Пироговский научный журнал). 2024; 8 (4): 49–54. Available from: https://doi.org/10.17116/operhirurg2024804149.
16. Weise H, Naros A, Weise C. Severe odontogenic infections with septic progress — a constant and increasing challenge: a retrospective analysis. BMC Oral Health Journal. 2019; 19 (1): 173. Available from: https://doi.org/10.1186/s12903-019-0866-6.
17. Dave M, Barry S, Coulthard P. An evaluation of sepsis in dentistry. British Dental Journal. 2021; 230 (6): 351–7. Available from: https://doi.org/10.1038/s41415-021-2724-6.
18. Kim J-K, Lee J-H. Clinical utility of procalcitonin in severe odontogenic maxillofacial infection. Maxillofacial Plastic and Reconstructive Surgery Journal. 2021; 43 (1): 3. Available from: https://doi.org/10.1186/s40902-020-00288-x.

DIAGNOSTIC POTENTIAL OF THE SOFTWARE-HARDWARE COMPLEX FOR ANALYSIS OF SELF-IDENTIFICATION PHENOMENON IN EARLY CHILDHOOD

Nikishina VB[1], Petrash EA[1] ✉, Chausov AS[1], Kanimetov KK[2]

[1] Pirogov Russian National Research Medical University, Moscow, Russia

[2] Neuro Speech Therapy Center "Above the Rainbow", Moscow, Russia

The relevance of the study provided results from the need to search for the objectifying methods to assess self-identification phenomenon in early childhood. The study aimed to evaluate the diagnostic potential of the software-hardware complex for analysis of self-identification phenomenon in young children. The sample consisted of 136 subjects of early age (12–36 months): 57 boys and 79 girls. Assessment methods: functional neuropsychological tests for evaluation of facial and optical-spatial gnosis; test 22 — mirror image series of the Bayley-III cognitive scale; self-recognition mirror test; the developed software-hardware complex for analysis of self-identification phenomenon in early childhood (SHC). The study conducted has shown that self-identification emerges at the age of 18 months, which has been also confirmed by the earlier research. However, the response to one's own reflection in the mirror as one sign of self-identification manifests itself in children at an earlier age and in some children turns out to be shaped by the age of 12 months, which is suggested by the facts of successful test execution in the group aged 12–17 months and low specificity of the method for self-identification. Thus, high SHC specificity for self-identification in early childhood is reported based on the findings.

Keywords: early age, self-identification, software-hardware complex

Author contribution: the authors contributed to the study equally.

Compliance with ethical standards: the study was approved by the Ethics Committee of the Pirogov Russian National Research Medical University (protocol No. 240 dated 20 May 2024); the informed consent was submitted by all study participants.

✉ **Correspondence should be addressed:** Ekaterina A. Petrash
Ostrovityanov, 1, Moscow, 117997, Russia; petrash@mail.ru

Received: 28.03.2025 **Accepted:** 14.04.2025 **Published online:** 25.04.2025

DOI: 10.24075/brsmu.2025.021

ДИАГНОСТИЧЕСКИЙ ПОТЕНЦИАЛ ПРОГРАММНО-АППАРАТНОГО КОМПЛЕКСА АНАЛИЗА ФЕНОМЕНА САМОИДЕНТИФИКАЦИИ ДЕТЕЙ РАННЕГО ВОЗРАСТА

В. Б. Никишина[1], Е. А. Петраш[1] ✉, А. С. Чаусов[1], К. К. Каниметов[2]

[1] Российский национальный исследовательский медицинский университет имени Н. И. Пирогова, Москва, Россия

[2] Нейрологопедический центр «Выше радуги», Москва, Россия

Актуальность предлагаемого исследования обусловлена необходимостью поиска объективизирующих методов оценки феномена самоидентификации детей раннего возраста. Целью исследования было оценить диагностический потенциал программно-аппаратного комплекса анализа феномена самоидентификации детей раннего возраста. Объем выборки составил 136 испытуемых раннего возраста (12–36 месяцев) — 57 мальчиков и 79 девочек. Методы исследования: функциональные нейропсихологические пробы оценки лицевого и оптико-пространственного гнозиса; проба 22 — Mirror image series когнитивной шкалы Bayley-III; Self-recognition mirror test; разработанный программно-аппаратный комплекс анализа феномена самоидентификации детей раннего возраста (ПАК). В результате проведенного исследования установлено, что самоидентификация появляется в возрасте 18 месяцев, что также подтверждено ранее проведенными исследованиями. Однако реакция на свое отражение в зеркале как одно из проявлений самоидентификации наблюдается у детей в более раннем возрасте и к 12 месяцам оказывается уже сформированной у части детей, на что указывают наличие успешных выполнений пробы в группе 12–17 месяцев и низкая специфичность методики для самоидентификации. Таким образом, на основании полученных результатов исследования зафиксирована высокая специфичность к самоидентификации детей раннего возраста ПАК.

Ключевые слова: ранний возраст, самоидентификация, программно-аппаратный комплекс

Вклад авторов: вклад авторов в исследование равнозначный

Соблюдение этических стандартов: исследование одобрено этическим комитетом РНИМУ имени Н. И. Пирогова (протокол № 240 от 20 мая 2024 г.); все участники подписали добровольное информированное согласие на обследование.

✉ **Для корреспонденции:** Екатерина Анатольевна Петраш
ул. Островитянова, д. 1, г. Москва, 117997, Россия; petrash@mail.ru

Статья получена: 28.03.2025 **Статья принята к печати:** 14.04.2025 **Опубликована онлайн:** 25.04.2025

DOI: 10.24075/vrgmu.2025.021

In today's psychological science there is a problem of measurability and accuracy of measurement of the early-onset complex mental phenomena. Currently, mental development in early childhood is assessed by observation and scaling methods, which are characterized by high degree of subjectivity. The following equipment is used to assess self-identification at older ages: various types of speech therapy mirrors, during working with which it is necessary not only to find parts of the face, but also to correctly execute actions of the articulatory system; the Sondsorry technique, according to which it is necessary to accurately reproduce movements after listening to music; the Timocco complex, which is used to control movements of the character through one's own movements (through the camera).

In the last decade (2014–2023), the artificial intelligence and machine learning technologies have gained tremendous development. The range of tasks that can be solved with the help of those is growing every year. The current level of the artificial intelligence technology development makes it possible to use hardware solutions for working on challenging diagnostic issues [1].

B. Amsterdam, who published his experiment involving the use of the self-recognition mirror test, modification of the mark test (designed for primate experiments by Gordon G. Gallup in 1970 [2]) aimed at determining human self-identification, in infants in 1972, was a pioneer in studies of human self-identification. The author found that children started to identify their reflection in the mirror as representation of their body at the age of 1.5–2 years [3]. Multiple subsequent studies aimed to develop the problem of self-identification in early childhood were associated with the following names: A. Aron, B. Fraley [4], B. I. Bertenthal, K. W. Fischer [5], D. Bischof-Köhler [6], T. Broesch [7], S. Duval, R. A. Wicklund [8], K. Guise [9], J. Kärtner [10], J. P. Keenan [11], M. Lewis [12], K. Musholt [13], P. Rochat [14], S. Savanah [15].

In 1977, it was shown that the mentally retarded individuals not always successfully passed the self-recognition mirror test [16]. Later a number of scientists [17–19] studied self-identification in various disorders, such as schizotypal personality disorder, Alzheimer's disease, Down syndrome, autism, schizophrenia, and split-brain syndrome.

In 1999–2001, a number of studies were conducted aimed at identifying neuropsychological correlates of human self-identification suggesting that in humans self-identification was localized in the right hemisphere [20]. In 1999 [21] and 2005 [22], it was shown that patients with local brain damage in the right prefrontal cortex were unable to identify their reflection in the mirror as their own, while recognition of faces of other people was preserved, even when using the mirror. One of the leading researches disclosing the current view of the self-identification brain substrate structure are van S. J. Veiuw and S. A. Chance, who used fMRI to reveal the structure of the cerebral cortex activation associated with self-identification in 2014. Based on the experimental results they concluded that the most important were prefrontal cortex and the temporoparietal tracts [23].

Thus, the historical and prospective analysis of the methods to assess the self-identification phenomenon has shown that the mark test and its modification, the self-recognition mirror test, are used to identify neurocognitive self-identification markers in animals and humans, including in clinical trials. The conditions of conducting the test vary depending on the task; globally, these can be divided into three types: experiment without any additional intervention (used to assess humans, who are familiar with the mirror); experiment involving spontaneous learning how to interact with the mirror (used for all animal species); experiment involving controlled learning how to interact with the mirror (used for the majority of animals, except some primate species).

Willingness to interact with their reflection, i.e. to examine it, smile at it, play with it, represents one of the factors of self-identification development in early childhood. Such a positive response to their reflection is reported in both children, who do not yet have self-identification due to age, and children, who have already developed self-identification [24, 25].

The concept by Johannes L. Brandl, according to which neurocognitive self-identification markers are defined as neurocognitive functions that ensure the child's self-identification, represents methodological substantiation of the study reported [26]. On the one hand, self-recognition in the mirror is implemented based on the knowledge, what one's face looks like; on the other hand, it is implemented based on integration of proprioceptive and exteroceptive sensations with visual information. This makes is possible to match a visible reflection to one's movements and define oneself as a source of these movements. The cerebral cortex activation in the zones responsible for facial gnosis that takes place during execution of self-identification tasks also confirms an important role of recognizing one's own face in the mirror in the development of self-identification [23]. Thus, the following are considered as neurocognitive self-identification markers: positive response to the reflection; proprioceptive and exteroceptive gnosis; visual gnosis (facial, simultaneous, optical-spatial).

Conceptually, our reasoning is based on the mental ontogenesis concept. In accordance with the ontogenetic patterns, the self-identification process initiation begins with the emergence of the revival complex being an innovation of infancy (at the age of 2.5–3 months) and characterized by the emergence of vocalization, motor activity, and smile upon seeing a primary caregiver (mother or father). Later, at the age of 7–8 months, differentiation of other people's faces occurs within the "friend or foe" boundaries. The infant begins to differentiate his/her face from the face of another person by the age of 18 months (Fig. 1).

The development of the software-hardware complex (SHC) will make it possible to objectify the procedure for assessment of mental development in early childhood (age 1–3 years), as well as to shape the system of measurable criteria.

The study aimed to evaluate the diagnostic potential of the software-hardware complex for analysis of self-identification phenomenon in early childhood.

METHODS

The total sample size was 136 individuals (57 (42%) boys and 79 (58%) girls); the average age was 25.35 ± 10.38 months. The sample was formed based on the selected inclusion and exclusion criteria. Inclusion criteria: age 1–3 years; female and male sex; age-appropriate neurotypical cognitive development. Exclusion criteria: age under 1 year or over 3 years; noncompliance with the cognitive development age norms; decompensated severe somatic disorder; hearing and vision impairment.

Three study groups were formed based on the age periods critical for self-identification [3]: toddlers aged 12–17 months, toddlers aged 18–23 months, and toddlers over the age of 24 months.

The study was conducted at the Veltischev Research Clinical Institute of Pediatrics and Pediatric Surgery (Pirogov Russian National Research Medical University), Russian Children's Clinical Hospital (branch of the Pirogov Russian National Research Medical University), and Roshal Children's Clinical Center. Examination time per subject was 20–35 min.

The study was conducted in two phases. The goal of the first phase was to assess facial gnosis in early childhood using functional neuropsychological tests. The child was positioned in front of the experimenter (most often on mother's knees). The experimenter attracted the child's attention, introduced him/herself and invited the child to play; after that he/she asked: "Show me where your nose (or other part of the face) is". The same procedure was used during the second test, but the child was asked to point at parts of the face of his/her primary caregiver. To perform the third test, the experimenter asked the primary caregiver to show images of relatives (mother, father, grandmother, grandfather, brother/sister) and ask the child,

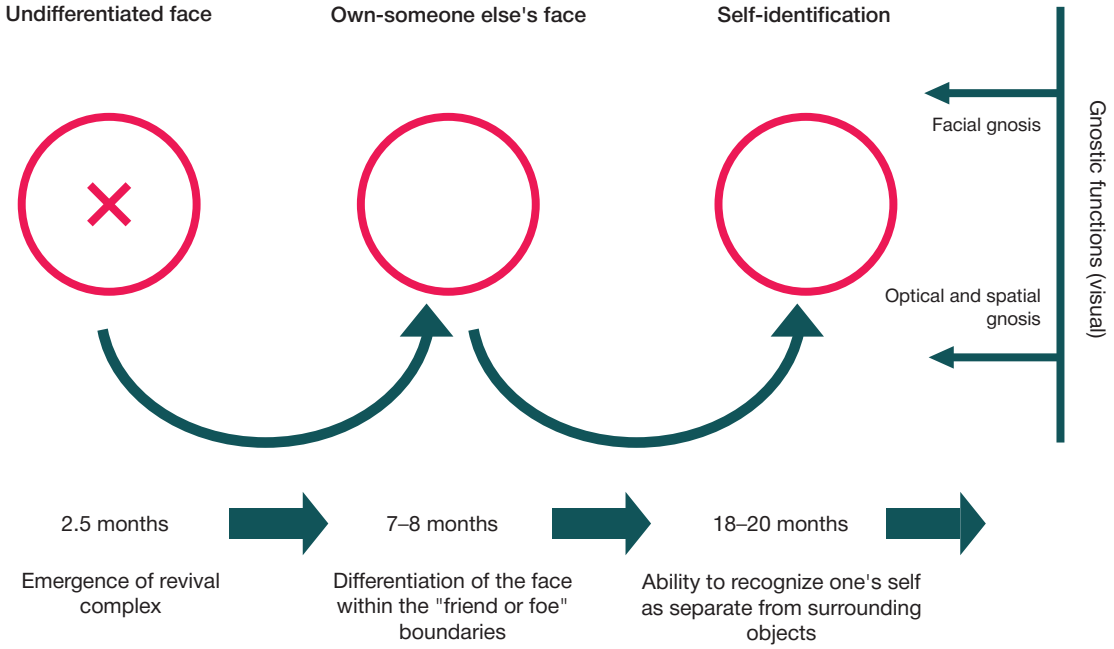

Fig. 1. Scheme of conceptual reasoning of ontogenesis of the self-identification phenomenon in early childhood

who was pictured. Facial gnosis was assessed based on the tempo, accuracy, and differentiation using the scale by Zh.M. Glozman: correct indication of the own face parts by the subject in accordance with the verbal instruction; correct indication of the other person's parts by the subject in accordance with the verbal instruction; recognition of the relative's face from a photograph.

The goal of the second phase was to assess self-identification in early childhood using the following: test 22 — mirror image series of the Bayley-III cognitive scale [27]; self-recognition mirror test (SMT) [3]; software-hardware complex (SHC) developed for analysis of self-identification phenomenon in early childhood [28].

The Bayley-III test procedure is as follows: the subject is shown a mirror sized 15 × 21 cm at a distance of 20–25 cm from the face, and the child's response to his/her reflection is assessed. Positive assessment is reported when the child is interested in the reflection, examines it and responds cheerfully.

The self-recognition mirror test procedure is as follows: the legal representative marks the subject's nose with bright cosmetics, and then the subject's behavior upon presentation of the mirror is recorded. The test is considered to be passed when the subject tries to touch or wipe the mark off his/her face, as well as when he/she uses a personal pronoun or says his/her name when asked "Who is this?" while pointing to the mirror. The test duration is 10 min, every 2 min 30 s the experimenter asks the legal representative to attract the subject's attention to the mirror, saying: "Look! Look! Look! Who is it?"

The procedure of testing using the SHC developed is as follows: the subject is positioned in front of the screen and video camera at a distance of 40–60 cm without any additional instructions. An image acquired using a video camera is displayed on the screen, with the marks drawn on the faces (Fig. 2).

If the child is distracted, one should draw his/her attention to the screen with the words: "Look!" If the subject does not respond to the mark within 20 s, the size of the mark is changed, and then, upon reaching the maximum size, its color is changed. If there is some response to the mark or all color

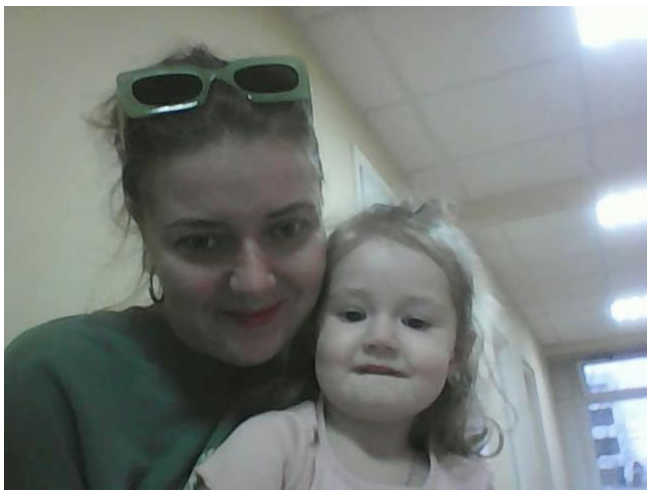

Image acquired using a video camera during assessment (35 months)

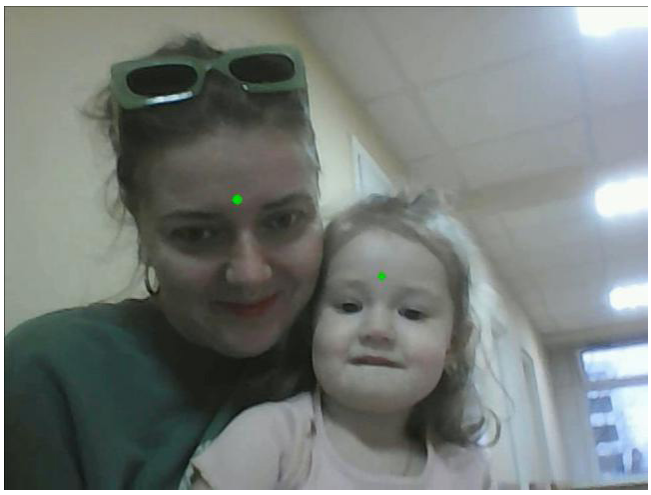

Image displayed on the screen during assessment (35 months)

Fig. 2. Example image acquired using the SHC

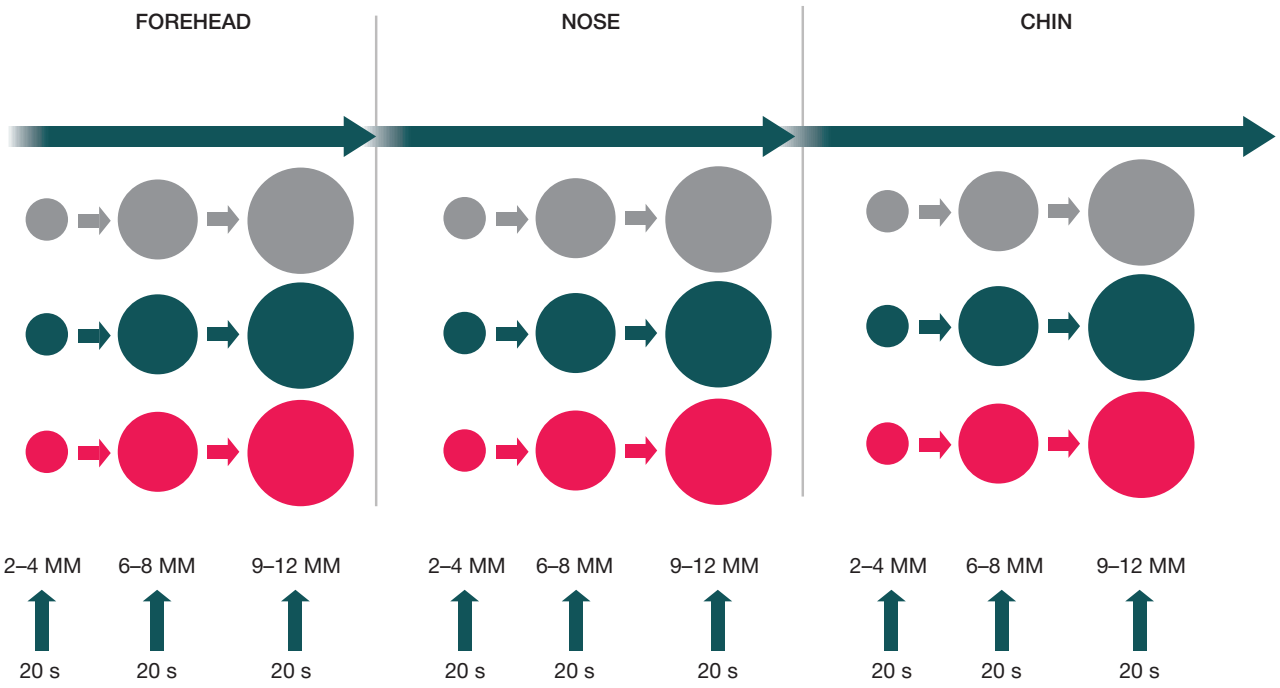

Fig. 3. Scheme of presenting the marks during the procedure of self-identification phenomenon assessment in early childhood using SHC

and size options presented, the position of the mark is changed to the next one. The marks are presented in the following order: green (first 2–4 mm, then 6–8 mm, and then 9–12 mm); blue (also as the size increases); red, as the size increases as well. The marks are presented sequentially in the following order of positioning: forehead, nose, chin (Fig. 3).

The diagnostic potential of the software and hardware computer vision technology for analysis of self-identification phenomenon in early childhood was assessed based on the sensitivity and specificity criteria. Sensitivity of the software and hardware technology characterizes accuracy of the diagnostic method, with which the program correctly determines the presence of the studied phenomenon and determines tolerance for type I errors (share of positive results defined as positive by the diagnostic method in the entire pool of the results obtained). Specificity characterizes accuracy of the diagnostic method when recording the studied trait (tolerance for type II errors) and shows the share of negative results determined as negative by the diagnostic method (in the entire pool of the results obtained).

Processing and interpretation of the acquired empirical study results

Quantitative data processing was performed using the descriptive and correlation statistics (Spearman's rank correlation), as well as using factor analysis with varimax rotation ($p < 0.05$).

RESULTS

Assessment of the results of performing functional neuropsychological tests for the diagnosis of facial and optical-spatial gnosis has shown, that children under the age of 18 months demonstrate low tempo, accuracy, and differentiation in all the tests proposed.

The age-specific features allowing one to trace the process of developing complex visual gnosis types in early childhood

Table 1. Results of correlation analysis of the mirror image series, SMT, and SHC tests in different age groups performed using Spearman's rank correlation

Indicators compared	Age groups (months)			
	12–17	18–23	24+	Total
SMT and SHC with the mark on the forehead	–	0.43	0.43	0.52**
SMT and SHC with the mark on the nose	–	0.68*	0.43	0.59**
SMT and SHC with the mark on the chin	–	0.68*	0.50*	0.66**
SMT and SHC	–	0.68*	0.50*	0.66**
SMT and Bayley-III	–	0.62	0.68**	0.64**
SHC with the mark on the forehead and SHC with the mark on the nose	–	0.62	0.58**	0.63**
SHC with the mark on the forehead and SHC with the mark on the chin	–	0.62	0.82**	0.79**
SHC with the mark on the nose and SHC with the mark on the chin	–	1**	0.82**	0.89**
Bayley-III and SHC with the mark on the forehead	–	0.25	0.27	0.33*
Bayley-III and SHC with the mark on the nose	–	0.41	0.27	0.38*
Bayley-III and SHC with the mark on the chin	–	0.41	0.33	0.42**
Bayley-III and SHC	–	0.41	0.33	0.42**

Note: * — $p < 0.05$; ** — $p < 0.01$.

Table 2. Results of factor analysis of facial gnosis and self-identification in early childhood

Variable		Factor 1	Factor 2	Factor 3
Indication of the own face part in accordance with the verbal instruction	Tempo	0.89	0.33	0.24
	Accuracy	0.91	0.25	0.23
	Differentiation	0.91	0.25	0.23
Indication of the other person's face part in accordance with the verbal instruction	Tempo	0.82	0.19	0.46
	Accuracy	0.82	0.17	0.48
	Differentiation	0.81	0.2	0.44
Recognition of the relative's photograph	Tempo	0.57	0.1	0.82
	Accuracy	0.57	0.1	0.82
	Differentiation	0.57	0.1	0.82
Bayley-III		0.17	0.34	0.83
Self-recognition mirror test		0.41	0.64	0.28
SHC with the mark on the face		0.13	0.84	0.09
SHC with the mark on the nose		0.16	0.89	0.11
SHC with the mark on the chin		0.19	0.95	0.12
SHC		0.19	0.95	0.12

have been identified based on the results obtained. The following sequence of phases have been determined: at the age of 16 months, the process of recognizing parts of another person's face is shaped (in accordance with the verbal instruction), which is associated with the rapid development of the nominative function of speech; then, by 18 months, optical-spatial gnosis is developed, specifically recognition of the spatially related parts of the face in a picture with the schematic view. Furthermore, within 16–18 months recognition of the parts of one's own face in accordance with the verbal instruction is developed. At the age of 18–22 months, arrangement of the details of the schematic face representation within the boundaries of face oval relative to each other becomes possible (ontogenetically accessible). This, in turn, provides the basis for recognition of faces of close and familiar people, and then for differentiation of faces of strangers (or unfamiliar people) in both real world and pictures (schematic or realistic). As for the tempo, accuracy, and differentiation criteria in terms of ontogenesis, the tempo characteristics are shaped first, than differentiation, and after that the accuracy characteristics.

The analysis of self-identification in early childhood was conducted by the following methods: self-recognition mirror test; test 22, mirror image series of the Bayley-III cognitive scale; SHC. The use of the specified instruments implies qualitative assessment of the results based on the execution criterion (identified — not identified). As a result, it has been found that the percentage of successful execution of all self-identification tests increases with age: children become able to successfully pass the self-recognition mirror test and SHC since the age of 18 months.

Then we performed assessment of the proposed SHC external validity, which consisted of two phases. In the first phase, we performed assessment based on the sensitivity and specificity criteria. The results of the self-recognition mirror test were determined as benchmark positive and negative values, while test 22, mirror image series of the Bayley-III cognitive scale, and SHC were determined as assessment methods to be compared. High SHC specificity is reported for the task of analyzing self-identification phenomenon in early childhood with the sensitivity increasing from the test with the mark on the forehead (45.45%) to the test with the mark on the nose (54.55%) and from the test with the mark on the nose to the test with the mark on the chin (63.64%). In general, the maximum SHC sensitivity is reported for the age group 18–23 months, but the test with the mark on the forehead shows the highest sensitivity in the older group (24+ months). It is impossible to assess SHC sensitivity in the group under the age of 18 months due to the lack of the facts of successful SMT execution by children of this age.

In the second phase, we assessed consistency of the results of analyzing self-identification in early childhood obtained using the SMT, SHC, and mirror image series methods. Table 1 provides the results of pairwise correlation analysis of the above methods performed using Spearman's rank correlation. When performing analysis of the SHC results, each test (with the mark on different parts of the face) was assessed separately, along with the indicator of passing of at least one of three tests during assessment of the subject.

The age group 18–23 months has shown a significant correlation between the SMT and SHC tests with the marks on the nose and chin, as well as with the indicator of successful execution of at least one test ($p < 0.05$). Furthermore, the results of the SHC tests with the marks on the nose and chin are fully consistent ($p < 0.01$). In the group over the age of 24 months, significant correlations of the SMT results with the SHC test with the mark on the chin and the indicator of successful execution of at least one test are observed ($p < 0.05$). Moreover, there are significant correlations between all SHC tests and between SMT and the Bayley-III score ($p < 0.01$). The analysis of the entire sample has revealed significant correlations of all the studied parameters. The highest correlation coefficients are reported for the correlations between SMT and the SHC test with the mark on the chin, indicator of successful execution of at least one test and the Bayley-III score, as well as for correlations between SHC tests.

To assess neurocognitive self-identification markers in early childhood, the factor analysis with varimax rotation was performed based on the results of assessing facial and optical and spatial gnosis, as well as self-identification scores obtained using the mirror image series, SMT, and SHC. Criteria were selected based on the Kaiser's criterion; to reduce the number of intersecting factors in the tested variables, we used orthogonal decomposition with varimax rotation. The fact of the variable belonging to the factor was determined based on the weight value ≥ 0.4. The factor analysis results are provided in Table 2.

We distinguished three factors based on the factor analysis of the indicators of facial and optical-spatial gnosis and the

methods to assess self-identification in early childhood. Factor 1: indication of one's own face part in accordance with the verbal instruction — 0.9 (the mean of the assessment criteria); indication of the other person's face part in accordance with the verbal instruction — 0.817 (the mean of the assessment criteria); recognition of the relative's photograph — 0.56 (the mean of the assessment criteria); self-recognition mirror test — 0.41. Factor 2: indicator of successful execution of at least one SHC test — 0.95; SHC tests: with the mark on the face — 0.82; with the mark on the nose — 0.89; with the mark on the chin — 0.95; self-recognition mirror test: 0.64. Factor 3: Bayley-III scale test — 0.83; recognition of the relative from the photograph — 0.8 (the mean of the assessment criteria); indication of the other person's face part in accordance with the verbal instruction — 0.46 (the mean of the assessment criteria). Based on the factors distinguished we can conclude that the self-recognition mirror test results are more strongly correlated to the SHC results, than to the Bayley-III scale test and facial gnosis assessment test results.

Consistency of variables within the factors was tested using the Cronbach's alpha; high consistency coefficients were reported: factor 1 — $\alpha = 0.97$; factor 2 — $\alpha = 0.93$; factor 3 — $\alpha = 0.97$.

DISCUSSION

Self-identification emerges at the age of 18 months, which is confirmed by the earlier reported research [3] and the results of our study, in which no cases of successful self-identification test execution have been revealed in the group aged 12–17 months. At the same time, the response to one's own reflection in the mirror registered using the mirror image series emerges in children at an earlier age and in some children turns out to be developed by the age of 12 months, which is suggested by the facts of successful test execution in the group aged 12–17 months and low method specificity for self-identification. Given the tandem with high sensitivity and the presence of significant correlations based on the external validity assessment results (obtained using the Bayley-III scale test and self-recognition mirror test) reported for the group over the age of 24 months and the entire sample, it can be concluded that interest in one's own reflection, examination of the reflection, and positive response represent a neurocognitive marker of self-identification in early childhood.

CONCLUSIONS

The software-hardware complex for analysis of self-identification phenomenon in early childhood shows high specificity for self-identification in young children, while the method sensitivity is not so high. We assume that sensitivity is affected by the mark characteristics and realism. The data obtained show the increase in sensitivity and correlation with the self-recognition mirror test from the first test presented to the last one, along with significant correlations between two last SHC tests in all age groups, which can result from the sequence effect. The factor analysis showed that the self-recognition mirror test belonged to two factors: factor of predominant association with facial gnosis; factor of predominant association with SHC. Furthermore, the self-recognition mirror test results turned out to be most important for the second factor, which confirmed the relationship between the SHC and self-recognition mirror test results. The fact that the self-recognition mirror test results belong to the first factor confirms the importance of facial gnosis for self-identification in early childhood. Accordingly, assessment of the influence of changing the color, shape of the mark, computer algorithms for positioning the mark relative to the subject's face and the use of realistic images as a mark on the SHC sensitivity and assessment of the influence of the sequence and position of the mark on the subject's face on the test execution success are considered as the potential of further research involving the use of the SHC developed.

References

1. Niilo V. Valtakari, Roy S. Hessels, Diederick C. Niehorster, Charlotte Viktorsson, Pär Nyström, Terje Falck-Ytter, Chantal Kemner, Ignace T.C. Hooge A field test of computer-vision-based gaze estimation in psychology. Behavior Research Methods. 2023; p. 1900–15.
2. Gallup GG. Chimpanzees: self-recognition. Science. 1970; p. 86–87.
3. Amsterdam B. Mirror self-image reactions before age two. Dev Psychobiol. 1972; p. 297–305.
4. Aron A, Fraley B. Relationship closeness as including other in the self: cognitive underpinnings and measures. Soc Cognit. 1999; p. 140–160
5. Bertenthal BI, Fischer KW. Development of self-recognition in the infant. Developmental Psychology. 1978; p. 44–50.
6. Bischof-Köhler D. Empathy and self-recognition in phylogenetic and ontogenetic perspective. Emotion Review. 2012; p. 40–48.
7. Broesch T, Callaghan T, Henrich J, Murphy C, Rochat P. Cultural variations in children's mirror self-recognition. Journal of Cross Cultural Psychology. 2010; p. 1–13.
8. Duval S, Wicklund RA. A theory of objective self-awareness. New York: Academic Press, 1972; 238 p.
9. Guise K, Kelly K, Romanowski J, Vogeley K, Platek SM, Murray E, et al. The anatomical and evolutionary relationship between self-awareness and theory of mind. Human Nature. 2007; p. 132–142.
10. Kärtner J, Keller H, Chaudhary N, Yovski RD. The development of mirror self-recognition in difference sociocultural contexts. Monographs of the Society for Research in Child Development. 2012; 316 p.
11. Keenan J, Gallup GG, Falk D. The face in the mirror: The search for the origin of consciousness. New York: Harper Collins. 2003; 304 p.
12. Lewis M. The origins and uses of self-awareness or the mental representation of me. Consciousness and Cognition. 2011; p. 120–129.
13. Musholt K. Thinking about oneself. The MIT Press. 2015; 232 p.
14. Rochat P. Self-recognition roots of human normativity // Phenomenology and the Cognitive Sciences. 2015; p. 741–753.
15. Savanah S. Mirror self-recognition and symbol-mindedness // Biology and philosophy. 2012; p. 657–673.
16. Harris LP. Self-recognition among institutionalized profoundly retarded males: A replication. Bulletin of the Psychonomic Society. 1977; p. 43–44.
17. Gallup GG, Anderson JR, Platek SM. Self-awareness, social intelligence and schizophrenia. The self in neuroscience and psychiatry. Cambridge UK: Cambridge University Press. 2003; p. 147–165.
18. Barnacz A, Johnson A, Constantino P, Keenan JP. Schizotypal personality traits and deception: The role of self-awareness. Schizophrenia Research. 2004; p. 115–116.
19. Cunningham C, Glenn S. Self-awareness in young adults with Down syndrome: I. Awareness of Down syndrome and disability. International Journal of Disability. Development and Education. 2004; p. 335–361.
20. Keenan JP, et al. Hand response differences in a self-identification task // Neuropsychologia. 2000; p. 1047–1053.
21. Breen N. Misinterpreting the mirrored self // Paper presented

at the Association for the Scientific Study of Consciousness, London, Ontario. 1999; p. 239–54.
22. Sherer M, Hart T, Whyte J, Nick TG, Yablon SA. Neuroanatomic basis of impaired self-awareness after traumatic brain injury: Findings from early computed tomography. Journal of Head Trauma and Rehabilitation. 2005; p. 287–300.
23. van Veluw SJ, Chance SA. Differentiating between self and others: An ALE meta-analysis of fMRI studies of self-recognition and theory of mind. Brain Imaging and Behavior. 2014; p. 24–38.
24. Dimaggio G, Lysaker PH, Carcione A, Nicolo G, Semerari A. Know yourself and you shall know the other . . . to a certain extent: Multiple paths of influence of self-reflection on mindreading. Consciousness and Cognition. 2008; p. 778–789.
25. Nielsen M, Dissanayake C. Pretend play, mirror self-recognition and imitation: A longitudinal investigation through the second year. Infant Behavior and Development. 2004; p. 342–365.
26. Brandl J. The puzzle of mirror self-recognition. Phemonenology and the Cognitive Sciences. 2016; p. 279–304.
27. Bayley N. Bayley scales of infant and toddler development. 3 изд. Harcourt Assessment Inc., 2006.
28. Nikishina VB, Chausov AS. Programmnyj kompleks analiza fenomena samoidentifikacii detej rannego vozrasta. Svidetel'stvo o registracii programmy dlja JeVM RU 2025611073, 16.01.2025. Russian.

Литература

1. Niilo V. Valtakari, Roy S. Hessels, Diederick C. Niehorster, Charlotte Viktorsson, Pär Nyström, Terje Falck-Ytter, Chantal Kemner, Ignace T.C. Hooge A field test of computer-vision-based gaze estimation in psychology. Behavior Research Methods. 2023; p. 1900–15.
2. Gallup GG. Chimpanzees: self-recognition. Science. 1970; p. 86–87.
3. Amsterdam B. Mirror self-image reactions before age two. Dev Psychobiol. 1972; p. 297–305.
4. Aron A, Fraley B. Relationship closeness as including other in the self: cognitive underpinnings and measures. Soc Cognit. 1999; p. 140–160
5. Bertenthal BI, Fischer KW. Development of self-recognition in the infant. Developmental Psychology. 1978; p. 44–50.
6. Bischof-Köhler D. Empathy and self-recognition in phylogenetic and ontogenetic perspective. Emotion Review. 2012; p. 40–48.
7. Broesch T, Callaghan T, Henrich J, Murphy C, Rochat P. Cultural variations in children's mirror self-recognition. Journal of Cross Cultural Psychology. 2010; p. 1–13.
8. Duval S, Wicklund RA. A theory of objective self-awareness. New York: Academic Press, 1972; 238 p.
9. Guise K, Kelly K, Romanowski J, Vogeley K, Platek SM, Murray E, et al. The anatomical and evolutionary relationship between self-awareness and theory of mind. Human Nature. 2007; p. 132–142.
10. Kärtner J, Keller H, Chaudhary N, Yovski RD. The development of mirror self-recognition in difference sociocultural contexts. Monographs of the Society for Research in Child Development. 2012; 316 p.
11. Keenan J, Gallup GG, Falk D. The face in the mirror: The search for the origin of consciousness. New York: Harper Collins. 2003; 304 p.
12. Lewis M. The origins and uses of self-awareness or the mental representation of me. Consciousness and Cognition. 2011; p. 120–129.
13. Musholt K. Thinking about oneself. The MIT Press. 2015; 232 p.
14. Rochat P. Self-recognition roots of human normativity // Phenomenology and the Cognitive Sciences. 2015; p. 741–753.
15. Savanah S. Mirror self-recognition and symbol-mindedness // Biology and philosophy. 2012; p. 657–673.
16. Harris LP. Self-recognition among institutionalized profoundly retarded males: A replication. Bulletin of the Psychonomic Society. 1977; p. 43–44.
17. Gallup GG, Anderson JR, Platek SM. Self-awareness, social intelligence and schizophrenia. The self in neuroscience and psychiatry. Cambridge UK: Cambridge University Press. 2003; p. 147–165.
18. Barnacz A, Johnson A, Constantino P, Keenan JP. Schizotypal personality traits and deception: The role of self-awareness. Schizophrenia Research. 2004; p. 115–116.
19. Cunningham C, Glenn S. Self-awareness in young adults with Down syndrome: I. Awareness of Down syndrome and disability. International Journal of Disability. Development and Education. 2004; p. 335–361.
20. Keenan JP, et al. Hand response differences in a self-identification task // Neuropsychologia. 2000; p. 1047–1053.
21. Breen N. Misinterpreting the mirrored self // Paper presented at the Association for the Scientific Study of Consciousness, London, Ontario. 1999; p. 239–54.
22. Sherer M, Hart T, Whyte J, Nick TG, Yablon SA. Neuroanatomic basis of impaired self-awareness after traumatic brain injury: Findings from early computed tomography. Journal of Head Trauma and Rehabilitation. 2005; p. 287–300.
23. van Veluw SJ, Chance SA. Differentiating between self and others: An ALE meta-analysis of fMRI studies of self-recognition and theory of mind. Brain Imaging and Behavior. 2014; p. 24–38.
24. Dimaggio G, Lysaker PH, Carcione A, Nicolo G, Semerari A. Know yourself and you shall know the other . . . to a certain extent: Multiple paths of influence of self-reflection on mindreading. Consciousness and Cognition. 2008; p. 778–789.
25. Nielsen M, Dissanayake C. Pretend play, mirror self-recognition and imitation: A longitudinal investigation through the second year. Infant Behavior and Development. 2004; p. 342–365.
26. Brandl J. The puzzle of mirror self-recognition. Phemonenology and the Cognitive Sciences. 2016; p. 279–304.
27. Bayley N. Bayley scales of infant and toddler development. 3 изд. Harcourt Assessment Inc., 2006.
28. Никишина В. Б., Чаусов А. С. Программный комплекс анализа феномена самоидентификации детей раннего возраста. Свидетельство о регистрации программы для ЭВМ RU 2025611073, 16.01.2025.

COMPARATIVE ANALYSIS OF THE HUMAN SPERM CELL ORGANELLE BIOCHEMICAL MARKERS BY CONFOCAL RAMAN SPECTROSCOPY

Nazarenko RV[1] ✉, Irzhak AV[2], Gvasalia BR[3], Pushkar DYu[3]

[1] Professor Zdanovsky Clinic LLC, Moscow, Russia

[2] Institute of Microelectronics Technology and High Purity Materials of the Russian Academy of Sciences, Chernogolovka, Russia

[3] Russian University of Medicine, Moscow, Russia

Despite widespread use of methods to assess structure and functional activity of spermatozoa, practical application of those in *in vitro* fertilization programs is currently rather limited. Limitations are primarily due to destructive nature of the methods. The study aimed to investigate the capabilities of confocal Raman spectroscopy in analysis of the human sperm organelle biochemical markers. Assessment of 176 spectra of spermatozoa collected from healthy sperm donors aged 18–35 years was performed using the Bruker Senterra confocal Raman microscope (Germany). Spectra were acquired from the sperm acrosome, nucleus, and midpiece. In addition, the spermatozoa suspension was exposed to a focused x-ray beam. As a result, bands were identified inherent to the sperm nuclear DNA — 1092 cm^{-1} and 780 cm^{-1}, typical for the head — 748 cm^{-1} (mitochondrial DNA marker); changes of shape of the triple band 420 cm^{-1}, 1445 cm^{-1} and 1486 cm^{-1} with predominance of the middle part 1445 cm^{-1} are typical for acrosomal spectra. No differences in the main Raman bands nherent to cells post DNA damage under exposure to x-ray radiation for 5 and 10 min relative to intact samples were reported. Confocal Raman spectroscopy is a promising noninvasive method to assess sperm ultrasctructure and biochemical processes.

Keywords: confocal Raman spectroscopy, sperm, DNA fragmentation, biochemical profile, metabolomics

Author contribution: Nazarenko RV — data acquisition and analysis, manuscript writing; Irzhak AV — data acquisition and analysis; Gvasalia BR, Pushkar DYu — manuscript editing.

Compliance with ethical standards: the study was approved by the Ethics Committee of the Kulakov National Medical Research Center for Obstetrics, Gynecology and Perinatology (protocol No. 10 dated 28 October 2021).

✉ **Correspondence should be addressed:** Ruslan V. Nazarenko
nazrusvad@gmail.com

Received: 22.02.2025 **Accepted:** 17.03.2025 **Published online:** 31.03.2025

DOI: 10.24075/brsmu.2025.016

СРАВНИТЕЛЬНЫЙ АНАЛИЗ БИОХИМИЧЕСКИХ МАРКЕРОВ КЛЕТОЧНЫХ ОРГАНЕЛЛ СПЕРМАТОЗОИДА ЧЕЛОВЕКА ПРИ ПОМОЩИ КОНФОКАЛЬНОЙ РАМАНОВСКОЙ СПЕКТРОСКОПИИ

Р. В. Назаренко[1] ✉, А. В. Иржак[2], Б. Р. Гвасалия[3], Д. Ю. Пушкарь[3]

[1] ООО «Клиника профессора Здановского», Москва, Россия

[2] Институт проблем технологии микроэлектроники и особо чистых материалов, Российской академии наук, Черноголовка, Россия

[3] Российский университет медицины, Москва, Россия

Несмотря на широкое распространение методов исследования структуры и функциональной активности сперматозоидов, их практическое применение в программах экстракорпорального оплодотворения на сегодняшнем этапе достаточно ограничено. Прежде всего, ограничение связано с деструктивным характером методов. Целью работы было исследование возможности конфокальной рамановской спектроскопии в анализе биохимических маркеров клеточных органелл сперматозоида человека. Анализ 176 спектров сперматозоидов, полученных от здоровых доноров спермы в возрасте 18–35 лет, выполняли на конфокальном рамановском микроскопе Senterra фирмы Bruker (Германия). Спектры снимали с акросомы, ядра и шейки сперматозоида. Дополнительно суспензию сперматозоидов подвергали воздействию фокусированного пучка рентгеновского излучения. В результате были выделены пики, присущие ДНК ядра сперматозоида — 1092 $см^{-1}$ и 780 $см^{-1}$, характерные для шейки — 748 $см^{-1}$ (маркер митохондриальной ДНК), для спектров с акросомы характерно изменение формы тройного пика 1420 $см^{-1}$, 1445 $см^{-1}$ и 1486 $см^{-1}$ с преобладанием средней части в области 1445 $см^{-1}$. Различий в основных рамановских пиках, присущих клеткам после повреждения ДНК при воздействии рентгеновского излучения в течение 5 и 10 мин, по сравнению с интактными образцами отмечено не было. Конфокальная рамановская спектроскопия является перспективным неинвазивным методом исследования ультраструктуры и биохимических процессов сперматозоида.

Ключевые слова: конфокальная рамановская спектроскопия, сперматозоид, фрагментация ДНК, биохимический профиль, метаболомика

Вклад авторов: Р. В. Назаренко — сбор и анализ данных, написание текста статьи; А. В. Иржак — сбор и анализ данных; Б. Р. Гвасалия, Д. Ю. Пушкарь — редактирование статьи.

Соблюдение этических стандартов: исследование одобрено этическим комитетом ФГБУ «НМИЦ АГП им. В. И. Кулакова» (протокол № 10 от 28 октября 2021 г.).

✉ **Для корреспонденции:** Руслан Вадимович Назаренко
nazrusvad@gmail.com

Статья получена: 22.02.2025 **Статья принята к печати:** 17.03.2025 **Опубликована онлайн:** 31.03.2025

DOI: 10.24075/vrgmu.2025.016

The last decades were marked by significant advances in various fields related to science-intensive technologies. Reproductive medicine was no exception. Every year more and more methods to assess biomaterials emerge that attract the scientists' attention.

One new method is Raman spectroscopy (or inelastic scattering spectroscopy), the principles of which were reported more than 80 years ago. Despite long history, only improvement of hardware and software made it possible to use the method to explore the detailed molecular structure ("fingerprint") of a biological sample.

There is a steadily growing interest of researchers in male infertility in general and identification of the sperm nuclear DNA damage in particular. It is well known that sperm can have good morphology and motility according to assessment criteria of the World Health Organization, but the embryo formed after fertilization of the oocyte with such sperm is characterized by low quality, low implantation rate and often stops developing [1–2]. Some DNA breakages in the sperm can be restored by the oocyte, but when the critical mass of damage is hit, the oocyte repair system is not enough. In this regard, there is growing interest in investigation of the sperm nuclear DNA and assessment of its functional state. Since the routine methods to assess ejaculate make it impossible to obtain such information using light microscopy, supplementary sperm assessment methods have recently became common. This is particularly true for sperm DNA fragmentation assessment methods [3–7]. These include staining with aniline blue, chromomycin A3, chromatin dispersion test (Comet), TUNEL, SCSA, etc. Unfortunately, all these methods are destructive and, therefore, provide very little practically useful information for using in assisted reproductive technologies. There is a demand for the method meeting the following criteria: allowing one to assess a single sperm without damaging it, allowing one to assess the sperm nuclear DNA integrity and its functional state, i.e. biochemical and metabolic profile, and to use this sperm for further fertilization by ICSI (Intra Cytoplasmic Sperm Injection). Considering the above requirements, it seems promising to study the confocal Raman spectroscopy capabilities in terms of obtaining more detailed information about the sperm structure and functional state.

Recently there have been more and more reports focused on using confocal Raman spectroscopy to assess biological tissues, living cells, subcellular organelles, and intracellular metabolic processes. However, there are not so many studies focused on assessing the sperm spectral characteristics. In 1980, Raman spectroscopy was applied to living cells, which involved the use of salmon sperm [8]. When comparing the Raman spectra acquired for sperm with normal and abnormal morphology [9], the researchers have drawn a conclusion that sperm morphology is not always correlated to proper packaging of its nuclear DNA. When assessing spectra acquired from subcellular organelles and the effects of UV radiation on those [10], spectra of the sperm acrosome, nucleus, and midpiece were reported. Other authors resumed working on the use of Raman spectroscopy for imaging of the sperm nuclear DNA damage [11]. They used UV radiation exposure to disrupt the DNA structure and reported typical band changes in the 1095/1050 cm^{-1} region. Oxidative DNA damage in the Fenton reaction with hydrogen peroxide was also reported [12]. The spectra acquired from spermatozoa damaged in this way fully matched the earlier reported ones [11]. We assumed the association between sperm morphology, its nuclear DNA integrity, and the Raman spectra acquired for the nuclear region [13]. Later these results were confirmed by other authors using the chromomycin A3, aniline blue, and acridine orange dyes for comprehensive assessment of the sperm nucleoprotein complex [14].

In the era of the omics (metabolomics, proteomics, etc.) revolution, Raman spectroscopy represents a powerful tool for investigation of biochemical processes in the cell. However, it is impossible to use the method and interpret the results without engaging experts, i.e. physicists, chemists, mathematicians, since the knowledge and skills essential for working with this method are far beyond the limits of biological or medical education.

The study aimed to acquire information about spectral characteristics of the human sperm cellular organelles, as well as to estimate the damaging effect of x-ray radiation on the human sperm nuclear nucleoprotein complex based on changes in Raman spectra.

METHODS

Healthy donors gave sperm samples through masturbation. The sexual abstinence period was 2–7 days.

Inclusion criteria for sperm donors: age 18–35 years; no hemotransmissive infection; no sexually transmitted infection; no severe chronic somatic disorder; no mental disorder; normal male karyotype 46 XY.

Exclusion criteria for sperm donors: fever at the moment of giving ejaculate; taking antibiotics, glucocorticoids, antidepressants at the moment of giving ejaculate; lack of the required (2–7 days) sexual abstinence period.

In each case routine semen analysis by light microscopy was performed. The results were interpreted in accordance with the WHO Guidelines 2010; the results corresponded to normozoospermia.

Sample preparation for confocal Raman spectroscopy

Ejaculate was centrifuged using the double density gradient technique (FertiPro, Breenem; Belgium) for 20 min at 415 g. After removing supernatant, precipitate was resuspended in phosphate buffered saline (PBS; Sigma–Aldrich, USA) at 37 °C and centrifuged again for 10 min at 415 g. Then 10 µL of the sperm suspension were applied to the aluminum substrate, the preparation was fixed using 70% ethanol and air dried.

Confocal Raman spectroscopy

The Senterra confocal Raman microscope (Bruker, Germany) was used for assessment. The instrument consists of two main blocks: a confocal binocular microscope with the image digitalization option and a spectrometer. A fully confocal system can adjust to three different excitation wavelengths ensuring the maximum possible spatial resolution. Since Senterra is based on the optical microscope, all the tools needed for visual characterization of the sample are available. Spectral analysis of various sperm compartments (nucleus, acrosome, midpiece) was performed at the laser excitation wavelength of 532 nm and power of 10 mW within the range of 280–1730 cm^{-1} with the 3–5 $см^{-1}$ resolution. The signal accumulation time for the point was 3x 20 s. Safety of the cell exposure to laser radiation and the lack of photo-induced damage with the specified power parameters have been confirmed in the literature [15].

Spectral pre-processing

Each spectrum was analyzed within the range of 680–1700 cm^{-1} after baseline correction through polynomial baseline fitting

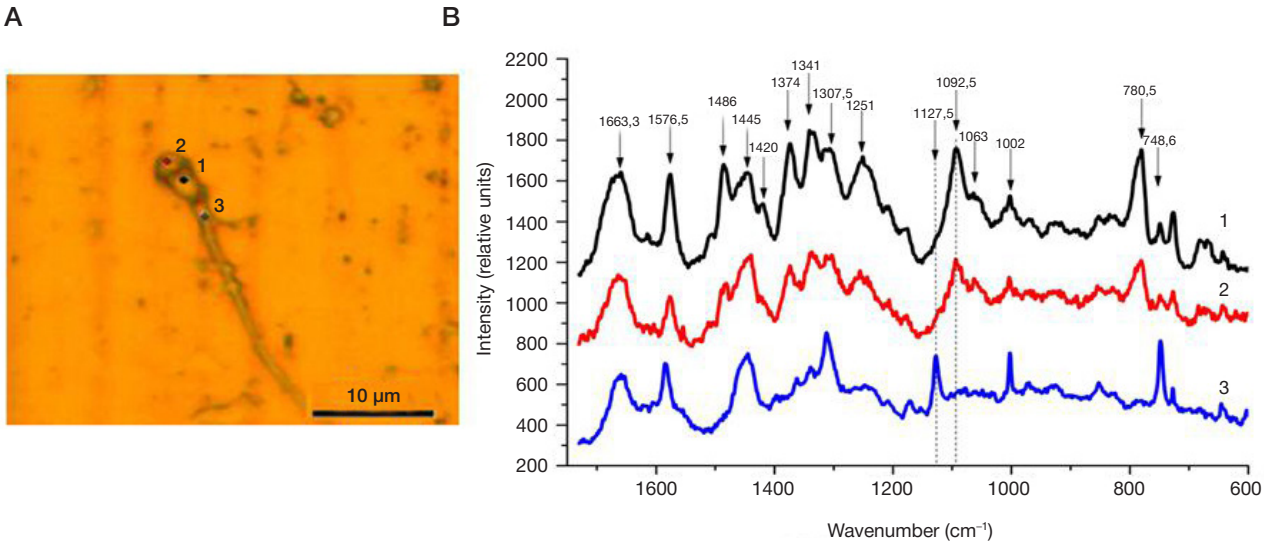

Fig. 1. A. Micrograph of the morphologically normal sperm. 1 (*black dot*) — beam focused on the sperm nuclear region; 2 (*red dot*) — beam focused on the acrosome; 3 (*blue dot*) — beam focused on the midpiece. **B.** Spectral characteristics obtained for the sperm nuclear region (*black line* — 1), acrosome (*red line* — 2), midpiece (*blue line* — 3)

and smoothing by the 21 point moving average method. Furthermore, standard normal variate (SNV) normalization was applied to all spectra.

The pre-processed spectra were used to make a data matrix X (176 × 510), where each row contained the Raman spectra intensities within the range of 680–1700 cm^{-1} with an increment of 2 cm^{-1} and the number of rows corresponded to the number of spectra.

In the second phase we assessed the sequelae of the x-ray radiation damaging effects on the sperm. For that the sperm suspension was divided into three aliquots. The first aliquot represented a control sample; the second and the third aliquots were exposed to the focused x-ray beam for 5 and 10 min, respectively. The results obtained were compared with each other.

RESULTS

A total of 19 sperm samples collected from 19 healthy donors aged 18–35 years were tested. A total of 176 spectra were acquired; the spectra inherent to sperm with normal morphology were identified.

Figure 1A presents a morphologically normal sperm. Dots mark the areas, for which spectra has been acquired. Label 1 corresponds to the sperm nucleus, label 2 corresponds to the acrosome, label 3 corresponds to the midpiece. Figure 1B presents a comparative chart of the spectral characteristics obtained for each area.

The Raman spectra acquired for nuclei of the intact spermatozoa and spermatozoa exposed to x-ray radiation for 5 and 10 min are provided in Fig. 2.

Despite different intensity of the spectra acquired, we noted no differences in the major Raman bands inherent to cells with DNA damage under 5 and 10 min exposure to x-ray radiation compared to intact samples.

DISCUSSION

The causes of abnormal sperm development or further damage are extremely diverse, and manifestations of such abnormalities are multivalent.

Based on the literature data we matched the bands we had acquired by Raman spectroscopy to the corresponding groups of atoms (see Table).

When assessing the sperm spectra (Fig. 1B), the following characteristic bands can be distinguished.

Inherent to nuclear DNA (1092 cm^{-1} and 780 cm^{-1}). The 1092 cm^{-1} band is B-DNA and Z-DNA marker. It is normally characterized by a gently sloping or horizontal arm in the 1063 cm^{-1} region. This feature is inherent to the nucleus with intact DNA. The band in the 780 cm^{-1} region corresponds to vibrations of thymine and cytosine, as well as to the DNA core. Some authors believe that this band is a marker of protamine DNA packaging, which has been confirmed by the later research [9, 16]. A triple band in the 1420 cm^{-1}, 1445 cm^{-1} and

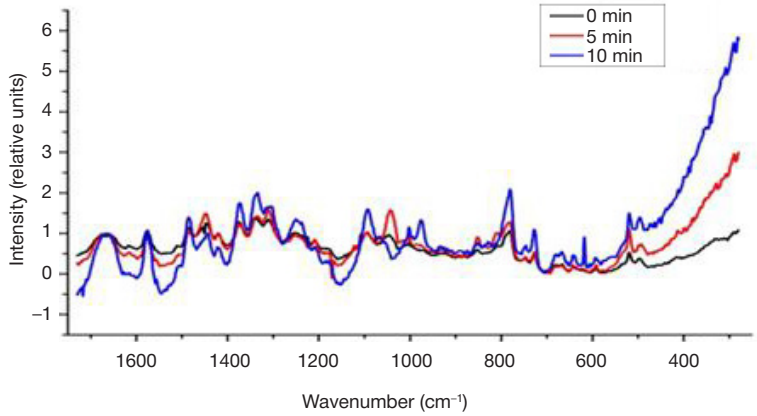

Fig. 2. Spectral characteristics obtained for the morphologically normal intact sperm (*black line*) exposed to x-ray radiation for 5 min (*red line*), 10 min (*blue line*)

Table. Major Raman bands and the corresponding groups of atoms [9, 17–21]

Wavenumber, cm^{-1}	Nucleic acid	Amino acids	Lipids
748	U, C		
782	T, C, DNA core		
1002		Phenylalanine	
1045	DNA damage marker		
1092	PO_2^- B-DNA and Z-DNA marker		
1251	A, C	N–H and C–H amide III	PO_2^- Phospholipids
1307	A	N–H и C–H amide III	
1341	G	N–H and C–H amide III	
1374	A, T, C		
1420	A		
1445			Methylene deformation (endogenous lipids)
1486	G, A		
1576	G, A		
1663	T	C=O amide I	C=C unsaturated lipid bonds

1486 cm^{-1} regions is characterized by specific ladder-like shape with the uppermost part in the 1486 cm^{-1} region. The band typical for phenylalanine amino acid (1002 cm^{-1}) is permanent, it is found in almost all graphs with different intensity.

Inherent to the acrosome. When assessing acrosomal spectral characteristics, it can be noted that there is an overall intensity reduction in almost all bands. Changes in the shape of the triple band 1420 cm^{-1}, 1445 cm^{-1}, and 1486 $см^{-1}$ with predominance of the middle part in the 1445 cm^{-1} region are typical, which corresponds to methylene deformation of endogenous lipids.

Inherent to the sperm midpiece (neck). Spectral characteristics of the midpiece are distinguished by the high intensity band in the 748 cm^{-1} region being a marker of the presence of mitochondria [4]. Intensity also grows of the 1576 cm^{-1} band, which, together with nucleic acids, corresponds to large amount of ATP [10]. Extinction of the 1092 cm^{-1} band and its transfer to the 1127 cm^{-1} region attract attention. This can be due to the presence of mitochondrial DNA, but we have found no confirmation in the literature.

The lack of significant spectral changes under exposure to x-ray radiation can be explained by high enough stability of the intact nucleoprotein complex of the mature sperm, in contrast to the actively dividing sperm precursor cells.

CONCLUSIONS

The pilot study conducted has made it possible to show the capabilities of Raman spectroscopy in terms of assessing the sperm biochemical processes and ultrastructure. We have created our own library of the spectra acquired for normal spermatozoa and the model with the sperm artificially damaged with the x-ray beam. The study involved fixed sperm. However, it is theoretically possible to select the intact live sperm for fertilization by ICSI using confocal Raman spectroscopy equipped with the optic (laser) tweezers. Further research in this field is necessary.

References

1. Speyer BE, Pizzey AR, Ranieri M, Joshi R, Delhanty JDA, Serhal P. Fall in implantation rates following ICSI with sperm with high DNA fragmentation. Human Reproduction. Oxford University Press (OUP). 2010; 25 (7): 1609–18. Available from: http://dx.doi.org/10.1093/humrep/deq116.
2. Fu W, Cui Q, Yang Z, Bu Z, Shi H, Bi B, et al. High sperm DNA fragmentation increased embryo aneuploidy rate in patients undergoing preimplantation genetic testing. Reproductive BioMedicine Online. 2023; 47 (6): 103366. Available from: http://dx.doi.org/10.1016/j.rbmo.2023.103366.
3. Evenson DP, Larson KL, Jost LK. Sperm Chromatin Structure Assay: Its Clinical Use for Detecting Sperm DNA Fragmentation in Male Infertility and Comparisons With Other Techniques. Journal of Andrology. Wiley-Blackwell. 2002; 23 (1): 25–43. Available from: http://dx.doi.org/10.1002/j.1939-4640.2002.tb02599.x.
4. Tesarik J, Mendoza-Tesarik R, Mendoza C. Sperm nuclear DNA damage: update on the mechanism, diagnosis and treatment. Reproductive BioMedicine Online. Elsevier BV. 2006; 12 (6): 715–21. Available from: http://dx.doi.org/10.1016/s1472-6483(10)61083-8.
5. Chi H-J, Chung D-Y, Choi S-Y, Kim J-H, Kim G-Y, Lee J-S, et al. Integrity of human sperm DNA assessed by the neutral comet assay and its relationship to semen parameters and clinical outcomes for the IVF-ET program. Clinical and Experimental Reproductive Medicine. The Korean Society for Reproductive Medicine (KAMJE); 2011; 38 (1): 10. Available from: http://dx.doi.org/10.5653/cerm.2011.38.1.10.
6. Sharma R, Iovine C, Agarwal A, Henkel R. TUNEL assay — Standardized method for testing sperm DNA fragmentation. Andrologia. 2020; 53 (2). Available from: http://dx.doi.org/10.1111/and.13738.
7. Andrabi SW, Ara A, Saharan A, Jaffar M, Gugnani N, Esteves SC. Sperm DNA fragmentation test: usefulness in assessing male fertility and assisted reproductive technology outcomes. Panminerva Medica. 2023; 65 (2). Available from: http://dx.doi.org/10.23736/s0031-0808.23.04836-x.
8. Kubasek WL, Wang Y, Thomas GA, Patapoff TW, Schoenwaelder KH, Van der Sande JH, et al. Raman spectra of the model B-DNA oligomer d(CGCGAATTCGCG)2 and of the DNA in living salmon sperm show that both have very similar B-type conformations. Biochemistry. American Chemical Society (ACS). 1986; 25 (23): 7440–5. Available from: http://dx.doi.org/10.1021/bi00371a028.
9. Huser T, Orme CA, Hollars CW, Corzett MH, Balhorn R. Raman spectroscopy of DNA packaging in individual human sperm cells distinguishes normal from abnormal cells. Journal of Biophotonics. Wiley-Blackwell. 2009; 2 (5): 322–32. Available from: http://dx.doi.org/10.1002/jbio.200910012.
10. Meister K, Schmidt DA, Bründermann E, Havenith M. Confocal Raman microspectroscopy as an analytical tool to assess the

mitochondrial status in human spermatozoa. The Analyst. Royal Society of Chemistry (RSC). 2010; 135 (6): 1370. Available from: http://dx.doi.org/10.1039/b927012d.
11. Mallidis C, Wistuba J, Bleisteiner B, Damm OS, Gross P, Wubbeling F, et al. In situ visualization of damaged DNA in human sperm by Raman microspectroscopy. Human Reproduction. Oxford University Press (OUP). 2011; 26 (7): 1641–9. Available from: http://dx.doi.org/10.1093/humrep/der122.
12. Sánchez V, Redmann K, Wistuba J, Wübbeling F, Burger M, Oldenhof H, et al. Oxidative DNA damage in human sperm can be detected by Raman microspectroscopy. Fertility and Sterility. Elsevier BV. 2012; 98 (5): 1124–9.e3. Available from: http://dx.doi.org/10.1016/j.fertnstert.2012.07.1059.
13. Nazarenko RV, Irzhak AV, Pomerantsev AL, Rodionova OYe. Confocal Raman spectroscopy and multivariate data analysis for evaluation of spermatozoa with normal and abnormal morphology. A feasibility study. Chemometrics and Intelligent Laboratory Systems. 2018; 182: 172–9. Available from: http://dx.doi.org/10.1016/j.chemolab.2018.10.002.
14. Jahmani MY, Hammadeh ME, Al Smadi MA, Baller MK. Label-Free Evaluation of Chromatin Condensation in Human Normal Morphology Sperm Using Raman Spectroscopy. Reproductive Sciences. 2021; 28 (9): 2527–39. Available from: http://dx.doi.org/10.1007/s43032-021-00494-6.
15. Edengeiser E, Meister K, Bründermann E, Büning S, Ebbinghaus S, Havenith M, Non-invasive chemical assessment of living human spermatozoa. RSC Adv. 2015; 5: 10424–9. Available from: https://doi.org/10.1039/c4ra12158a.
16. Li M, Ji Y, Wang D, Zhang Y, Zhang H, Tang Y, et al. Evaluation of Laser Confocal Raman Spectroscopy as a Non-Invasive Method for Detecting Sperm DNA Contents. Frontiers in Physiology. 2022; 13. Available from: http://dx.doi.org/10.3389/fphys.2022.827941.
17. Li X, Wang M, Chen H, Li Q, Yang H, Xu H, et al. Flow cytometric and near-infrared Raman spectroscopic investigation of quality in stained, sorted, and frozen-thawed buffalo sperm. Animal Reproduction Science. Elsevier BV. 2016; 170: 90–9. Available from: http://dx.doi.org/10.1016/j.anireprosci.2016.04.008.
18. Ellis DI, Cowcher DP, Ashton L, O'Hagan S, Goodacre R. Illuminating disease and enlightening biomedicine: Raman spectroscopy as a diagnostic tool. The Analyst. Royal Society of Chemistry (RSC). 2013; 138 (14): 3871. Available from: http://dx.doi.org/10.1039/c3an00698k.
19. Ferrara M, Di Caprio G, Managò S, De Angelis A, Sirleto L, Coppola G, et al. Label-Free Imaging and Biochemical Characterization of Bovine Sperm Cells. Biosensors. MDPI AG. 2015; 5 (2): 141–57. Available from: http://dx.doi.org/10.3390/bios5020141.
20. Li N, Chen D, Xu Y, Liu S, Zhang H. Confocal Raman microspectroscopy for rapid and label-free detection of maleic acid-induced variations in human sperm. Biomedical Optics Express. The Optical Society. 2014; 5 (5): 1690. Available from: http://dx.doi.org/10.1364/boe.5.001690.
21. Rimskaya E, Gorevoy A, Shelygina S, Perevedentseva E, Timurzieva A, Saraeva I, et al. Multi-Wavelength Raman Differentiation of Malignant Skin Neoplasms. International Journal of Molecular Sciences. 2024; 25 (13): 7422. Available from: http://dx.doi.org/10.3390/ijms25137422.

Литература

1. Speyer BE, Pizzey AR, Ranieri M, Joshi R, Delhanty JDA, Serhal P. Fall in implantation rates following ICSI with sperm with high DNA fragmentation. Human Reproduction. Oxford University Press (OUP). 2010; 25 (7): 1609–18. Available from: http://dx.doi.org/10.1093/humrep/deq116.
2. Fu W, Cui Q, Yang Z, Bu Z, Shi H, Bi B, et al. High sperm DNA fragmentation increased embryo aneuploidy rate in patients undergoing preimplantation genetic testing. Reproductive BioMedicine Online. 2023; 47 (6): 103366. Available from: http://dx.doi.org/10.1016/j.rbmo.2023.103366.
3. Evenson DP, Larson KL, Jost LK. Sperm Chromatin Structure Assay: Its Clinical Use for Detecting Sperm DNA Fragmentation in Male Infertility and Comparisons With Other Techniques. Journal of Andrology. Wiley-Blackwell. 2002; 23 (1): 25–43. Available from: http://dx.doi.org/10.1002/j.1939-4640.2002.tb02599.x.
4. Tesarik J, Mendoza-Tesarik R, Mendoza C. Sperm nuclear DNA damage: update on the mechanism, diagnosis and treatment. Reproductive BioMedicine Online. Elsevier BV. 2006; 12 (6): 715–21. Available from: http://dx.doi.org/10.1016/s1472-6483(10)61083-8.
5. Chi H-J, Chung D-Y, Choi S-Y, Kim J-H, Kim G-Y, Lee J-S, et al. Integrity of human sperm DNA assessed by the neutral comet assay and its relationship to semen parameters and clinical outcomes for the IVF-ET program. Clinical and Experimental Reproductive Medicine. The Korean Society for Reproductive Medicine (KAMJE); 2011; 38 (1): 10. Available from: http://dx.doi.org/10.5653/cerm.2011.38.1.10.
6. Sharma R, Iovine C, Agarwal A, Henkel R. TUNEL assay — Standardized method for testing sperm DNA fragmentation. Andrologia. 2020; 53 (2). Available from: http://dx.doi.org/10.1111/and.13738.
7. Andrabi SW, Ara A, Saharan A, Jaffar M, Gugnani N, Esteves SC. Sperm DNA fragmentation test: usefulness in assessing male fertility and assisted reproductive technology outcomes. Panminerva Medica. 2023; 65 (2). Available from: http://dx.doi.org/10.23736/s0031-0808.23.04836-x.
8. Kubasek WL, Wang Y, Thomas GA, Patapoff TW, Schoenwaelder KH, Van der Sande JH, et al. Raman spectra of the model B-DNA oligomer d(CGCGAATTCGCG)2 and of the DNA in living salmon sperm show that both have very similar B-type conformations. Biochemistry. American Chemical Society (ACS). 1986; 25 (23): 7440–5. Available from: http://dx.doi.org/10.1021/bi00371a028.
9. Huser T, Orme CA, Hollars CW, Corzett MH, Balhorn R. Raman spectroscopy of DNA packaging in individual human sperm cells distinguishes normal from abnormal cells. Journal of Biophotonics. Wiley-Blackwell. 2009; 2 (5): 322–32. Available from: http://dx.doi.org/10.1002/jbio.200910012.
10. Meister K, Schmidt DA, Bründermann E, Havenith M. Confocal Raman microspectroscopy as an analytical tool to assess the mitochondrial status in human spermatozoa. The Analyst. Royal Society of Chemistry (RSC). 2010; 135 (6): 1370. Available from: http://dx.doi.org/10.1039/b927012d.
11. Mallidis C, Wistuba J, Bleisteiner B, Damm OS, Gross P, Wubbeling F, et al. In situ visualization of damaged DNA in human sperm by Raman microspectroscopy. Human Reproduction. Oxford University Press (OUP). 2011; 26 (7): 1641–9. Available from: http://dx.doi.org/10.1093/humrep/der122.
12. Sánchez V, Redmann K, Wistuba J, Wübbeling F, Burger M, Oldenhof H, et al. Oxidative DNA damage in human sperm can be detected by Raman microspectroscopy. Fertility and Sterility. Elsevier BV. 2012; 98 (5): 1124–9.e3. Available from: http://dx.doi.org/10.1016/j.fertnstert.2012.07.1059.
13. Nazarenko RV, Irzhak AV, Pomerantsev AL, Rodionova OYe. Confocal Raman spectroscopy and multivariate data analysis for evaluation of spermatozoa with normal and abnormal morphology. A feasibility study. Chemometrics and Intelligent Laboratory Systems. 2018; 182: 172–9. Available from: http://dx.doi.org/10.1016/j.chemolab.2018.10.002.
14. Jahmani MY, Hammadeh ME, Al Smadi MA, Baller MK. Label-Free Evaluation of Chromatin Condensation in Human Normal Morphology Sperm Using Raman Spectroscopy. Reproductive Sciences. 2021; 28 (9): 2527–39. Available from: http://dx.doi.org/10.1007/s43032-021-00494-6.
15. Edengeiser E, Meister K, Bründermann E, Büning S, Ebbinghaus S, Havenith M, Non-invasive chemical assessment of living human spermatozoa. RSC Adv. 2015; 5: 10424–9. Available from: https://doi.org/10.1039/c4ra12158a.
16. Li M, Ji Y, Wang D, Zhang Y, Zhang H, Tang Y, et al. Evaluation of Laser Confocal Raman Spectroscopy as a Non-Invasive Method for Detecting Sperm DNA Contents. Frontiers in Physiology. 2022; 13. Available from: http://dx.doi.org/10.3389/fphys.2022.827941.
17. Li X, Wang M, Chen H, Li Q, Yang H, Xu H, et al. Flow cytometric and near-infrared Raman spectroscopic investigation of quality

in stained, sorted, and frozen-thawed buffalo sperm. Animal Reproduction Science. Elsevier BV. 2016; 170: 90–9. Available from: http://dx.doi.org/10.1016/j.anireprosci.2016.04.008.
18. Ellis DI, Cowcher DP, Ashton L, O'Hagan S, Goodacre R. Illuminating disease and enlightening biomedicine: Raman spectroscopy as a diagnostic tool. The Analyst. Royal Society of Chemistry (RSC). 2013; 138 (14): 3871. Available from: http://dx.doi.org/10.1039/c3an00698k.
19. Ferrara M, Di Caprio G, Managò S, De Angelis A, Sirleto L, Coppola G, et al. Label-Free Imaging and Biochemical Characterization of Bovine Sperm Cells. Biosensors. MDPI AG. 2015; 5 (2): 141–57. Available from: http://dx.doi.org/10.3390/bios5020141.
20. Li N, Chen D, Xu Y, Liu S, Zhang H. Confocal Raman microspectroscopy for rapid and label-free detection of maleic acid-induced variations in human sperm. Biomedical Optics Express. The Optical Society. 2014; 5 (5): 1690. Available from: http://dx.doi.org/10.1364/boe.5.001690.
21. Rimskaya E, Gorevoy A, Shelygina S, Perevedentseva E, Timurzieva A, Saraeva I, et al. Multi-Wavelength Raman Differentiation of Malignant Skin Neoplasms. International Journal of Molecular Sciences. 2024; 25 (13): 7422. Available from: http://dx.doi.org/10.3390/ijms25137422.

THERAPEUTIC STRATEGIES FOR WILSON'S DISEASE: CURRENT STATE AND PROSPECTS

Ivanenko AV, Starodubova VD, Shokhina AG ✉

Pirogov Russian National Research Medical University, Moscow, Russia

Wilson's disease is a rare hereditary disorder caused by the *ATP7B* gene mutations that leads to copper metabolism disturbances and toxic copper accumulation in the liver, brain, and other organs. The main manifestations include liver damage, neurological and psychiatric symptoms. The use of advanced treatment methods (D-penicillamine, trientine, zinc salts) improves the outcome, but is limited by side effects and complexity of adherence to therapy. Liver transplantation is used in severe forms, but it is limited by the donor shortage and the need for immunosuppression. In our opinion, promising areas include gene therapy involving the use of AAV vectors and CRISPR/Cas9, mRNA platforms, and cell technologies. However, these approaches require further research for the efficacy, safety, and accessibility improvement.

Keywords: Wilson's disease, monogenic disorder, ATP7B, copper overload, gene therapy, cellular therapy

Funding: the study was supported by the Russian Science Foundation grant (RSF grant No. 24-74-10106).

Author contribution: Ivanenko AV, Starodubova VD — manuscript writing; Shokhina AG — developing the concept, manuscript writing and editing, obtaining funding.

✉ **Correspondence should be addressed:** Arina G. Shokhina
Ostrovityanova, 1, str. 1, Moscow, 117513, Russia; a.g.shokhina@yandex.ru

Received: 02.04.2025 **Accepted:** 20.04.2025 **Published online:** 28.04.2025

DOI: 10.24075/brsmu.2025.022

ТЕРАПЕВТИЧЕСКИЕ СТРАТЕГИИ ДЛЯ ЛЕЧЕНИЯ БОЛЕЗНИ ВИЛЬСОНА–КОНОВАЛОВА: СОВРЕМЕННОЕ СОСТОЯНИЕ И ПЕРСПЕКТИВЫ

А. В. Иваненко, В. Д. Стародубова, А. Г. Шохина ✉

Российский национальный исследовательский медицинский университет имени Н. И. Пирогова, Москва, Россия

Болезнь Вильсона-Коновалова — редкое наследственное заболевание, вызванное мутациями гена *ATP7B*, приводящее к нарушению метаболизма меди и ее токсическому накоплению в печени, мозге и других органах. Основные проявления — поражение печени, неврологические и психиатрические симптомы. Применение современных методов лечения (D-пеницилламин, триентин, соли цинка) улучшает прогноз, но ограничено побочными эффектами и сложностью соблюдения терапии. Трансплантацию печени применяют при тяжелых формах, однако она ограничена дефицитом доноров и необходимостью иммуносупрессии. Перспективные направления, на наш взгляд, включают генную терапию с использованием AAV-векторов и CRISPR/Cas9, мРНК-платформы и клеточные технологии, однако эти подходы требуют дальнейших исследований для повышения эффективности, безопасности и доступности.

Ключевые слова: болезнь Вильсона–Коновалова, моногенное заболевание, ATP7B, перегрузка медью, генная терапия, клеточная терапия

Финансирование: работа поддержана денежными средствами гранта Российского научного фонда (грант РНФ №24-74-10106).

Вклад авторов: А. В. Иваненко, В. Д. Стародубова — написание статьи; А. Г. Шохина — разработка концепции, написание и редактирование статьи, получение финансирования.

✉ **Для корреспонденции:** Арина Геннадиевна Шохина
ул. Островитянова, д. 1, стр. 1, г. Москва, 117513, Россия; a.g.shokhina@yandex.ru

Статья получена: 02.04.2025 **Статья принята к печати:** 20.04.2025 **Опубликована онлайн:** 28.04.2025

DOI: 10.24075/vrgmu.2025.022

Wilson's disease (WD) is a rare autosomal recessive disorder caused by the *ATP7B* gene mutations that leads to copper metabolism disturbances and toxic copper accumulation in the liver, brain, and other organs. Clinical manifestations include primarily liver damage (hepatitis, cirrhosis, acute liver failure), neurological symptoms (tremor, dystonia, parkinsonism), and mental disorders (depression, mood swings). The diagnosis is based on the combination of clinical data, laboratory tests (ceruloplasmin levels, copper in blood and urine), and molecular genetic testing. The use of advanced treatment methods significantly improves the patients' outcomes, but it is still limited by side effects, complexity of adherence to treatment regimen, and insufficient symptom control efficacy. The paper considers evolution of therapeutic approaches to treatment of WD: from conventional pharmacological methods to promising genetic and cell technologies.

Advanced pharmacological approaches: copper overload control

D-penicillamine (DPA) and trientine are the major chelating agents that enhance urinary copper excretion and return blood free copper levels back to normal after 1–2 years or 6–48 months of therapy, respectively [1]. However, DPA causes severe side effects, such as immune-mediated nephritis and neurological deterioration in 14–21% of patients having neurological symptoms. Trientine is a safer alternative, but it is also associated with the risk of neurological complications [2].

Zinc salts inhibit copper absorption through induction of metallothionein expression in enterocytes. Despite the fact that the method is relatively safe, several months of zinc therapy are needed to achieve the effect, and zinc therapy is not suited for

acute conditions [3]. Furthermore, there are cohorts of patients that do not respond to zinc salt therapy.

Tetrathiomolybdate (TTM) and methanobactins represent innovative exprerimental agents that have shown promising results in pre-clinical trials [4, 5]. However, the development of TTM was terminated during the phase III clinical trial due to mixed efficacy and side effects (anemia, neutropenia) [6]. Pre-clinical and clinical trials of methanobactin have not yet been completed.

Transplantation: radical but limited approach

Liver transplantation is a radical treatment method for patients with WD suffering from acute liver failure or not responding to drug therapy. However, the use of this method is limited by the donor organ shortage, perioperative risk, and the need for lifelong immunosuppression. Immunosuppression increases susceptibility to infections and malignant tumors, which makes transplantation an extreme measure.

Hepatocyte transplantation represents a minimally invasive alternative, in which isolated donor cells are injected into the hepatic portal vein. The animal model studies have shown the decrease in copper levels and improved survival rate [7, 8]. However, such problems, as low cell engraftment effectiveness, immune rejection, and disturbed liver repopulation, limit the clinical use.

Gene therapy: addressing the root cause

Gene therapy is aimed at restoring the *ATP7B* function through functional gene delivery in hepatocytes. The use of recombinant adeno-associated viruses (rAAV) has shown promising results in pre-clinical and early clinical trials: tATP7b (UX701) (truncated *ATP7B* variant delivered via AAV8) has shown a persistent therapeutic effect in mice; it is currently through phase I/II/III clinical trials [9]. MiniATP7B (VTX-801) represents one more truncated variant that has shown dose-dependent efficacy in mice and is tested in phase I/II clinical trials [10].

The CRISPR/Cas9 method provides an opportunity to ensure the directed correction of mutations. However, the use of the method faces such problems, as low editing effectiveness in non-dividing hepatocytes and potential off-target effects [11]. Base editors and prime editors expand the possibilities of adjustment without creating double-strand breaks, but require further optimization for clinical use.

mRNA technologies represent a promising approach of Wilson's disease treatment. In contrast to viral vectors (such as AAV), mRNA does not integrate into the genome, which minimizes the risk of insertion mutagenesis. Lipid nanoparticles (LNPs) used to deliver mRNA show tropism for the liver. Despite the fact that direct trials of mRNA therapy for WD are yet to be launched, advances in treatment of other liver diseases using mRNA platforms (for example, transthyretin amyloidosis) confirm their performance [12]. In particular, the NTLA-2001 therapy based on CRISPR has already shown promising results [13].

Stem cell-based therapy: liver function restoration

Induced pluripotent stem cells (iPSCs) can be differentiated into hepatocytes for autologous stem cell transplantation, which potentially eliminates the risk of immune rejection. However, the current protocols allow to create immature hepatocyte-like cells with reduced functionality compared to mature cells of the mature organism [14]. 3D cell culture is the main area which, in the long term, will improve cell maturation and engraftment effectiveness [15].

Combining gene therapy with the stem cell-based technologies can ensure a renewable source of the genetically adjusted hepatocytes for transplantation, thereby solving the problem of genetic defects, and the need for liver regeneration.

CONCLUSION

Therapeutic approaches of Wilson's disease treatment evolve rapidly from symptomatic management to potentially radical methods aimed to eliminate the genetic cause of the disease. Despite the fact that conventional methods remain important for ongoing treatment, innovations in gene therapy, genome editing, and stem cell-based technologies have serious potential for long-term management of the disease and its complete cure.

Further research is needed to optimize these methods in order to ensure clinical use, safety, efficacy, and accessibility for all patients suffering from this severe disorder.

References

1. European Association for the Study of the Liver. EASL Clinical Practice Guidelines: Wilson's disease. Journal of Hepatology. 2012; 56 (3): 671–85. DOI: 10.1016/j.jhep.2011.11.007.
2. Weiss KH, et al. Zinc Monotherapy Is Not as Effective as Chelating Agents in Treatment of Wilson Disease. Gastroenterology. 2011; 140 (4): 1189–98.e1. DOI: 10.1053/j.gastro.2010.12.034.
3. Munk DE, et al. Effect of oral zinc regimens on human hepatic copper content: a randomized intervention study. Sci Rep. 2022; 12 (1): 14714. DOI: 10.1038/s41598-022-18872-8.
4. Solovyev N, Ala A, Schilsky M, Mills C, Willis K, Harrington CF. Biomedical copper speciation in relation to Wilson's disease using strong anion exchange chromatography coupled to triple quadrupole inductively coupled plasma mass spectrometry. Analytica Chimica Acta. 2020; 1098: 27–36. DOI: 10.1016/j.aca.2019.11.033.
5. Snijders RJALM, et al. An open-label randomised-controlled trial of azathioprine vs. mycophenolate mofetil for the induction of remission in treatment-naive autoimmune hepatitis. Journal of Hepatology. 2024; 80 (4): 576–85. DOI: 10.1016/j.jhep.2023.11.032.
6. Medici V, Sturniolo GC. Tetrathiomolybdate, a copper chelator for the treatment of Wilson disease, pulmonary fibrosis and other indications. IDrugs. 2008; 11 (8): 592–606.
7. Fujiyoshi J, et al. Therapeutic potential of hepatocyte-like-cells converted from stem cells from human exfoliated deciduous teeth in fulminant Wilson's disease. Sci Rep. 2019; 9 (1): 1535. DOI: 10.1038/s41598-018-38275-y.
8. Sauer V, et al. Repeated transplantation of hepatocytes prevents fulminant hepatitis in a rat model of Wilson's disease. Liver Transplantation. 2012; 8 (2): 248–59. DOI: 10.1002/lt.22466.
9. Leng Y, et al. Long-Term Correction of Copper Metabolism in Wilson's Disease Mice with AAV8 Vector Delivering Truncated ATP7B. Human Gene Therapy. 2019; 30 (12): 1494–504. DOI: 10.1089/hum.2019.148.
10. Murillo O, et al. Liver Expression of a MiniATP7B Gene Results in Long–Term Restoration of Copper Homeostasis in a Wilson Disease Model in Mice. Hepatology. 2019; 70 (1): 108–26. DOI: 10.1002/hep.30535.
11. Pöhler M, et al. CRISPR/Cas9-mediated correction of mutated copper transporter ATP7B. PLoS ONE. 2020; 15 (9): e0239411. DOI: 10.1371/journal.pone.0239411.
12. Fontana M, et al. Vutrisiran in Patients with Transthyretin

Amyloidosis with Cardiomyopathy. N Engl J Med. 2025; 392 (1): 33–44. DOI: 10.1056/NEJMoa2409134.
13. Gillmore JD, et al. CRISPR-Cas9 In Vivo Gene Editing for Transthyretin Amyloidosis. N Engl J Med. 2021; 385 (6): 493–502. DOI: 10.1056/NEJMoa2107454.
14. Baxter M, et al. Phenotypic and functional analyses show stem cell-derived hepatocyte-like cells better mimic fetal rather than adult hepatocytes. Journal of Hepatology. 2015; 62 (3): 581–9. DOI: 10.1016/j.jhep.2014.10.016.
15. Suominen S, et al. Improvements in Maturity and Stability of 3D iPSC-Derived Hepatocyte-like Cell Cultures. Cells. 2023; 12 (19): 2368. DOI: 10.3390/cells12192368.

Литература

1. European Association for the Study of the Liver. EASL Clinical Practice Guidelines: Wilson's disease. Journal of Hepatology. 2012; 56 (3): 671–85. DOI: 10.1016/j.jhep.2011.11.007.
2. Weiss KH, et al. Zinc Monotherapy Is Not as Effective as Chelating Agents in Treatment of Wilson Disease. Gastroenterology. 2011; 140 (4): 1189–98.e1. DOI: 10.1053/j.gastro.2010.12.034.
3. Munk DE, et al. Effect of oral zinc regimens on human hepatic copper content: a randomized intervention study. Sci Rep. 2022; 12 (1): 14714. DOI: 10.1038/s41598-022-18872-8.
4. Solovyev N, Ala A, Schilsky M, Mills C, Willis K, Harrington CF. Biomedical copper speciation in relation to Wilson's disease using strong anion exchange chromatography coupled to triple quadrupole inductively coupled plasma mass spectrometry. Analytica Chimica Acta. 2020; 1098: 27–36. DOI: 10.1016/j.aca.2019.11.033.
5. Snijders RJALM, et al. An open-label randomised-controlled trial of azathioprine vs. mycophenolate mofetil for the induction of remission in treatment-naive autoimmune hepatitis. Journal of Hepatology. 2024; 80 (4): 576–85. DOI: 10.1016/j.jhep.2023.11.032.
6. Medici V, Sturniolo GC. Tetrathiomolybdate, a copper chelator for the treatment of Wilson disease, pulmonary fibrosis and other indications. IDrugs. 2008; 11 (8): 592–606.
7. Fujiyoshi J, et al. Therapeutic potential of hepatocyte-like-cells converted from stem cells from human exfoliated deciduous teeth in fulminant Wilson's disease. Sci Rep. 2019; 9 (1): 1535. DOI: 10.1038/s41598-018-38275-y.
8. Sauer V, et al. Repeated transplantation of hepatocytes prevents fulminant hepatitis in a rat model of Wilson's disease. Liver Transplantation. 2012; 8 (2): 248–59. DOI: 10.1002/lt.22466.
9. Leng Y, et al. Long-Term Correction of Copper Metabolism in Wilson's Disease Mice with AAV8 Vector Delivering Truncated ATP7B. Human Gene Therapy. 2019; 30 (12): 1494–504. DOI: 10.1089/hum.2019.148.
10. Murillo O, et al. Liver Expression of a MiniATP7B Gene Results in Long–Term Restoration of Copper Homeostasis in a Wilson Disease Model in Mice. Hepatology. 2019; 70 (1): 108–26. DOI: 10.1002/hep.30535.
11. Pöhler M, et al. CRISPR/Cas9-mediated correction of mutated copper transporter ATP7B. PLoS ONE. 2020; 15 (9): e0239411. DOI: 10.1371/journal.pone.0239411.
12. Fontana M, et al. Vutrisiran in Patients with Transthyretin Amyloidosis with Cardiomyopathy. N Engl J Med. 2025; 392 (1): 33–44. DOI: 10.1056/NEJMoa2409134.
13. Gillmore JD, et al. CRISPR-Cas9 In Vivo Gene Editing for Transthyretin Amyloidosis. N Engl J Med. 2021; 385 (6): 493–502. DOI: 10.1056/NEJMoa2107454.
14. Baxter M, et al. Phenotypic and functional analyses show stem cell-derived hepatocyte-like cells better mimic fetal rather than adult hepatocytes. Journal of Hepatology. 2015; 62 (3): 581–9. DOI: 10.1016/j.jhep.2014.10.016.
15. Suominen S, et al. Improvements in Maturity and Stability of 3D iPSC-Derived Hepatocyte-like Cell Cultures. Cells. 2023; 12 (19): 2368. DOI: 10.3390/cells12192368.

TWO-STEP AAV8 GENE DELIVERY IN A CHILD WITH CRIGLER–NAJJAR SYNDROME TYPE I

Rebrikov DV[1,2] ✉, Degtyareva AV[1], Yanushevich YuG[2], Gautier MS[1], Gorodnicheva TV[1,2], Bavykin AS[1,2], Ushakova LV[1], Filippova EA[1], Degtyarev DN[1], Sukhikh GT[1]

[1] Kulakov National Medical Research Center for Obstetrics, Gynecology and Perinatology, Moscow, Russia

[2] Pirogov Russian National Research Medical University (Pirogov University), Moscow, Russia

Crigler–Najjar syndrome type I, an orphan *UTG1A1* enzyme deficiency, manifests at birth with severe unconjugated hyperbilirubinemia. Here we describe sustained clinical response in a pediatric patient with Crigler–Najjar syndrome type I treated with two consecutive doses of AAV8 delivering the UTG1A1 coding sequence. Infusion I (6×10^{12} vg/kg) afforded sustained decrease in serum bilirubin, allowing substantial relaxation of the phototherapy from 12 h to 4 h daily. Infusion II at a double dose was made in 6 months; the decision was intended at complete elimination of phototherapy. However, the elimination led to a sharp increase in bilirubin levels necessitating resumption of phototherapy. The patient is currently stable on 4 h daily phototherapy for 80 weeks since the resumption and 107 weeks since the AAV8 therapy initiation. No toxic side effects were encountered. A slow incremental dynamics in serum bilirubin opens the issue of clinical advisability for subsequent infusions of the drug.

Keywords: Crigler–Najjar syndrome type I, AAV8, gene therapy

Funding: This work was supported by the Ministry of Health of the Russian Federation (No. 124020400004-9).

Author contribution: Rebrikov DV — literature analysis, study planning, development of study concept and design, development of drug concept, data interpretation, manuscript preparation; Degtyareva AV — literature analysis, study planning, development of study concept and design, patient examination, data interpretation; Gautier MS, Ushakova LV, Filippova EA — patient examination; Yanushevich YuG, Gorodnicheva TV, Bavykin AS — drug development, data interpretation, manuscript preparation; Degtyarev DN, Sukhikh GT — development of study concept and design, data interpretation.

Compliance with ethical standards: the therapy was approved by Ethics Committee at the Kulakov National Medical Research Center for Obstetrics, Gynecology and Perinatology on Dec 01 2022, Protocol #12 for infusion I, and on Jul 20 2023, Protocol #7 for infusion II. The patient's legal representatives provided voluntary informed consents for the study and for each infusion of the drug.

✉ **Correspondence should be addressed:** Denis V. Rebrikov
Ostrovityanova, 1, Moscow, 117997, Russia; drebrikov@gmail.com

Received: 25.04.2025 **Accepted:** 29.04.2025 **Published online:** 30.04.2025

DOI: 10.24075/brsmu.2025.025

ДВУХЭТАПНАЯ AAV8-ГЕНОТЕРАПИЯ РЕБЕНКА С СИНДРОМОМ КРИГЛЕРА–НАЙЯРА 1-ГО ТИПА

Д. В. Ребриков[1, 2] ✉, А. В. Дегтярёва[1], Ю. Г. Янушевич[2], М. С. Готье[1], Т. В. Городничева[1,2], А. С. Бавыкин[1,2], Л. В. Ушакова[1], Е. А. Филиппова[1], Д. Н. Дегтярёв[1], Г. Т. Сухих[1]

[1] Национальный медицинский исследовательский центр акушерства, гинекологии и перинатологии имени В. И. Кулакова, Москва, Россия

[2] Российский национальный исследовательский медицинский университет имени Н. И. Пирогова (Пироговский Университет), Москва, Россия

Синдром Криглера–Найяра 1-го типа (СКН1) является следствием дефицита фермента уридиндифосфатглюкуронозилтрансферы 1А1, кодируемого геном *UTG1A1* и проявляется при рождении тяжелой неконъюгированной гипербилирубинемией. В работе описан устойчивый клинический ответ у ребенка с СКН1, которого лечили двумя последовательными дозами AAV8-генотерапии, доставляющей кодирующую последовательность UTG1A1. Инфузия I (6×10^{12} вг/кг) обеспечила устойчивое снижение сывороточного билирубина, что позволило ослабить фототерапию с 12 ч до 4 ч в день. Инфузия II в двойной дозе была сделана через 6 месяцев; данное решение было принято с целью полной отмены фототерапии. Однако отмена привела к резкому повышению уровня билирубина, что потребовало возобновления фототерапии. В настоящее время состояние пациента стабильно на 4-часовой ежедневной фототерапии в течение 80 недель с момента возобновления и 107 недель с момента начала терапии генопрепаратом. Токсических побочных эффектов не наблюдалось. Плавный прирост уровня билирубина в сыворотке крови ставит вопрос о клинической целесообразности ежегодных инфузий препарата.

Ключевые слова: синдром Криглера–Найяра 1-го типа, AAV8, генная терапия

Финансирование: работа выполнена при поддержке Министерства здравоохранения Российской Федерации (№ 124020400004-9).

Вклад авторов: Д. В. Ребриков — анализ литературы, планирование исследования, разработка концепции и дизайна исследования, разработка концепции препарата, интерпретация данных, подготовка рукописи; А. В. Дегтярёва — анализ литературы, планирование исследования, разработка концепции и дизайна исследования, обследование пациента, интерпретация данных; М. С. Готье, Л. В. Ушакова, Е. А. Филиппова — обследование пациента; Ю. Г. Янушевич, Т. В. Городничева, А. С. Бавыкин — разработка препарата, интерпретация данных, подготовка рукописи; Д. Н. Дегтярёв, Г. Т. Сухих — разработка концепции и дизайна исследования, интерпретация данных.

Соблюдение этических стандартов: исследование одобрено этическим комитетом ФГБУ «НМИЦ АГП им. В. И. Кулакова» Минздрава России (протокол № 12 от 01 декабря 2022 г. (для инфузии I) и протокол № 7 от 20 июля 2023 г. (для инфузии II)). Законные представители пациентки дали информированное добровольное согласие на исследование и на каждую инфузию препарата.

✉ **Для корреспонденции:** Д. В. Ребриков
ул. Островитянова, д. 1, г. Москва, 117997, Россия; drebrikov@gmail.com

Статья получена: 25.04.2025 **Статья принята к печати:** 29.04.2025 **Опубликована онлайн:** 30.04.2025

DOI: 10.24075/vrgmu.2025.025

Crigler-Najjar syndrome (CNs) is an orphan enzymopathy caused by loss-of-function variants in *UGT1A1* [1]. The lack of active uridine diphosphate glucuronosyltransferase 1A1, which leads to accumulation of bilirubin conjugates clinically represented by jaundice and severe neurological impairments, is potentially fatal in infancy. The diagnosis involves biochemical and molecular genetic tests for, respectively, unconjugated bilirubin and *UGT1A1* variants. No specific pathogenetic treatment for the condition has been proposed apart from transplantation of the liver in CNs type I, the severe form. The patients require constant observation and are on continual bilirubin clearance by plasmapheresis and (or) phototherapy, which is physiologically straining and profoundly affects the lifestyle options in young patients.

The potential of using adeno-associated virus serotype 8 for the treatment of Crigler-Najjar syndrome has been substantiated in preclinical studies *in vivo* [2, 3]. In 2023, D'Antiga et al. reported successful treatment of Crigler-Najjar syndrome (CNs) type I in adult patients using a gene drug with AAV-mediated delivery [4]. In pediatric patients, the efficiency could (speculatively) interfere with the high rates of growth and physiological renewal of liver cells. Here we describe a sustained clinical response (107 weeks by the time of writing) in a pediatric patient with CNs type I using *UGT1A1* coding sequence delivered by two consecutive doses of adeno-associated viral vector serotype 8 (AAV8). This is the first report on AAV therapy in a two-dose delivery mode.

Case description

Vector design and purification

cDNA from a healthy donor with wild-type *UGT1A1* sequence was used as a template. The coding sequence was cloned into pAAV-TBG plasmid. The pAAV-TBG-*UGT1A1* construct was packaged in HEK293 cells.

The particles were purified in an iodixanol stepwise density gradient (OptiPrep, StemCell Technologies, USA) at 350,000 g, +18 °C for 1.5 hours (Optima-XPN ultracentrifuge; Beckman, USA). The 60% fraction and a half of the 40% iodixanol fraction were collected, purified by dialysis (Spectrum™, Fisher Scientific #0867140; pore size 100 kDa) against (1x) PBS/350 mM NaCl/0.001% Pluronic F-68 buffer at 4°C for 14–18 h, concentrated with Amicon® centrifugal filters, pore size 100 kDa (Millipore Sigma, USA) and additionally sterilized by 0.22 µm syringe filtration. The product, alphaglucuronosyltransferasegene unoparvovec, was quantitated by real-time PCR with plasmid DNA as a reference. All purity indicators were found to be within the reference limits for clinical use; the product contained endotoxin <0.64 EU/ml (Endosafe® LAL; Charles River Endosafe, USA), BSA < 159 ng/ml (BSA ELISA Kit; Wuhan Fine Biotech, PRC), HEK293 residual proteins <2 ng/ml (HEK293 HCP ELISA Kit; Cygnus Technologies, USA) and was *Mycoplasma*-negative.

Preclinical study

In vitro tests were carried out on HeLa cells (ATCC, USA).

Animal study was authorized by the Institutional Animal Care and Use Committee at the Pirogov University. *In vivo* tests on C57BL6 mice were performed in three rounds: dose-response assessment, overdose toxicity assessment and fade-out assessment in adolescence. The control group received identical volume of dilution buffer instead of the drug in all experiments.

Dose-response assessment was performed on 8-month-old mice in groups $n(c)=11$, $n(L)=11$, $n(M)=11$, $n(H)=11$. Toxicology and biodistribution studies involved monitoring of leukocyte counts and biochemical tests at 3, 4, and 5 weeks post-infusion, and post-mortem assessment of blood parameters and biodistribution of the drug to muscle and viscera on week 6. Immunohistochemistry revealed selective biodistribution of the human *UGT1A1* coding sequence to the liver. The hUGT1A1 signal increased incrementally with the dose by both the intensity and the spread into the liver parenchyma from veins of the lobules (Fig. 1).

Overdose toxicity assessment of the maximum of potential therapeutic dose was performed by administering a 1.2×10^{14} vg/kg dose to 8-month-old mice in control and experimental groups ($n = 6$ each) with the same check points and controlled parameters as above. No significant toxicity effects were detected.

Fade-out assessment in adolescence was assessed on 5-week-old mice ($n = 24$) received tail vein 1.2×10^{13} vg/kg drug injections. At 2 weeks post-infusion and then every 3 weeks until the end of experiment (at the age of 19 weeks), groups of mice ($n = 6, 4, 4, 4, 6$) were euthanized with livers taken for qPCR analysis of viral genome copies and quantitative protein detection by immunohistochemistry (liver sections stained with hUGT1A1-specific antibody). Quantitative PCR showed a 2-fold decrease in the vector DNA content every 6 weeks (4-fold over the experiment). Quantitative protein analysis showed that hUGT1A1 levels increased up to 5 weeks post-infusion and remained stable until the end of the experiment.

Patient

A girl with CNs type I, confirmed by *UGT1A1* gene sequencing and manifested as severe unconjugated hyperbilirubinemia, under continuous observation at the Kulakov National Medical Research Center for Obstetrics, Gynecology and Perinatology, was maintained on 12 h daily phototherapy, which afforded a neat confinement of indirect bilirubin levels within the toxicity limit of 300–350 µmol/l.

The AAV therapy was approved by Ethics Committee at the Kulakov National Medical Research Center for Obstetrics, Gynecology and Perinatology on Dec 01 2022, Protocol #12 for infusion I, and on Jul 20 2023, Protocol #7 for infusion II. Application for clinical trial phase I–II No. 13571. The patient's legal representatives provided voluntary informed consents for the study and for each infusion of the drug.

Treatment and outcome

The gene therapy was initiated at an age of 7 years 5 months. The patient received two intravenous infusions of alphaglucu ronosyltransferasegene unoparvovec: 6×10^{12} viral genomes per kg body weight (vg/kg) on week 0 and 1.2×10^{13} vg/kg on week 27 (Fig. 2). The safety was monitored by transaminase levels and patient-reported well-being. The efficacy was assessed by reduction in serum bilirubin levels. A chart of indirect bilirubin levels over 3.5 years, including an extensive time length preceding the treatment, is given in Fig. 2. The phototherapy regimen was continuously adjusted in accordance with the indirect bilirubin levels. Both infusions were accompanied by prednisolone support to mitigate immune reactions: the patient received prednisolone daily, in oral doses reduced stepwise from 1 mg/kg to 0 in the course of 8 and 2 weeks since the infusion, respectively (Fig. 2). In addition, on day of infusion II,

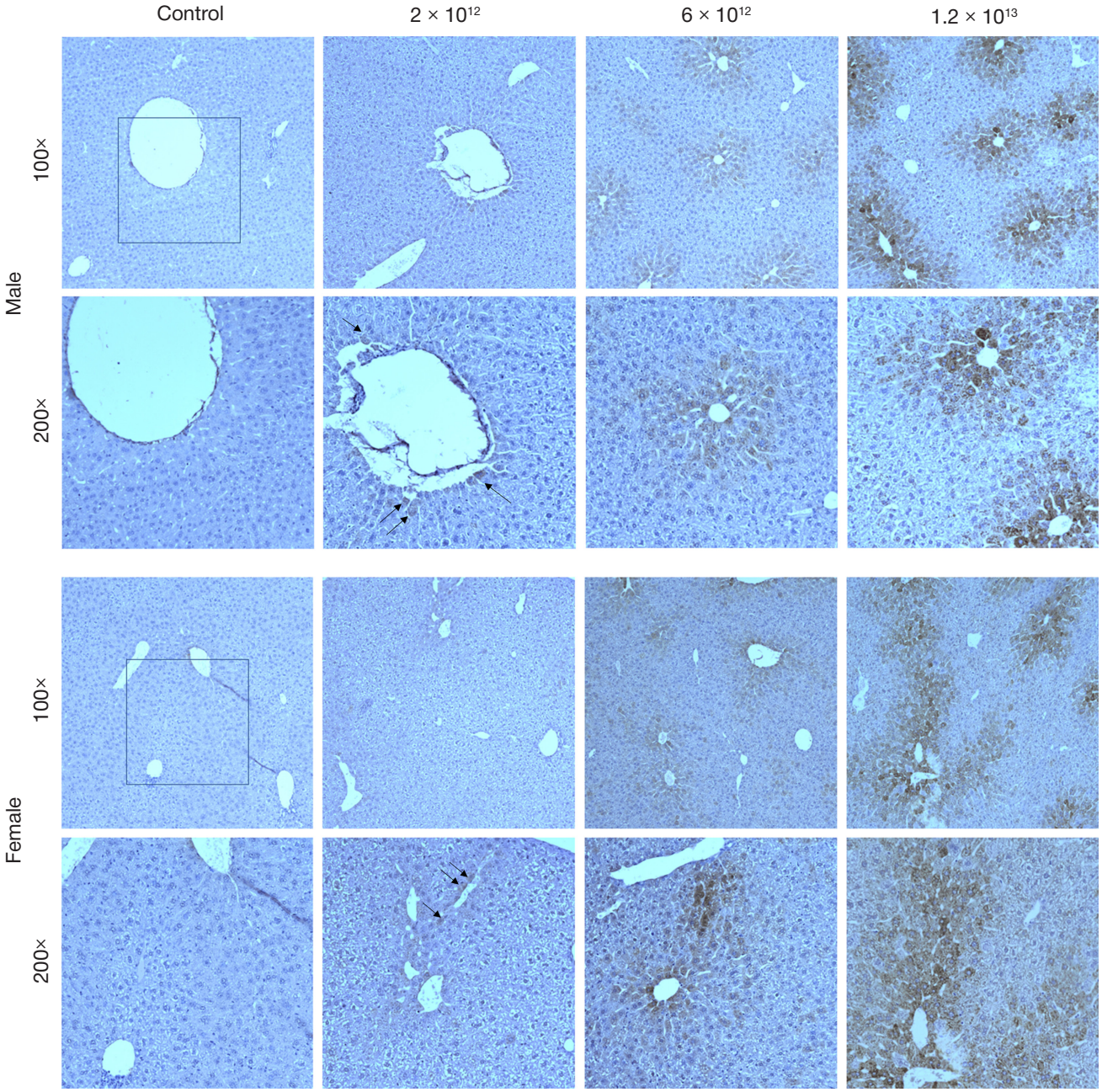

Fig. 1. Immunohistochemistry for human UDP-glucuronosyltransferase 1A1 in mouse liver, post-infusion week 6. The sections counterstained with hematoxylin were assessed using antibodies to human UGT1A1 topped with HRP-conjugated second antibody. Vector doses, vg/kg, are indicated. *Black arrows* in the low-dose images indicate perivascular localization of the signal

the patient received 250 mg (10 mg/kg) methylprednisolone intravenously.

No neutralizing antibodies to AAV8 were detectable before infusion I. The positive immunological reaction with AAV8 epitopes persisted post-infusion.

Infusion I reduced the serum bilirubin 2-fold, the minimum achieved throughout weeks 2–9. As the daily phototherapy doses were gradually reduced to 4 h by week 8, serum bilirubin concentrations rebound to ~250 μmol/l starting from week 10. The clinical decision on infusion II was intended at complete elimination of phototherapy. Infusion II on week 27 produced no toxic effects and afforded a further ~20% reduction in serum bilirubin concentrations by week 29. Considering the positive dynamics, the phototherapy support was discontinued, but resumed 2 weeks later at the same limited dose of 4 h, as serum bilirubin concentrations rapidly increased to ~400 μmol/l. The re-initiated phototherapy provided rapid correction of serum bilirubin concentrations to ~250 μmol/l. The liver enzyme profiles remained normal throughout the observation period. At the time of writing (week 97), the patient is stable on phototherapy administered 4 h daily, without systemic complaints.

Case discussion

The treatment produced no toxic side effects. Although complete discontinuation of the phototherapy proved unfeasible at this stage, the treatment afforded a lasting 3-fold reduction in daily exposure compared with initial values.

CONCLUSION

The use of liver-specific gene therapy in pediatric patients is associated with accelerated loss of the restored function,

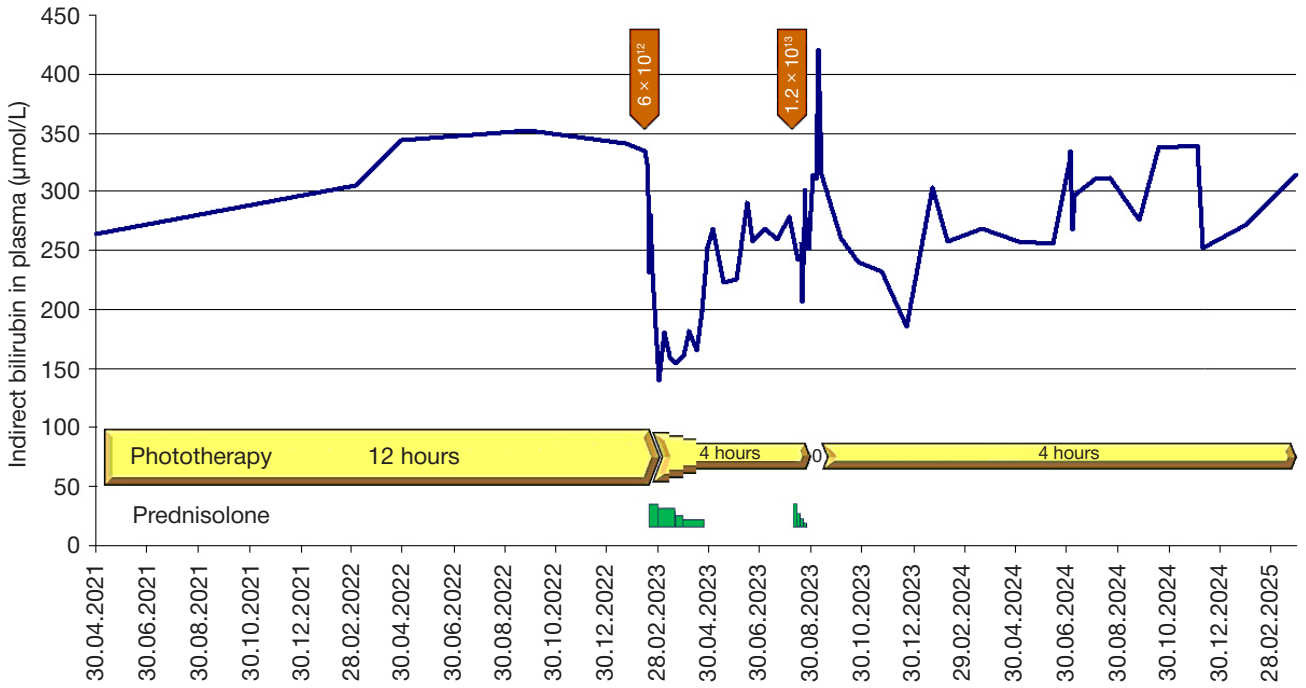

Fig. 2. Dynamics of indirect bilirubin levels with regard to alphaglucuronosyltransferasegene unoparvovec infusions I and II, adjusted phototherapy regimens and prednisolone support (oral doses, starting from 1 mg/kg daily)

apparently due to the high physiological regeneration capacity and liver growth. The opportunity of safe repeated administration of AAV8 vector allows satisfactory control of the critical biochemical indicator.

The Gene Therapy for Crigler-Najjar Syndrome Type I is currently in a Phase 1/2 trial (https://clinicaltrials.gov/study/NCT06641154) and could be applicable to other patients aged 3 months to 10 years.

References

1. Dhawan A, Lawlor MW, Mazariegos GV, McKiernan P, Squires JE, Strauss KA, Gupta D, James E, Prasad S. Disease burden of Crigler-Najjar syndrome: Systematic review and future perspectives. J Gastroenterol Hepatol. 2020; 35 (4): 530–43. DOI: 10.1111/jgh.14853.
2. Collaud F, Bortolussi G, Guianvarc`h L, et al. Preclinical Development of an AAV8-hUGT1A1 Vector for the Treatment of Crigler-Najjar Syndrome. Mol Ther Methods Clin Dev. 2018; 12: 157-74.
3. Greig JA, Nordin JML, Draper C, et al. AAV8 Gene Therapy Rescues the Newborn Phenotype of a Mouse Model of Crigler-Najjar. Hum Gene Ther. 2018; 29 (7): 763–70.
4. D'Antiga L, Beuers U, Ronzitti G, et al. Gene Therapy in Patients with the Crigler-Najjar Syndrome. N Engl J Med. 2023; 389 (7): 620–31. DOI: 10.1056/NEJMoa2214084.

Литература

1. Dhawan A, Lawlor MW, Mazariegos GV, McKiernan P, Squires JE, Strauss KA, Gupta D, James E, Prasad S. Disease burden of Crigler-Najjar syndrome: Systematic review and future perspectives. J Gastroenterol Hepatol. 2020; 35 (4): 530–43. DOI: 10.1111/jgh.14853.
2. Collaud F, Bortolussi G, Guianvarc`h L, et al. Preclinical Development of an AAV8-hUGT1A1 Vector for the Treatment of Crigler-Najjar Syndrome. Mol Ther Methods Clin Dev. 2018; 12: 157-74.
3. Greig JA, Nordin JML, Draper C, et al. AAV8 Gene Therapy Rescues the Newborn Phenotype of a Mouse Model of Crigler-Najjar. Hum Gene Ther. 2018; 29 (7): 763–70.
4. D'Antiga L, Beuers U, Ronzitti G, et al. Gene Therapy in Patients with the Crigler-Najjar Syndrome. N Engl J Med. 2023; 389 (7): 620–31. DOI: 10.1056/NEJMoa2214084.